



**University of  
Nottingham**  
UK | CHINA | MALAYSIA

# **Dynamics of ligand and nanobody binding at CXCR4/EGFR complexes**

**Dehan Comez**

**University of Nottingham**

**School of Life Sciences**

Supervisors:

Stephen J Hill

Laura E Kilpatrick

Stephen J Briddon

Meritxell Canals

Thesis submitted to the University of Nottingham

for the degree of Doctor of Philosophy

September 2024

This thesis submitted for the degree of Doctor of Philosophy is entirely the candidate's own work. The experiments described in this thesis were performed by the author between September 2020 and December 2023 in the Cell Signalling Research Group, University of Nottingham, UK and at QVQ Ltd., Utrecht, Netherlands. No part of the material has been submitted previously for a degree or any other qualification at any university. All proximity ligation assay (PLA) work was performed and supervised as part of collaborative research team comprising of Dr Stephanie M Anbuhl, Dr Raimond Heukers, Prof Marco Siderius, Prof Martine J. Smit at QVQ Ltd., Utrecht, Netherlands and Division of Medicinal Chemistry, Amsterdam Institute of Molecular and Life Sciences (AIMMS) Vrije Universiteit (VU), Amsterdam, Netherlands.

**Abstract**

Understanding the cell signalling of cancer has the potential to impact the development of anti-cancer therapeutics. The dimerisation of cell membrane receptors is one of the key modulators of cancer cell signalling. G-protein coupled receptors (GPCRs) and receptor tyrosine kinases (RTKs) are two prominent receptor families regulating various cellular processes in normal physiology and cancer progression. The abnormalities in membrane receptors, such as mutations, overexpression or enhanced receptor-receptor interaction are relevant for many cancer types. CXCR4 is significantly upregulated in numerous cancers, which correlates to cancer progression. Epidermal growth factor receptor (EGFR) is one of the major growth hormone receptors critical to various cancers, promoting cancer progression, proliferation, survival, and metastasis. This thesis aimed to elucidate the dynamics of CXCR4 and EGFR complexes. NanoLuciferase Bioluminescence Resonance Energy Transfer (NanoBRET) was used to quantify interacting characteristics of CXCR4/EGFR dimerisation with NanoLuciferase and fluorophore tags on receptors. Proximity Ligation Assay (PLA) was also used to detect endogenously expressed CXCR4/EGFR dimers on HeLa cells with receptor specific nanobodies conjugated to oligonucleotides.

We have shown that, in the presence of the NLuc substrate furimazine, energy transfer occurs from NLuc-tagged donor (NLuc\_EGFR or NLuc\_CXCR4) to the closely located acceptor fluorophore- tagged receptor (SNAP\_CXCR4 or HaloEGFR). Similar results were observed for oligonucleotide conjugated nanobody-based proximity ligation assay (PLA) with endogenously expressed or CRISPR-edited CXCR4/EGFR. Additionally, the dynamics of various receptor selective agonists/antagonists (CXCL12, EGF, TGF- $\alpha$ , AMD3100, IT1t, Erlotinib, etc.) and nanobodies (VUN400, Q44, etc.) binding at CXCR4/EGFR complex, demonstrated monomerising or dimerising effects. These data revealed that there is close proximity (<10nm) between EGFR and CXCR4 on the cellular membrane, and this proximity can be impacted by several EGFR/CXCR4 receptor ligands and nanobodies. These data improve our understanding of CXCR4/EGFR complex and its potential therapeutic utilization especially for cancer biology.

**Publications arising from this thesis****Journal articles**

Comez D, Glenn J, Anbuhl SM, Heukers R, Smit MJ, Hill SJ, Kilpatrick LE. Fluorescently tagged nanobodies and NanoBRET to study ligand-binding and agonist-induced conformational changes of full-length EGFR expressed in living cells. *Front Immunol.* 2022 Nov 23;13:1006718. doi: 10.3389/fimmu.2022.1006718. PMID: 36505413; PMCID: PMC9726709.

van den Bor J, Bergkamp ND, Anbuhl SM, Dekker F, Comez D, Perez Almeria CV, Bosma R, White CW, Kilpatrick LE, Hill SJ, Siderius M, Smit MJ, Heukers R. NanoB2 to monitor interactions of ligands with membrane proteins by combining nanobodies and NanoBRET. *Cell Rep Methods.* 2023 Mar 13;3(3):100422. doi: 10.1016/j.crmeth.2023.100422. PMID: 37056381; PMCID: PMC10088090.

Dekkers S, Comez D, Karsai N, Arimont-Segura M, Canals M, Caspar B, de Graaf C, Kilpatrick L.E, Leurs R, Kellam B, Hill S.J, Briddon S.J, and Stocks M.J. Small Molecule Fluorescent Ligands for the Atypical Chemokine Receptor 3 (ACKR3). *ACS Medicinal Chemistry Letters* 2024 15 (1), 143-148 DOI: 10.1021/acsmchemlett.3c00469

### Conference Abstracts

Detection of Spatial Organisation of CXCR4 and complexes with EGF receptor. Dehan Comez, Stephanie Anbuhl, Martine J. Smit, Laura E. Kilpatrick, Stephen J. Hill, 2023, Gordon Research Conference, Molecular Pharmacology, Les Diablerets, Switzerland.

Detecting the binding of fluorescent nanobodies to full-length EGFR expressed on HEK293 cell membranes using NanoBRET., Dehan Comez, Stephanie Anbuhl, Martine J. Smit, Laura E. Kilpatrick, Stephen J. Hill, 2023, 19<sup>th</sup> World Congress of Basic and Clinical Pharmacology, Glasgow, Scotland, UK.

Detection of Spatial Organisation of CXCR4 and complexes with EGF receptor. Dehan Comez, Stephanie Anbuhl, Martine J. Smit, Laura E. Kilpatrick, Stephen J. Hill, 2023, 11th Adrenoceptor Symposium Adrenoceptors and GPCR Signalling, Glasgow, Scotland, UK

The effect of ligand and nanobody binding dynamics on EGFR/CXCR4 complex, Dehan Comez, Stephanie Anbuhl, Raimond Heukers, Marco Siderius, Martine J. Smit, Laura E. Kilpatrick, Stephen J. Hill, 2024, 14<sup>th</sup> EMBO Young Scientists' Forum, Izmir, Turkey.

## **Acknowledgements**

First, I would like to thank my supervisory team. Prof. Steve Hill and Dr. Laura Kilpatrick have been incredible supervisors during my PhD. I have learned a lot from them. Thanks, Steve, for being a role model for me and showing how to be a kind a fair supervisor. You have been always rational and supportive. Your critical approach to the data has been teaching for me. Thanks, Laura, for being there for me literally 24-7. Your emotional support and kindness were life saving for me for many times during this journey. Your extensive knowledge in different scientific areas and lab experience helped me incomprehensibly. I will always miss you being around and chatting in the lab in my future lab work.

Second, I want to thank everyone in the Cell Signalling Research Group and COMPARE. Thanks to you, it was home for me during my three years in Nottingham. Desisleva Nesheva, Nicola Dijon, Charlie Lay, Eddy Wragg, Clare Harwood, Lydia Ogrodzinski, Sean Cullum, Laura Humphrys, George Coney, Kelvin Cheung, Simon Platt, Patrizia Panucci, Mark Soave, Owen Underwood, Marleen Groenen, James Farmer, Chloe Peach, Hannah Lockington, Julie Sanchez. It was quite nice to have a chat with you all and knowing that you were there in the lab whenever I need.

Special thanks to Marieke van Daele, Noemi Karsai and Cemre Tuzer. We have started this journey together. You were always there at each step of my PhD supporting me. I enjoyed all the time we spent outside of the lab. Our travels were amazing. I am so happy that I have lifetime friendships with you.

Third, I would like to thank everyone in ONCORNET consortium for providing amazing scientific and friendly environment. It was a great scientific opportunity to share knowledge and experience with each other. I had a great time during our gathering in different cities. Thanks Prof Federico Mayor Jr, Dr Viviana Marolda, Raimond Heukers and Dr Stephanie M Anbuhl for hosting me in Madrid and Utrecht during my secondments. Thanks Prof. Steve Briddon and Prof Meritxell Canals for supporting me in Nottingham.

A big thank you to all my loved ones all around the world. To my mum Vicdan Comez, my dad Ayhan Comez and my sister Nihan Comez for supporting me all the way through my career. A special thank you to my grandma Rasime Comez whom I have lost during my PhD. Thanks for the unconditional love and always smiling eyes when

you see me since my childhood. My nephews Kerem and Baran. I missed you growing up. I wish I could spend more time with you. My cousins Selin, Pelin and Ezgi. All my friends/family Cise, Berceste, Ezgi, Yasemin, Peyda, Gulsun, Yeliz, Aykan, Nurcan, Busra, Meryem, Ozlem, Deniz, Mert, Aybike, Kemal.

---

**Abbreviations**

A1	Adenosine receptor subtype 1
A3	Adenosine receptor subtype 3
ACKR3	Atypical chemokine receptor 3
AF	Alexa fluor®
AREG	Amphiregulin
BTC	Betacellulin
BRET	Bioluminescence resonance energy transfer
BODIPY	4,4-difluoro-4-bora-3a,4a-diaza-s-indacene
BSA	Bovine serum albumin
cAMP	3,'5'-cyclic adenosine monophosphate
CB <sub>2</sub>	Cannabinoid receptor 2
CXCL11	C-X-C chemokine ligand 11
CXCL12	C-X-C chemokine ligand 12
CXCR4	C-X-C chemokine receptor type 4
CAS	CRISPR-associated protein
CRISPR	Clustered regularly interspaced short palindromic repeats
CR	Cysteine rich domain
DMEM	Dulbecco's modified Eagle's medium
DMSO	Dimethyl sulphoxide
ECM	Extracellular matrix
ECD	Extracellular domain
ECL	Extracellular loop
E. coli	<i>Escherichia coli</i>
EDTA	Ethylenediaminetetraacetic acid
EGF	Epidermal growth factor

---

EGFR	Epidermal growth factor receptor
EREG	Epiregulin
ERK	Extracellular-signal regulated kinase
FBS	Fetal bovine serum
GPCR	G protein-coupled receptor
GRB2	Growth factor receptor-bound protein 2
Hb-EGF	Heparin-binding EGF-like growth factor
HBSS	HEPES buffered saline solution
HEK293T	Human embryonic kidney clone 293, SV40 large T antigen
HEPES	(4-(2-hydroxyethyl)-1-piperazineethanesulfonic acid
HIV	Human immunodeficiency virus
HL	HiLyte®
IC <sub>50</sub>	Concentration at which half maximal inhibition occurs
ICD	Intracellular domain
ICL	Intracellular loop
IG	Immunoglobulin
K <sub>d</sub>	Concentration at which half the receptors are occupied
LB	Luria broth
MAPK	Mitogen-activated protein kinases
Min	Minute
Nb	Nanobody
NLuc	NanoLuciferase; commercially sold as NanoLuc®
pIC <sub>50</sub>	Concentration required for 50% inhibition of responses (IC <sub>50</sub> ) expressed as a negative logarithm
PBS	Phosphate buffered saline
PFA	Paraformaldehyde

---

PI3K	Phosphoinositide 3-kinase
PKA	Protein kinase A
RTK	Receptor tyrosine kinases
RTKI	Receptor tyrosine kinase inhibitor
SAR	Structure-activity relationship
SD	Standard deviation
Sec	Second
S.E.M.	Standard error of the mean
SHC	Src homology domain-containing adaptor protein C
TGF- $\alpha$	Transforming growth factor- $\alpha$
TCEP	Tris(2-carboxyethyl)phosphine
TM	Transmembrane
VEGFR2	Vasoactive endothelial growth factor receptor 2
VHH	Variable domain for heavy chain of heavy chain antibody
WT	Wild-type

---

**Table of Contents**

<i>Abstract</i> .....	3
<i>Publications arising from this thesis</i> .....	4
<i>Acknowledgements</i> .....	6
<i>Abbreviations</i> .....	8
<i>Table of Contents</i> .....	11
<i>Chapter 1: Introduction</i> .....	15
1.1 G protein-coupled receptors (GPCRs) .....	16
1.2 GPCR Signalling.....	17
1.3 Chemokines and Chemokine Receptors .....	24
1.4 The Structure of CXCR4.....	26
1.5 CXCR4 Signalling .....	32
1.6 ACKR3 Structure .....	36
1.7 ACKR3 Signalling.....	38
1.8 CXCR4 and ACKR3 signalling in cancer .....	39
1.9 Receptor Tyrosine Kinases .....	41
1.10 The Structure of EGFR .....	42
1.11 EGFR Signalling .....	48
1.12 The EGFR in Cancer .....	50
1.13 GPCR/RTK Crosstalk.....	51
1.14 CXCR4/ EGFR Crosstalk.....	53
1.15 Fluorescent Ligands .....	55
1.16 Nanobodies .....	56
1.17 Hypothesis and aims .....	57
<i>Chapter 2: Materials and Methods</i> .....	59
2.1 Materials.....	60
2.2 Vectors and cloning .....	63

---

<b>2.3 Luria Broth with agar plate preparation .....</b>	<b>68</b>
<b>2.4 Transformation of the competent bacteria cells .....</b>	<b>68</b>
<b>2.5 Luria broth preparation .....</b>	<b>69</b>
<b>2.6 Maxiprep DNA purification .....</b>	<b>69</b>
<b>2.7 DNA Sequencing .....</b>	<b>70</b>
<b>2.8 Cell Culture.....</b>	<b>70</b>
2.8.1 Freezing of cells.....	71
2.8.2 Thawing of cells.....	71
2.8.3 Passaging of cells.....	71
2.8.4 Cell seeding for NanoBRET assays .....	72
<b>2.9 Transfection of HEK293 cells with Fugene HD .....</b>	<b>73</b>
<b>2.10 Membrane preparation from stably transfected HEK293 cells .....</b>	<b>73</b>
<b>2.11 Clonal selection of stably transfected cell lines (dilution cloning) .....</b>	<b>74</b>
<b>2.12 Preparation of Hank's Balanced Solution (HBSS) .....</b>	<b>74</b>
<b>2.13 Nanoluciferase bioluminescence resonance energy transfer (NanoBRET) Assays</b>	<b>75</b>
<b>2.14 NanoBRET Ligand Binding Assay.....</b>	<b>77</b>
2.14.1 NanoBRET saturation binding assay .....	78
2.14.2 NanoBRET ligand displacement assay (competition assay).....	79
<b>2.15 NanoBRET Receptor-Receptor Dimerisation Assay.....</b>	<b>79</b>
<b>2.16 NanoBRET kinetic assay .....</b>	<b>81</b>
<b>2.17 NanoBIT Internalisation assay .....</b>	<b>81</b>
<b>2.18 SNAPTag and HaloTag Labelling .....</b>	<b>83</b>
<b>2.19 Bioluminescent imaging.....</b>	<b>84</b>
<b>2.20 Production and purification of nanobodies .....</b>	<b>85</b>
<b>2.21 Conjugation of VUN416c and Q44c with oligonucleotides .....</b>	<b>85</b>
<b>2.22 Determining Nb-oligo binding (ELISA).....</b>	<b>86</b>
<b>2.23 Proximity ligation assays.....</b>	<b>86</b>
<b>2.24 Data analysis .....</b>	<b>87</b>
2.24.1 Saturation Binding .....	87

---

---

2.24.2 Competition Binding .....	88
2.24.3 Statistical analysis .....	89
<b><i>Chapter 3: Binding properties of fluorescently labelled CXCR4 and ACKR3 ligands determined using NanoBRET.....</i></b>	<b>90</b>
<b>3.1 Introduction .....</b>	<b>91</b>
<b>3.2 Results .....</b>	<b>95</b>
3.2.1 Determination of CXCR4 ligand binding by NanoBRET.....	95
3.2.2 Determination of novel ACKR3 ligands binding by NanoBRET .....	99
<b>3.3 Summary and Discussion .....</b>	<b>105</b>
<b>3.4 Conclusion.....</b>	<b>107</b>
<b><i>Chapter 4: NanoBRET studies to investigate the binding of EGFR ligands/nanobodies and agonist-induced conformational changes of EGFR.....</i></b>	<b>108</b>
<b>4.1 Introduction .....</b>	<b>109</b>
<b>4.2 Results .....</b>	<b>111</b>
4.2.1 Expression and localisation of NLuc_EGFR in HEK293 cells.....	111
4.2.2 Ligand and nanobody binding studies to NLuc_EGFR .....	112
4.2.3 Internalisation of EGFR by EGF nanobody binding .....	126
<b>4.3 Discussion .....</b>	<b>128</b>
<b>4.4 Conclusion.....</b>	<b>132</b>
<b><i>Chapter 5: Determination of CXCR4/EGFR Homodimerisation and Heterodimerisation using NanoBRET.....</i></b>	<b>133</b>
<b>5.1 Introduction .....</b>	<b>134</b>
<b>5.2 Results .....</b>	<b>136</b>
5.2.1 Formation of CXCR4 and EGFR homodimers and heterodimers .....	136
5.2.2 Impact of the serum starvation on EGFR/CXCR4 heterodimerisation .....	144
5.2.3 Impact of ligand and nanobody binding on CXCR4/EGFR heterodimers. ....	147
5.2.4 The effect of ligand binding on CXCR4/EGFR homodimers/heterodimers .....	150
5.2.5 Detection of endogenous receptor heterodimerisation of CXCR4/EGFR .....	160
5.2.6 Detection of CXCL12 and EGF binding at EGFR and CXCR4 respectively.....	167
5.2.7 Investigation of conformational change of EGFR with co-expression of CXCR4 .....	172
<b>5.3 Summary and Discussion .....</b>	<b>174</b>

---

---

<b>5.4 Conclusion.....</b>	<b>179</b>
<b><i>Chapter 6: General Discussion and Conclusions .....</i></b>	<b><i>182</i></b>
<b>6.1 General Discussion .....</b>	<b>183</b>
<b>6.2 Future directions .....</b>	<b>187</b>
<b><i>Chapter 7: Appendix .....</i></b>	<b><i>189</i></b>
<b>7.1 Amino acid sequences of the receptors .....</b>	<b>190</b>
7.1.1 NLuc_CXCR4 (rat 5-HT <sub>3a</sub> Signal peptide).....	190
7.1.2 NLuc_EGFR (IL6 signal peptide) .....	191
7.1.3 Halo_EGFR (EGFR native signal peptide) .....	192
7.1.4 SNAP_CXCR4 (rat 5-HT <sub>3a</sub> signal peptide).....	193
7.1.5 HiBiT_EGFR (IL6 signal peptide) .....	194
7.1.6 Sequencing primers for EGFR .....	195
<b><i>Chapter 8: References.....</i></b>	<b><i>198</i></b>

# Chapter 1: Introduction

## 1.1 G protein-coupled receptors (GPCRs)

The G protein-coupled receptor family is the largest family of cell membrane receptors and drug targets in the human genome (Benovic, 2018a; Erlandson et al., 2018; Kogut-Günthel et al., 2024; Weis & Kobilka, 2018). With more than 800 family members, they control various physiological functions such as vision, taste, olfaction, neurotransmission, immunity, and endocrine regulation (Rosenbaum et al., 2009). They are a notable therapeutic avenue, with around 35% of drugs approved by the Food and Drug Administration (FDA) targeting 108 GPCRs (Hauser et al., 2019). They are classified into five main families: glutamate, rhodopsin, adhesion, frizzled/taste2 and secretin (Fredriksson et al., 2003). Another nomenclature for GPCRs uses A, B, C, D, E, F letters to classify them as: class A—rhodopsin-like receptors; class B—secretin family; class C—metabotropic glutamate receptors; class D—fungal mating pheromone receptors; class E—cAMP receptors, and class F—frizzled (FZD) and smoothed (SMO) receptors (Attwood & Findlay, 1994). The Class A are the most prominent of the GPCR subfamilies of which the chemokine receptors are a member of (**Figure 1.1**) (S. Zhao et al., 2019). Rhodopsin was the first GPCR crystal structure solved (Palczewski et al., 2000).

According to their architecture, GPCR members have several common properties. They share a common seven transmembrane (7TM) structure spanning the cell membrane in a counter-clockwise manner. These transmembrane regions are linked by three extracellular (ECL) and three intracellular (ICL) loops (Kobilka, 2007a). GPCRS also contain an extracellular amino terminus and an intracellular carboxyl terminus (Kobilka, 2007b). The position of the ligand-binding pocket, however, can vary greatly depending on the GPCR sub-family. The endogenous ligands of several class A GPCRs (e.g. beta-adrenoceptors, muscarinic receptors etc) bind to an orthosteric ligand-binding site within the 7TM domains (Kobilka, 2007a). The ligands of the class B GPCRs bind to both the seven-transmembrane domain and extracellular domain. For class C GPCRs, a Venus flytrap (VFT) region in the extracellular domain provides the site of ligand binding (Basith et al., 2018a). Class F GPCRs have an extracellular domain containing extracellular cysteine-rich domain (CRD) for ligand binding (**Figure 1.2**) (Fredriksson et al., 2003) (Basith et al., 2018b). Ligand binding initiates the conformational change in the GPCR family, leading to intracellular

signalling protein recruitment such as heterotrimeric G proteins (GTP binding proteins) and  $\beta$ -arrestins (Nathan J. Pavlos, 2017a).

## 1.2 GPCR Signalling

GPCRs are regulatory receptors essential for healthy physiology and signal transduction (Gurevich & Gurevich, 2019a; Nathan J. Pavlos, 2017b; Rosenbaum et al., 2009; Weis & Kobilka, 2018). Hormones, neurotransmitters, ions and photons are some the ligands that allow communication of cells within their environment (Syrovatkina et al., 2016a). Upon activation by ligands, multiple conformational changes can occur in GPCRs that leads to activation of downstream signalling (Pavlos, 2017a). G proteins are heterotrimeric proteins formed of  $\alpha$ ,  $\beta$  and  $\gamma$  subunits (Pavlos, 2017b). After GPCR activation, they act as guanyl nucleotide exchange factors (GEFs) promoting the exchange of GDP (guanidine diphosphate) for GTP (guanidine triphosphate) at the  $\alpha$  subunit (Gilman, 1987a). Following this, the  $\beta$  and  $\gamma$  subunits dissociate from the  $\alpha$  subunit (Gilman, 1987b). G proteins are classified according to their  $\alpha$  subunits,  $G_{\alpha s}$ ,  $G_{\alpha i}$  (Gi),  $G_{\alpha q}$  and  $G_{\alpha 12/13}$  (Milligan & Kostenis, 2006a).  $G_{\alpha s}$  family consists of  $G_{\alpha s}$  and  $G_{\alpha olf}$  subunits (Milligan & Kostenis, 2006a).  $G_{\alpha i}$  family has multiple members:  $G_{\alpha i1}$ ,  $G_{\alpha i2}$ ,  $G_{\alpha i3}$ ,  $G_{\alpha o}$ ,  $G_{\alpha t}$ ,  $G_{\alpha g}$ , and  $G_{\alpha z}$  (Smrcka, 2019a). The  $G_{\alpha q}$  family contains  $G_{\alpha q}$ ,  $G_{\alpha 11}$ ,  $G_{\alpha 14}$ , and  $G_{\alpha 16}$  subunits (Milligan & Kostenis, 2006b). There are also 5  $G_{\beta}$  and 12  $G_{\gamma}$  subunit isoforms (Smrcka, 2019b). When the agonist stimulated exchange of GDP to GTP on the  $\alpha$  subunit occurs, this subunit is activated and dissociates from  $\beta$  and  $\gamma$  subunits. Upon dissociation, the  $G_{\alpha s}$  subtype can activate the enzyme adenylyl cyclase leading to the production of cAMP (cyclic adenosine monophosphate) from ATP (Pavlos, 2017b; Zhou et al., 2019). cAMP-dependent PKA (protein kinase A) consists of two regulatory and two catalytic subunits. cAMP binding to the regulatory subunits of PKA releases the catalytic subunits which can then enter the nucleus, phosphorylate cAMP-binding protein (CREB) and activate transcription factors to regulate various cellular functions (Neves et al., 2002).



**Figure 1.1 GPCR classification phylogenetic tree.** Branches of GPCR families have shown as Adhesion (purple), Secretin (pink), Glutamate (orange), Frizzled/Taste2 (dark and light green), Rhodopsin (blue). Four chemokine structures, including CXCR4, are shown in the Rhodopsin branch (Figure taken from Zhao et al., 2019).

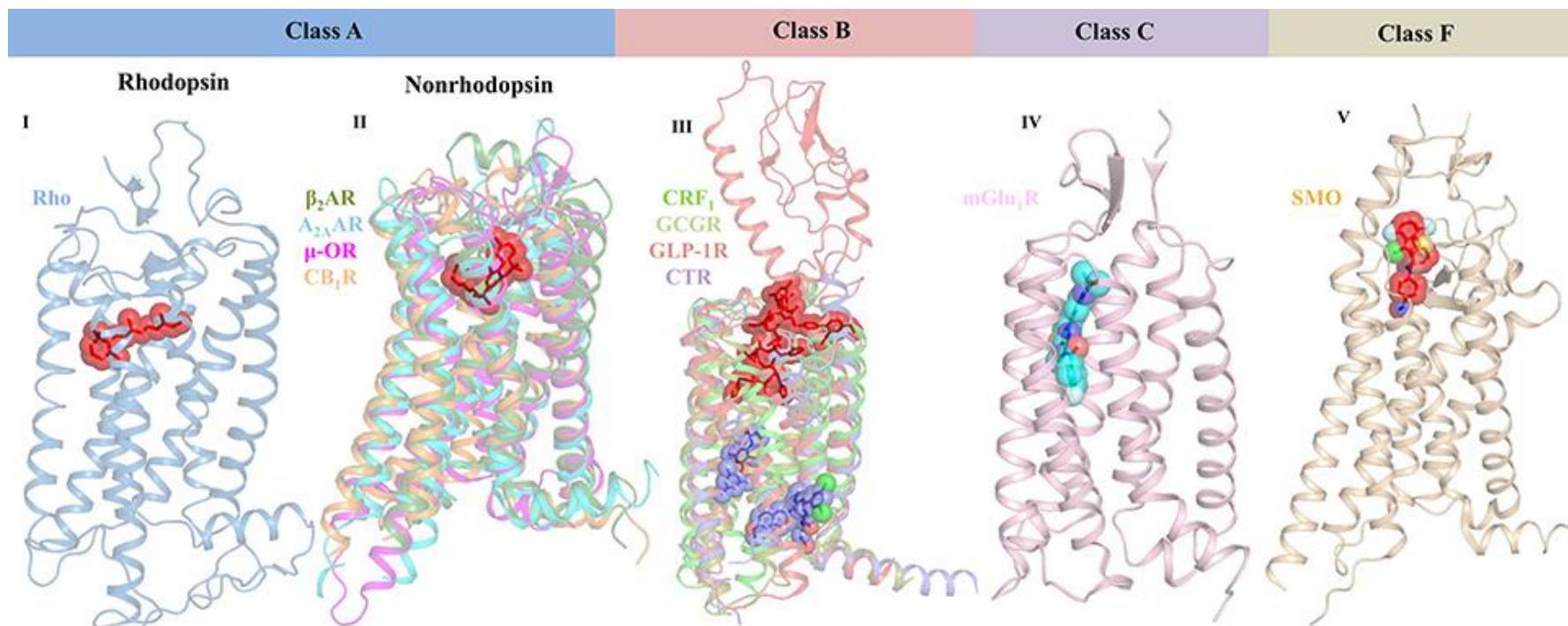


**Figure 1.2 Crystal structure of class A, B, C and F GPCRs.** Common architecture of GPCR classes includes seven transmembrane domains. Their ligand-binding pockets show diversity (shown in red and blue). The ligands of the class A receptors bind in the 7TM region, class B receptors bind in both 7TM and extracellular regions, class C the venus trap region helps the binding of ligands and class F has cysteine-rich extracellular binding domain (Figure taken from Basith et al., 2018b).

In contrast, for the G protein subtype  $G_{\alpha i}$  ( $G_i$ ), its activation results in the inhibition of the activity of adenylyl cyclase and inhibition of subsequent production of cAMP (Dorsam & Gutkind, 2007a) (Syrovatkina et al., 2016a). Activation of the  $G_{\alpha q}$  subtype leads to increased phospholipase C- $\beta$  activity causing the hydrolysis of the membrane lipid  $PIP_2$  (Phosphatidylinositol 4,5-bisphosphate) to  $IP_3$  (inositol 1,4,5-trisphosphate) and DAG (diacylglycerol) (Dorsam & Gutkind, 2007b).  $IP_3$  in the cytoplasm activates  $IP_3$  gated calcium channels located on the membrane of the endoplasmic reticulum and leads to the release the  $Ca^{2+}$  into the cytoplasm (Syrovatkina et al., 2016a) (Dorsam & Gutkind, 2007a). This calcium release and DAG together activate protein kinase C (PKC), leading to phosphorylation and activation of downstream signalling molecules (Syrovatkina et al., 2016b).  $IP_3$ , DAG and  $Ca^{2+}$  play roles as secondary messengers in this pathway (Dorsam & Gutkind, 2007a)(Syrovatkina et al., 2016a). Additionally,  $G_{\alpha 12}$  activates the monomeric GTPase RhoA and inhibits Rho kinase to regulate similar cellular functions.  $G_{\beta\gamma}$  subunits regulate MAPK (mitogen-activated protein kinase) and ion channels (Smrcka, 2019b) (**Figure 1.3**). GPCR signalling is regulated by other proteins such as GPCR kinases (GRKs) and arrestins (Gurevich & Gurevich, 2019a). GRKs phosphorylate various GPCRs on several serine and threonine residues leading to  $\beta$ -arrestin binding. This binding prevents G protein binding to GPCRs and inhibits downstream pathways (Gurevich & Gurevich, 2019b).  $\beta$ -arrestin binding can also induce desensitisation and internalisation of some GPCRs through clathrin-coated vesicles (Shenoy & Lefkowitz, 2011)(Benovic, 2018b).

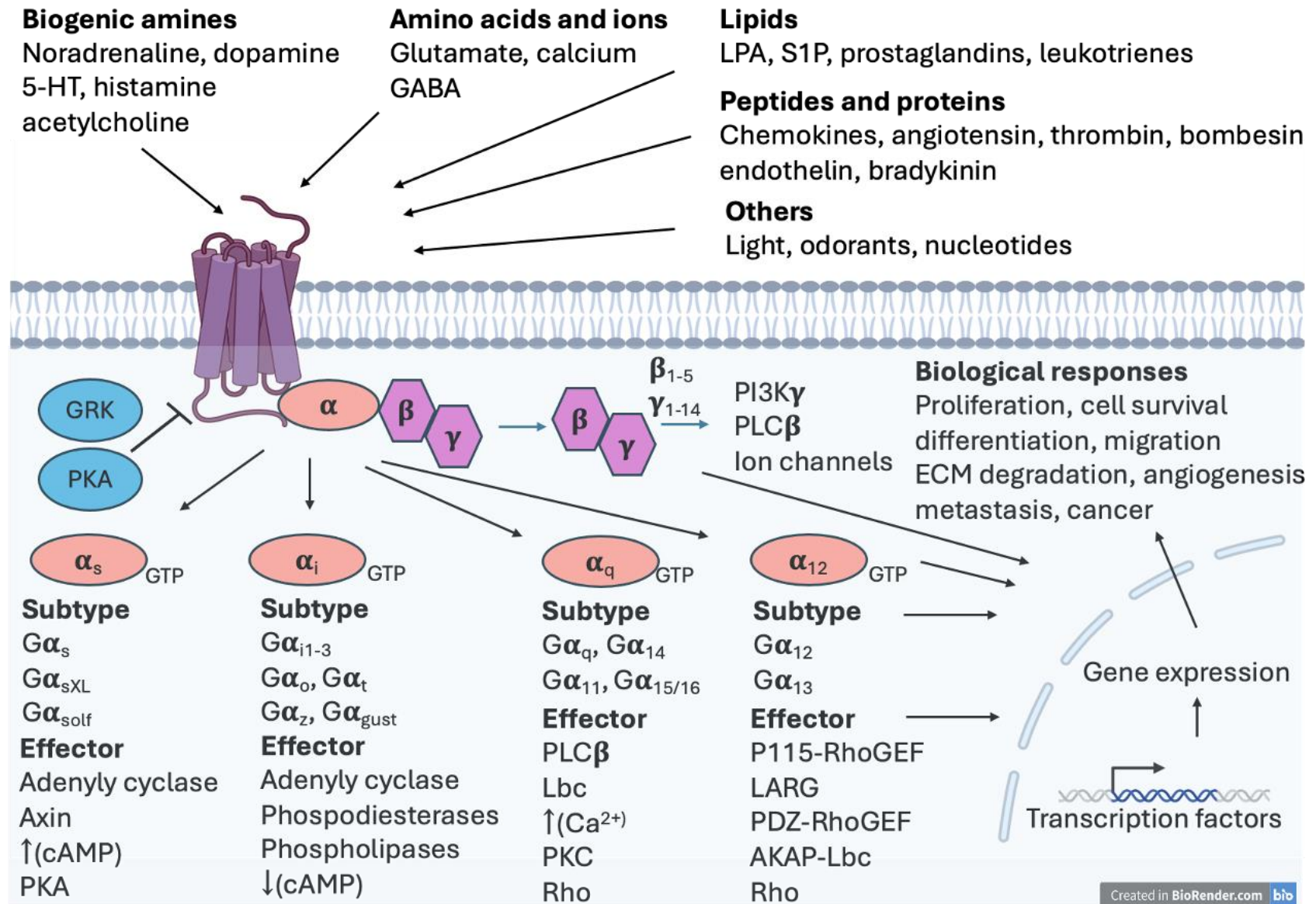
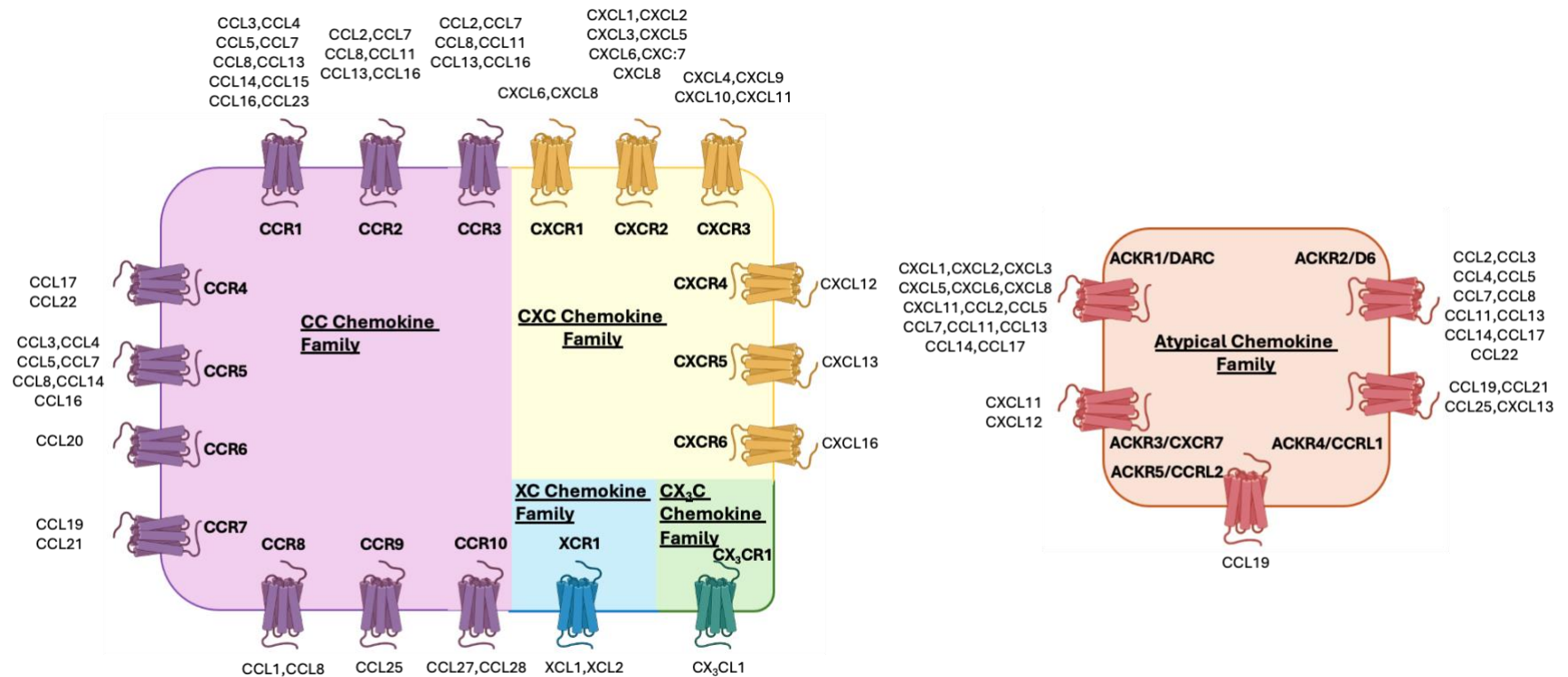


**Figure 1.3 GPCR signalling through G proteins and their downstream signalling pathway.** Upon activation following agonist binding, GPCRs signal through heterotrimeric G proteins consisting of  $G_\alpha$  and  $G_{\beta\gamma}$  subunits. G proteins are classified according to their  $G_\alpha$  subunits, and they interact with different downstream signalling molecules leading to various cellular responses. Figure adapted from (Dorsam & Gutkind, 2007a) and created using Biorender.

### 1.3 Chemokines and Chemokine Receptors

Chemokines are small molecules which belong to the cytokine superfamily. They have 8-10 kDa molecular weight range (Rossi & Zlotnik, 2000). The chemokine classification and nomenclature are formed according to conserved cysteine residues on their N-terminal sites. While the C-chemokine subfamily consists of one cysteine, CC-family contains two adjacent cysteines. When cysteines are separated via one other amino acid, the chemokine family is called CXC. The 3 amino acid separated family is called CX3C (Bachelierie et al., 2014). Chemokines function as signalling molecules between various types of cells through binding to a group of membrane proteins called chemokine receptors. The conventional chemokine receptors are GPCRs which couple with heterotrimeric G proteins. The second and atypical group of chemokine receptors which are not able to signal through G proteins are called atypical chemokine receptors (ACKRs) (Lodowski & Palczewski, 2009). The receptor nomenclature is based on their binding chemokine class (e.g. CXCR is the receptor family that binds CXC chemokines) (Murphy et al., 2000). So far, there are 10 CCRs, 6 CXCRs, 1 CX3CR, 1 XCR and 5 ACKRs identified (**Figure 1.4**). Most of these receptors bind more than one chemokine with different binding affinities (Elemam et al., 2021a). The main biological role of the chemokines and their receptors is cell migration, termed chemotaxis that plays an important role in immunity and cancer biology (Rossi & Zlotnik, 2000). Chemokines can modulate the proliferation and metastasis of cancer cells as well as immune cell recruitment in the cancer microenvironment (Poeta et al., 2019).



Created in BioRender.com

**Figure 1.4 Chemokine receptors and their predominant binding chemokines.** The nomenclature of the chemokine receptor family aligns with the chemokines that they bind such as CC, CXC, CX<sub>3</sub>C, XC. The ACKR receptors were named after their atypical features since they do not signal through G proteins. Figure adapted from (Elemam et al., 2021a). Created with Biorender.

#### 1.4 The Structure of CXCR4

The C-X-C chemokine receptor type 4 (CXCR4) is a member of the class A G protein-coupled receptor (GPCR) superfamily. There have been four different structures of CXCR4 determined. Wu et al. (2010) obtained the crystal structures of CXCR4 bound to either the small molecule IT1T (isothiourea derivative; at a resolution of 2.5 Å) or CVX15 (16-residue cyclic peptide analogue of horseshoe crab peptide polyphemusin) at a resolution of 2.9 Å. (Qin et al., 2015a) acquired the viral chemokine antagonist vMIP-II bound CXCR4 crystal structure at 3.1 angstrom resolution. A recent study showed the cryo-EM structure of the CXCL12-CXCR4-Gi monomeric complex at active state at 2.65 Å (Y. Liu et al., 2024).

The endogenous ligand for CXCR4, CXCL12 contains an N terminus loop, a CXC motif followed by an N loop and three  $\beta$  strands ( $\beta_1$ ,  $\beta_2$  and  $\beta_3$ ) connect by 30s and 40s loops. Residues C9 and C34 and C11 and C50 are bonded with disulfide bonds (**Figure 1.5**) (Y. Liu et al., 2024). Molecular modelling has suggested a “two-site” binding mode, with site one referring to the receptor binding domain for the ligand and site two being the N-terminus of the CXCL12. This means that the core of the chemokine binds to the N-terminus and extracellular loop of the receptor and, as a second step, the N-terminus then interacts with the seven transmembrane domain of the receptor which is called orthosteric pocket (Qin et al., 2015b) (Adlere et al., 2019).

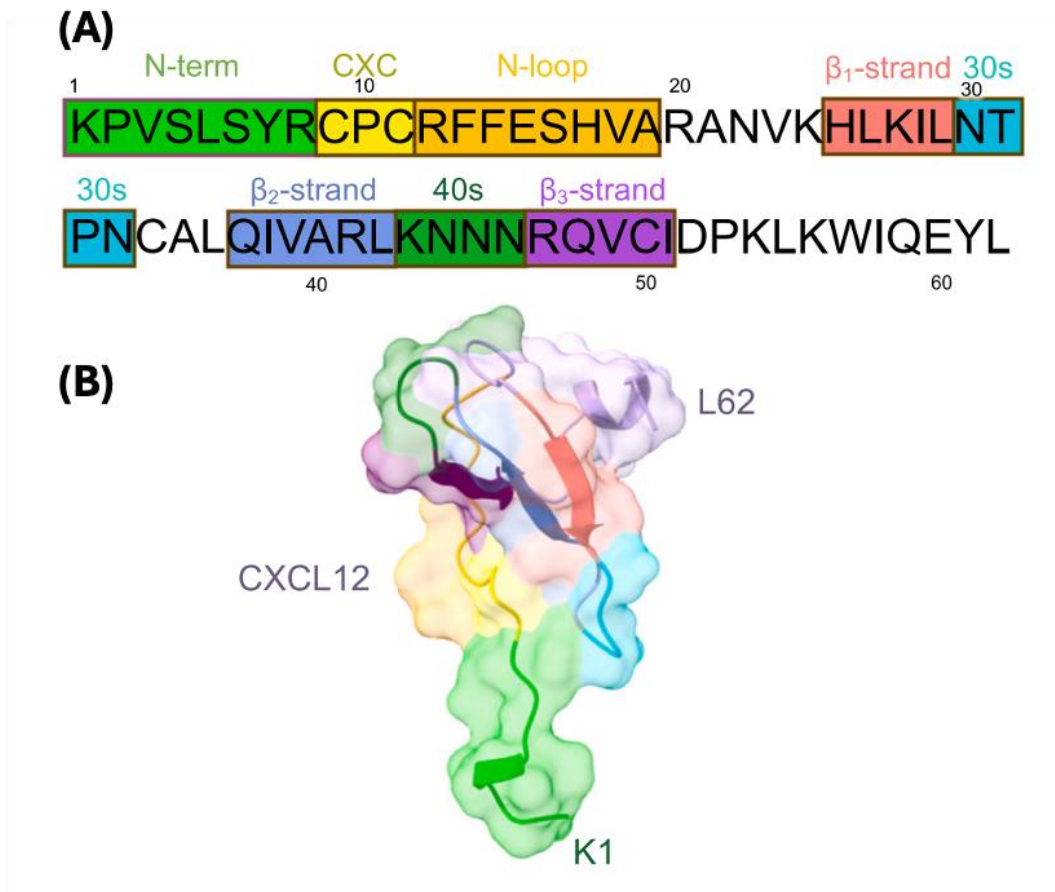


**Figure 1.5** The coloured amino acid sequence (A) and the cryo-EM structure (B) of CXCL12. Chemokine N-terminal K1-R8 residues (light green), CXC motif (yellow), N-terminal loop (orange),  $\beta_1$  strand of CXCL12 (salmon), 30s loop connecting the  $\beta_1$  strand and  $\beta_2$  strand (cyan),  $\beta_2$ -strand of CXCL12 (marine blue), 40s loop connecting the  $\beta_2$  strand and  $\beta_3$  strand (grass green), the third  $\beta$  strand of CXCL12 (purple) (Y. Liu et al., 2024).

In keeping with the “two-site” mode of chemokine binding, CXCL12 binds to N terminus of CXCR4 chemokine recognition site 1 (CRS1) through CXCL12 globular core. CXC motif of CXCL12 interacts with PC motif of CXCR4 which is CRS1.5 (an intermediate region between CRS1 and CRS2) and N terminus of CXCL12 interacts with transmembrane (TM) binding pocket of CRS1.5 of CXCR4. CXCL12 contains proline 10 (P10) which is a unique position among CXC chemokines, interacts with C28NT on N terminus of CXCR4 (**Figure 1.6**). This N terminus interaction help CXCL12 to navigate it binding into the TM pocket at CRS2. The binding interactions between CXCL12 and CXCR4 contains K1 (N terminus) of CXCL12 forms polar interactions with C186<sup>ECL2</sup> and D187<sup>ECL2</sup> in ECL2 of CXCR4. V3 of CXCL12 forms

a hydrogen bond with E288<sup>7.39</sup> of CXCR4. S4 of CXCL12 has multiple polar interactions with H281<sup>7.32</sup> and E288<sup>7.39</sup> of CXCR4 defining an upward turn from the horizontal pose toward the extracellular region. L5 to R8 takes a vertical pose in CRS2. Y7 of CXCL12 has polar interactions with D187<sup>ECL2</sup> of CXCR4, while R8 of CXCL12 forms a hydrogen bond with D262<sup>6.58</sup> of CXCR4. CXCL12 also forms hydrophobic interactions with CRS2 of CXCR4 residues L41<sup>1.35</sup>, W94<sup>2.60</sup>, H113<sup>3.29</sup>, Y116<sup>3.32</sup>, I185<sup>ECL2</sup>, F189<sup>ECL2</sup>, Y255<sup>6.51</sup>, I259<sup>6.55</sup>, L266<sup>6.62</sup>, E268<sup>6.64</sup>, and S285<sup>7.36</sup>. P2 of CXCL12 has forms hydrophobic interactions with W94<sup>2.60</sup> and Y116<sup>3.32</sup>, L5 forms nonpolar interactions with L41<sup>1.35</sup> and H113<sup>3.29</sup>, and S6 has short-range hydrophobic interaction with I185<sup>ECL2</sup> (**Figure 1.6**)

The interaction between CXCL12 and extracellular region of CXCR4 is provided with P32 (30s loop connecting the  $\beta_1$ , and  $\beta_2$  strand) residue from CXCL12 and residue S178<sup>ECL2</sup> of CXCR4 which defines CRS3. This P32-S178<sup>ECL2</sup> interaction at CRS3 supports the stabilization of the ECL2 conformation. The stability of CXCL12 binding to N terminus of CXCR4 is provided by non-polar interactions between K25NT, E26NT, P27NT, and F29NT residues of CXCL12 and I185<sup>ECL2</sup>, F189<sup>ECL2</sup> amino acids of CXCR4. These interactions extending from the extracellular CRSs to the transmembrane domain of CXCR4 start a conformational change led by CXCL12 binding (Y. Liu et al., 2024). Even though this structure lacks resolution for CRS1 due to its CXCR4s instability at this region, CXCL12 binding to CXCR4 might apply the “two-step” model. This model hypothesize CRS1 starts the recognition and recruitment of the chemokine and helping its N terminus insertion into the CRS2 of the chemokine receptor. This insertion of the CXCL12 is the deepest in the receptor in comparison with other chemokine receptors (Y. Liu et al., 2024). Interestingly the interaction between vCCL2 and CXCR4 is shallower compared to the CXCL12-CXCR4 binding (Y. Liu et al., 2024; Qin et al., 2015a)

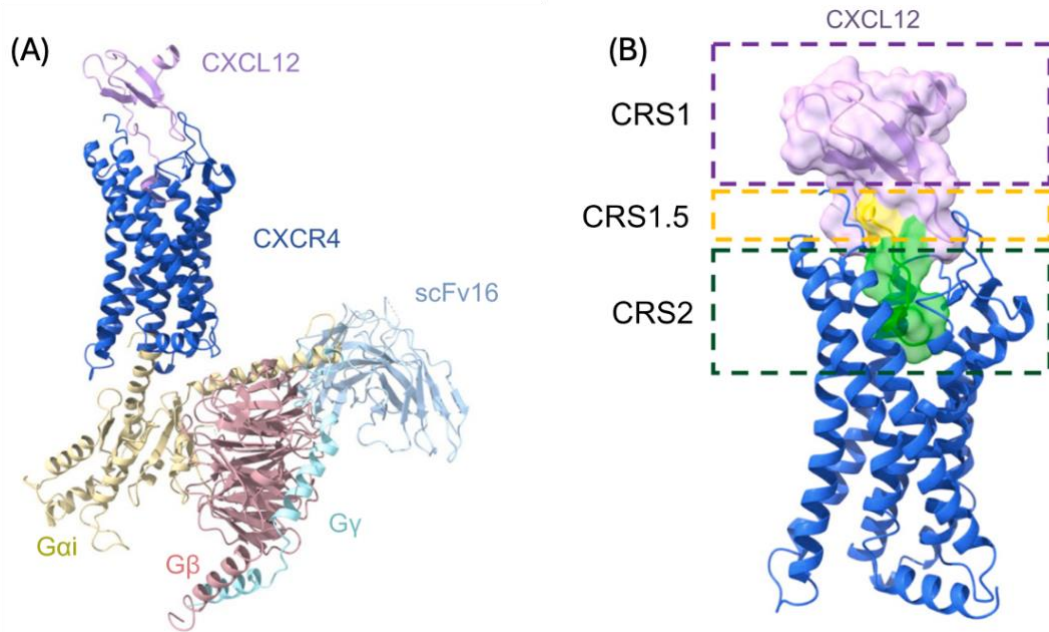


**Figure 1.6 Cryo-EM the structure of CXCL12-CXCR4-Gi complex.** (A) Side view of the structure of the CXCL12-CXCR4-Gi complex. CXCR4 is depicted in blue, CXCL12 in light pink,  $G_{\alpha i}$  in yellow,  $G_{\beta}$  in salmon,  $G_{\gamma}$  in cyan, and scFv16 in slate blue. (B) Side view of the structure of CXCR4-CXCL12 complex with chemokine recognition sites (CRS). The receptor is shown as a blue cartoon, and the chemokine is displayed as a cartoon and transparent surface. Green, N terminus; yellow, CXC motif; light pink, the globular core of CXCL12. CRS1, CRS1.5, and CRS2 are highlighted (Y. Liu et al., 2024).

The crystal structures from Wu et al. (2010) showed that CXCR4, like other GPCRs, has seven transmembrane  $\alpha$ -helices, an extracellular side with extracellular loops (ECL) and three intracellular loops (ICLs) that connect the 7 TM  $\alpha$ -helices. ECL1 ties together helices II and III, ECL2 ties helices IV and V while ECL3 links helices VI and VII. ECL2 is the largest of the ECLs and its sequence differs between various Class A GPCRs. The disulphide bonds between residues of ECLs and the N-terminal segment (residues of 16-34) are crucial for ligand binding of IT1T and CVX15, and they form the pocket for ligand docking (B. Wu et al., 2010a). The intracellular side of CXCR4 accommodates intracellular loop 1 (ICL1) and ties helices I and II, with ICL2 linking helices III and IV and ICL3 helices V and VI and the CXCR4 C-terminus. Crystal structures that have been obtained using the viral chemokine antagonist vMIP-II complexed with CXCR4 can be seen in **Figure 1.7** (Qin et al., 2015). The crystal structures obtained for CXCR4 with different ligands, suggest that

the intracellular portion of CXCR4 is more highly conserved between structures and shows similar architecture with other GPCRs than seen for the extracellular portion (B. Wu et al., 2010a). These structures also showed that CXCR4 has several properties distinct from other Class A GPCRs such as the location of the ligand binding site being in closer proximity to the extracellular surface (B. Wu et al., 2010a). While IT1t binds to the minor pocket of CXCR4 having ionic interactions with D97<sup>2.63</sup> and E288<sup>7.39</sup> amino acids, CVX15 interacts with the major pocket via D187<sup>ECL2</sup> and D262<sup>6.58</sup> (Qin et al., 2015b). CXCL12 also mainly occupies the minor sub-pocket surrounded by TM1 and TM2 of CXCR4 (Y. Liu et al., 2024).

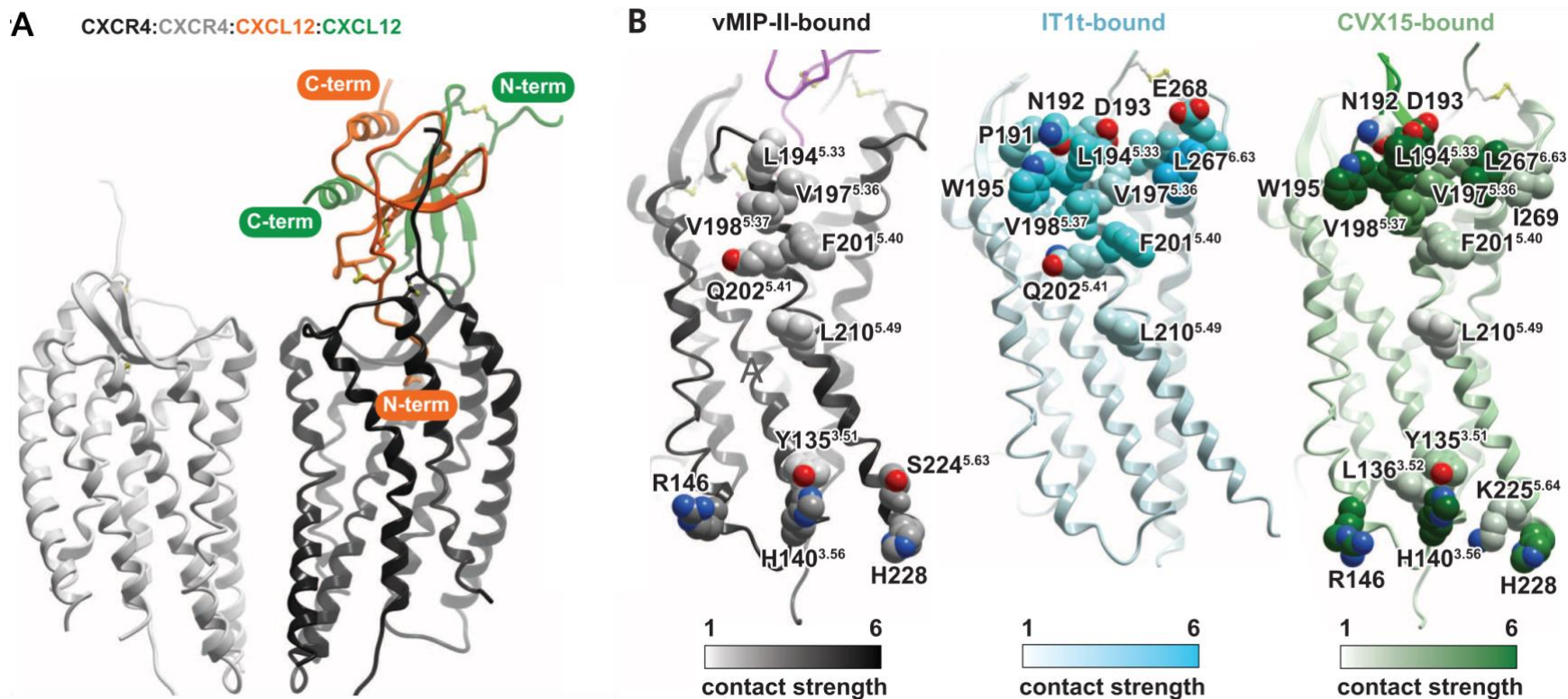


**Figure 1.7 CXCR4 structure.** (A) Molecular modelling of CXCL12 binding to the CXCR4 N-terminus predicted from the crystal structure determined with: vMIP-II bound CXCR4. (B) Crystal structures of CXCR4 when bound to vMIP-11, IT1t or CVX15. CXCR4 homodimer formation provided by the top halves of helix V and VI. Additional interactions were provided by intracellular parts of helices III and V. Residues that contribute to CXCR4 homodimer formation are shown as spheres; color intensities represent contact strength (Qin et al., 2015).

The crystal structures obtained by Wu et al. (B. Wu et al., 2010a), suggest a symmetric dimer architecture for CXCR4. In IT1t-bound CXCR4 structures, two CXCR4 receptors were suggested to bind to each other at the extracellular side of helices V and VI. In contrast, in CVX15 bound CXCR4 dimers, they showed additional interactions at the intracellular portion of helices III and IV and ICL2. This suggests that CVX15 binding starts a structural change in the N terminus portion of helix V and causes a closer proximity of the two receptor monomers at their intracellular portion which might lead to positive cooperativity between them. This phenomenon postulates that ligand binding at one receptor can affect the binding affinity of the interacting receptor via conformational change at the other receptor (B. Wu et al., 2010a). IT1t bound CXCR4 dimer interaction mostly involve hydrophobic bonds of Leu194<sup>5.33</sup>/Val197<sup>5.36</sup>/Val198<sup>5.37</sup> residues. More interactions between opposing monomers include residues Phe201<sup>5.40</sup>-Phe201<sup>5.40</sup>, Met205<sup>5.44</sup>-Met205<sup>5.44</sup>, and Leu210<sup>5.49</sup>-Leu210<sup>5.49</sup>. A substantial role is also played by a Trp195<sup>5.34</sup>-Leu267<sup>6.63</sup> contact, which includes both side-chain stacking and a hydrogen bond from Trp195<sup>5.34</sup> (NE1) to the main chain carbonyl oxygen of Leu267<sup>6.63</sup>. Polar interaction between side chains of Asn192 and Glu268 residues involving main-chain carbonyl oxygens of Leu266<sup>6.62</sup> and Trp195<sup>5.34</sup> of opposing monomers also play a role for dimers (**Figure 1.8B and Figure 1.8E**). CVX15 bound dimerisation includes the hydrophobic interactions of Tyr135<sup>3.51</sup>, Leu136<sup>3.52</sup>, His140 and Pro147 side chains of helices intracellular ends of helices III and IV, and ICL2 (**Figure 1.8C and Figure 1.8F**) (B. Wu et al., 2010b).

### 1.5 CXCR4 Signalling

CXCR4 is activated via the binding of its ligand CXCL12 (Stromal Cell-Derived Factor-1, SDF-1). The activation of CXCR4 starts a signalling cascade through heterotrimeric G proteins, mainly of the Gi subtype (Busillo & Benovic, 2007). Following the activation of CXCR4, Gi proteins mostly inhibit adenylyl cyclase and reduce cAMP signalling (Heuninck et al., 2019). Apart from G-protein dependent pathway, CXCR4 signalling can be regulated independently of G-proteins via  $\beta$ -arrestin and GRKs (G protein-coupled receptor kinases) (Z. J. Cheng et al., 2000a). GRKs are serine/threonine kinases, and they phosphorylate CXCR4 on its C-terminus following activation via CXCL12 binding. Specifically, GRK2 and GRK3

---

phosphorylation occurs on Ser346/347 while GRK6 phosphorylates at Ser324/5, Ser330 and Ser339 (Busillo et al., 2010a) (Fumagalli et al., 2019). While the phosphorylation of the C-terminus of CXCR4 via GRK2 and GRK3 are essential for  $\beta$ -arrestin recruitment to the receptor, phosphorylated amino acids produced following the action of GRK6 inhibits the recruitment of  $\beta$ -arrestin (Mueller et al., 2013).  $\beta$ -arrestin recruitment mostly plays a role in receptor desensitisation via internalisation of the receptor in clathrin-coated vesicles (Cheng et al., 2000). On the other hand,  $\beta$ -arrestin recruitment can mediate downstream signalling by acting as a scaffold protein for intracellular signalling molecules, such as ERK, MEK and Raf, important for cellular processes such as cancer progression (Peterson & Luttrell, 2017).  $G_i$  inhibition of cAMP production causes the activation of Src family tyrosine kinases and initiates the intracellular Ras/Raf/MEK/ERK signalling cascade leading to regulation of the cell cycle. Hence CXCR4 signalling is not only dependent on  $G_i\alpha$  and  $\beta$ -arrestins but they might also signal through  $G\beta\gamma$  subunits, since these subunits can also mediate downstream signalling processes such as phosphatidylinositide 3-kinases (PI3Ks) and PLC- $\beta$  (calcium accumulation) regulating cell adhesion and migration through AKT (Pozzobon et al., 2016a) (Rubin, 2009) (Zielińska & Katanaev, 2020a).

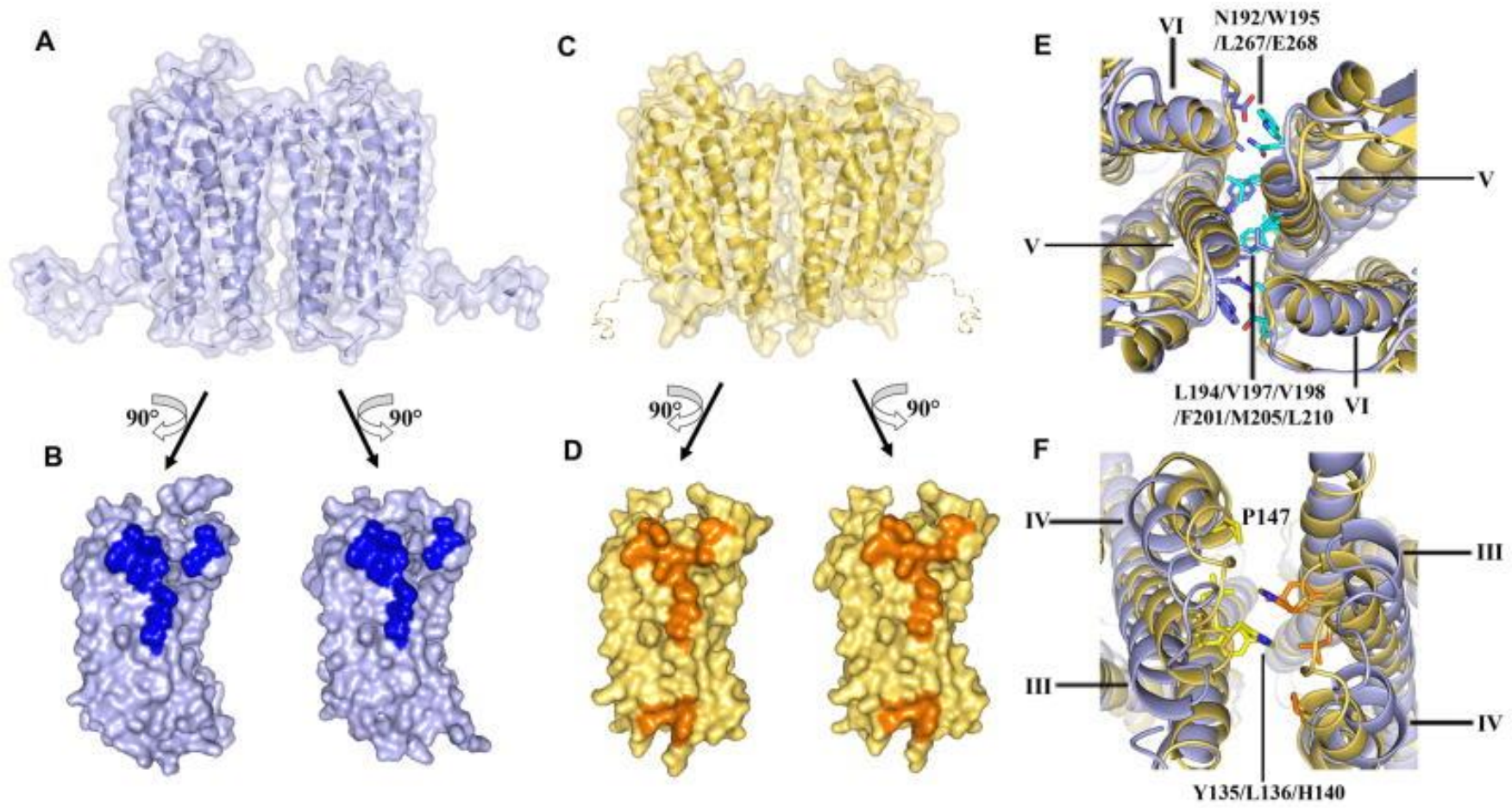


**Figure 1.8 Crystal structure of CXCR4 homodimerisation.** (A) Molecular surface representation of the IT1t bound CXCR4 (blue). (B) IT1t bound CXCR4 dimerisation interface (dark blue). (C) Molecular surface representation of the CVX15 bound CXCR4 (yellow). (D) CVX15 bound CXCR4 dimerisation interface (orange). (E) Top view of the extracellular side of the dimers of IT1t and CVX15 bound CXCR4 which show similar interactions via helices V and VI. Residues of IT1t bound CXCR4 involved in the dimer interaction are shown in stick representation, and coloured blue in monomer A, cyan in monomer B. Bottom view of the intracellular side of the dimers. Contacts can only be observed at the intracellular tips of helices III and IV, and ICL2 in CVX15 bound CXCR4. The residues involved in the dimer interaction are shown in stick representation, and coloured yellow and orange. These interactions are not present in the IT1t bound CXCR4 (Wu et al., 2010).

## 1.6 ACKR3 Structure

The structure of ACKR3 bound to different agonists has been recently elucidated (Yen et al., 2022) using cryo-electron microscopy. Yen et al., (2022) used CXCL12 in conjunction with two distinct Fabs (fragment antigen-binding region) that bind to the extracellular face (CID25) or intracellular site (CID24) of ACKR3 to stabilize a receptor conformation conducive to cryo-EM (**Figure 1.9**) (Yen et al., 2022). The extracellular binding fab CID25 had a small effect on the binding pose of CXCL12 to ACKR3 but no effect on  $\beta$ -arrestin recruitment (Yen et al., 2022). The agonists used to determine the structure of ligand bound ACKR3 were wild- type CXCL12 (CXCL12WT), CXCL12LRHQ (a higher-affinity variant of CXCL12 with alterations at its N terminus), and the small- molecule agonist CCX662 (Yen et al., 2022). The resultant structures showed that wild- type CXCL12 and CXCL12LRHQ showed similar modes of binding to ACKR3 (Yen et al., 2022).

CXCL12 binding to ACKR3 occurs in a different way than to canonical chemokine receptors like CXCR4. The rotation of CXCL12 leads to an interaction firstly with the N terminus of TM5 and ECL3 of ACKR3, rather than with the extended ECL2 of CXCR4 (Yen et al., 2022). This rotation of CXCL12 permits the  $\beta$ -1 strand of the chemokine (26-Leu, Lys, Iso, Leu, Asp-30) to form a parallel  $\beta$ -strand interaction with the N-terminal residues 28-Val, Val, Asp, Thr, Val, Met, Cys-34 of ACKR3 (Yen et al., 2022). This is a different pattern than canonical chemokine receptors where the N terminus of the receptors bind to a shallow groove of CXCL12 flanked by the chemokine N-loop” and “40s-loop,” named as chemokine recognition site 1 (CRS1) (Yen et al., 2022). This is consistent with a previous data showing that the dimer formation of CXCL12 shows lower affinity ( $K_d < 1 \mu\text{M}$ ) for ACKR3 because CXCL12 forms dimers through their  $\beta$ 1 strand (Devree et al., 2016) . However, the dimeric form of CXCL12 shows inhibited CXCR4 binding because CXCL12 binds to CXCR4 via different regions of the chemokine ( $K_d=28 \text{ nM}$ ) (Devree et al., 2016).

The orthosteric ligand binding site of ACKR3 for CXCL12 has been named as chemokine recognition site 2 (CRS2). The N terminus of CXCL12 has also been shown to bind to the minor pocket of ACKR3 formed by residues in TM1, TM2, TM3, and TM7. The Lys1 amino acid of CXCL12 can reach to the major receptor binding pocket (formed by TM3 to TM7) of ACKR3 (Yen et al., 2022). Pro2 and Val3 amino acids

---

of CXCL12 also bind to side chains of ACKR3. The conformational heterogeneity of these side chain provides promiscuity to the receptor allowing the binding of two different ligands (CXCL12 and CXCL11). The lack of a disulfide bond between the N terminus and ECL3 of ACKR3 also helps to confer deformability of the orthosteric pocket by various ligands (Yen et al., 2022).

The  $\beta$ -arrestin bias of ACKR3 has been linked to the lack of a kink at the cytoplasmic end of TM4 in ICL2 which directly interacts with G proteins in many class A receptors (Yen et al., 2022). This lack of a kink does not prevent GRK or arrestin binding to ACKR3 (Yen et al., 2022). This ICL2 feature is not conserved between other ACKRs and may suggest that all ACKRs may differ in their extent of G-protein binding (Yen et al., 2022). The other feature of ACKR3 that decreases G-protein binding has been suggested to be the smaller size of its cytoplasmic cleft (Suomivuori et al., 2020). Curiously, BRET based G protein recruitment assays have shown ACKR3 in close proximity with G protein but probably not physically coupling (Yen et al., 2022). Alternatively, ICL3 might be helping with the recruitment of G proteins but to the lack of interaction with ICL2 prevents G protein activation (Yen et al., 2022). Additionally, CXCL12 treatment seemed to have no effect on G protein recruitment to ACKR3 in opposition to CXCR4 (Yen et al., 2022).

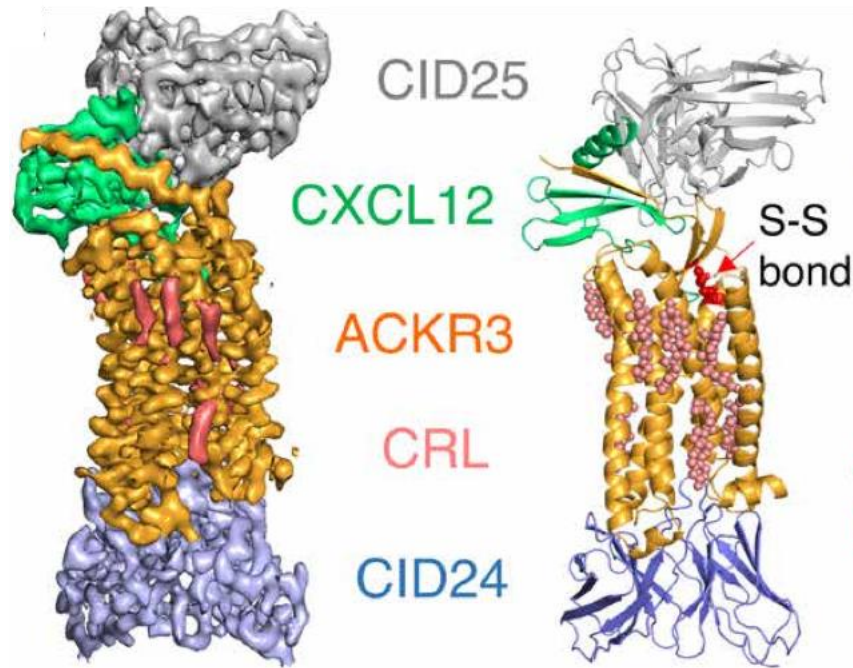


**Figure 1.9 The cryo-EM structure of ACKR3.** The cryo-EM structure of ACKR3 bound with CID25 and CID24 Fabs and CXCL12. Cryo-EM map threshold contoured at  $10\sigma$  (left) and corresponding atomic model (right). (CRL, cholesterol). (Figure taken from Yen et al., 2022).

### 1.7 ACKR3 Signalling

ACKR3 is a member of the atypical chemokine receptor subfamily (Graham et al., 2012) (Bachelierie et al., 2015). The members of this family are characterised as unable to bind to G proteins, and  $\beta$ -arrestin preferentially mediates the internalisation of ACKR3 (Graham et al., 2012)(Lodowski & Palczewski, 2009). ACKR3 has been previously known as RDC-1/ CXCR7 when it was originally discovered as an orphan receptor (Balabanian et al., 2005) (Sánchez-Martín et al., 2013). It can bind to its ligands CXCL11 and CXCL12 (the latter shared with CXCR4) (Janssens et al., 2018). CXCL12 binds to ACKR3 ( $K_d = 0.4$  nM) with tenfold higher binding affinity than observed at CXCR4 (Balabanian et al., 2005). ACKR3 is also called a scavenging receptor because it scavenges CXCL12 and prevents CXCR4 activation via CXCL12 (Naumann et al., 2010). This mechanism is driven by constitutive internalisation and recycling of ACKR3 in addition to lysosomal degradation of CXCL12 which is transported intracellularly when remaining bound to ACKR3 (Luker et al., 2010). CXCL12 binding of ACKR3 initiates downstream signalling through a pathway

involving GRK phosphorylation and  $\beta$ -arrestin recruitment (Quinn et al., 2018a). ACKR3 expression does not seem to be sufficient for the activation of ERK1/2 signalling in the absence of CXCR4 co-expression (Meyrath et al., 2020). ACKR3 is expressed in various cell types such as hematopoietic cells, endothelial cells, and neuronal progenitor cells (Koenen et al., 2019). Studies in knock out mice indicate that loss of ACKR3 results in defects in cardiac development (Sierro et al., 2007). ACKR3 plays a significant role in cancer cellular behaviours such as survival and adhesion (Miao et al., 2007).

### **1.8 CXCR4 and ACKR3 signalling in cancer**

CXCR4 and ACKR3 are co-expressed in various cells such as T and B lymphocytes, vascular endothelial cells, dendritic cells and cancer cells derived from patients with NSCLC (Non-small-cell lung cancer) (Iwakiri et al., 2009), breast cancer (Sun et al., 2010) and cervical cancer (Xu et al., 2021) (M. Neves et al., 2019a). The interaction of ACKR3 and CXCR4 can lead to phosphorylation of CXCR4/ACKR3 complexes via GRKs, and recruitment of  $\beta$ -arrestin subsequent to either CXCL12 scavenging or downstream ERK1/2 pathway activation (Lounsbury, 2020) (Meyrath et al., 2020) (**Figure 1.10**). This scavenging effect of CXCL12 by ACKR3, alters the CXCR4/G protein complex leading to decreased calcium signalling and plays a critical role in several cancers' proliferation, adhesion and metastasis (Levoye et al., 2009a).

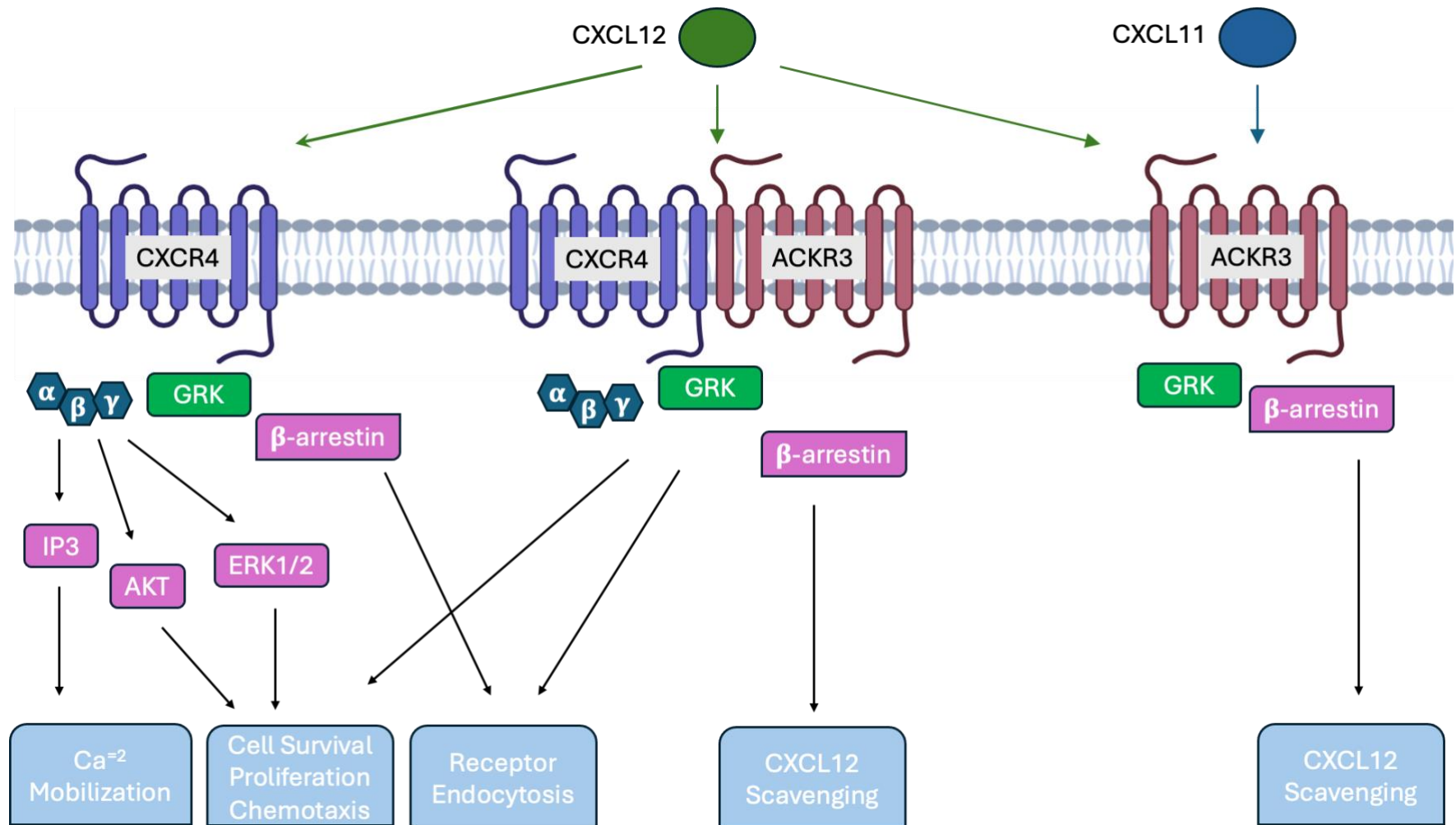


**Figure 1.10 CXCR4/ACKR3 axis in cancer.** The downstream signalling of CXCR4 is regulated by G proteins, GRKs and  $\beta$ -arrestin. They lead to alteration of cellular behaviours through IP3, ERK and AKT signalling pathways in cancer. ACKR3 downstream signalling is mostly regulated by  $\beta$ -arrestin and GRK. Adapted from (Lounsbury, 2020). Created with Biorender.

## 1.9 Receptor Tyrosine Kinases

Receptor tyrosine kinases (RTKs) are a family of cell surface growth factor receptors. They regulate cell-to-cell communication, coordinate cellular mechanisms such as proliferation, motility, differentiation, and metabolism (Gschwind et al., 2004) (Zhao et al., 2020). RTKs mostly consist of an extracellular domain responsible for ligand binding, a single transmembrane helix and an intracellular region that accommodates a juxtamembrane regulatory region and a functional domain responsible for its tyrosine kinase activity, along with a carboxyl (C-) terminal tail (Hubbard, 1999)(Cadena and Gill, 1992).

RTKs are located on the cell membrane, typically as monomers, and once ligand-binding occurs, they dimerise with another available monomer (Trenker and Jura 2020). Homodimerisation occurs when the same RTK member dimerises with itself; however, many RTKs can also form heterodimers with other RTKs or complexes with other cell membrane receptors such as GPCRs (Di Liberto et al., 2019a). The dimerisation of the RTK causes a conformational change, which leads to trans autophosphorylation of RTK monomers at their C terminus at specific tyrosine residues facilitated by the inherent kinase activity of the receptor. This autophosphorylation provides docking sites to recruit adaptor proteins and kinases containing Src homology-2 (SH2) or phosphotyrosine-binding (PTB) domains to the intracellular domain of the RTK, initiating downstream cell signalling cascade activation. The general activation mechanism can be seen in (**Figure 1.11**) (Lemmon & Schlessinger, 2010a) (Tian et al., 2020).

RTKs orchestrate physiological cellular mechanisms regulating cellular survival, proliferation, apoptosis and migration (Pottier et al., 2020; Takeuchi & Ito, 2011). Therefore, dysfunctional RTK expression or signalling can ultimately promote cancer initiation and progression (Du and Lovly, 2018). This can occur through various mechanisms, with most ultimately increasing RTK activation. Gain-of-function mutations or chromosomal rearrangements are the genetic mechanisms governing constitutively active RTKs (Da Cunha Santos et al., 2011a; Hsu et al., 2018; Lahiry et al., 2010). Receptor amplification, autocrine activation or receptor-receptor oligomerisation can also be seen in cancer cells (Oikawa et al., 2017)(Chen et al., 2016). The oncogenic role of different types of RTKs has been characterised in various

---

cancers, notably involving the epidermal growth factor receptor (EGFR), Insulin Receptor, HER2/ErbB2, fibroblast growth factor receptor (FGFR), vascular endothelial growth factor receptor 2 (VEGFR2) and c-MET as well as other RTK family members (Du and Lovly, 2018), (Lemmon & Schlessinger, 2010a) (Trenker and Jura 2020).

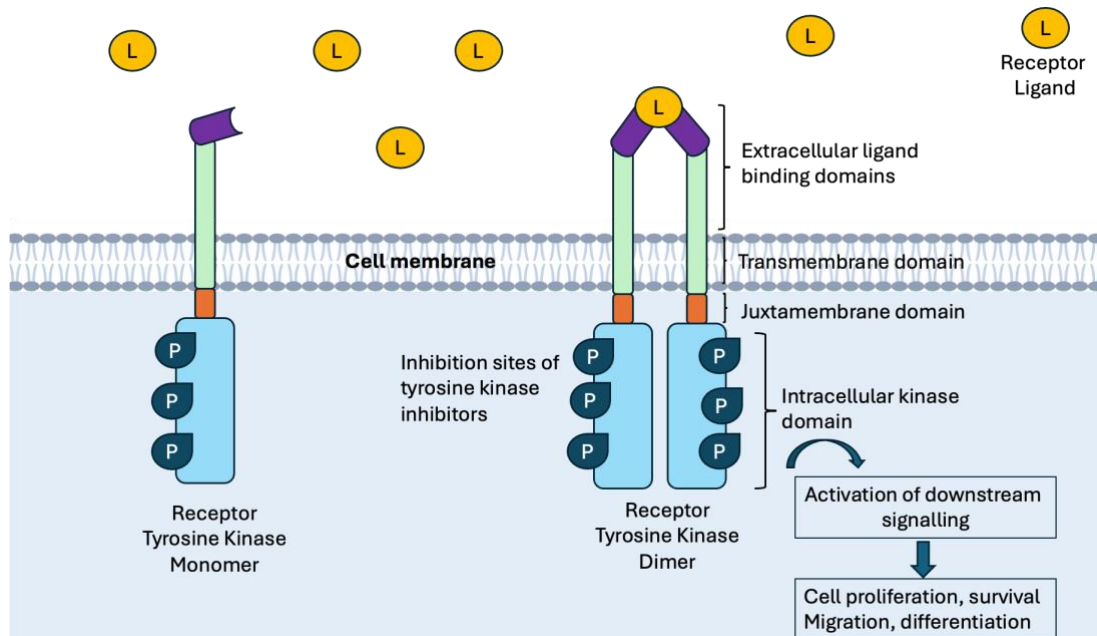


**Figure 1.11 The general activation mechanisms of RTKs in oncogenic signalling.** Specific ligand binding at monomer RTKs induces the dimerisation at the cell membrane. Dimerisation leads to autophosphorylation of receptors within the intracellular kinase domain. This starts the downstream cascade of various cellular behaviours via recruitment of adaptor proteins. Adapted from (Tian et al., 2020).

### 1.10 The Structure of EGFR

The epidermal growth factor receptor (EGFR), also named ErbB1 or HER1, is a receptor tyrosine kinase located on the cell membrane (G. Guo et al., 2015; Sigismund et al., 2018). Three homologs of EGFR (ErbB-1) have been identified in humans, ErbB-2 (HER2), ErbB-3 (HER3), and ErbB-4 (HER4) (Jorissen et al., 2003a). EGFR binds to several growth factors grouped as high-affinity binding ligands, which are epidermal growth factor (EGF), transforming growth factor- $\alpha$  (TGF $\alpha$ ), betacellulin (BTC), and heparin-binding EGF-like growth factor (HB-EGF), and the low-affinity

ligands are epiregulin, epigen and amphiregulin which bind 1 to 10 fold more weakly to EGFR (Jones et al., 1999)(Freed, 2017a) (Burgess, 2008a). EGF is a monomeric polypeptide chain containing 53 amino acids, including six cysteine residues that form three disulfide bonds (Kumar et al., 2008a). The human EGFR consists of 1186 amino acids (170-kDa mass). N-linked glycosylation of the EGFR is required for translocation of the EGFR to the cell surface and for its function (Zhen et al., 2003). The extracellular part of the protein is responsible for EGF binding, with this region consisting of four domains I–IV concurrently called L1, S1, L2, and S2. Domains II and IV are homologous cysteine-rich domains (CR1 and CR2), and domains I and III share 37% amino acid identity (Ferguson, 2008).

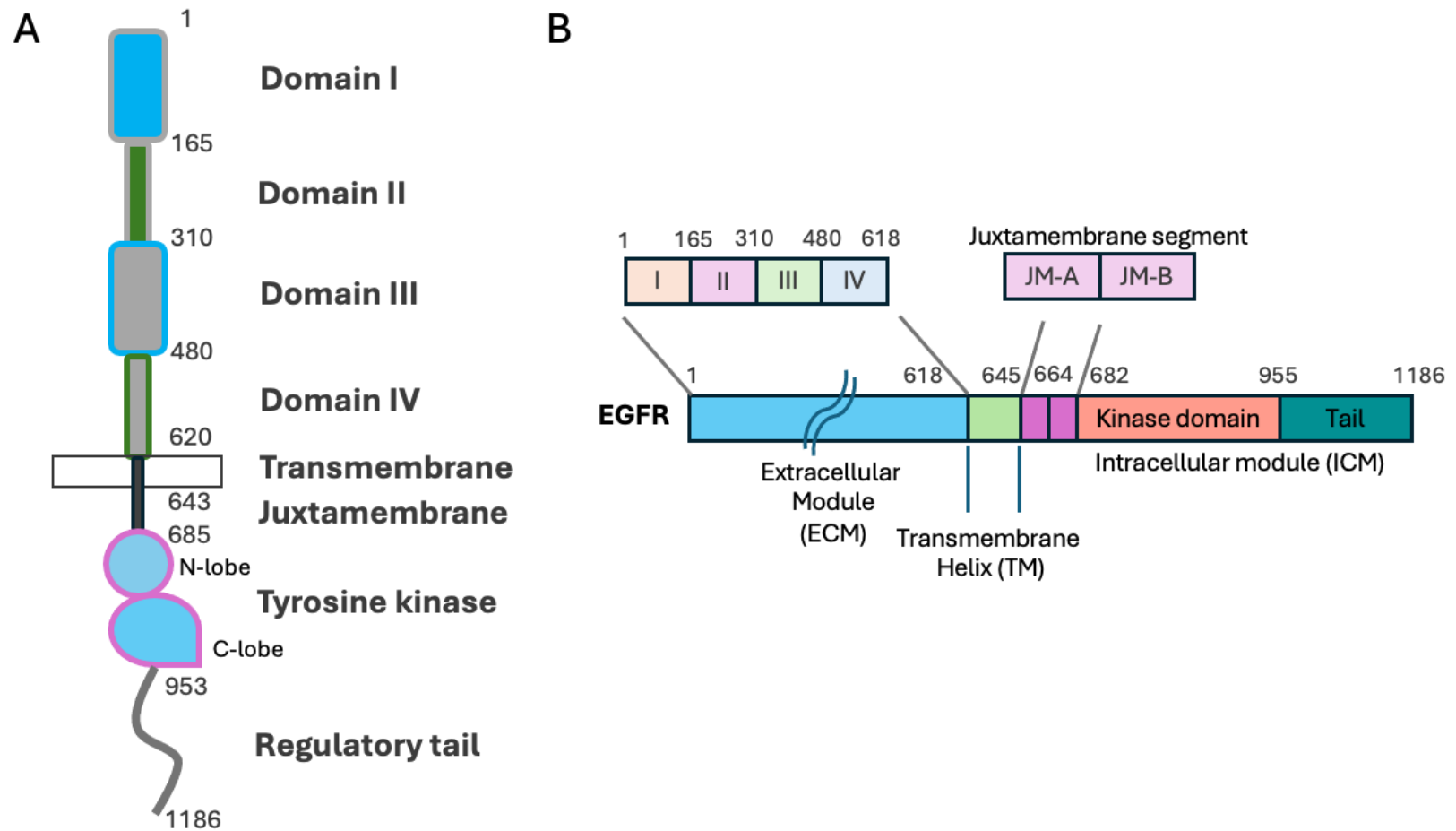


**Figure 1.12 Structural domains of EGFR.** A- The structural domains of the EGFR. B- Linear depiction of the borders of each domain. Adapted from (Ferguson, 2008) and (Kovacs et al., 2015). The EGFR consists of extracellular domains, transmembrane and juxtamembrane regions, tyrosine kinase domain and a regulatory tail. The extracellular region contains four domains called as domain I, II, III and IV.

A crystal structure of EGFR indicated EGF docking occurs at the extracellular domains of EGFR within domains I–III, which adopt a C shape conformation (Ogiso et al., 2002a). The amino acid residues Tyr13, Ile23, Arg41, and Leu47 are the main residues of monomeric EGF responsible for binding to EGFR (Ogiso et al., 2002a). Moreover, transforming growth factor (TGF- $\alpha$ ) can also activate EGFR by binding to a distinct site in the extracellular domain (Freed et al., 2017). However, TGF-  $\alpha$  cannot bind to extracellular domain I of EGFR due to the difference in its B loop structure but it may have similar binding interactions to EGF with domains II and III of EGFR (Ogiso et al., 2002b) (Bessman, Freed, et al., 2014). EGF binding between domain I and III breaks the tethered formation of domains II and IV leading to an extended formation of domain II. Extended domain II plays acts as a dimerisation arm between two EGFR monomers' extracellular regions (Bessman, Bagchi, et al., 2014a).

EGF binding to the extracellular site of EGFR induces intracellular kinase domain autophosphorylation at key tyrosine residues on the carboxyl-terminus of EGFR, leading the two monomer receptors to dimerise and interact with SH2 domain-containing proteins such as growth factor receptor-bound protein 2 (GRB2) (**Figure 1.12**)(Ferguson, 2008) (Dawson et al., 2005a). This dimerisation followed by proximity autophosphorylation starts a signal transduction cascade leading to activation of other downstream kinases or kinase-linked cytokine receptors (Burgess, 2008a) (Ray et al., 2018).

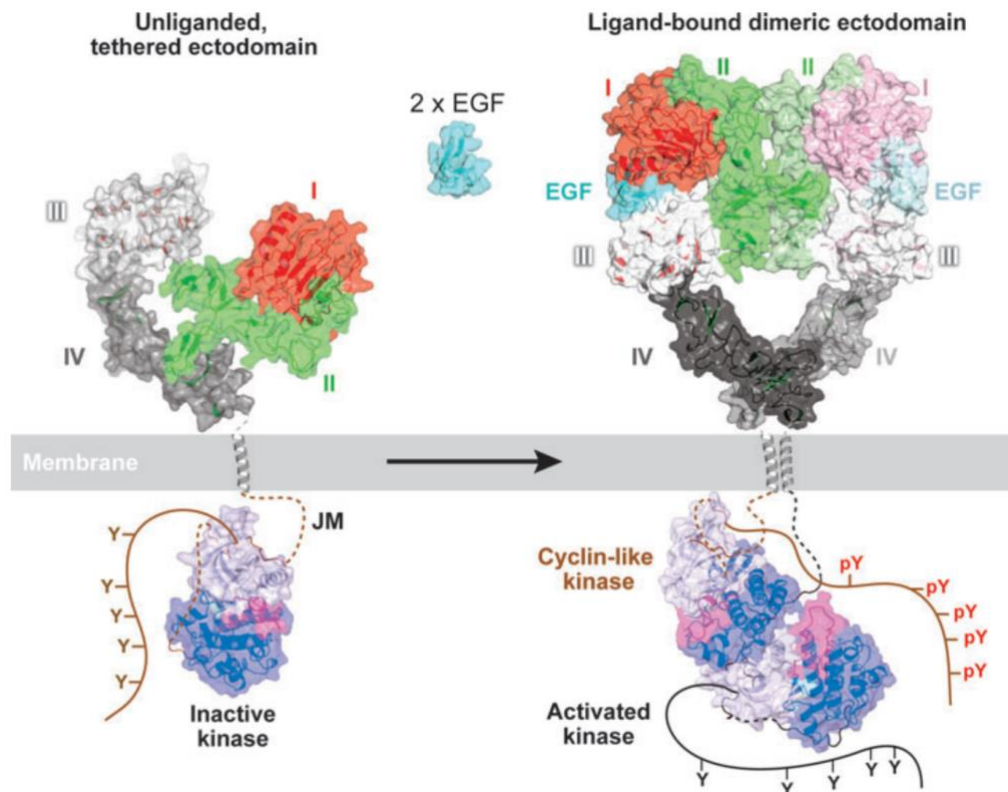


**Figure 1.13** Cartoon representation extrapolated from the crystal structures of EGFR. Illustration of the conformational changes occurring upon EGFR activation in response to EGF binding. Unliganded monomer (left) and ligand-bound and dimerised EGFR (right). The different sites have different colours. EGF-light blue, site I-red and pink, site II-green, site III-white, site IV-light and dark grey, transmembrane domain light grey on membrane (Figure taken from Ferguson, 2008).

The homo and heterodimerisation motifs of the EGFR family members have been identified between the kinase domain, the Leu955-Val956-Ile957 segment of EGFR (“LVI”), facilitating ligand-independent dimerisation between different subfamilies of the EGFR family (Mudumbi et al., 2023; Stamos et al., 2002). The NH<sub>2</sub>-terminal lobe (N-lobe) of the kinase domain structure is formed by five  $\beta$ -strands ( $\beta$ 1 and  $\beta$ 2) and one  $\alpha$ -helix. The COOH-terminal lobe (C-lobe) of the kinase domain is mainly formed by five  $\alpha$ -helices ( $\alpha$ E,  $\alpha$ F,  $\alpha$ G,  $\alpha$ H,  $\alpha$ I) (Stamos et al., 2002). The residues between these two sites are where ATP, ATP analogues, and ATP-competitive inhibitors bind and is called the cleft. The glycine-rich nucleotide phosphate-binding loop (Gly695-Gly700) on the N-lobe functions as the catalytic kinase machinery. On the C-lobe DFG motif (Asp831-Gly833), a catalytic Asp813, the catalytic loop (Arg812-Asn818), and

the A-loop (Asp831-Val852) located for this function (Stamos et al., 2002). The structural domains of EGFR can be seen in (**Figure 1.12**)(**Figure 1.13**).

The autocatalytic C-terminal tail of EGFR is the site of the ATP binding pocket within the kinase domain close to phosphorylation residues such as Tyr974, Tyr992, Tyr1048, Tyr1068, Tyr1086, Tyr1101 and Tyr1173. These phosphorylated tyrosines work as docking sites to recruit molecules, containing SH2 (Src homology 2) and phosphotyrosine-binding (PTB) domains. Phosphorylation of tyrosine residues of EGFR leads to downstream signalling pathway activation such as RAS-RAF-MEK-ERK pathway and the PI3K-AKT-mTOR pathways orchestrating cellular proliferation, survival and other cellular behaviours (**Figure 1.14**)(Martin-Fernandez et al., 2019) (Da Cunha Santos et al., 2011b)

The juxtamembrane segment contains two main sites JM-A (residues 645–663) and JM-B (residues 664–682). JM-B provides a clamp from the N-lobe of the receiver kinase domain to provide engagement to the C-lobe of the activator kinase domain of another EGFR monomer upon dimer formation leading to asymmetric dimerisation. A C-terminal 19 residue deletion and T654 and T669 phosphorylation of juxtamembrane domain has been shown to destabilise the dimerisation of EGFR. (Kovacs et al., 2015a).

Interestingly, it has been shown that either the extracellular domains (ECD) or intracellular domains (ICD) of EGFR are able to form homodimers independent from each other meaning that the lack of ICD on EGFR does not affect the homodimerisation abilities of isolated ECD domains (Mudumbi et al., 2023) Although ligand binding has been shown to induce EGFR homodimerisation, pre-formed dimers have also been observed without ligand binding (Mudumbi et al., 2023). (Purba et al., 2022).(Tao & Maruyama, 2008). Structural and cellular studies have demonstrated that two lower affinity EGFR ligands, epiregulin and epigen, induce the purified EGFR extracellular domains to form dimers, each resulting in distinct conformations (Freed et al., 2017). The resulting ligand-induced dimers were weaker and more short-lived than those induced by EGF (Freed et al., 2017). Unexpectedly, this weakened dimerisation elicited more sustained responses than EGF, evoking responses in breast cancer cells associated with differentiation rather than pro-proliferative responses typically induced by EGF (Freed et al., 2017).

### 1.11 EGFR Signalling

The knowledge about the physiology and pathophysiology of the EGFR family came initially from mouse models; knock-out of EGFR caused embryonic or postnatal death due to implantation, cardiac or central nervous system disorders such as defects of hippocampal development or neurodegeneration after birth (Sibilia et al., 1998). As previously mentioned, EGFR binds to several growth factors beyond EGF such as epigen, epiregulin, TGF- $\alpha$ , heparin binding-EGF (Hb-EGF), betacellulin (BTC), amphiregulin (AR) and neuregulin-1 (NRG-1) (Burgess, 2008a). ErbB family members have different activation mechanisms in response to ligand binding and influenced by asymmetric interactions with other family members (Freed et al., 2017). For example, HER2 (ErbB2) activation does not occur via ligand binding but by dimerisation with other family members (Nevoltris & Chames, 2015). At normal receptor expression levels, EGFR homodimers can directly or indirectly activate several downstream signalling pathways such as Ras/Raf-1/MAPK, PI3K/Akt/mTOR, PKC, STAT (**Figure 1.14**) (Da Cunha Santos et al., 2011b). It is also capable of direct interactions and dimerisation with other membrane receptors such as GPCRs and other RTKs (VEGFR) or intracellular receptor-associated kinases (JAKs) (Burgess, 2008a) (Jorissen et al., 2003a). The activation of various downstream signalling pathways orchestrates cellular behaviours such as cell proliferation, survival, migration and angiogenesis (Guo et al., 2015; Santos et al., 2021; Sigismund et al., 2018).

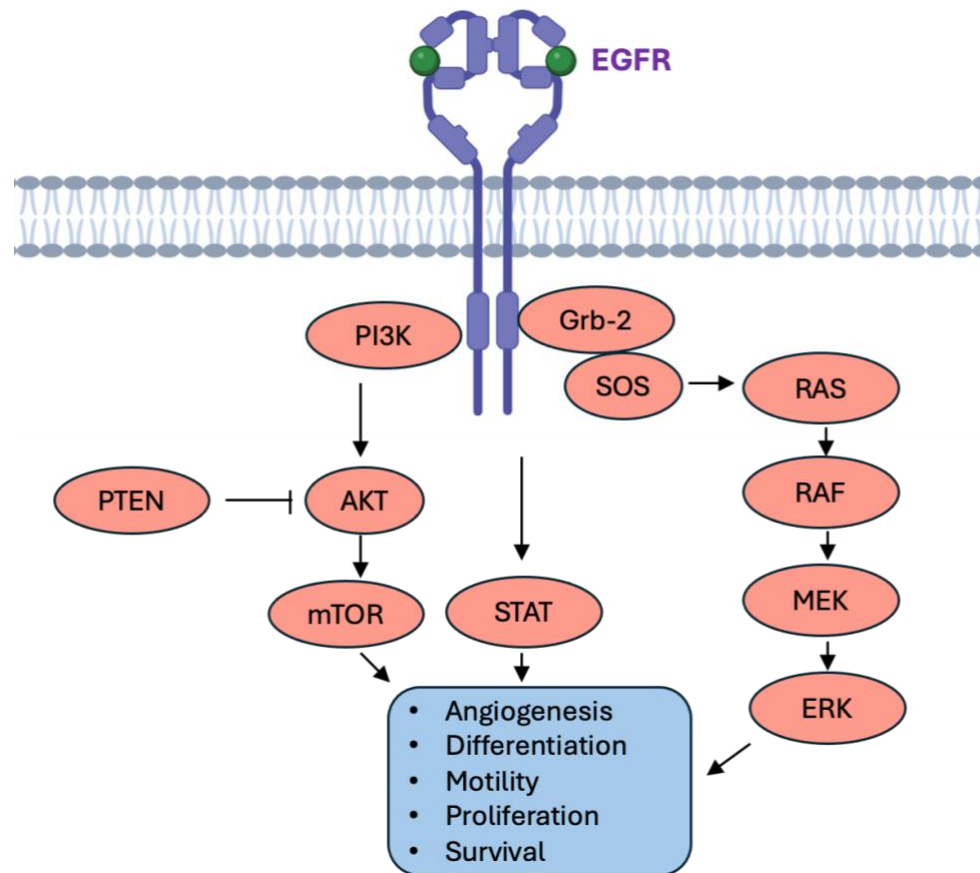


**Figure 1.14 EGFR downstream signalling cascade mechanism and cellular responses.** Autophosphorylation of EGFR via ligand binding leads to recruitment of SH2 (Src homology 2) domain-containing proteins such as GRB2 and PI3K. This starts the downstream pathway cascade activation such as AKT/mTOR, SOS/RAS/RAF/MEK/ERK to regulate cellular behaviours like angiogenesis, differentiation, motility, proliferation, and survival. Adapted from (Da Cunha Santos et al., 2011). Created with Biorender.

### 1.12 The EGFR in Cancer

The EGFR was first recognised as an oncogenic mediator due to its similarity with v-ErbB, a retroviral protein from the avian erythroblastosis virus (Downward et al., 1984). Its relevance with cancer has been recognised in various cancer types, particularly epithelial tumours such as lung (Da Cunha Santos et al., 2011b), breast (Masuda et al., 2012) or colon cancer (Pabla et al., 2015). Clinical studies have shown that EGFR overexpression or mutation can act as a biomarker for reduced survival, lymph node metastasis and poor chemosensitivity in different cancers (Guardiola et al., 2019a)(Zeng et al., 2014). EGFR mutations are categorised according to their nucleic acid changes, mostly within the kinase domain. Class I mutations are short in-frame deletions within exon 19. Class II mutations are single-nucleotide substitutions within exon 18 to 21. Class III mutations are in-frame duplications or insertions within exon 20 (Shigematsu et al., 2005). Most of the kinase domain mutations are exon 19 deletions and an exon 21 point mutation of L858R (leucine to arginine substitution) (**Figure 1.15**) (Shigematsu et al., 2005) (Da Cunha Santos et al., 2011b). Kinase domain mutations such as L858R cause an alteration from an inactive form to a constitutively active kinase form (50-fold more active than the wild type receptor). This mutant form prevents the binding of lapatinib (a receptor tyrosine kinase phosphorylation inhibitor (RTKI) to the ATP-binding cleft. However, at the same time, another RTKI gefitinib shows a 20-fold higher binding affinity to this mutant form of EGFR (Yun et al., 2007) (Kumar et al., 2008b). In addition to amplification, overexpression or mutation, crosstalk between EGFR and other partner proteins has been observed in different cancer types (Zobair et al., 2013) (Salazar et al., 2014a).

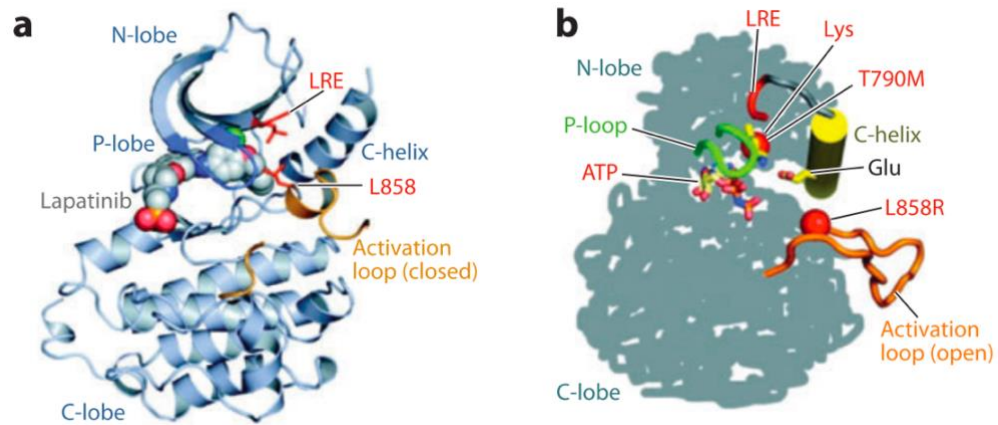


**Figure 1.15 The intracellular kinase domain mutations of EGFR.** A- Lapatinib bound kinase domain and its different lobes of EGFR. The inactive form of the kinase domain due to unmutated Leu858. The activation loop is closed due to Lapatinib binding. B- As a result of the 858 Leucine to Arginine mutation, the kinase domain is constitutively activated, and lapatinib can no longer bind to the ATP-cleft. (LRE is leucine-747 to glutamic acid-749 (LRE) deletion; T790M is a Threonine to methionine mutation at position 790) (Da Cunha Santos et al., 2011b)

### 1.13 GPCR/RTK Crosstalk

GPCRs and RTKs are both families of cell surface receptors that are crucial regulators of cell signalling and share similar downstream signalling molecules with data suggesting that they can regulate each other (Di Liberto et al., 2019b). Activation of an RTK by a GPCR agonist (not a direct binding to the RTK) was first shown via EGFR activation by endothelin-1, lysophosphatic acid and thrombin (Daub et al., 1996). GPCR/RTK crosstalk can be classified as ligand-dependent and ligand-independent mechanisms. The ligand-dependent process relies on the activation of metalloproteases (MMPs) such as ADAM (disintegrin and metalloprotease) family members to cleave pro-ligands (immature molecules which are cleaved into the mature, pharmacologically active forms) of various RTKs, which activate their cognate RTKs and consequently initiate intracellular signalling (Ohtsu et al., 2006) (Prenzel et al., 1999). A second way is a ligand-independent activation which requires physical interaction between GPCRs and RTKs (Di Liberto et al., 2019a) or shared intracellular downstream molecules following GPCR activation such as  $\text{Ca}^{2+}$  ions, PKC, Src kinase,  $\beta$ -arrestin, and reactive oxygen species (ROS) which can activate the

RTKs via different mechanisms (**Figure 1.16**) (Cattaneo et al., 2014) (Di Liberto et al., 2019a). There have been several studies showing oligomeric complexes of GPCRs and RTKs (Bergelin et al., 2010; Blasco-Benito et al., 2019; Di Liberto et al., 2019c; Kilpatrick et al., 2019; Kilpatrick & Hill, 2021; Maudsley et al., 2000). Thus, signalling complexes between vasoactive endothelial growth factor receptor 2 (VEGFR2) and the GPCR sphingosine-1-phosphate receptor have been reported in thyroid cancer cells (Bergelin et al., 2010). Signalling complexes have also been reported between the  $\beta$ 2-adrenoceptor and both EGFR (Maudsley et al., 2000) and VEGFR2 (Kilpatrick et al., 2019). CB<sub>2</sub> and HER2 receptor interaction is one of the key examples for GPCR/RTK interaction shown with co-immunoprecipitation in HEK293 cells (Pérez-Gómez et al., 2015) and with proximity ligation assay (PLA) in tissue microarray and xenograft models (Blasco-Benito et al., 2019). There have been various studies showing transactivation and direct heterodimerisation between EGFR and AT1R (type 1 angiotensin II (AngII) receptor) via BRET, FRET, FLIM and co-IP (Gekle et al., 2024; Johnstone et al., 2021; O'Brien et al., 2018).

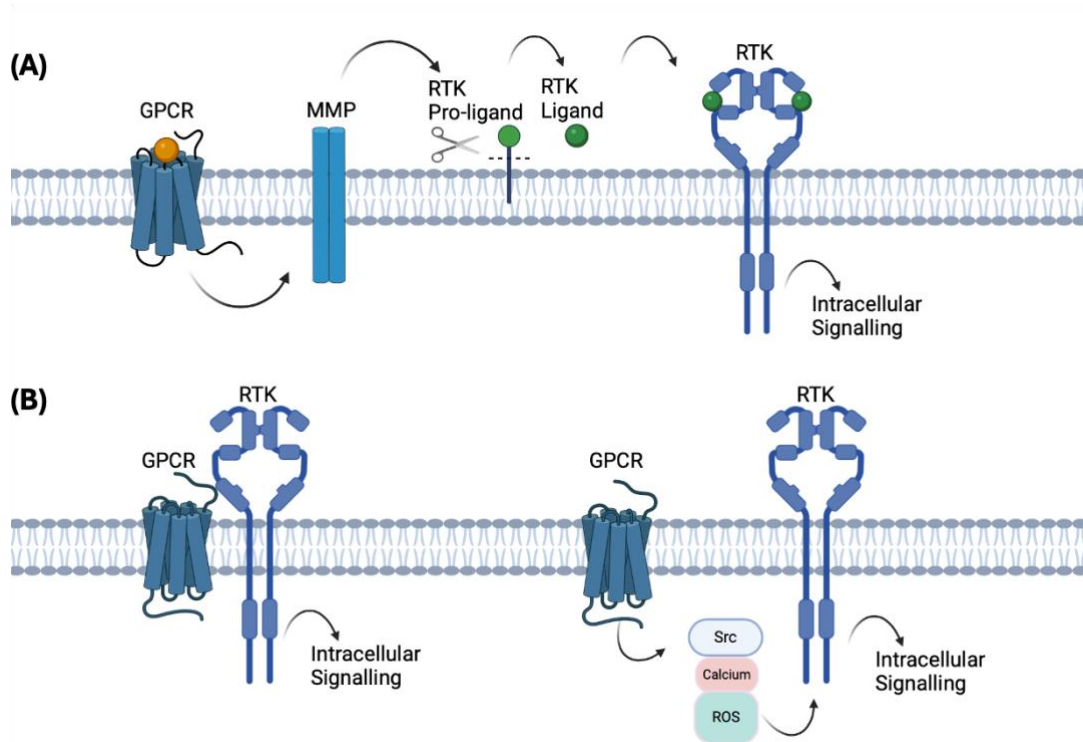


**Figure 1.16 Transactivation of RTKs via ligand-dependent and ligand-independent mechanisms.** (A) As a ligand-dependent mechanism, GPCR ligand binding can lead MMPs to cleave RTK pro-ligands, subsequently activating RTKs. (B) As a ligand-independent mechanism, GPCRs and RTKs can physically form heterocomplexes. GPCRs can also activate RTKs via their recruitment of downstream signalling molecules. Adapted from Liberto et al., 2018). Created with Biorender.

#### 1.14 CXCR4/ EGFR Crosstalk

The significance of CXCR4, ACKR3 or EGFR receptors have been studied separately in various cancers for many years (Neves et al., 2019b) (Shigematsu et al., 2005). The potential for crosstalk interactions between EGFR and CXCR4 has been an interesting question in cancer biology. There have been several studies showing signalling cross-talk between CXCR4 and EGFR using various approaches (Phillips et al., 2005) (Zobair et al., 2013) (Wu et al., 2020a)(Guo et al., 2007a) (Porcile et al., 2004)(Tsai et al., 2015a)(Cabioglu et al., 2007)(Zuo et al., 2017)(Zuo et al., 2017). One of the first approaches to study the relationship between EGFR and CXCR4 was to use specific ligands to activate either receptor in cells where both receptors were expressed (Phillips et al., 2005). EGF treatment increased the expression level of CXCR4 mRNA and/or protein levels in A549 non-small cell lung cancer NSCLC (Phillips et al., 2005)

(Zobair et al., 2013) (J. Wu et al., 2020b) and in SKOV ovarian cancer cells (Guo et al., 2007b). CXCL12 treatment has also been shown to increase EGFR expression levels in A549 cells (Wu et al., 2020b). Apart from the increased expression levels of the receptors, EGF stimulation was able to induce the phosphorylation of CXCR4 at Ser339 in glioblastoma cells (Woerner et al., 2005) and Ser324/325 and Ser330 in the breast cancer T47D cell line (Sosa & Lopez-Haber, 2010). Furthermore, the inhibition of EGFR by the kinase inhibitor AG1478 has been shown to decrease CXCR4 expression in A549 cells (Zobair et al., 2013) and decrease CXCL12 dependent cell proliferation of OC134, a human ovarian cancer cell line (Porcile et al., 2004). Interestingly, the overexpression of CXCR4 has been demonstrated to increase EGFR expression in A549 cells (Zuo et al., 2017). Silencing of EGFR decreased the level of CXCR4 while CXCR4 knockdown decreased EGFR protein levels in MDA-MB-231 breast cancer cells (Li et al., 2017). Interestingly, transactivation of CXCR4 downstream mediators G $\alpha$ i protein activation by EGF and EGFR which requires GIV scaffold protein that links the EGFR G $\alpha$ I leading to EGF-dependent trysoine phosphorylation of G $\alpha$ i have been shown (Neves et al., 2020; Roy et al., 2024).

The alteration of EGFR/CXCR4 expression levels had significant effects on cellular behaviour. Simultaneous silencing of EGFR and CXCR4 led to reduced invasion and migration capacity of breast cancer (Li et al., 2017) and gastric cancer cells (Y. Cheng et al., 2017a). Co-expression of CXCR4 and EGFR is associated with poor prognosis, aggressive phenotype, shorter overall survival and disease-free survival rates in breast cancer (Cabioglu et al., 2007; Li et al., 2017) (Li et al., 2017) pancreatic ductal adenocarcinoma (H. Wu et al., 2015) and non-small cell lung carcinoma (Zobair et al., 2013) patients. Furthermore, breast cancer patients with lymph node metastasis showed co-expression of CXCR4, CCR7 and EGFR expression (Y. Liu et al., 2010).

Another aspect might be specific mutations of EGFR and their effects on EGFR/CXCR4 crosstalk. An EGFR mutation, the Leu858Arg (L858R) substitution, significantly increased the extent of malignant pleural effusions (MPE) in lung adenocarcinoma patients. It has been shown that patients with Leu858Arg (L858R) mutations have higher CXCR4 expression levels (Tsai et al., 2015b). Silencing of CXCR4 resulted in the decreased invasion capacity of lung cancer cells carrying Leu858Arg (L858R) mutation (Tsai et al., 2015b).

Along with EGFR/CXCR4 interaction, EGFR/ACKR3 crosstalk might be a promising candidate to understand RTK/GPCR interactions in cancer. ACKR3 overexpression has been shown to promote EGFR phosphorylation in non-cancerous prostate cells (R. K. Singh & Lokeshwar, 2011). Additionally, ACKR3 silencing decreased the EGFR phosphorylation in prostate cancer (R. K. Singh & Lokeshwar, 2011) and breast cancer cells (Salazar et al., 2014a). Furthermore, the proximity of EGFR and ACKR3 complexes have been shown using coimmunoprecipitation assays in prostate cancer cells (R. K. Singh & Lokeshwar, 2011) and proximity ligation assays in breast cancer cell lines and tissues from patients (Salazar et al., 2014a).

### **1.15 Fluorescent Ligands**

Several tools and approaches have been developed to understand the pharmacology and molecular mechanisms of GPCRs and RTKs. Receptor selective fluorescent ligands are one of them. Fluorescent ligands are useful to monitor expression and function of these receptors and can allow the quantification of receptor-ligand interactions both at endogenous receptor levels and overexpressed receptors (Soave, Briddon, et al., 2020a). Fluorescent ligands consist of a pharmacophore, linked to a fluorophore via a short linker (Stoddart, Kilpatrick, et al., 2015a). The pharmacophore is the functional part of the molecule such as a selective agonist or antagonist for the receptor of interest (Stoddart, Kilpatrick, et al., 2015b). Some of the main classes of fluorophores that have been used to label pharmacophores are from the 4,4-difluoro-4-bora-3a,4a-diaza-s-indacene (BODIPY) series (Allen et al., 2000), AlexaFluor series (Brand et al., 2008) or rhodamine derivatives (Castro et al., 2005). For peptide based fluorescent ligands, amine or thiol reactive fluorophores can be conjugated via lysine or cysteine side chains (Harikumar et al., 2006). Small molecule compounds are conjugated via a linker to separate pharmacophores and fluorophore to provide access of the pharmacophore to the binding site of the receptor and introduce flexibility. It is worth noting that the choice of fluorophore used can change the chemical properties and lipid solubility of the ligand and potentially effect the binding affinity of the pharmacophore to the receptor (Baker et al., 2010a).

### 1.16 Nanobodies

Along with fluorescent ligands, nanobodies have been utilized to understand receptor pharmacology. While conventional human immunoglobulins contain paired heavy and light chains (~150 kDa), it has been found that camelid and shark species have heavy chain only antibodies (HCAbs) (~80 kDa) (Cheloha et al., 2020)(Conrath et al., 2003). The VHHs (variable domain for heavy chain of heavy chain antibody) or nanobodies are single domain antibody fragments (~15 kDa) that contain a variable region to recognize different epitopes (Muyldermans, 2021) (**Figure 1.17**). The advantages of nanobodies are their small size, solubility and higher permeability, stability, amenability to genetic modification to form libraries and ease of labelling for various utilization (Bannas et al., 2017a). They can be utilized to carry a variety of molecules such as small drugs to a selective target (drug conjugates), or RNAs into cells and be used for imaging or therapeutic purposes in cancer or vasculature diseases (Sun et al., 2021) (Jovčevska & Muyldermans, 2020). They have been also used as stabilizers for structural biology studies particularly with GPCRs (Manglik et al., 2017) or to study protein dynamics as conformational sensors that bind to their targets in a conformation-specific way when combined with bioluminescence resonance energy transfer (BRET) or Förster or fluorescence resonance energy transfer (FRET) assays (Nevoltris et al., 2015a) (Dmitriev et al., 2016)(Leemans et al., 2020)(Che et al., 2020)(Galazzo et al., 2020).

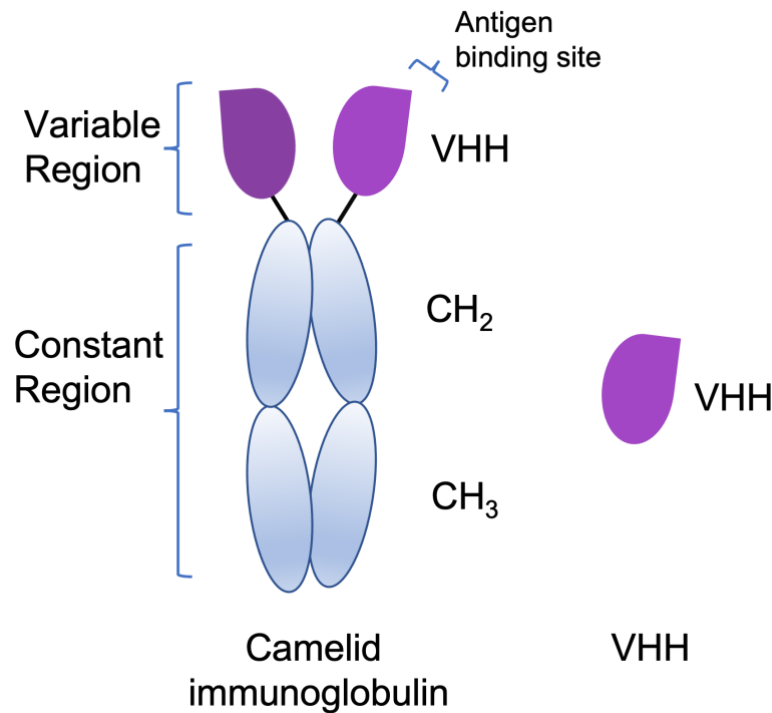


**Figure 1.17 Domains of camelid immunoglobulin and VHH.** VHHs (variable domain for heavy chain of heavy chain antibody) or nanobodies are heavy chain only antibodies consisting of variable region of camelid immunoglobulin.

### 1.17 Hypothesis and aims

Although the significance of CXCR4 and EGFR individually has been shown, the CXCR4/EGFR complex signalling has not been elucidated. Interestingly, CXCR4/EGFR might signal differently than its subcomponents. Hence EGFR/CXCR4 complex can be a novel therapeutic target for cancer therapy. Therefore, we hypothesized that CXCR4 and EGFR can form dimers and most probably it influences the behaviour of several types of cancer cells. Nevertheless, it is not easy to hypothesize if CXCR4/EGFR complexes play cancer inducing role like receptor homodimers or act as an inhibitory factor for cancer cells. Regardless, it is an important phenomenon to understand for long-term future aim to continue to utilise targeted cancer therapy for CXCR4 and EGFR with various tools such as antibodies and small molecule inhibitors.

In the light of these, we specifically aimed these for this thesis:

1. To characterize the binding properties of labelled and unlabelled novel compounds for CXCR4 and ACKR3. To this aim, NanoBRET at NanoLuc-tagged receptors was used.
2. To gain insight into the binding properties of various EGFR ligands and nanobodies (specially Q44 and Q86). To this aim, NanoBRET was used at NanoLuc-tagged EGFR stably transfected in HEK293 cells.
3. To characterize protein-protein interactions between CXCR4/EGFR and the influence of various receptor selective ligands and nanobodies on these dimer complexes. To this aim, NanoBRET and PLA were used in HEK293 and HeLa cells.

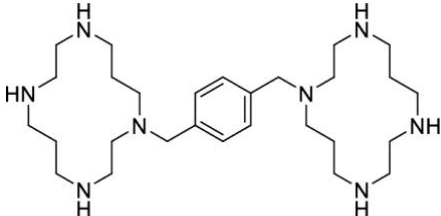
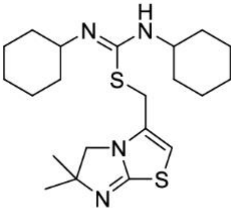
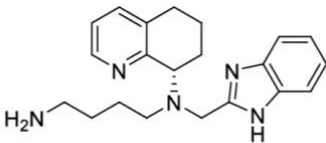
# Chapter 2: Materials and Methods

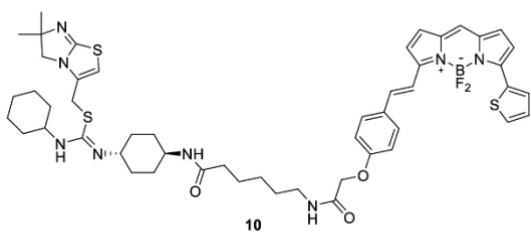
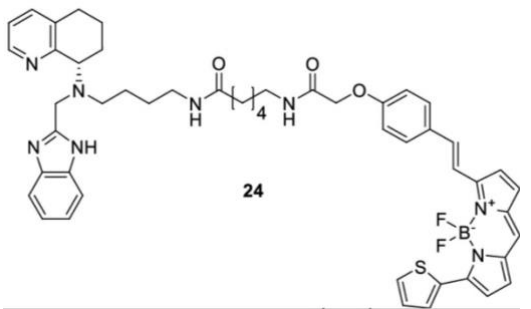
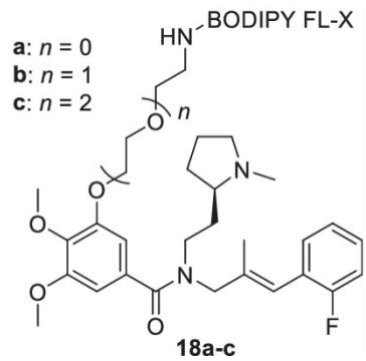
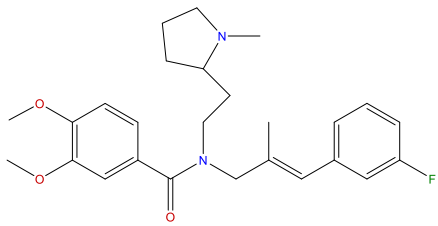
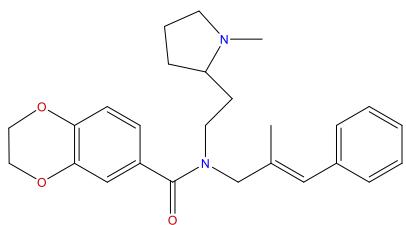
## 2.1 Materials

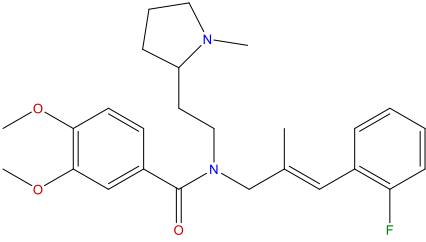
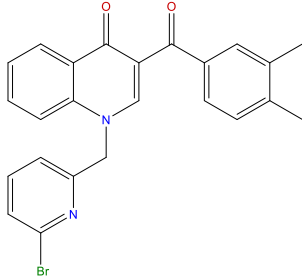
CXCL12-488 (Oregon Green® 488 on penultimate lysine) and CXCL12-647 (AlexaFluor® 647) (CAF-11) were obtained from ALMAC (Edinburgh, UK). Unlabelled chemokine ligands CXCL12 (300-28A) was from PeproTech (London, UK), AMD3100 (239820) from Sigma Aldrich (Gillingham, UK), IT1t (4596) from Tocris Bioscience (Bristol, UK) and AMD070 (Mavorixafor trihydrochloride) (HY-50101A) was from MedChemExpress (New Jersey, USA). Epidermal Growth Factor biotinylated complexed to AlexaFluor 488® streptavidin (E13345) or AlexaFluor 647® streptavidin (E35351) were obtained from Thermo Fischer Scientific (Waltham, USA). Human recombinant TGF- $\alpha$  (239-A-100), human recombinant amphiregulin (262-AR-100), human recombinant betacellulin (261-CE-010), human recombinant epiregulin (1195-EP-025), human recombinant epigen (6629-EP-025), human recombinant EGF (236-EG-200) were purchased from R&D Systems (Minnesota, USA) and heparin-binding EGF-like growth factor (E4643) was purchased from Sigma Aldrich (Gillingham, UK), erlotinib (A3397) was purchased from ApexBio (Houston, USA). Novel ACKR3 fluorescent compounds (18a, 18b, 18c) were synthesised by Dr Sebastian Dekkers and Professor Michael Stocks the School of Pharmacy, University of Nottingham. Novel CXCR4 fluorescent compounds 11 and 24 were synthesised by Dr Sebastian Dekkers at the School of Pharmacy, University of Nottingham (Dekkers et al., 2024). Novel unlabelled ACKR3 compounds VUF11072 (20), VUF11074 (19), VUF11403(9) and VUF16545(4) were synthesised and provided by Professor Dr Rob Leurs from the Division of Medicinal Chemistry, Vrije Universiteit Amsterdam (Dekkers et al., 2024). Fluorescently labelled or unlabelled EGFR and CXCR4 nanobodies Q44c, Q44c-HL488, Q86c, Q86c-HL488, VUN400c, VUN401, VUN415c, containing an unpaired or fluorescent label paired cysteine in the C-terminal tag, were provided by QVQ (Utrecht, The Netherlands). Purified LgBiT (N3030), FuGENE HD Transfection Reagent (E2311) and furimazine (N1110) were purchased from Promega Corporation (Southampton, UK). Opti-MEM reduced serum medium (31985062) was purchased from (Gibco, Thermo Fisher, MA, USA). Fetal bovine serum (F7524) was purchased from Sigma Aldrich (Gillingham, UK). HaloTag ligand AlexaFluor® 488 (G1002) was purchased from Promega Corporation (Southampton, UK), and SNAP-Surface-AlexaFluor488® (S9129S) was obtained from New England BioLabs (Ipswich, USA). All tissue culture

plasticware was purchased from Fischer Scientific (Loughborough, UK). Unless otherwise stated, all cell culture reagents and media were purchased from Sigma-Aldrich, (Gillingham, Dorset, UK). 96-well, F-Bottom, white cell culture microplate (655983) was purchased from Greiner Bio-One GmbH (Frickenhausen, Germany). Cellview glass bottom cell culture dish (627860) was purchased from Greiner Bio-One GmbH (Frickenhausen, Germany). The chemicals used for Hank's Balanced Salt Solution (HBSS) preparation were purchased from ; HEPES (H3375) Sigma Aldrich (Gillingham, UK), potassium chloride (101985M) BDH Laboratory Supplies (Poole, UK), magnesium sulfate heptahydrate (M1880) Sigma Aldrich (Gillingham, UK), calcium chloride 2-hydrate (C-2661) Sigma Aldrich (Gillingham, UK), sodium bicarbonate (S7277) Sigma Aldrich (Gillingham, UK), sodium pyruvate (P5280) Sigma Aldrich (Gillingham, UK) and sodium chloride (S9625) Honeywell (North Caroline, USA) .

**Table 2.1 The CXCR4 and ACKR3 compounds used in this thesis and their chemical structures.**

Compound	Chemical Structure
AMD3100 (Sigma Aldrich, Gillingham, UK)	
IT1t (Tocris Bioscience, Bristol, UK)	
AMD070 (Mavorixafor) (MedChemExpress, New Jersey, USA)	

<p>Compound 10 (IT1t derivative)</p> <p>(Provided by Dr Sebastian Dekkers and Prof Michael Stocks, University of Nottingham)</p>	 <p>Chemical structure of Compound 10, an IT1t derivative. It features a central cyclohexane ring with a thiazolidine ring and a sulfonamide group attached. The sulfonamide group is linked to a long chain containing a secondary amide, a primary amide, and a carboxylic acid group. The chain ends with a complex boron-containing heterocyclic system.</p>
<p>Compound 24 (AMD070 derivative)</p> <p>(Provided by Dr Sebastian Dekkers and Prof Michael Stocks, University of Nottingham)</p>	 <p>Chemical structure of Compound 24, an AMD070 derivative. It consists of a central chain with a secondary amide, a primary amide, and a carboxylic acid group. The chain is substituted with a quinoline ring system and a complex boron-containing heterocyclic system.</p>
<p>Compounds 18a-c (VUF11207 derivative)</p> <p>(designed by Dr Maikel Wijtmans).</p>	 <p>Chemical structure of Compounds 18a-c, VUF11207 derivatives. The structure shows a central core with a methoxy group, a methyl group, and a fluorine atom. The core is linked to a chain containing a secondary amide, a primary amide, and a carboxylic acid group. The chain is substituted with a BODIPY FL-X fluorophore and a complex boron-containing heterocyclic system. The variable <math>n</math> is defined as:</p> <ul style="list-style-type: none"><li>a: <math>n = 0</math></li><li>b: <math>n = 1</math></li><li>c: <math>n = 2</math></li></ul>
<p>20 (VUF11072)</p> <p>(Provided by Prof Rob Leurs, Vrije Universiteit Amsterdam)</p>	 <p>Chemical structure of Compound 20, VUF11072. It features a central core with a methoxy group and a fluorine atom. The core is linked to a chain containing a secondary amide, a primary amide, and a carboxylic acid group. The chain is substituted with a complex boron-containing heterocyclic system.</p>
<p>19 (VUF11074)</p> <p>(Provided by Prof Rob Leurs, Vrije Universiteit Amsterdam)</p>	 <p>Chemical structure of Compound 19, VUF11074. It features a central core with a methoxy group and a fluorine atom. The core is linked to a chain containing a secondary amide, a primary amide, and a carboxylic acid group. The chain is substituted with a complex boron-containing heterocyclic system.</p>

<p>9 (VUF11403) (Provided by Prof Rob Leurs, Vrije Universiteit Amsterdam)</p>	
<p>4 (VUF16545 (GD325)) (Provided by Prof Rob Leurs, Vrije Universiteit Amsterdam)</p>	

## 2.2 Vectors and cloning

**Table 2.2 The table of DNA constructs and their parent vectors used.**

Construct	Parent Plasmid
NLuc_CXCR4	pcDNA3.1/Neo
NLuc_ACKR3	pcDNA3.1/Neo
SNAPTag_CXCR4	pcDNA3.1/Neo
HiBiT_CXCR4	pcDNA3.1/Neo
SNAPTag_A1	pcDNA3.1/Neo
SNAPTag_A3	pcDNA3.1/Neo
NLuc_EGFR	pNKF1-secN CMV
HiBiT_EGFR	pNKF1-secN CMV
HaloTag_EGFR	pNKF1-secN CMV

pcDNA3.1(+) plasmids containing antibiotic resistance cassettes for ampicillin (bacterial) and neomycin (mammalian) and encoding N terminal tagged NLuc\_CXCR4, SNAPTag\_CXCR4, HiBiT\_CXCR4 or NLuc\_ACKR3 were made by Dr Birgit Caspar, during her PhD studentship at the University of Nottingham (Caspar, 2018). CXCR4 and ACKR3 cDNA was obtained from Professor Martine Smit's lab at Vrije University of Amsterdam. TOP10F Chemically Competent *E. Coli* cells (Invitrogen, Waltham, USA) were used for transformations. Plasmids encoding N terminal SNAPTag adenosine receptor subtype 1 (A<sub>1</sub>) or adenosine receptor subtype 3 (A<sub>3</sub>) cDNA were made by Dr Mark Soave.

Dr Birgit Caspar amplified CXCR4 and ACKR3 cDNA sequences via a polymerase chain reaction. She cloned SNAPTag or Nanoluciferase cDNA sequence from the previously generated pcDNA3.1 (Invitrogen, Waltham, USA) or pcDNA3.1 with NLuc (Promega, Southampton, UK) or SNAP tags (New England BioLabs, Ipswich, USA). All the CXCR4, ACKR3, A<sub>1</sub> or A<sub>3</sub> plasmids contained a rat 5-HT<sub>3</sub> receptor signal sequence (amino acids MRLCIPQVLLALFLSMLTGPGEGRK) upstream of the N terminal NLuc or SnapTag sequence and GS linker to facilitate surface expression of tagged receptors. They all contain ampicillin resistance gene for selection (**Figure 2.1** and **Figure 2.2**).

cDNA encoding N terminal fusions of EGFR to NLuc, HiBiT or HaloTag were a kind gift from Promega Corporation, with the EGFR ORF obtained initially from the Kazusa DNA Research Institute (Kisarazu, Japan). NLuc\_EGFR lacking its native signal sequence peptide was cloned into a pNKF1-secN CMV vector fusing the signal peptide sequence of IL-6 onto the N terminus of NLuc and a GSSGIAI linker between NLuc and EGFR. For N-terminal HiBiT tagged constructs, HiBiT (VSGWRLFKKIS) was inserted after the IL6 signal peptide and fused to EGFR using a GSSGGGGSGGGGSSGAIA linker (termed HiBiT\_EGFR). For the N-terminal HaloTag EGFR construct, the HaloTag sequence was inserted after the EGFR natural signal peptide and fused to EGFR using a linker GSSGGGGSGGGGSSGAIA (termed HaloTag\_EGFR). They all contain neomycin/kanamycin resistance gene for selection (**Figure 2.3**). The signalling peptide sequences are cleaved off during membrane translocation.

---

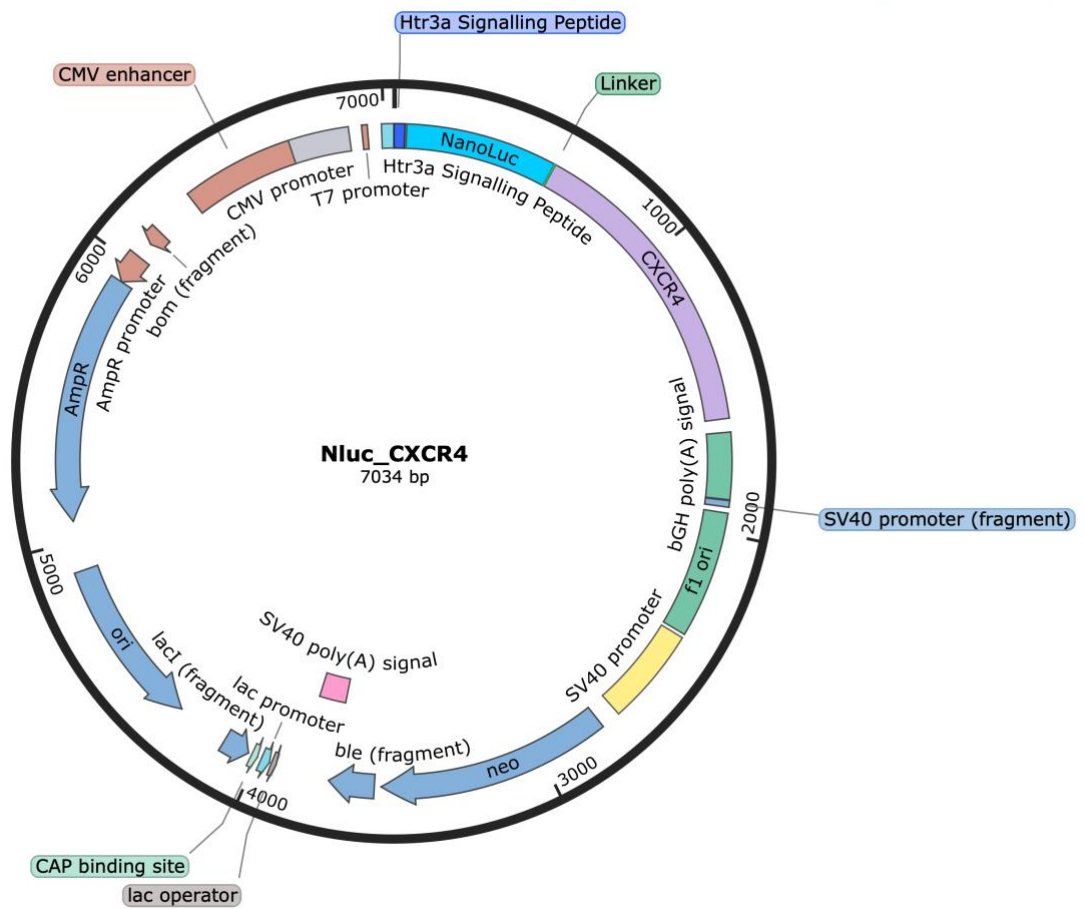


**Figure 2.1** Vector map of NLuc\_CXCR4 (pcDNA3.1). (Figure generated using SnapGene Viewer 7.0.3)

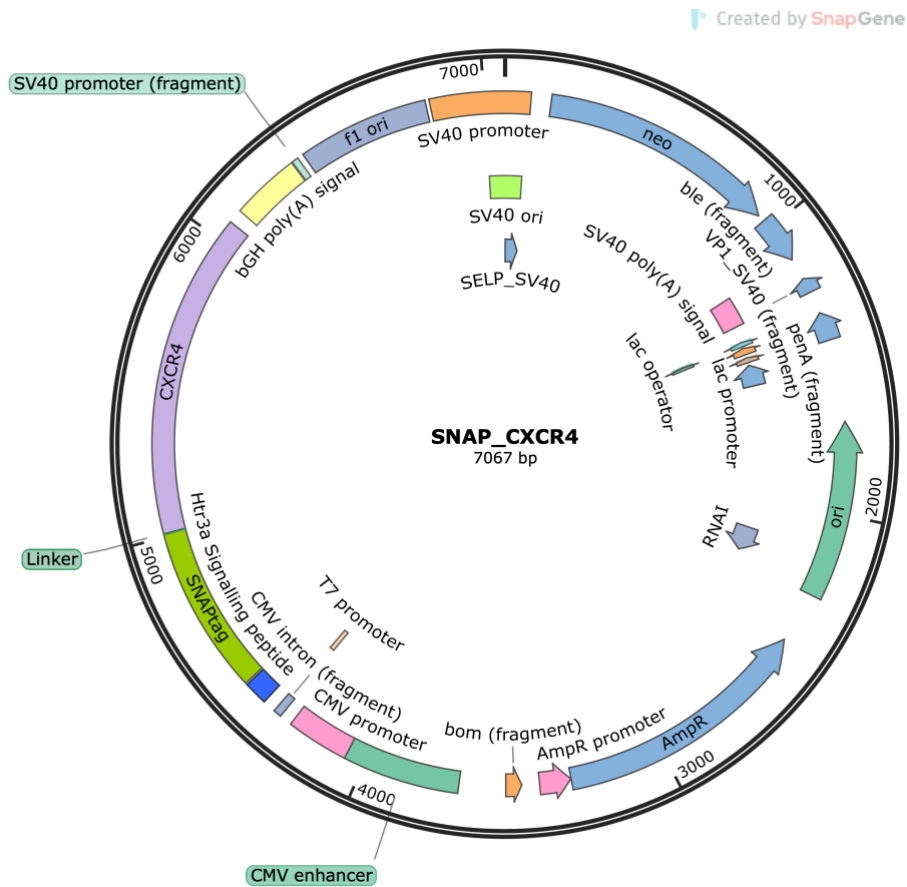


**Figure 2.2** Vector map of SNAPTag\_CXCR4 (pcDNA3.1). (Figure generated using SnapGene Viewer 7.0.3)

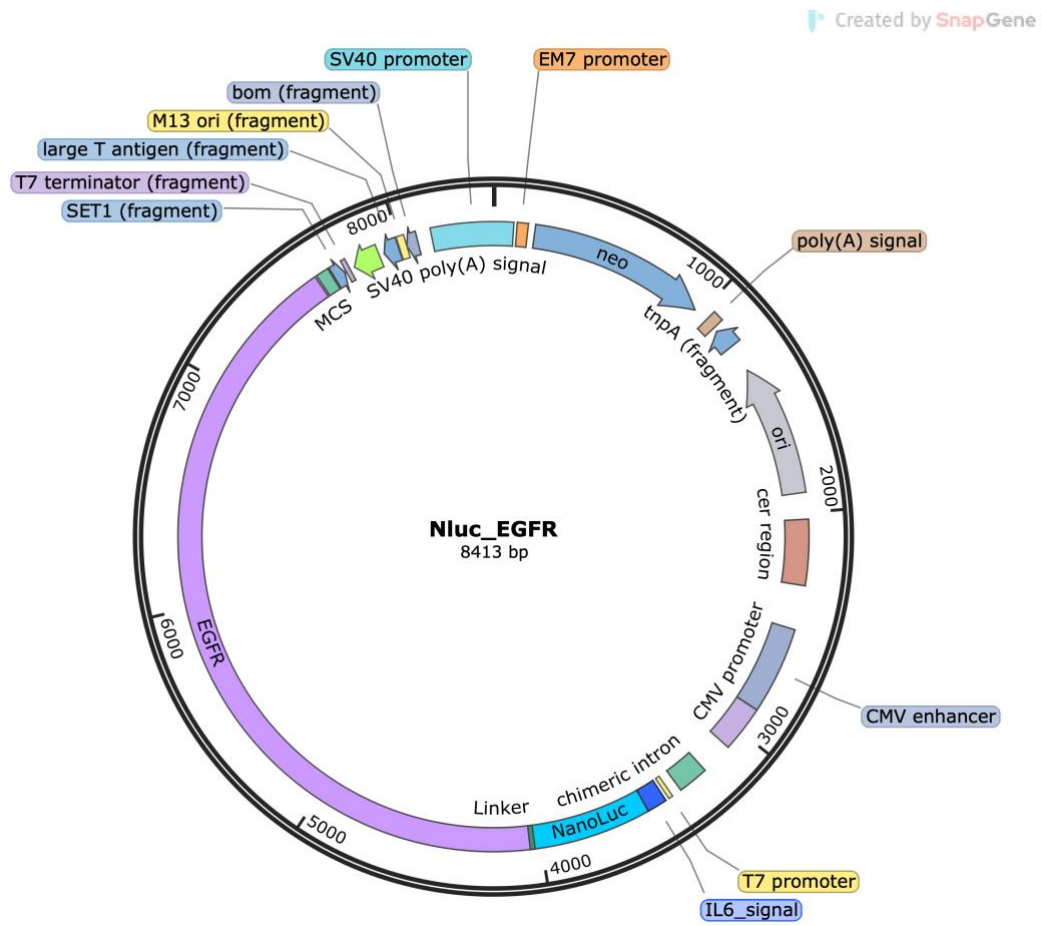


**Figure 2.3** Vector map of NLuc\_EGFR. (Figure generated using SnapGene Viewer 7.0.3)

### 2.3 Luria Broth with agar plate preparation

Thirty-five grams of Luria Broth with agar (Lennox) (L2897-1KG) from Sigma Aldrich (Gillingham, UK) was added to 1 litre of Milli Q water. After autoclaving and cooling to a hand-hot temperature, ampicillin (100 µg/ml) or kanamycin (30 µg/ml) were added and agar poured into the petri dishes (approximately 20ml per plate). Once the agar had set, plates were stored for up to one month in the fridge at 4°C until needed.

### 2.4 Transformation of the competent bacteria cells

DH5α (18265017; Invitrogen) or One Shot® TOP10F chemically competent (C303003; Invitrogen) *Escherichia coli* bacteria strains and cDNA samples were defrosted on ice. 17 µl of competent bacteria and 1 or 2 µl (approximately 100 ng) of cDNA samples, depending on their stock concentrations, were added to 1.5ml Eppendorf tubes, mixed and left on ice for 30 minutes. Cells were heat shocked for 30 seconds at 42°C and then returned to ice for 3 minutes. 250 µl of LB broth ([see 2.5](#)) for DH5α cells or Super Optimal broth with Catabolite repression (S.O.C) media for TOP10F cells was added on each tube and flicked gently. Tubes were placed on a shaker at 225 rpm at 37°C for an hour. After one hour of incubation, 50 µl of LB broth and 50 µl of transformed bacteria culture were mixed and spread on pre-warmed LB agar plates ([see 2.3](#)) with appropriate resistance antibiotic. After a few minutes, the agar plates were placed agar side up (to avoid water contamination caused by moisture) in a hotbox set to 37°C. The next day, colonies that were picked with the help of a pipette tip by scraping, and bacteria cultures were started in either 5 ml or 200 ml of LB broth with the appropriate resistance antibiotic. Cultures were shaken overnight at 225 rpm at 37°C.

## 2.5 Luria broth preparation

Twenty grams of Luria Broth (Lennox) (L3022-1KG; Sigma Aldrich, Gillingham, UK) was added to 1 litre of Milli Q water in glass bottles. After autoclaving and subsequent cooling of the broth, ampicillin (100 µg/ml) or kanamycin (30 µg/ml) antibiotics were added. The bacteria colonies that were picked up from LB agar plates were added to the prepared LB broth to start and grow bacteria cultures.

## 2.6 Maxiprep DNA purification

After growing the bacteria culture overnight in 200 ml of LB broth, the cultures were centrifuged at 3,400 x g for 10 minutes at 4 °C and the pellets were stored in -20 °C. At the day of plasmid purification, the pellets were thawed on ice. A ZymoPURE™ II Plasmid Maxiprep Kit (Zymo Research; (D4203) California, US) was used to purify plasmids. The pellet was resuspended in 14 ml of resuspension buffer and vortexed. Next, 14 ml of lysis buffer was added to lyse bacterial cells, and the tubes were gently inverted six times and incubated at room temperature for 2-3 minutes. 14 ml of neutralisation buffer was added, and the tubes were gently inverted five more times. The lysate was transferred to ZymoPURE™ Syringe Filter-X and left for 5-8 minutes to allow filtration of the precipitation. Luer Lock plug from the bottom of the syringe was removed and the filter was placed into a clean 50 ml conical tube. The solution was pushed through the filter. 14 ml of binding buffer was added on it. Using a vacuum pump manifold (Vac-Man, A7231; Promega Corporation, USA), the filter was washed two times with 10 ml of washing solutions. The column was placed in a collection tube and centrifuged at 16,000 x g for 1 minute to remove any residual wash buffer. The column was transferred to a new 1,5 ml collection tube, and 400 µl of elution buffer was added. After 2 minutes, the collection tube was centrifuged at 16,000 x g for 1 minute. The entire eluate was added to EndoZero™ Spin-Column and centrifuged for another 1 minute at 10,000 x g to remove residual endotoxins. Purified plasmid absorbance was measured via DS-11 FX+ spectrometer/fluorometer (DeNovix, Wilmington, DE, USA). The maxiprep procedure typically resulted in an approximate yield of 350 µl DNA preparation with a 500-1500 ng/µl DNA concentration and a 260/280 absorbance ratio of 1.8-1.9. The samples having 260/280 absorbance ratio is between 1.8-2.0 is accepted pure for dsDNA. The 260 nm

absorbance is specific for double bonds between purine and pyrimidine rings of double strand DNA. The samples having absorbance below 1.6 accepted as contaminated with proteins or phenol since they absorb at 280 nm. All purified DNA was stored at -20°C.

## 2.7 DNA Sequencing

For plasmid sequencing, Sanger sequencing (Next Generation Sequencing Facility, D Floor, School of Life Sciences, University of Nottingham) was performed using 100 ng/μl DNA and T7 forward primer and a BGH reverse primer were used for CXCR4 and ACKR3 constructs in pcDNA3.1. Sixteen primers were used for EGFR constructs in NaLuc, HiBiT and HaloTag plasmids to sequence the whole EGFR DNA sequence (see Appendix). Along with Sanger sequencing, whole plasmid DNA sequencing service via Oxford Nanopore Technologies was performed by Plasmidsaurus (Oregon, United States).

## 2.8 Cell Culture

Human embryonic kidney (HEK) 293 cells are an immortalised well-characterised model cell line used in biological research due to their easy cell culture maintenance, short division time and high transfection efficiency and expression of recombinant proteins (Thomas & Smart, 2005). They were created by Graham et al. via the transformation of human embryonic kidney cells with adenovirus type 5 DNA (Graham et al., 1977). The HEK293T cell line was developed as a derivative of HEK293 cells via stable expression of SV40 large T-antigen (Dubridge et al., 1987). This derivative gave further improvements to plasmid transfection efficiency and recombinant protein expression. HEK293-GloSensor™ (termed HEK293G cells) are HEK293 cells stably transfected with the pGloSensor™-20F cAMP plasmid by Promega Corporation, Southampton, UK. HEK293T wild-type cells or HEK293-GloSensor™ cells stably expressing NLuc\_CXCR4, NLuc\_ACKR3 or NLuc\_EGFR tagged at their respective N termini with Nanoluciferase (NLuc) were cultured in Dulbecco's Modified Eagle's Medium-high glucose (DMEM; D6429, Sigma Aldrich, Gillingham, UK) supplemented with 10% Fetal Calf Serum (FCS) at 37°C/5% CO<sub>2</sub>.

### **2.8.1 Freezing of cells**

Cells were passaged as described above; however, following centrifugation, they were resuspended in 1 ml of complete DMEM/10% FCS containing cell culture grade 10% DMSO Dimethyl Sulfoxide (DMSO). DMSO prevents the crystallisation of the cells during the freezing process. Cell aliquots were added to cryogenic storage vials. They were put in Mr. Frosty™ containers for 24 hours at -80°C to avoid cell death due to crystallization during cell freezing. Mr. Frosty™ provides a slow freezing process via decreasing the temperature 1°C/minute. After 24 hours, cryovials were moved into liquid nitrogen for long-term cryopreservation of the cells (liquid or vapour phase).

### **2.8.2 Thawing of cells**

Cells stored in 1.5ml cryovials long-term in liquid nitrogen were thawed at room temperature. They were added to 5 ml of DMEM and resuspended. They were centrifuged at 1000 rpm for 4 minutes, and the resultant pellet was resuspended in 1 ml of DMEM and cultured in a T75 cell culture flask containing 20 ml of DMEM with 10% FCS.

### **2.8.3 Passaging of cells**

After cell confluency reached at 70%, culture media DMEM was aspirated and 5 ml of 1x Phosphate Buffered Saline (PBS) (Sigma Aldrich, Gillingham, UK) was added on flask. After washing the cells with PBS, PBS was aspirated from the flask, and 1 ml of trypsin/EDTA (0.5 g/l trypsin, 0.2 g/l EDTA) was added for 3-4 minutes to detach the cells. 5 ml of DMEM was added, and cells were transferred to a 30 ml universal tube and centrifuged at 1000 rpm for 4 minutes. After centrifugation, the supernatant was poured off, and the cell pellet was resuspended in 5 ml of DMEM/10% FCS. Cells were transferred into a T75 cell culture flask containing 20 ml of DMEM/10% FCS, typically at a split ratio of 1:5.

### 2.8.4 Cell seeding for NanoBRET assays

#### *96 well plate format*

For NanoBRET experiments, 96 well flat bottom,  $\mu$ CLEAR® white CELLSTAR® TC plates (Greiner Bio-One 655098, Stonehouse, UK) were coated with sterile poly-D-lysine (Sigma Aldrich, Gillingham, UK) at 10 ng/ml concentration in 50  $\mu$ l volume per well for 30 minutes at room temperature. After coating, each well was washed with 1x PBS once and stored at room temperature until use. The media from the T75 flasks were aspirated, and cells were washed with 1x PBS. Cells were trypsinised and centrifuged as described ([see 2.8.3](#)) After centrifugation, the supernatant was aspirated, and the cell pellet was resuspended in 5 ml of DMEM/10% FCS. Cells were then counted using a haemocytometer, resuspended in DMEM/10% FCS to the desired number of cells and seeded onto the poly-D-lysine coated 96-well plates at 40,000 cells/well (day 1) for experiments performed on the next day (day 2). Alternatively, if cells were to be transfected, cells were plated at 15,000 cells/well (day 1), transfected the next day (day 2) and the experiment performed on day 3. Cells were left to grow overnight at 37°C/5% CO<sub>2</sub>.

#### *Six well plate format*

Cells were trypsinised and centrifuged as described at ([2.8.3](#)). After centrifugation, the supernatant was aspirated, and the cell pellet was resuspended in 5 ml of DMEM/10% FCS. Cells were then counted using a haemocytometer, resuspended in DMEM/10% FCS to the desired number of cells per ml and seeded in a 6-well plate at 1 million cells per well. The following day, cells were transfected ([see 2.9](#)) with a plasmid of interest and incubated overnight at 37°C/5% CO<sub>2</sub>. The following day, cells were trypsinised, resuspended, counted, and seeded in 96-well plates for NanoBRET experiments as described as above.

## **2.9 Transfection of HEK293 cells with Fugene HD**

HEK293T cells were transfected a day before the experiments according to the FuGENE HD Transfection Reagent (E2311) protocol provided by the manufacturer (Promega Corporation). The cDNA of interest and transfection mix was prepared in Opti-MEM reduced serum medium (31985062) purchased from (Gibco, Thermo Fisher, MA, USA) and incubated for 10 minutes as the protocol suggested. Transfection mix was added to cells plated in either a 96-well- or 6-well plates in a 3:1 ratio of DNA: FuGENE HD in DMEM containing 10% FCS. Cells were left to grow for 16 hours.

## **2.10 Membrane preparation from stably transfected HEK293 cells**

HEK293T cells stably expressing NLuc\_EGFR or NLuc\_CXCR4 were grown to 70–80% confluency in T175 flasks. Cells were washed with 1x PBS. They were scraped in 15 mL of PBS using a cell scraper. The cell suspension was transferred into a 50-mL tube and centrifuged at 378 x g for 10 min at 4 °C after centrifugation, the supernatant was aspirated, and the pellet was kept at 80 °C. On the day of membrane preparation, pellets were thawed and resuspended in 15 mL of 1x PBS and homogenised using an electronic handheld IKA T10 Ultra Turrax homogeniser in 10 times 3 seconds burst at 15,000 rpm. Unbroken cells and nuclei were removed by centrifugation at 1,500 g for 20 min at 4 °C. The supernatant was centrifuged at 41,415 x g for 30 min at 4 °C. The pellet was resuspended in 2 mL of ice-cold PBS and, transferred to a borosilicate glass homogeniser mortar and homogenised 15 times using an IKA RW16 overhead stirrer attached to a serrated pestle (Kartell) at 1,000 rpm. Protein concentrations were obtained using a BCA assay (Pierce™ BCA Protein Assay, Thermo Fisher Scientific) and absorbance values were measured using a Dynex Technologies 4.25 plate reader. Membranes were stored at 80 °C until use in NanoBRET assays.

### **2.11 Clonal selection of stably transfected cell lines (dilution cloning)**

Stably transfected clonal Human embryonic kidney 293 (HEK293)-GloSensor™ (Promega, Southampton, UK) cells expressing NLuc\_CXCR4 and NLuc\_ACKR3 (constructs map provided above) cells were generated by Dr. Birgit Caspar (Cell Signalling Lab, University of Nottingham). For this HEK293-GloSensor™ cells were transfected using FuGENE® HD reagent (Promega Corporation, Southampton, UK) and transfected cells were selected using 1 mg/ml geneticin (G418) 24 hours after transfection. The complete DMEM media containing G418 was changed every two days. After the cell death reached the plateau phase, the concentration of geneticin was decreased to 0.5 mg/ml. Cells were grown until they reached their confluency, and then they were diluted for clonal selection. Cells were trypsinised, counted and diluted to give cell numbers of 4 and 40 cells per 100 µl in 96-well plates. Colonies started to form in approximately 2-3 weeks. Cells were checked for single colonies, which were grown to 50% confluency, and then transferred to 24-well plates and later 25 cm<sup>2</sup> flasks. The clonally selected cells were screened for selection (luminescence indicative of NanoLuciferase expression) and frozen until further use ([see 2.8.1](#))

### **2.12 Preparation of Hank's Balanced Solution (HBSS)**

10x HBSS was prepared according to the following recipe and with final molar concentrations of ingredients (20 mM of sodium pyruvate, 1450 mM of NaCl, 50 mM of KCl, 10 mM of MgSO<sub>4</sub>, 100 mM of HEPES, 13 mM of CaCl<sub>2</sub>, 15 mM NaHCO<sub>3</sub>) dissolved in 900 ml of ddH<sub>2</sub>O. The pH of the 10x solution was adjusted to 7.45, and the solution diluted to 1 litre using ddH<sub>2</sub>O. After autoclaving, a working solution of 1x HBSS was made by diluting the 10x HBSS to 1x HBSS and adding D-glucose at a final concentration of 10 mM. Before each experiment, 0.1 % or 0.2% bovine serum albumin (BSA) was added (Sigma Aldrich, Gillingham, UK) to the 1x HBSS solution in 20 ml or 50 ml universal tubes and then warmed up to 37°C in the absence of CO<sub>2</sub>.

### 2.13 Nanoluciferase bioluminescence resonance energy transfer (NanoBRET) Assays

Bioluminescence Resonance Energy Transfer (BRET) is a technique based on energy transfer from a bioluminescent donor molecule to a fluorescent acceptor that is dependent on close proximity (within 10 nm) of the bioluminescent and fluorescent tags (Stoddart, Johnstone, et al., 2015). Nanoluciferase (NLuc) is a bioluminescent enzyme engineered from the deep-sea shrimp *Oplophorus gracilirostris* (Dixon et al., 2016). It is substantially smaller than *Renilla* luciferase (19 vs 38kDa) and is 150- fold brighter (Machleidt et al., 2015). NLuc oxidises its substrate (furimazine) which produces a bioluminescence signal which can be measured by appropriate detecting devices (Hall et al., 2012). The efficient spectral overlap between the donor emission and excitation wavelength of the acceptor fluorophore/fluorescent protein used is essential for NanoBRET (Stoddart et al., 2016) (**Figure 2.4**). The NanoBRET technique can determine protein-protein interactions such as GPCR-GPCR or GPCR-RTK or ligand-receptor interactions in live cells and isolated membranes to understand their binding kinetics, affinity and allosteric regulation as well as interactions of these receptors with their downstream regulations (Stoddart et al., 2018). To study the binding of fluorescently labelled ligands, receptors of interest can be tagged with Nanoluciferase on their extracellular termini to allow binding of a fluorescent ligand to be monitored using NanoBRET. NanoBRET can be used to perform ligand saturation binding assays, competition binding assays or ligand binding kinetic assays in live cells to monitor real-time molecular interactions (**Figure 2.5**). (Stoddart et al., 2018) Additionally, NanoBRET can be used to detect protein-protein interactions (Kilpatrick et al., 2019). To study the receptor-receptor interactions, one receptor can be tagged with NanoLuciferase enzyme (donor) and a second receptor with a fluorophore or fluorescent protein for resonance energy transfer. Close proximity (<10 nm) of the two receptors leads to energy transfer between donor and receptor and produces a BRET signal (Kilpatrick et al., 2019) (**Figure 2.6**).

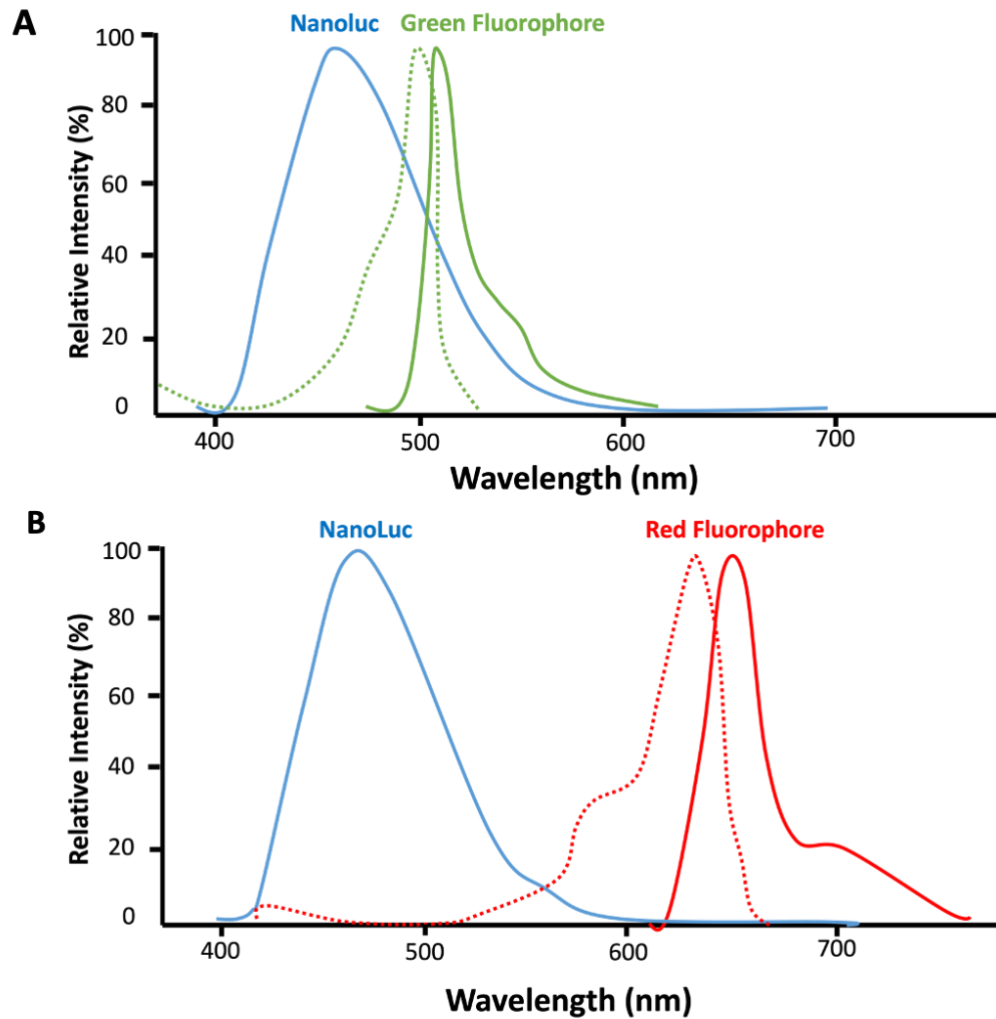


**Figure 2.4** Schematic of the overlap between the spectral wavelength of NLuc and the excitation and emission spectra of fluorophores typically used in bioluminescence resonance energy transfer (BRET). The wavelengths overlap between NLuc emission (blue line) and excitation (broken line) and emission (solid line) of A-) green-shifted acceptor (BODIPY-FL-X) and B-) red-shifted BRET (BODIPY 630/650) acceptor fluorophores. Adapted from (Stoddart et al., 2018).

### 2.14 NanoBRET Ligand Binding Assay

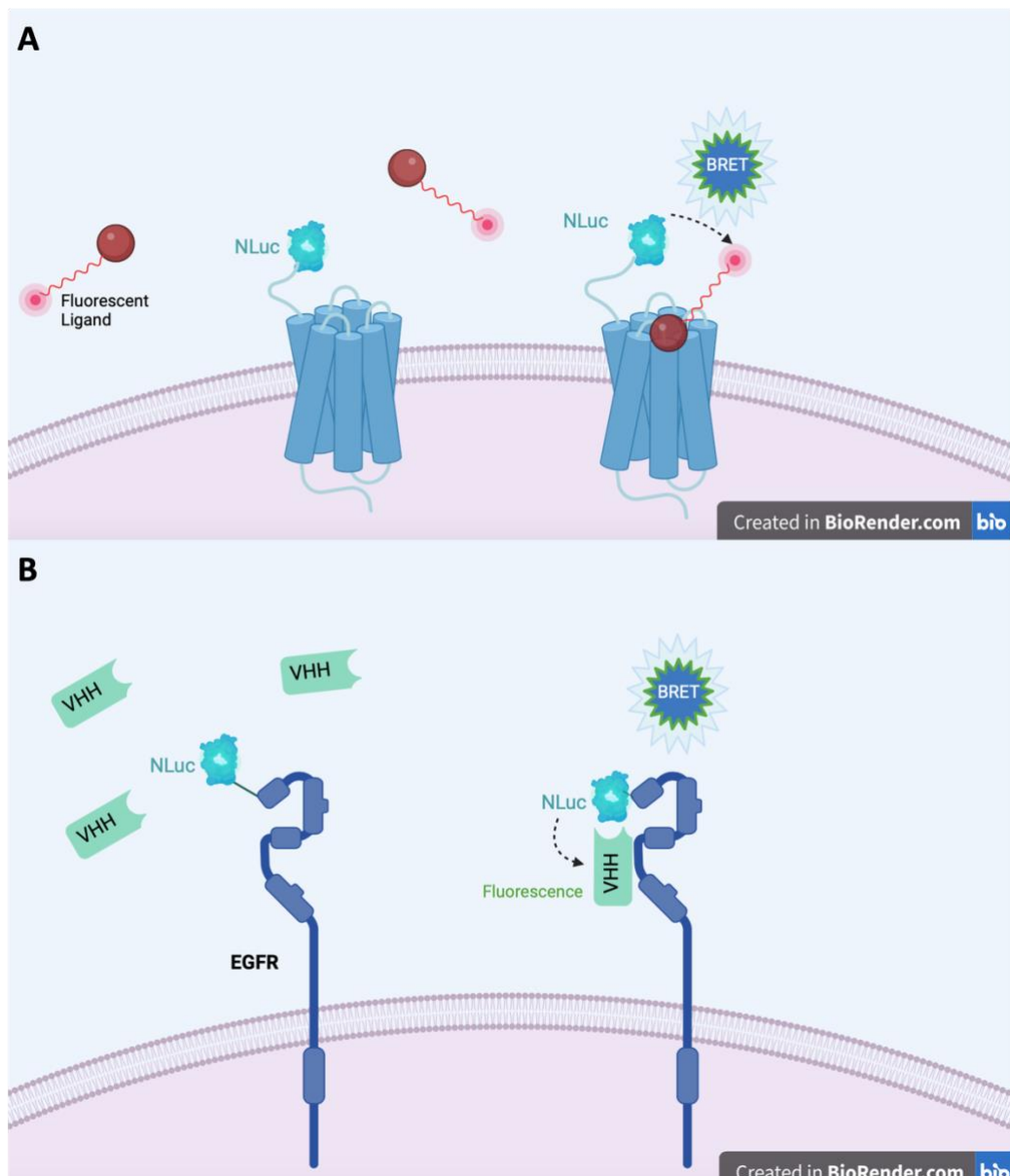


**Figure 2.5 The mechanism of NanoBRET ligand/nanobody binding assay.** Schematic representation of a NLuc binding assay using fluorescently labelled ligands and nanobodies and NLuc tagged A-) G-protein coupled receptors (CXCR4/ACKR3) and B-) tyrosine kinase receptor (EGFR) (Figure was created with BioRender).

To study the binding of fluorescently labelled ligands, receptors of interest are tagged with NLuc on their extracellular N-terminus to allow the binding of a fluorescent ligand/nanobody to be monitored using NanoBRET. In presence of NLuc's substrate furimazine, resonance energy transfer occurs if the fluorescent ligand/nanobody is

within sufficient proximity (less than 10nm). This leads the emitted light cause excitation of the fluorophore of the fluorescent ligand/nanobody, which then emits its own fluorescence (**Figure 2.5**). Both fluorescence and luminescence emissions can be detected simultaneously using appropriate instrumentation (eg. a BMG PheraStar). BRET ratios can then be calculated by dividing fluorescence emissions by luminescence emissions. NanoBRET can be used to perform ligand saturation binding assays, competition binding assays or ligand binding kinetic assays. (Stoddart et al., 2018)

#### **2.14.1 NanoBRET saturation binding assay**

For ligand binding experiments, HEK293G or HEK293T live cells, stably or transiently transfected or purified membranes prepared from these cells were used. Live cells were seeded into poly-D-lysine coated white clear bottom 96-well plates mentioned at [section 2.8.4](#). Purified membranes were added to white opaque bottom 96-well plates, with 2.5 µg of purified membranes/well used for ligand binding experiments. Stock fluorescent ligands were diluted in 1x HBSS containing 0.1 or 0.2 % BSA (Bovine Serum Albumin) to give a concentration range of various ligands for CXCR4, ACKR3 or EGFR. Non-specific binding was determined using an appropriate unlabelled compound which is a competitor for the receptor of interest ligand binding in HBSS/BSA. (The competitor concentration should be high enough to displace labelled ligand/compound/nanobody. For example, 100 ng of unlabelled EGF was used against fluorescently labelled EGFR ligands and nanobody experiments) Cells were washed once with HBSS, and then compounds were added to each well (triplicates, quadruplicates or five replicates) in a total volume of 50 or 100 µl. Plates were incubated at 37°C for 30 minutes (The incubation time differs on different receptors and compounds/ligands) (for EGFR ligands and nanobodies binding), (1 or 2 hours for CXCR4 and ACKR3 compounds and ligands). 5 µl of the NLuc substrate furimazine (Promega Corporation, Southampton, UK) was then added as 1/400 final dilution. After 5 minutes of incubation, fluorescence and luminescence emissions were simultaneously read using a PHERAstar FS dual plate reader (BMG Labtech, UK). Red fluorescent ligands were measured using module 610-LP with 460-80 filters and >610 nm emission filters), and green fluorescent ligands were measured using the BRET1 optical module (475 nm and 535 nm emission filters for

luminescence and fluorescence signals respectively). The raw BRET ratio was calculated by dividing fluorescence emissions by luminescence emissions, and the results were plotted as non-linear regression-curve fit (see 2.24) on GraphPad Prism version 10 (GraphPad Software, La Jolla, CA).

#### **2.14.2 NanoBRET ligand displacement assay (competition assay)**

Competition assays were performed the same way as ligand binding assays using live cells or membranes prepared from these cells. For cells and membranes, a constant concentration ( $K_d$  or half of the  $K_d$  concentration) of fluorescent ligand or nanobody and a fixed concentration of unlabelled competing ligands were added to wells. After 30, 60 minutes or 2 hours of incubation (for EGFR ligands and nanobodies binding), (1 or 2 hours for CXCR4 and ACKR3 compounds and ligands) at 37°C/5% CO<sub>2</sub> in the dark. Furimazine was added to each well as 1/400 final dilution. As described previously, fluorescence and luminescence were measured simultaneously using a PHERAstar FS dual plate reader (see 2.14.1). The raw BRET ratio was calculated by dividing fluorescence emissions by luminescence emissions, and the results were plotted as described at 2.24 on GraphPad Prism version 10 (GraphPad Software, La Jolla, CA).

#### **2.15 NanoBRET Receptor-Receptor Dimerisation Assay**

HEK293T cells were seeded at 15,000 per well for 96-well plates. The following day, cells were transfected transiently with appropriate plasmids, as mentioned 2.9. To obtain a BRET signal between donor and acceptor tagged receptors, receptors must be closer than 10 nm and in an orientation that allows efficient energy transfer (**Figure 2.6**). Two different receptor-tag combinations were used for receptor-receptor dimerisation assay: 1- NLuc\_CXCR4 expressed with HaloTag\_EGFR and 2- NLuc\_EGFR expressed with SNAPTag\_CXCR4. Cells were transfected with FuGENE HD Transfection Reagent using a 3:1 DNA/FuGENE HD ratio in OptiMEM following the manufacturer's instructions. For receptor-receptor dimerisation saturation experiments, a constant amount of donor (NLuc) tagged receptor cDNA and an increasing amount of acceptor tagged receptor cDNA (SNAPTag or HaloTag) were transfected. For ligand induced experiments, a constant amount of donor and acceptor

receptor cDNA was used (20 ng per well for both). 60 ng per well of empty vector pcDNA3.1 was used to give a total cDNA concentration per well of 100 ng. After 16-24 hours of transfection, culture media was removed, and cells were labelled with either HaloTag (AlexaFluor® 488 (G1002)) (0.2  $\mu$ M final concentration) or SNAP-Surface-AlexaFluor488® (0.2  $\mu$ M final concentration) labels (see 2.18). If ligand induced experiments were performed, the cells were then incubated for 30 minutes with various ligands such as CXCL12 and EGF which are natural ligands of CXCR4 and EGFR respectively, small molecule antagonists (IT1t, AMD3100 etc), receptor tyrosine kinase inhibitors (Erlotinib etc), nanobodies (VUN400c, Q44c etc) at 37°C. Fluorescence emissions from HaloTag or SNAPTag receptors were read prior to adding furimazine using PHERAstar FS platereader (BMG Labtech) using filters for excitation at 485 nm and emission at 520 nm to check the transfection efficiency of fluorescently labelled receptors. After that, cells were incubated with 1/400 final dilution of furimazine for 5 minutes, and fluorescence and luminescence then measured simultaneously using a PHERAstar FS dual plate reader using the BRET1 optical module (475 nm and 535 nm (30 nm band-pass filter for each) emission filters for luminescence and fluorescence signals respectively), as described at 2.14.1.

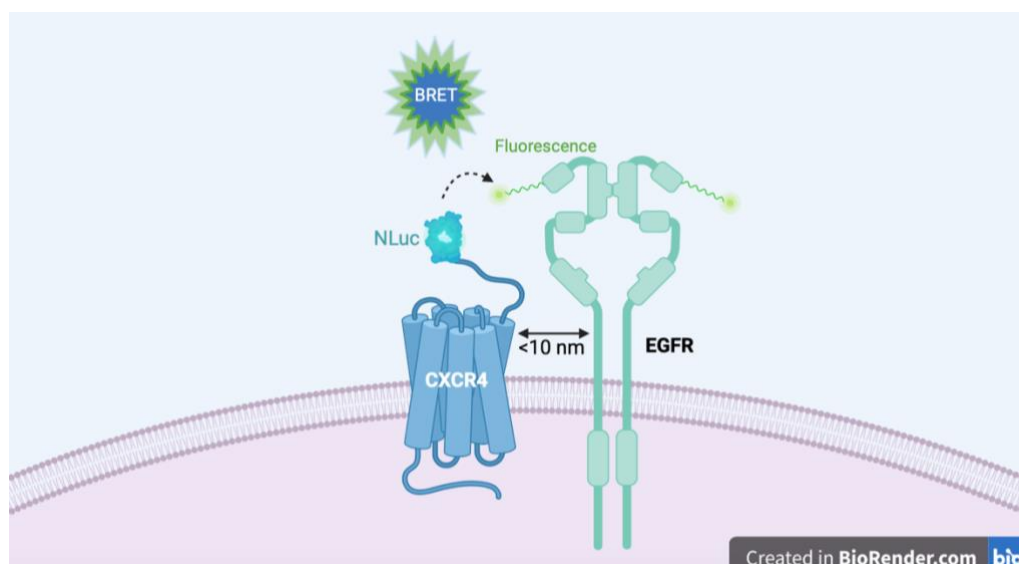


**Figure 2.6 The mechanism of NanoBRET receptor-receptor dimerisation assay.** Schematic representation of NLuc receptor-receptor dimerisation assay using fluorescently labelled (HaloTag and SNAPTag) and NLuc tagged receptors. (Figure was created with Biorender).

### 2.16 NanoBRET kinetic assay

Kinetic assays were performed either using live HEK293 cells or membranes prepared from these cells. Live HEK293 cells stably or transiently expressing NLuc tagged receptors (40,000/well) were plated onto poly-D-lysine-coated white 96-well plates as described in [2.8.4](#) and incubated overnight at 37°C/5% CO<sub>2</sub>. The following day, cells were washed with 100 µL of HBSS containing 0.2% BSA. 45 µL of HBSS containing furimazine (1/400 final dilution) was added to each well. For experiments using membrane preparations, an aliquot of defrosted membrane was added to each well at a concentration of 2.5 µg in 10 µl along with 70 or 80 µL of HBSS containing furimazine (1/400 final dilution). Baseline BRET values were read using a PHERAstar FS dual plate reader for 15 minutes at 37°C every 15, 30 or 60 seconds. After baseline measurements, unlabelled or fluorescently labelled ligands at various concentrations were added to the cells. Plates were then read for 2 hours at 37°C.

### 2.17 NanoBIT Internalisation assay

HiBiT internalisation assay is based on NanoBIT complementation. While protein-fragment complementation assays are used widely in protein-protein interaction assays, several studies used NanoBIT complementation to investigate receptor internalisation (Soave, Heukers, et al., 2020), (Reyes-Alcaraz et al., 2022). Nanoluciferase (NLuc) is an engineered luciferase derived from a deep-sea shrimp (Dixon et al., 2016). The full length enzyme is 19 kDa. The subunits derived from NLuc enzyme are LgBiT (LargeBiT) (18 kDa), SmBiT (SmallBiT) (1.3 kDa) and HiBiT (1.3 kDa) (11 amino acid) (Schwinn et al., 2018). While SmBiT shows weak affinity against LgBiT for self-association ( $K_d = 190 \mu\text{M}$ ) (Dixon et al., 2016), HiBiT has higher affinity ( $K_d = 700 \text{pM}$ ) (Schwinn et al., 2018). In this thesis HiBiT-LgBiT complementation strategy was used to investigate receptor internalisation. The HiBiT tagged receptors on the cell surface give luminescent signal after the complementation with purified LgBiT and NLuc substrate furimazine. Contrary, internalized HiBiT tagged receptors cannot complement with membrane impermeable purified LgBiT and don't produce luminescent signal. Hence, in this method, low luminescence signal signifies high internalisation level while high luminescence signal depicts high

number of receptors localised on cellular membrane. To perform HiBiT internalisation experiment we have used the following protocol.

HEK293 cells (20,000/well) were plated onto poly-D-lysine coated white 96-well plates as mentioned [2.8.4](#) and incubated at 37°C 5% CO<sub>2</sub> overnight. The following day, cells were transfected with 50 ng per well of HiBiT\_EGFR cDNA and 50 ng of empty pcDNA 3.1 plasmid or 50 ng of SNAP\_CXCR4 cDNA using FuGENE HD Transfection Reagent at a 3:1 DNA/FuGENE HD ratio in OptiMEM following manufacturer's instructions. Cells were then incubated at 37°C/5% CO<sub>2</sub> for 16-24 hours. The following day, culture media was removed, and cells were washed with HBSS once. Cells were incubated with various ligands to induce internalisation for 120, 60, 30 or 5 minutes for time course experiments and 30 minutes for time point experiments at 37°C. No ligand induced/only HBSS plus 0.02% BSA groups were used as control. After the ligand incubation time, 10 nM of purified LgBiT and furimazine (1/400 dilution) diluted in HBSS/0.02% BSA, were added to each well for 20 minutes at 37°C. Using the LUM Plus optical module (filters between 475-505 nm), luminescence was measured using a PHERAstar FS plate reader (BMG Labtech, Offenburg, Germany) (**Figure 2.7**).

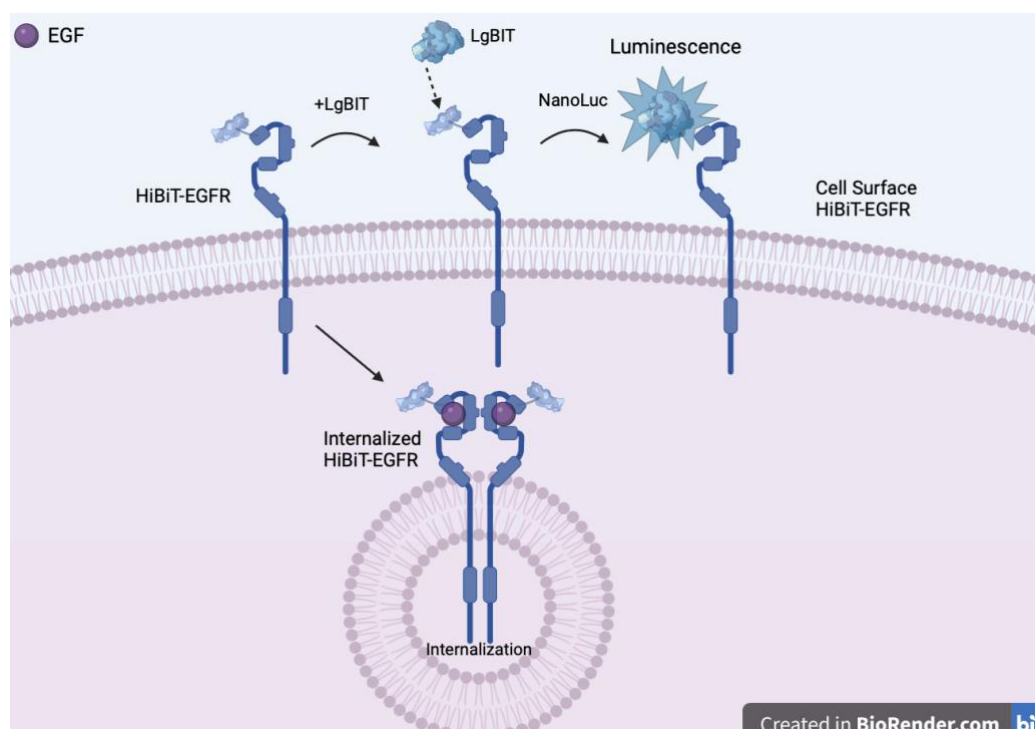


**Figure 2.7** The mechanism of NanoBIT internalisation assay. Schematic representation of HiBiT tagged EGFR internalisation. (Figure was adapted from Soave et al., 2018 and created with Biorender).

### 2.18 SNAPTag and HaloTag Labelling

Site-specific tagging of proteins with small peptides and proteins helps us to create tools to understand receptor functions in live cells(Cole, 2013). In this thesis we used SNAPTag and HaloTag to label CXCR4 and EGFR to be able to do receptor-receptor interaction BRET experiments. The SNAPTag (20 kDa) is a modified form of the DNA repair enzyme, human O6-alkylguanine-DNA-alkyltransferase (AGT)(Cole, 2013). A self-labelling reaction creates a covalent bond between reactive cysteine residue in the tag with O6-benzylguanine (BG) derivatives with variable fluorophore labels(Cole, 2013) (**Figure 2.8**).

HaloTag (33 kDa) is a modified haloalkane dehalogenase protein designed to covalently bind to synthetic ligands of HaloTag (Georgyi V. Los, 2008). The synthetic ligands comprise a chloroalkane linker can be attached to a several flurescent dyes similar to SNAPTag (Urh, 2012). A covalent ester bond is formed during catalysis between an aspartate in the enzyme and the hydrocarbon substrate(Georgyi V. Los, 2008).

The advantages of self-labeling proteins with peptide tags like SNAPTag and HaloTAG are their high reaction rate and specificity of labelling with sppecific bond between synthetic substrates and the tags. Also, the large number of various fluorophore conjugated substrates are commercially available (Urh, 2012)(Cole, 2013). Another advantage for SNAPTag and HaloTag is it is possible to choose membrane permeable or impermeable labelling ligands. We have used membrane impermeable labelling strategy to detect membrane located receptors in this thesis.

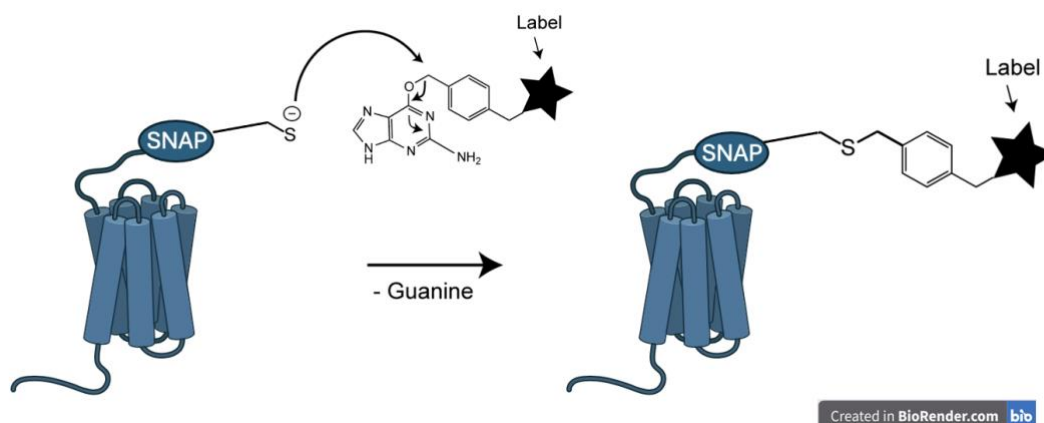


**Figure 2.8 SNAPTag labelling of protein of interest.** (Figure was adapted from N.Cole, 2013 and created with Biorender).

SNAPTag and HaloTag were used for CXCR4-EGFR homodimer and heterodimer BRET experiments in this thesis (see [2.15](#)). For this, cells were labelled with either HaloTag (AlexaFluor® 488 (G1002)) (0.2  $\mu$ M final concentration) or SNAP-Surface-AlexaFluor488® (0.2  $\mu$ M final concentration) labels in 50  $\mu$ L of complete media for 30 minutes at 37°C. Cells were then washed with 100  $\mu$ L of HBSS containing 0.2% BSA three times for 5 minutes. After this the BRET protocol was continued as mentioned section [2.15](#).

### 2.19 Bioluminescent imaging

HEK293 cells stably expressing NLuc\_EGFR (500.000 cells/dish) were plated onto poly-D-lysine-coated 35 mm cellview glass bottom cell culture dish in DMEM/10% FCS. After an overnight incubation at 37°C/5% CO<sub>2</sub>, the culture media was aspirated, and cells were washed with via adding 3 ml of HBSS containing 0.2% BSA and aspirating it. 1.5 ml of HBSS/0.2% BSA added on dish and furimazine was added as 1:500 dilution. Immediately after furimazine addition bright-field and bioluminescence imaging was performed using Olympus Luminoview 200 (LV200) inverted microscope (Olympus, Southend, UK). Cells were imaged live with PanApochromat 60x NA1.42 oil immersion objective with 0.5x tube length, resulting in 30x final magnification. Images were captured with brightfield (exposure 50 ms, gain 50) and luminescence (exposure 20 seconds, gain 200) filters.

## 2.20 Production and purification of nanobodies

VUN400, VUN401 [29], VUN415, VUN416, and Q44, Q86 [14] were cloned into the pYQVQ11 plasmid (QVQ, Utrecht, The Netherlands) and produced in *Saccharomyces cerevisiae* as previously described [14]. All proteins were purified using an Amsphere™ A3 column (JSR Life Sciences) on an ÄKTA start purification system (Cytiva) as described previously [33] and dialyzed against PBS. Protein concentration was determined by UV-VIS spectrometry and protein integrity was assessed by SDS PAGE.

## 2.21 Conjugation of VUN416c and Q44c with oligonucleotides

VUN416c and Q44c nanobodies with an unpaired cysteine in the C-terminus were prepared at high concentration (>3 g/l) and incubated with a 10-fold molar excess of tris(2-carboxyethyl) phosphine (TCEP) for 3 hours at 37°C, which was removed afterwards by two 0.5 ml Zeba spin columns (#89882, Thermo Fisher Scientific). The reduced nanobodies were incubated with a 10-fold molar excess of DBCO-Maleimide (#760668, Sigma Aldrich), which again was removed afterwards by two 0.5 ml Zeba spin columns. Nb-DBCO conjugates were quantified using absorbance at 280 and 310 nm and subsequently incubated with azide-modified oligonucleotides (Integrated DNA Technologies (IDT), Coralville, IA, USA) in a 1:1 molar ratio. Oligonucleotides 1 and 2 (oligo1, oligo2) were based on those described previously [34].

Oligo1: 5'-azide-AAA AAA AAA AGA CGC TAA TAG TTA AGA CGC TT-3'

Oligo2: 5'-azide-AAA AAA AAA ATA TGA CAG AAC TAG ACA CTC TT-3'

The yield of conjugations of Nb-DBCO and azide-oligonucleotides was assessed by SDS PAGE and PageBlue staining and was >90%.

## 2.22 Determining Nb-oligo binding (ELISA)

Genome-edited NLuc-CXCR4 expressing HeLa cells were seeded at 30,000 cells per well into a clear cell culture 96-well plate (Greiner) one day prior to the experiment. On the day of the experiment, the medium was refreshed with full medium with/without unlabeled VUN416 or Q44 (1  $\mu$ M) as competitors and incubated for 1 hour at 37°C, 5% CO<sub>2</sub>. Cells were washed with PBS and fixed with 4% PFA, washed again, and then incubated with blocking buffer (5% BSA, 0.05 mg/ml sheared salmon sperm DNA (#AM9680, Thermo Fisher Scientific) in PBS) with/without unlabeled VUN416 or Q44 (1  $\mu$ M) for 1 hour at RT, shaking at 300 RPM. Nb-oligos were incubated in presence/absence of competitors (1  $\mu$ M) for 1 hour at RT, and the unbound fraction then washed away (Duolink wash buffer A). Biotin-conjugated anti-sense-oligonucleotides (Anti-oligo1-Biotin: 5'-Biotin-AAG CGT CTT AAC TAT TAG CGT CTT TTT TTT T; Anti-oligo2-Biotin: 5'-Biotin-AAG AGT GTC TAG TTC TGT CAT ATT TTT TTT TT, ordered from IDT, each 100 nM diluted in blocking buffer) were added and incubated for 1 hour at RT, shaking at 300 RPM. Cells were again washed with wash buffer A and subsequently incubated with streptavidin-HRP (1:5000, #21130, Thermo Fisher Scientific). After washing with wash buffer A and PBS, TMB (#34028, Thermo Fisher Scientific) was added and incubated until sufficient coloration was achieved, and the reaction was stopped with H<sub>2</sub>SO<sub>4</sub> (1 M). Absorbance at 450 nm was quantified using a ClarioStar Plus (BMG Labtech).

## 2.23 Proximity ligation assays

An alternative method to study receptor-receptor interactions is proximity ligation where oligonucleotides conjugated to receptor-targeted antibodies can act as probes to target a protein complex. These oligonucleotides can be joined by ligation if they have been brought into close proximity by receptor oligomerisation (Söderberg et al., 2008). The DNA ligation product formed can then act as a template for PCR amplification of a single-stranded rolling circular product that can be visualized by hybridization of a fluorescently-labelled complementary oligonucleotide detection probe (Söderberg et al., 2008). The resulting labelled rolling circle amplified DNA product can then be imaged microscopically (Raykova et al., 2016).

HeLa cells were seeded at 30,000 cells per well into a poly-L-lysine-coated black clear-bottom PhenoPlate (Perkin Elmer, for imaging) one day prior to the experiment. On the day of the experiment, the medium was refreshed by full medium with/without unlabeled VUN400, VUN416, or Q44 (1  $\mu$ M) as competitors and incubated for 1 hour at 37°C, 5% CO<sub>2</sub>. Cells were washed with PBS and fixed with 4% PFA, washed again, and then incubated with blocking buffer (Duolink blocking buffer for antibody-based PLA; 5% BSA, 0.05 mg/ml sheared salmon sperm DNA in PBS for Nb-based PLA). Nb-oligos (10 nM) were incubated in presence/absence of unlabeled nanobodies (1  $\mu$ M) for 1 hour at 37°C. Each Nb-oligo incubation was followed by washing with wash buffer A. Ligation, amplification, and detection of bound oligonucleotides were done using the PLA detection kit Red (#DUO92008, Sigma Aldrich) and according to the manufacturer's instructions. Cells were imaged using the Axiovert 5 Microscope (Zeiss) using a 20x objective, 1 s exposure time and 4x gain. Images were analyzed for mean grey value in ImageJ (Version 2.14.0/1.54f).

## 2.24 Data analysis

All data were analysed using Prism version 10 (GraphPad Software, San Diego, CA, USA). Plasmid sequences were viewed and edited using Benchling (San Francisco, USA) and SnapGene Viewer 7.0.3 (GSL Biotech, USA). All data obtained from the NanoBRET assays were calculated as BRET ratios using Microsoft Excel (Equation 1).

$$BRET\ ratio = \frac{Emission\ from\ acceptor\ channel}{Emission\ from\ donor\ channel} \quad \text{Equation 1}$$

### 2.24.1 Saturation Binding

The data were transferred into a new GraphPad Prism 10 worksheet and fitted with the “one-site-total and non-specific binding” setting using the following equation (Equation 2).

$$Total\ binding = B_{max} \cdot \frac{[L]}{[L] + K_D} + M \cdot [L] + C \quad \text{Equation 2}$$

In this equation,  $B_{\max}$  is the maximum specific binding,  $[L]$  is the concentration of fluorescent ligand in nM,  $K_d$  is the equilibrium dissociation constant in nM,  $M$  is the slope of the non-specific binding component, and  $C$  is the intercept with the y axis (Soave, Goulding, et al., 2020) (**Figure 2.9**).

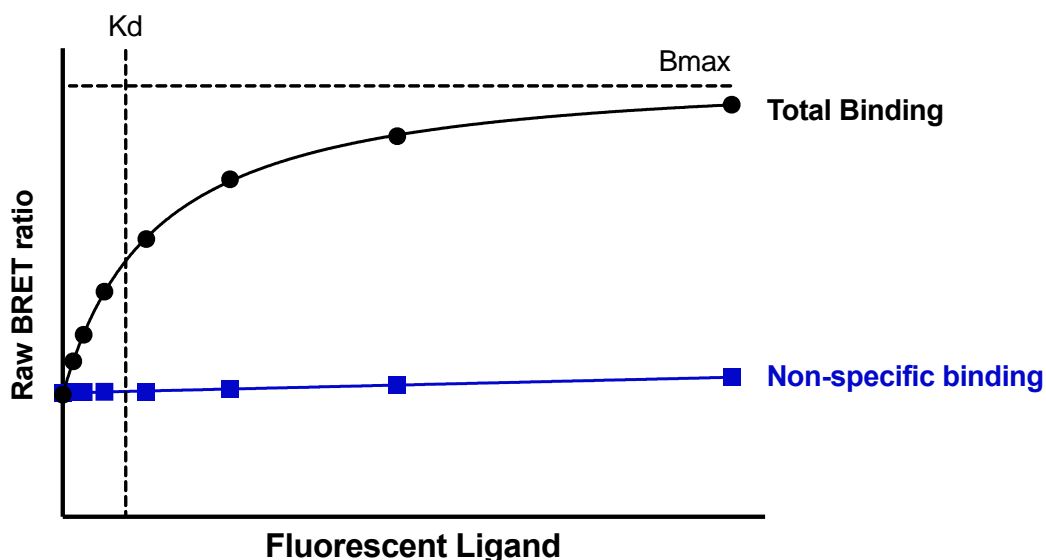


**Figure 2.9** Total and non-specific binding curve depicted using GraphPad Prism. Plot showing the determination of  $B_{\max}$  and  $K_d$  values on total binding and non-specific binding curves.

### 2.24.2 Competition Binding

For the competition curve analysis, the BRET ratio data was calculated in Microsoft Excel, transferred to GraphPad Prism, and fitted into the following equation.

$$\text{Specific Binding} = 100 - \frac{100 \times [I]^{Hc}}{[I]^{Hc} + IC_{50}^{Hc}} \quad \text{Equation 3}$$

Specific Binding is the specific binding of a labelled ligand to a receptor (fit to four-parameter model),  $[I]$  is the concentration of competing ligand,  $IC_{50}$  is the concentration of competitor ligand required to generate 50% of inhibition of specific binding, and  $Hc$  is the Hill coefficient, describing the curve's steepness.

To determine the % inhibition of specific binding, the data was fit to nonlinear regression, using a ‘One site – Fit logIC<sub>50</sub> model was chosen, which uses the following equation (Equation 4).

$$\% \text{ Inhibition of specific binding} = \frac{100 \times [A]}{[A] + IC_{50}} \quad \text{Equation 4}$$

[A] is the concentration of competing ligands, and the IC<sub>50</sub> is the molar concentration of ligand required to inhibit 50% of the specific binding of the fluorescent ligand.

To obtain the K<sub>i</sub> (dissociation constant of unlabelled ligand) value for competing ligands, the K<sub>d</sub> (equilibrium dissociation constant of the labelled ligand) value for the fluorescent ligand (obtained from saturation binding experiments) was used in the following equation based on the Cheng–Prusoff correction (Equation 3) IC<sub>50</sub> (concentration of unlabelled ligand required to inhibit the specific binding of labelled ligand by 50%) (Soave, Goulding, et al., 2020).

$$K_i = \frac{IC_{50}}{1 + \frac{[L]}{K_D}} \quad \text{Equation 5}$$

### 2.24.3 Statistical analysis

The graphs plotted as either the mean ± SEM (Standard Error of the Mean) of all experiments or one representative experiment. An unpaired t-test was used to determine statistical significance between two unpaired observations. One-way analysis of variance (ANOVA) tests was performed to compare three or more sets of data. Statistical significance was defined as p<0.05.

**Chapter 3: Binding  
properties of fluorescently  
labelled CXCR4 and  
ACKR3 ligands  
determined using  
NanoBRET**

### 3.1 Introduction

The IT1T or CVX15-bound crystal structures of CXCR4 have been determined by (B. Wu et al., 2010b). F87 and E288 amino acids on TM domains have been showed to be significantly crucial for binding of 11 different antagonists (HC4319, DV3, DV1, DV1 dimer, V1, vMIP-II, CVX15, LY2510924, IT1t, AMD3100, and AMD11070) of CXCR4 (B. Wu et al., 2010b)(Meng et al., 2023). It has also been suggested that AMD3100 binding is affected by W94A (TM2) and D97A (TM2) mutations in the minor subpocket and D171 and D262 mutations in the major subpocket (Meng et al., 2023). These observations suggested that AMD3100 binds to the major and minor subpockets simultaneously, which differs from previous studies suggesting it interacts with only the major pocket (Jørgensen et al., 2021). The binding modes of AMD070 (AMD11070) and IT1t have been shown to be similar, primarily interacting with the minor subpocket (Meng et al., 2023) (**Figure 3.1**), with IT1t mainly having ionic interactions with D97 and E288 amino acids (B. Wu et al., 2010b).

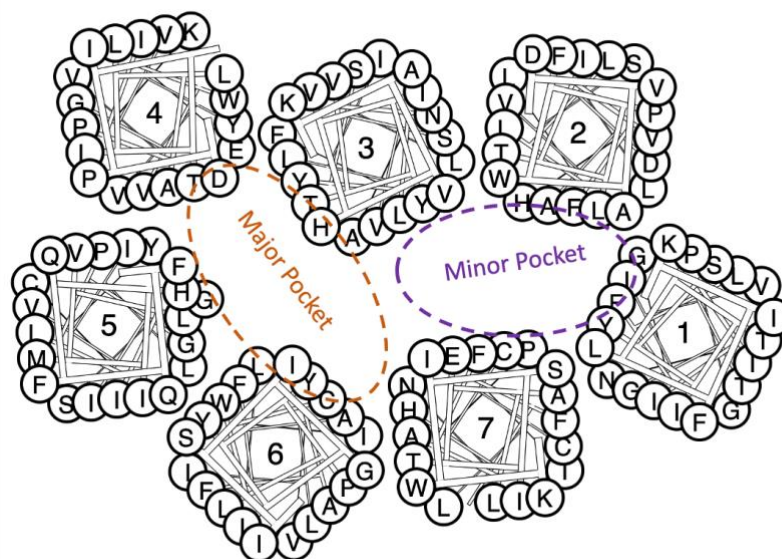


**Figure 3.1** The major and minor binding sub pockets of CXCR4. Serpentine diagram of CXCR4. The numbers refer to transmembrane alpha helices, the letters are single amino acid codes. The figure is depiction of the CXCR4 from above. The figure was adapted from (Meng et al., 2023).

CXCR4 is commonly expressed in hematopoietic cells such as neutrophils, monocytes, and macrophages, but it is also found in neuronal stem cells, astrocytes, and microglia (Pozzobon et al., 2016b). CXCR4-knockout mice show defects in B cell lymphopoiesis and bone marrow colonisation as well as late gestational lethality, illustrating that it plays a crucial role in embryonic development (Nagasawa et al., 1996; Zou et al., 1998). While CXCR4 is not expressed in many healthy cell types, it is highly upregulated and leads to increased proliferation, migration and invasion in several cancers like breast cancer (Shi et al., 2020), multiple myeloma (Ito et al., 2021), non-small cell lung cancer (Cavallaro, 2013) and liver cancer (Ghanem et al., 2014). The CXCR4-CXCL12 axis stimulates the migration of CXCR4-expressing cells towards CXCL12 gradients, which leads to the homing of immune cells to sites of inflammation controlling the cancer microenvironment (Mezzapelle et al., 2022) as well as metastasis of primary cancer cells to secondary homing sites (Cavallaro, 2013). It has also been shown that CXCR4 plays a role as a helper receptor for HIV-1 entry to the cell as a co-receptor of CD4 to interact with HIV envelope protein, gp120 (Nickoloff-Bybel et al., 2021). This gives importance to the discovery and development of CXCR4 antagonists (Zhang et al., 2020). Efforts to develop small-molecule inhibitors have yielded many different chemical classes of highly potent antagonists (Debnath et al., 2013; Grande et al., 2017) (Woodard & Nimmagadda, 2011). As a result of this research, one small molecule antagonist, AMD3100 was clinically approved, and other small molecules also currently undergoing clinical trials for cancer and HIV infection treatment (Bridger et al., 2010; De Clercq, 2019; Debnath et al., 2013; Wang et al., 2020; Zhang et al., 2020)

Regarding its cognate ligands, ACKR3 shares CXCL12 with CXCR4 and CXCL11 with CXCR3 respectively (Janssens et al., 2018). CXCL12 binds to ACKR3 ( $K_d= 0.4$  nM) with ten times higher affinity than it does to CXCR4 (Balabanian et al., 2005). ACKR3 is expressed in various cell types, such as hematopoietic, endothelial, and neuronal progenitor cells (Koenen et al., 2019). Studies in knock-out mice indicate that loss of ACKR3 results in defects in cardiac development (Sierro et al., 2007). ACKR3 also plays a significant role in the development of many cancers, increasing tumour cell proliferation, migration, adhesion, and angiogenesis capacity (Miao et al., 2007).

Although the physiological function of ACKR3 is not fully clear, it has been shown that it can scavenge various ligands such as CXCL11, CXCL12, the viral chemokine vCCL20, adrenomedullin, MIF and opioids (Meyrath et al., 2020; Quinn et al., 2018b). It has been demonstrated that CXCL12 scavenging by ACKR3 stimulates the metastasis and growth of CXCR4-positive breast cancer cells (Hattermann & Mentlein, 2013). CXCR4 and ACKR3 are co-expressed in various cells such as T and B lymphocytes, vascular endothelial cells, dendritic cells and cancer cell lines derived from patients with NSCLC (Iwakiri et al., 2009), breast cancer (X. Sun et al., 2010) and cervical cancer (Xu et al., 2021)(M. Neves et al., 2019a).

Due to the increasing documentation on the role of ACKR3 in disease, several structurally diverse small molecule ACKR3 ligands such as AMD3100 (which also can bind to CXCR4) (Kalatskaya et al., 2009), VUF11207 (Wijtmans et al., 2012), LN6023 (Bayrak et al., 2022a) have been reported.

Cell membrane receptors play a significant role in cellular physiology in health and disease. Several tools, including receptor selective fluorescent ligands, have been used to understand their dynamics and mechanisms. They can be used to monitor the expression and the function of these receptors with several methods, such as confocal microscopy, Fluorescence Correlation Spectroscopy (FCS), Bioluminescence Resonance Energy Transfer (BRET) or Fluorescence Resonance Energy Transfer (FRET) assays to probe receptor pharmacology, molecular mobility, localisation or trafficking (Soave, Briddon, et al., 2020b). Small molecule ligands are conjugated to such fluorophores with a linker to introduce flexibility and provide access of the pharmacophore to the receptor's binding site. It is worth noting that the addition of fluorophores can change a ligand's chemical properties and lipid solubility and potentially affect the binding affinity of the conjugated pharmacophore to the receptor (Baker et al., 2010). Fluorescent ligands should therefore be considered as unique pharmacological entities requiring their own validation in respect to affinity, selectivity and imaging properties (Stoddart, Kilpatrick, et al., 2015a). Synthetic strategies for linker and fluorophore attachment were developed with the help of structure-activity relationship (SAR) and in silico design. (Dekkers et al., 2023, 2024)

One of the most widely used ligands to study CXCR4 and ACKR3 is labelled and unlabelled CXCL12 (Y. Cheng et al., 2017b; Levoye et al., 2009b; Yamada et al., 2015). Additionally, commercially available antibodies and nanobodies have been

---

used (Maussang et al., 2013; Tripathi et al., 2016). However, developing and producing these protein-based tools is expensive and time-consuming. Small molecule ligands selectively targeting CXCR4 and ACKR3 can be used as cost-effective alternatives to those protein-based tools as they are more accessible to synthetic chemistry and are relatively easy to conjugate to fluorophore analogues (Soave, Briddon, et al., 2020b; Stoddart, Kilpatrick, et al., 2015a).

This chapter will describe the pharmacological evaluation of recently developed and synthesised non-fluorescent and fluorescent CXCR4 probes based on IT1t and AMD070 as well as ACKR3 probes based on VUF11207. The CXCR4 compounds were developed by Dr Sebastian Dekkers, Dr Nicholas D. Kindon, Professors Barrie Kellam and Michael Stocks at the University of Nottingham. The ACKR3 compounds were developed by Dr Sebastian Dekkers, Dr Marta Arimont-Segura, Dr Chris de Graaf and Professor Rob Leurs from the Vrije Universiteit Amsterdam in collaboration with Professors Barrie Kellam and Michael Stocks using classical medicinal chemistry approach. The chapter has the following objectives:

- To develop and optimise an *in vitro* NanoBRET assay to assess the direct binding of the ligands and known compounds for CXCR4 and ACKR3.
- Characterisation of the binding properties of labelled and unlabelled novel compounds for CXCR4 and ACKR3.

To achieve the objectives for this chapter, NanoBRET technology was used (see section [2.14](#)). For NanoBRET ligand binding experiments, stably transfected N-terminal tagged NLuc\_CXCR4 and NLuc\_ACKR3 (full-length) expressed in living HEK293 GloSensor cells were used (**Figure 2.5**). NanoBRET saturation or competition (displacement) experiments were then performed using fluorescently labelled ligands (CXCL12-green, compounds 10 and 24) or unlabelled CXCR4 and ACKR3 targeting ligands (CXCL12, AMD3100, IT1t and compounds 4, 9, 19, 20, 18a, 18b, 18c). Compounds targeting CXCR4 and ACKR3 have been listed in **Table 2.1**.

## 3.2 Results

### 3.2.1 Determination of CXCR4 ligand binding by NanoBRET

Initially, to determine the binding affinity of fluorescently labelled CXCL12-green at N terminal NanoLuciferase-tagged stably-transfected receptor (NLuc\_CXCR4) in living HEK293 GloSensor cells, NanoBRET saturation binding assays were performed. 10  $\mu$ M AMD3100 was used to determine non-specific binding. The dissociation constant ( $K_d$ ) for CXCL12-green (Oregon Green® 488) binding to CXCR4 was determined to be  $78.8 \pm 27.8$  nM (n=5) (**Figure 3.2**).

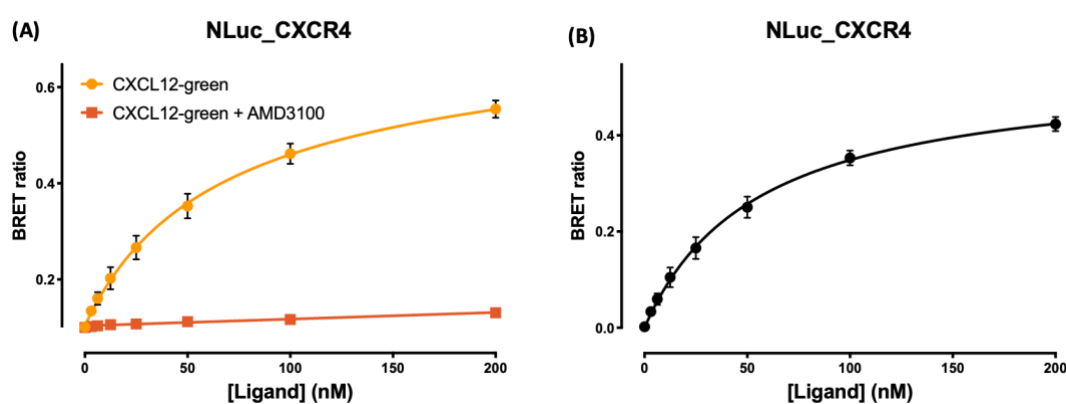


**Figure 3.2 Saturation binding of CXCL12-green in HEK293G NLuc\_CXCR4 cells.** HEK293G NLuc\_CXCR4 cells were treated with increasing concentrations of green fluorescently labelled CXCL12 (CXCL12-Green) (Oregon Green® 488) and total, (A) non-specific and (B) specific binding were calculated in the presence or absence of 10  $\mu$ M AMD3100. Compounds were added simultaneously, and cells incubated for 60 minutes at 37 °C. Experiments were performed in HBSS containing 0.2 % BSA. The NLuc substrate furimazine (1:400 final dilution) was added, and, plates were incubated for 5 minutes, before luminescence and fluorescence emissions were measured on a PheraStar FS plate reader. The raw BRET ratio was calculated by dividing the fluorescent signal by the bioluminescent signal. Specific binding was calculated by deducting the non-specific binding from the total binding values. Data points are mean  $\pm$  SEM, of 5 independent experiments performed in triplicate wells.

The NanoBRET assay was also used to determine the affinity of competing ligands using competition binding experiments with a fixed concentration of CXCL12-green (25 nM). IT1t, AMD3100 and unlabelled CXCL12 could displace CXCL12-green at high concentrations. The equilibrium dissociation constants obtained were  $pK_i = 6.8 \pm 0.08$  for AMD3100,  $pK_i = 7.6 \pm 0.1$  for IT1t, and  $pK_i = 6.4 \pm 0.2$  for CXCL12 (**Figure 3.3**).

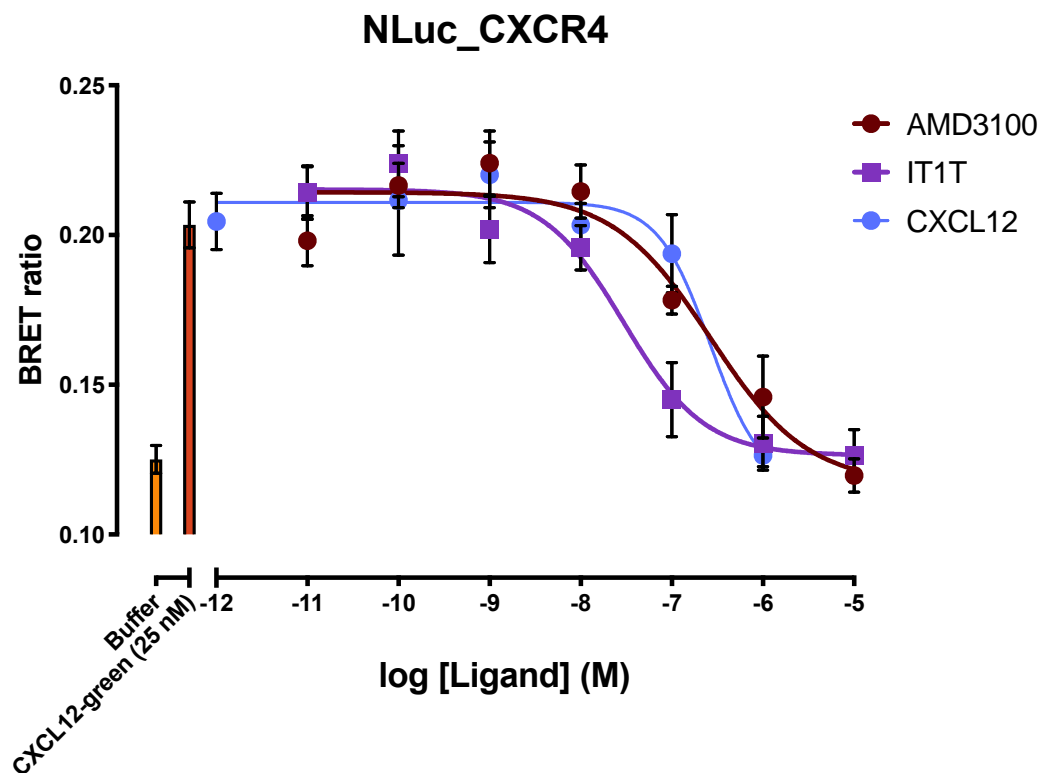


**Figure 3.3 Competition binding of CXCL12-green with AMD3100, IT1t and CXCL12.** HEK293G NLuc\_CXCR4 cells were treated with 25 nM of CXCL12-green and increasing concentrations of AMD3100, IT1t and unlabelled CXCL12 simultaneously for 60 minutes at 37 °C. Experiments were performed in HBSS containing 0.2 % BSA. The NLuc substrate furimazine (1:400 final dilution) was added, and, plates were incubated for 5 minutes, and luminescence and fluorescence emissions were measured on a PheraStar FS plate reader. The error bars depict the mean  $\pm$  SEM of 4 independent experiments performed in triplicate wells. The raw BRET ratio was calculated by dividing the fluorescent signal by the bioluminescent signal.

After the verification of the NLuc\_CXCR4 system with CXCL12-green, fluorescent ligands, the affinity of two novel fluorescently labelled compounds conjugated to BODIPY 630/650-X (BY630/650-X) designed to target CXCR4 were tested using NanoBRET saturation binding assays (**Figure 3.4**).

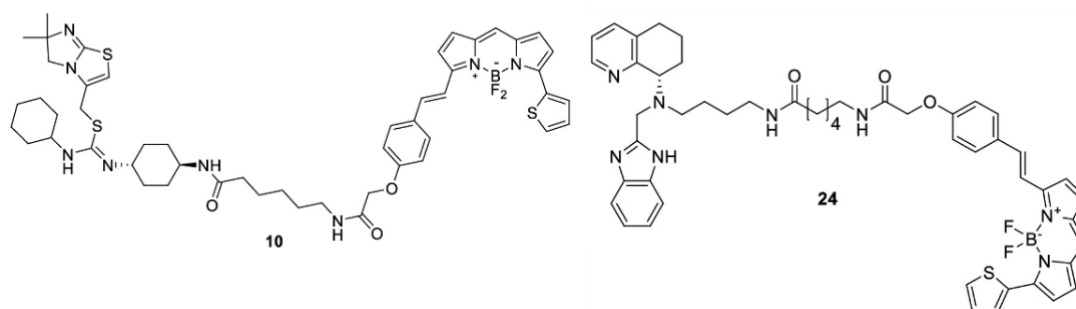


**Figure 3.4** Chemical structure of compounds **10** and **24**. BODIPY 630/650-X (BY630/650-X) labelled CXCR4 antagonists derived from IT1t (compound 10) and AMD070 (compound 24) designed and synthesised by Dr Sebastian Dekkers and Dr Nicholas D. Kindon (Dekkers et al., 2023).

Compound **10** (IT1t derivative) and compound **24** (AMD070 derivative) both showed saturable binding at NLuc\_CXCR4 with  $K_d$  values  $295.5 \pm 44$  (N=6) and  $284.5 \pm 7.3$  (N=4) respectively (**Table 3.1**). The binding of the IT1t-based compound 10 was fully displaced by unlabelled AMD3100 and IT1t. The binding of the AMD070-based compound 24 was mostly inhibited by IT1t and partially inhibited by AMD3100 showing relatively higher non-specific binding (**Figure 3.5**).

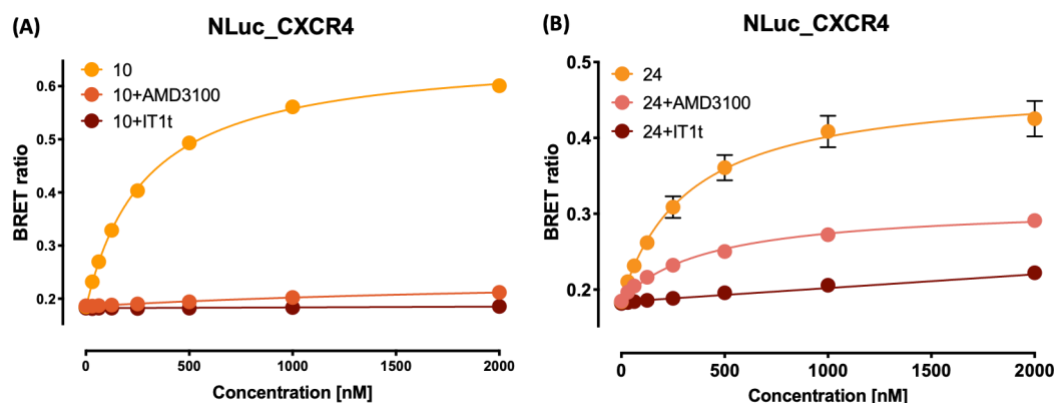


**Figure 3.5 Saturation binding of fluorescently labelled 10 and 24 compounds in HEK293G NLuc\_CXCR4 cells.** HEK293G NLuc\_CXCR4 cells were treated with compounds (A) **10** and (B) **24** in the absence or presence of 10  $\mu$ M of AMD3100 or IT1t. NanoBRET experiments were performed using full-length N terminal nanoluciferase CXCR4 stably expressing HEK293 cells. Compounds were added simultaneously and incubated for 60 minutes at 37  $^{\circ}$ C. Experiments were performed in HBSS containing 0.2 % BSA. The NLuc substrate furimazine (1:400 final dilution) was added, and plates were incubated for 5 minutes then, luminescence and fluorescence emissions were measured using a BMG Pherastar FS. Data are combined mean  $\pm$  SEM from (A) six and (B) four independent experiments, respectively, where each experiment was performed in triplicate. Where not shown the error bars were within the size of the symbol. The raw BRET ratio was calculated by dividing the fluorescent signal by the bioluminescent signal.

**Table 3.1 Binding Affinities of the Novel Fluorescent Ligands Determined in HEK293G Cells Stably Expressing NLuc\_CXCR4.**

Compound	$K_d$ (nM)	$pK_d$	n
10	$295.5 \pm 44$	$6.54 \pm 0.05$	6
24	$284.5 \pm 7.3$	$6.54 \pm 0.09$	4

Data are expressed as mean  $\pm$  SEM from 4-6 independent experiments (n) from triplicate wells. Equilibrium binding parameters were derived from saturation binding experiments (Figure 3.6 and Figure 3.7).  $pK_d$  values are the negative log of the  $K_d$  values.

### 3.2.2 Determination of novel ACKR3 ligands binding by NanoBRET

The same approach was used to determine the binding affinity of CXCL12-green at NLuc-tagged ACKR3 stably expressed in HEK293 G cells. The mean dissociation constant obtained for CXCL12-green binding to ACKR3 was  $3.3 \pm 0.8$  nM (n=5) (**Figure 3.6**). Non-specific binding was determined in the presence of 10  $\mu$ M unlabelled CXCL12. The specific binding of CXCL12-green was obtained by deducting the non-specific binding from the total binding values.

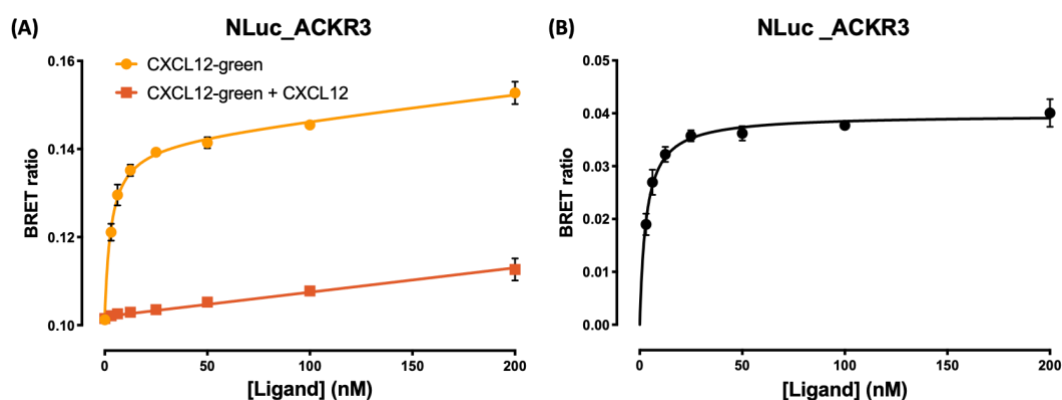


**Figure 3.6 Saturation binding of CXCL12-green in HEK293G NLuc\_ACKR3 cells.** HEK293G stably expressing NLuc\_ACKR3 cells were treated with green fluorescently labelled CXCL12 (CXCL12-green) (A) total, non-specific and (B) specific binding was calculated in the presence or absence of 10  $\mu$ M unlabelled CXCL12. Compounds were added simultaneously and incubated for 60 minutes at 37  $^{\circ}$ C. Experiments were performed in HBSS containing 0.2 % BSA. The NLuc substrate furimazine (1:400 final dilution) was added, and, plates were incubated for 5 minutes, and luminescence and fluorescence emissions were measured on a PheraStar FS plate reader. The raw BRET ratio was calculated by dividing the fluorescent signal by the bioluminescent signal. Specific binding was calculated by deducting the non-specific binding from the total binding values. Data points are mean  $\pm$  SEM. of 5 replicate experiments performed in triplicate wells.

The unlabelled ACKR3 agonist VUF11207 molecule was designed and synthesised by Dr Maikel Wijtmans and colleagues (Wijtmans et al., 2012) from Vrije University Amsterdam. Dr Sebastian Dekkers developed and synthesised the three different BODIPY-FL-X labelled derivatives of VUF11207, which differed in the length of the linkers used (atom numbers) (**Figure 3.7**). The number of atoms for linkers are 13, 16, and 19 for 18a, 18b and 18c, respectively.

The characterisation of these compounds at HEK293G cells stably expressing NLuc\_ACKR3 HEK293G cells with saturation binding BRET experiments showed clear saturable specific binding to the NLuc\_ACKR3 with low levels of non-specific binding (determined in the presence of 10  $\mu$ M unlabeled VUF11207. The dissociation constants of the compounds were  $12.6 \pm 0.2$  nM for **18a**,  $81 \pm 2.7$  nM for **18b** and  $150 \pm 10.7$  nM for **18c** (**Figure 3.8**). Obtained equilibrium dissociation constants can be found in **Table 3.2**.

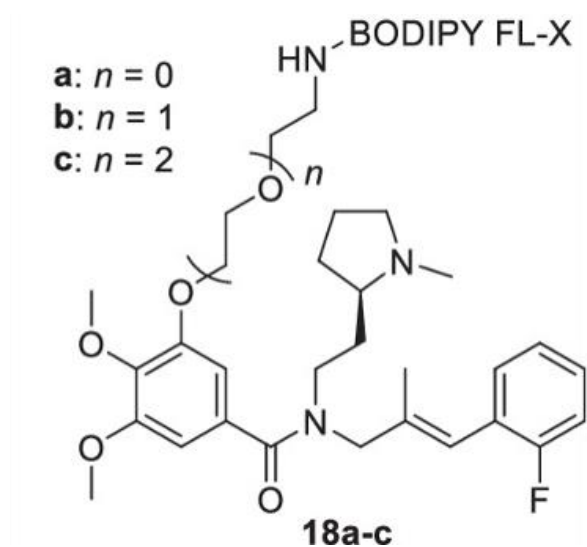


**Figure 3.7** Chemical structure of **18 a-c** compounds. BODIPY FL-X labelled ACKR3 agonists derived from VUF11207 (designed by Dr Maikel Wijtmans).

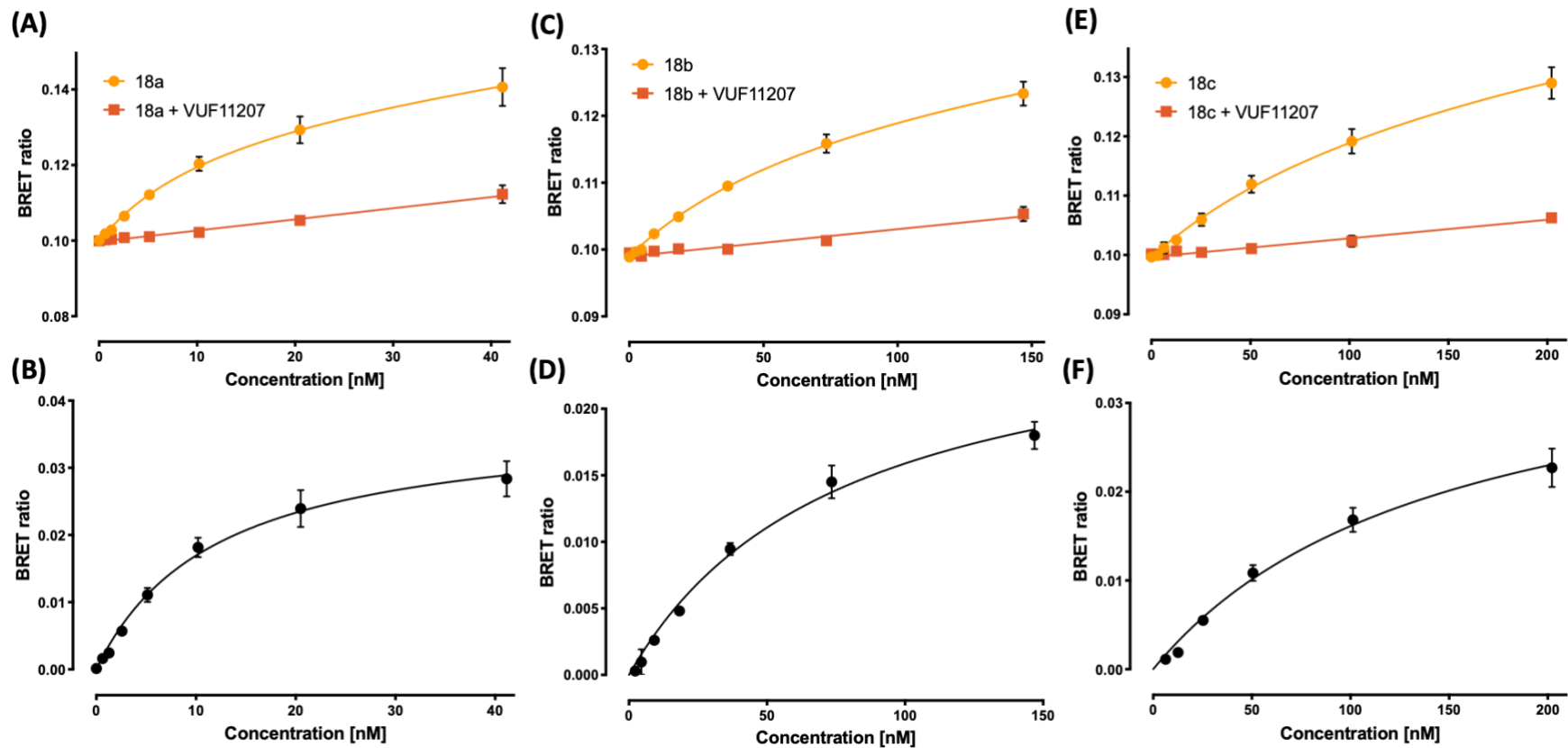


**Figure 3.8 Saturation binding of VUF11207 derivatives fluorescently labelled 18a, 18b, 18c in HEK293G Nluc\_ACKR3 cells.** HEK293G cells stably expressing NLuc\_ACKR3 were treated with (A, B) 18a, (C, D) 18b, (E, F) 18c ligands in the absence or presence of 10  $\mu$ M of unlabelled VUF11207. Compounds were added simultaneously and incubated for 60 minutes at 37 °C. Experiments were performed in HBSS containing 0.2 % BSA. The NLuc substrate furimazine (1:400 final dilution) was added, and plates were incubated for 5 minutes then, luminescence and fluorescence emissions were measured using a BMG Pherastar FS. Data are combined mean  $\pm$  SEM from four independent experiments, where each experiment was performed in triplicate. The raw BRET ratio was calculated by dividing the fluorescent signal by the bioluminescent signal. Specific binding (B-D-F) was calculated by subtracting the non-specific binding from the total binding (A-C-E) values.

**Table 3.2 Binding Affinities of the Novel Fluorescent Ligands Determined in HEK293G Cells Stably Expressing NLuc\_ACKR3.**

Compound	K <sub>d</sub> (nM)	pK <sub>d</sub>	Length of the linker (atom no)	n
18a	12.6 ± 0.2	7.8 ± 0.009	13	4
18b	81 ± 2.7	7.09 ± 0.01	16	4
18c	150 ± 10.7	6.8 ± 0.03	19	4

Data are expressed as mean ± SEM from 4 independent experiments using triplicate wells. Equilibrium binding parameters were derived from saturation binding experiments (Figure 3.11). pK<sub>d</sub> values are the negative log of the K<sub>d</sub> values.

Since compound 18a has the highest affinity of other compound 18 derivatives, it was then taken forward as a fluorescent probe in NanoBRET displacement assays to determine the affinities of the unlabelled compounds, 4, 9, 19, and 20 ligands at NLuc ACKR3 (**Figure 3.9**). A fixed concentration of 32.4 nM of 18a was simultaneously added with increasing concentrations of the unlabelled compounds. The binding affinities (pK<sub>i</sub>) of 4, 9, 19, and 20 were determined to be 7.4 ± 0.13, 6.6 ± 0.07, 5.0 ± 0.10, 6.2 ± 0.07 respectively (**Table 3.3**). While compound 4 has the highest competition for VUF11207-based 18a binding, the competition curves appear to have two components within it must be noted that it might bind to receptor on two sites. Compounds 9 and 20 were able to fully compete with 18a, whereas compound 19 partially displaced 18a at higher concentrations (**Figure 3.9**).

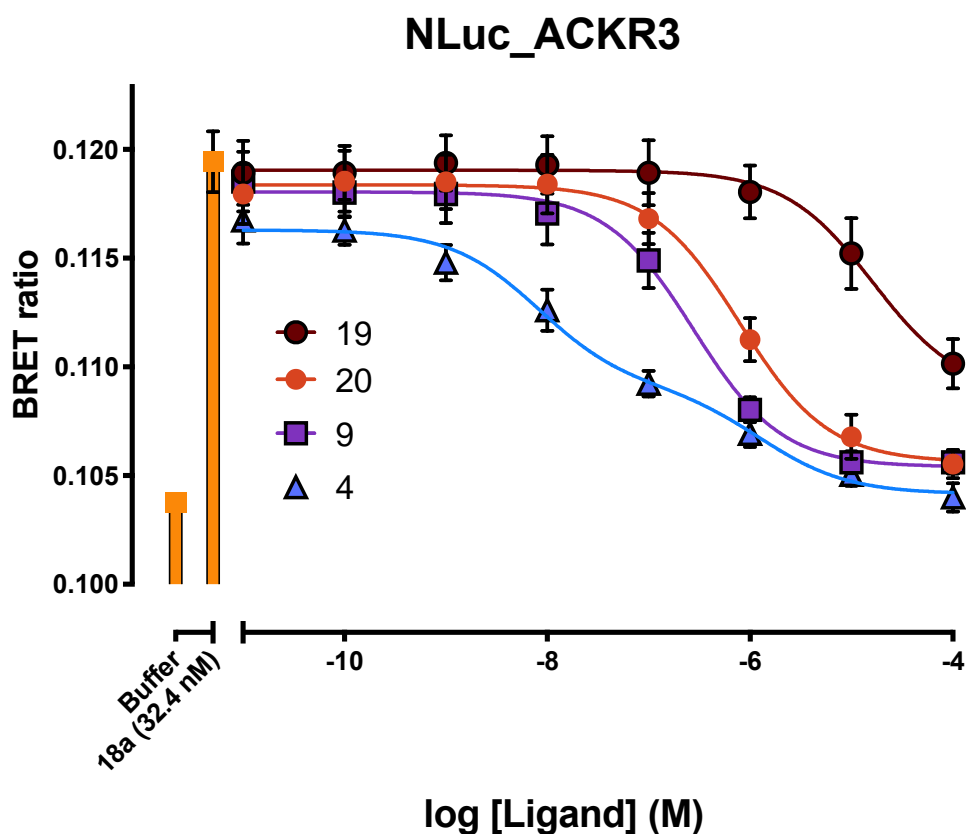


**Figure 3.9 NanoBRET Competition binding experiments of 4, 9, 19, 20 using the fluorescent VUF11207 derivative 18a (32.4 nM) in HEK293G stably expressing NLuc\_ACKR3 cells.** NanoBRET experiments were performed using full-length N terminal nanoluciferase ACKR3 stably expressing HEK293 cells. Compounds were added simultaneously and incubated for 60 minutes at 37 °C. Experiments were performed in HBSS containing 0.2 % BSA. The NLuc substrate furimazine (1:400 final dilution) was added, and plates were incubated for 5 minutes then, luminescence and fluorescence emissions were measured using a BMG Pherastar FS. Data are combined mean  $\pm$  SEM from at least five independent experiments, where each experiment was performed in triplicate. The raw BRET ratio was calculated by dividing the fluorescent signal by the bioluminescent signal.

**Table 3.3 Binding Affinities of Known ACKR3 Ligands Determined in HEK293G Cells Stably Expressing NLuc\_ACKR3.**

Compound	pKi	n
4	$7.4 \pm 0.13$	5
9	$6.6 \pm 0.07$	6
19	$5.0 \pm 0.10$	5
20	$6.2 \pm 0.07$	6

Data are expressed as mean  $\pm$  SEM from 5-6 independent experiments using triplicate wells. Equilibrium binding parameters were derived from competition binding experiments (Figure 3.12). Competition experiments were fit to a non-linear regression, and the curves were used to determine the pKi of each unlabeled ACKR3 compound.

### 3.3 Summary and Discussion

This chapter reports on the properties of new receptor selective red-emitting fluorescent ligands targeting CXCR4 and green-emitting fluorescent ligands targeting ACKR3. The development of these ligands will allow the monitoring of receptor dynamics, such as cell surface expression levels, ligand binding affinities, and internalisation of the receptors at both endogenous and overexpression levels in cancer cells. They also open the way to discovering new agonists and antagonists for these two important receptors by allowing testing new compounds without fluorescent tags. The distance and orientation constraints of NanoBRET are advantageous in characterising/validating these fluorescent probes with respect to their affinity and selectivity. These data show that the fluorescent ligand CXCL12-green can bind to both CXCR4 and ACKR3 receptors with high nanomolar affinity; however, ACKR3 showed higher affinity than CXCR4 as seen in a previous study (Gustavsson et al., 2019). The previous BRET ligand binding observations from (White et al., 2020a) using CXCL12-red showed pK<sub>d</sub> of  $7.15 \pm 0.04$  (K<sub>d</sub> = 72.1 nM) binding at CRISPR-Cas9 edited NLuc\_CXCR4 HEK293 cells were comparable to our results with CXCL12-green  $7.19 \pm 0.13$  pK<sub>d</sub> (K<sub>d</sub> = 78.8 nM) HEK293 cells exogenously expressing NLuc\_CXCR4. The two important points here that the green and red labelled CXCR4 are comparable although they have different fluorescent labels. And

the second point is CRISPR-Cas9 edited endogenously expressing CXCR4 cells have a similar binding affinity result as overexpressed CXCR4. This illustrates the sensitivity of NanoBRET as it would be difficult to quantify binding at endogenous receptor levels from changes in fluorescent values alone. CXCL12 binding at NLuc\_ACKR3 for CXCL12-green was  $8.52 \pm 0.10$  pK<sub>d</sub> (K<sub>d</sub> =  $3.3 \pm 0.8$  nM) comparable with (CXCL12-red) binding  $8.12 \pm 0.10$  pK<sub>d</sub> from (White et al., 2020a). The unlabelled orthosteric antagonists IT1t and AMD3100 competed with CXCL12-green for binding to CXCR4. The observed equilibrium dissociation constants were AMD3100 (pK<sub>i</sub> =  $6.8 \pm 0.08$ ) and IT1t (pK<sub>i</sub> =  $7.6 \pm 0.1$ ).

The production and purification of peptide ligands like CXCL12 is expensive. Instead, synthesis of small molecule inhibitors is cost efficient. Hence, here we have studied novel BODIPY 630/650-X conjugated CXCR4 antagonists. Compound 10 (IT1t based), and 24 (AMD070 based) maintained their affinity toward the CXCR4 receptor even though fluorophore attached to them almost double the size of the molecules. IT1t is an isothioureia CXCR4 antagonist (Thoma et al., 2008), which is highly potent (IC<sub>50</sub> = 8.0 nM), displaying excellent bioavailability and in vivo activity. IT1t binds to a relatively shallow part of the orthosteric binding pocket of CXCR4, mainly at the minor subpocket, compared to the endogenous ligand CXCL12 or to AMD3100 (Meng et al., 2023). The IT1t-based compound 10 showed selective binding at NLuc\_CXCR4 with an affinity of pK<sub>d</sub> =  $6.54 \pm 0.05$  and could be displaced by unlabelled IT1t and AMD3100 in intact HEK293 cells. Previous results (Dekkers et al., 2023) showed compound 10 had a higher affinity to NLuc\_CXCR4 (pK<sub>d</sub> =  $7.01 \pm 0.11$ ) in purified membranes prepared from NLuc\_CXCR4 expressing HEK293 cells. In contrast to our results, AMD3100 could not fully compete with compound 10 in purified membranes (Dekkers et al., 2023), while we have shown that both AMD3100 and IT1t completely displaced compound 10 (Dekkers et al., 2023). This might suggest that in intact cells, the membrane dynamics alter the competitive properties of AMD3100, which might lead to a non-competitive interaction resembling allosterism. Furthermore, while compound 10 reaches saturation at a concentration approximately 0.5 μM in purified membranes (Dekkers et al., 2023), this effect was not seen until concentrations above 1 μM in intact cells. Recent docking studies have shown that AMD070 mainly binds to minor subpockets on CXCR4 and shows binding modes similar to that observed for IT1t (Meng et al., 2023). BODIPY-630/650-X conjugated AMD070 ligand 24 also

showed clear specific binding at CXCR4. IT1t almost entirely displaced 24, while AMD3100 partially competed with it in intact cells and purified membranes (Dekkers et al., 2023). Similar to 10, compound 24 reached saturation at about 0.5  $\mu\text{M}$  in purified membranes (Dekkers et al., 2023), whereas this was at concentrations above 1  $\mu\text{M}$  in intact cells.

Additionally, we have studied small molecules targeting ACKR3. Fluorescent conjugates of VUF11207 (Wijtmans et al., 2012) labelled with BODIPY FL-X with linkers of three different lengths, with PEG chains ranging from 0 to 2 were tested. The three fluorescent conjugates produced clear saturable specific binding to the ACKR3 receptor associated with low levels of non-specific binding. The binding affinity of ligands determined for 18a, 18b and 18c were  $\text{pK}_d = 7.8 \pm 0.009$  ( $K_d = 12.6 \pm 0.2$ ),  $\text{pK}_d = 7.09 \pm 0.01$  ( $K_d = 81 \pm 2.7$ ),  $\text{pK}_d = 6.8 \pm 0.03$  ( $K_d = 150 \pm 10.7$ ) respectively. Since it has been known that the length of the linker influences ligand binding (Baker et al., 2010b; Stoddart, Kilpatrick, et al., 2015a), ligand 18a, which has the shortest linker, seems to have the highest binding affinity. Accordingly, 18a was therefore used for further ligand binding experiments to test the affinity of a panel of unlabelled ligands with different binding modes. Compounds 4, 9, 19 and 20 were shown to be fully competitive at higher concentrations with 18a.

### **3.4 Conclusion**

Expanding the CXCR4 and ACKR3 receptor toolkit was one of the primary objectives of our study. Nevertheless, the novel fluorescent ligands developed in this study can be used as probes in future screening assays for novel small molecule agonists and antagonists targeting CXCR4 or ACKR3. To extend the utilization of both CXCR4 (Figure 6 in (Dekkers et al., 2023)) and ACKR3 (Figure 4 in (Dekkers et al., 2024)) fluorescent ligands, they were used for confocal imaging successfully.

**Chapter 4: NanoBRET  
studies to investigate the  
binding of EGFR  
ligands/nanobodies and  
agonist-induced  
conformational changes of  
EGFR**

## 4.1 Introduction

The epidermal growth factor receptor (EGFR), also called ErbB1 or HER1, is a member of the RTK family on the cell surface. It is a crucial receptor for targeted therapies in several cancers, such as lung and brain cancers (Jorissen et al. 2003). The human EGFR contains 1186 amino acids (170-kDa mass)(Zhen et al., 2003). The extracellular protein region consists of four domains (I–IV) (Ogiso et al., 2002b) (Burgess, 2008a). A crystal structure of EGFR indicated EGF docking occurs at the extracellular domains of EGFR within domains I–III, which adopt a C shape conformation; thus, EGF binding leads to a conformational change (Ogiso et al., 2002b). EGF binding to extracellular domains I and III leads to a conformational change that exposes a dimerisation interface in domain II (Freed et al., 2017).

EGFR binds to several growth factors grouped as high-affinity binding ligands, which are epidermal growth factor (EGF), transforming growth factor- $\alpha$  (TGF $\alpha$ ), betacellulin (BTC), and heparin-binding EGF-like growth factor (HB-EGF), and the low-affinity ligands are epiregulin, epigen and amphiregulin which bind 1 to 10 fold more weakly to EGFR (Jones et al., 1999)(Freed, 2017a) (Burgess, 2008a).

Human immunoglobulins consist of paired heavy and light chains (~150 kDa) (Bannas et al., 2017b). Camelid and shark species produce heavy chain-only antibodies which do not contain light chains (HCAbs) (~80 kDa) (Cheloha et al., 2020)(Conrath et al., 2003). The VHHs (variable domain for heavy chain of heavy chain antibody) named nanobodies are single domain antibody fragments (~15 kDa) that contain variable regions capable of recognising different epitopes (Muyldermans, 2021). There are some pre-existing heavy-chain antibodies targeting EGFR (Roovers et al., 2007), developed by different groups for several purposes, such as monitoring EGFR oligomerisation (Hofman et al., 2010a), tumour imaging (Piramoon et al., 2017), tumour growth inhibitor (Roovers et al., 2007) and determination of conformational status (Nevoltris et al., 2015a) (Sharifi et al., 2021). Different nanobodies have been discovered that bind to a similar site to EGF on the receptor that compete with EGF (Hofman et al., 2008a)(Schmitz et al., 2013a) and others that bind to EGFR but do not compete for EGF binding and do not activate the receptor (Hofman et al., 2008a) (Low-Nam et al., 2011a). One such EGFR nanobody is EgB4 that has been used to discover movements of the extracellular domains of EGFR in conjunction with a fluorescent membrane dye (Zanetti-Domingues et al., 2018).

---

Discovery of the nanobodies is one of the recent breakthroughs for the targeted cancer treatment with antibodies. Hence, understanding the pharmacology of nanobodies targeting EGFR a very prominent receptor in several cancer is imperative for the field. In this chapter, we have used N-terminal nanoluciferase-tagged EGFR and NanoBRET to investigate the pharmacological properties of a derivative of EgB4 fluorescently labelled with HiLyte 488 fluorophore (termed Q86c-HL488). Another fluorescent EGFR targeting nanobody, termed Q44c-HL488 was also used that bind to the EGF-binding site in a similar but not the same manner to the previously described 7D12 nanobody in (Schmitz et al., 2013b). This chapter aims to determine the binding properties of EGFR targeting nanobodies and natural EGFR ligands. The chapter has the following objectives:

- To gain insight into the binding properties of various EGFR ligands and nanobodies at stably transfected N-terminus tagged NLuc\_EGFR in HEK293 cells.
- To elucidate the binding interactions between nanobodies and EGFR ligands.
- To understand the suggested conformational sensor properties of the EGFR nanobody Q86.
- To quantify the binding affinities, kinetics and internalisation properties of the nanobodies Q44c or Q86c.

To achieve the objectives for this chapter, NanoBRET technology was used (see section [2.14](#)). For NanoBRET ligand and nanobody binding experiments, NanoLuc was engineered onto the N terminus of EGFR (full length receptor) ( **Figure 2.3**). The resulting construct (NLuc EGFR) was stably expressed in living HEK293 cells (ReLuc2P line) and purified membranes prepared from these cells (see section [2.11](#)) (**Figure 4.1**). NanoBRET saturation, displacement or kinetics experiments were then performed using fluorescently labelled EGF ligands (EGF-AlexaFluor488 (EGF-AF488) or EGF-AlexaFluor647 (EGF-AF647)) or fluorescently labelled EGFR targeting nanobodies (Q44c- HL488 and Q86c-HL488). A 11 amino acid fragment of NanoLuc, termed HiBiT was engineered onto the N terminus of EGFR. This construct was expressed in HEK293T cells and used for HiBiT internalisation assays to examine receptor internalisation (see section [2.17](#)).

---

## 4.2 Results

### 4.2.1 Expression and localisation of NLuc\_EGFR in HEK293 cells

Firstly, the expression level and localisation of NLuc\_EGFR stably expressed in HEK293 cells were determined with bioluminescence imaging using an Olympus LV200 (see [2.19](#)). This microscope collects the short emission from wavelengths of NLuc (460 nm) in a dark imaging chamber excluding external light. Cells were imaged immediately after furimazine addition to imaging chambers in the absence of any ligand. Bioluminescence imaging showed that NLuc\_EGFR expression was abundant, and predominantly localised on the cellular membrane even though a small amount of intracellular expression was also observed (**Figure 4.1**).

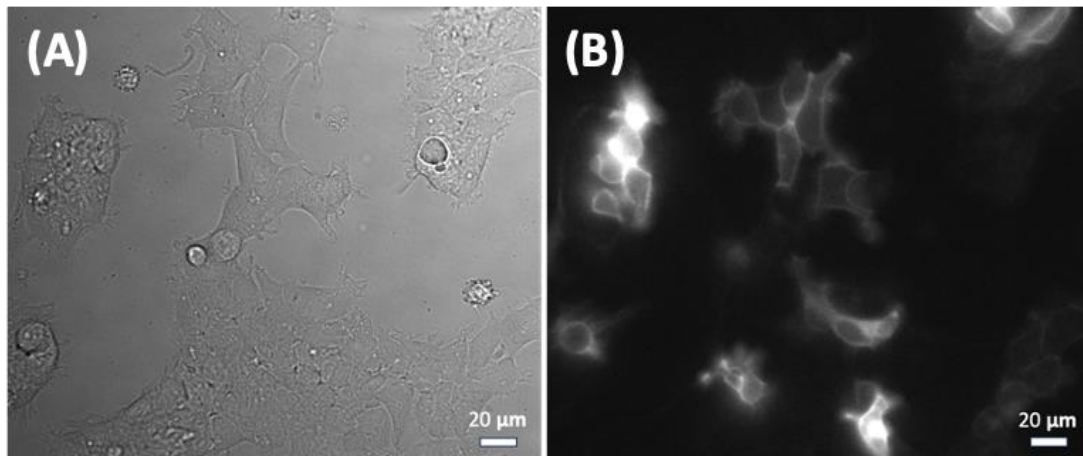


**Figure 4.1 Bioluminescence emission imaging of a stably transfected NLuc\_EGFR HEK293 cell line using an Olympus LV200.** HEK293 cells stably transfected with NLuc\_EGFR were plated on 25 mm<sup>2</sup> cellview glass-bottomed dishes. The following day, the NanoLuc substrate furimazine was added (1:500 dilution) in HBSS/0.2% BSA, and five minutes after furimazine addition, (A) bright-field and (B) live bioluminescence imaging was performed using an Olympus LV200 inverted microscope. Images are representative of 2 independent experiments.

### 4.2.2 Ligand and nanobody binding studies to NLuc\_EGFR

Initial experiments were performed to investigate the binding of fluorescently labelled EGF analogues to the N-terminal nanoluciferase tagged full-length EGFR (NLuc\_EGFR) receptor expressed in living HEK293 cells. NanoBRET saturation binding experiments showed that both EGF-AF488 (Alexa fluor 488®) and EGF-AF647 (Alexa Fluor 647 ®) exhibited saturable binding to the NLuc\_EGFR, which was displaceable by 100 nM unlabelled EGF (**Figure 4.2 A and C**). The mean  $K_d$  values obtained for EGF-AF488 and EGF-AF647 were  $2.30 \pm 0.09$  nM (n=5) and  $3.49 \pm 0.21$  nM (n=5) respectively. Additionally, the binding of EGF-AF488 (**Figure 4.2B**) and EGF-AF647 (**Figure 4.2D**) used in four different concentrations were efficiently inhibited by increasing concentrations of unlabelled EGF. The  $pK_i$  values for unlabelled EGF were  $9.35 \pm 0.02$  (n=5) and  $9.61 \pm 0.06$  (n=5) respectively.

Furthermore, binding of 3 nM of EGF-AF488 (**Figure 4.3A**) was potently inhibited by increasing concentrations of the unlabelled EGFR ligands EGF, Hb-EGF, and BTC (high-affinity binding ligands including TGF- $\alpha$ ). While TGF- $\alpha$  partially inhibited the binding of EGF-AF488, the inhibitory effect of EREG, AREG and Epigen (low-affinity ligands) was relatively minor. EGF-AF647 (**Figure 4.3B**) showed similar results with the same rank of potency, except no data was obtained for TGF- $\alpha$ . The rank order of potency of EGF>BTC=Hb-EGF>TGF can be seen in (**Table 4.1**).

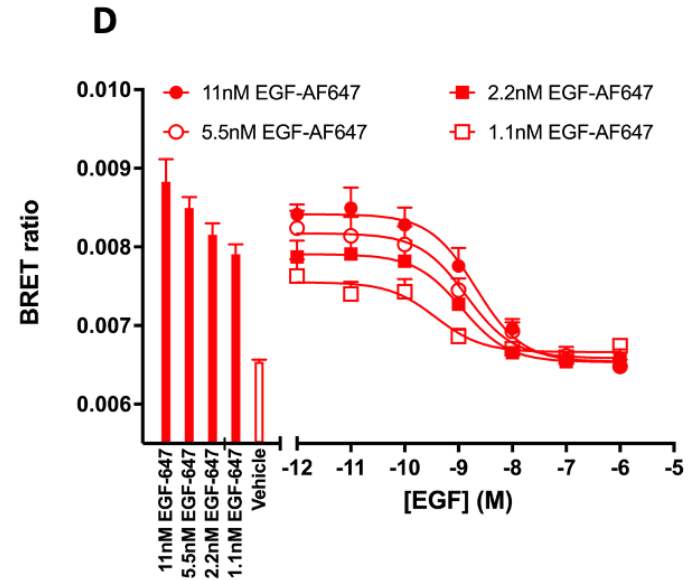
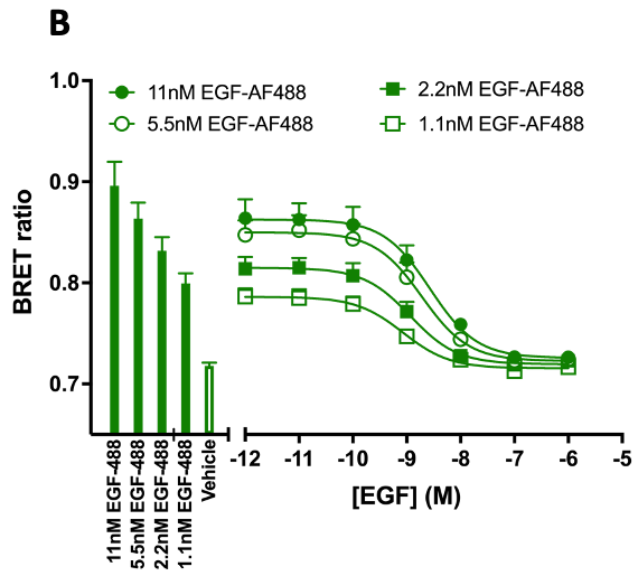
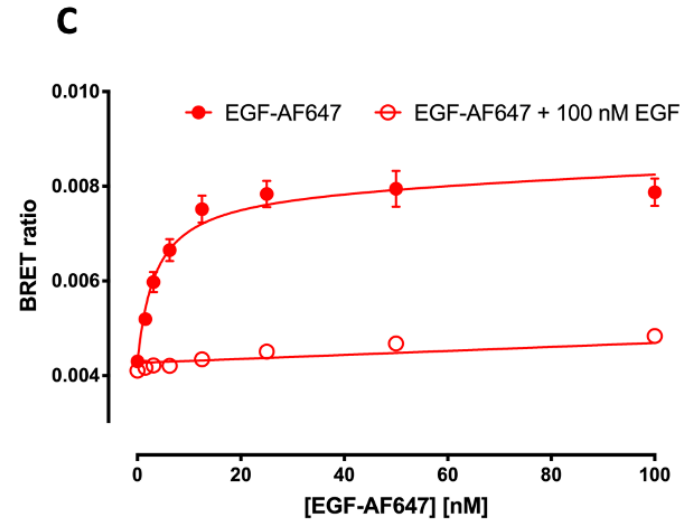
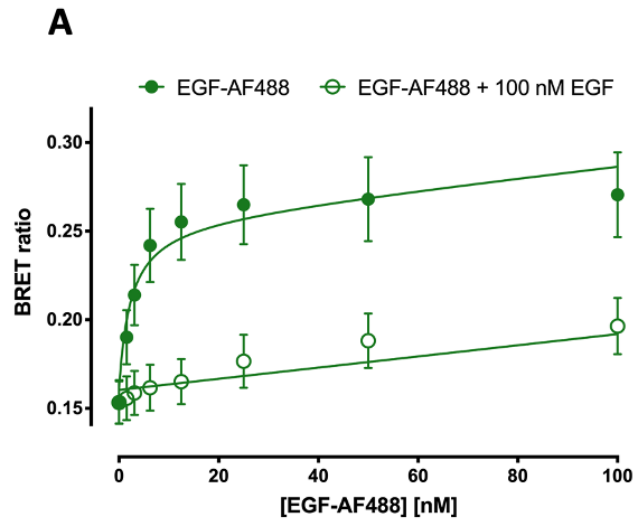


**Figure 4.2 Quantification of fluorescent EGF binding to HEK293 cells stably expressing a full-length N-terminal nanoluciferase tagged EGFR (NLuc\_EGFR) measured using NanoBRET.** Saturation binding of fluorescently labelled (A) EGF-AF488 and (C) EGF-AF647 in the absence (closed circles) or presence (open circles) of 100 nM unlabelled EGF added simultaneously and incubated for 30 minutes at 37°C. Saturation experiments were performed in HBSS containing 0.2 % BSA. Displacement experiments using fixed concentrations of (B) EGF-AF488 or (D) EGF-AF647 by increasing concentrations of unlabelled EGF. Both ligands were added simultaneously, and cells were incubated for 60 minutes at 37°C. The NLuc substrate furimazine (1/400 final dilution) was added, and the plates were incubated for 5 minutes. Then, luminescence and fluorescence emissions were measured using a BMG Pherastar FS. Displacement experiments were performed in HBSS containing 0.1 % BSA. Closed bars represent fluorescent EGF alone, with open bars representing vehicle (HBSS/0.1% BSA). Data are combined mean  $\pm$  SEM from five independent experiments, where each experiment was performed in triplicate.

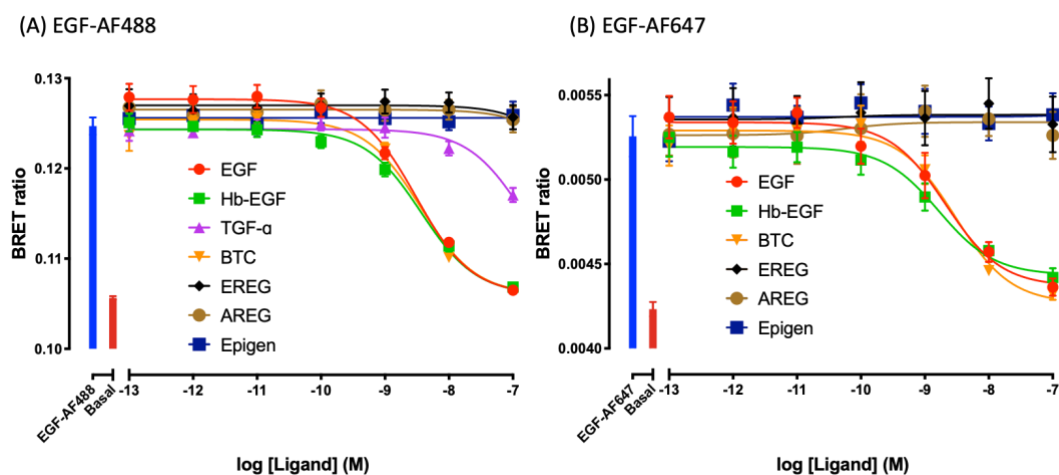


**Figure 4.3 Effect of unlabelled EGFR ligands on the binding of fluorescently labelled EGF.** N-terminal NLuc\_EGFR stably expressed in HEK293 cells were simultaneously treated with unlabelled and EGF-AF488 (A) or EGF-AF647 (B) ligands incubated for 30 minutes at 37°C. Experiments were performed in HBSS containing 0.2 % BSA. The NLuc substrate furimazine (1/400 final dilution) was added, and plates were incubated for 5 minutes. Then, luminescence and fluorescence emissions were measured using a BMG Pherastar FS. Blue bars represent BRET ratios obtained for total EGF-AF488 or EGF-AF647 in the absence of competing ligands, whereas red bars represent those measured for HBSS/0.2% BSA buffer alone (basal). Data are combined mean  $\pm$  SEM from five independent experiments for EGF-AF488 and four independent experiments for EGF-AF647 where each experiment was performed in triplicate.

The next step was to determine the displacement of fluorescently labelled EGF by increasing concentrations of unlabelled Q44c and Q86c EGFR nanobodies. The displacement experiments would help us to test whether the EGF binding is displaced by the unlabelled nanobodies, hence the overlap between binding regions of EGF and nanobodies. Q44c was able to potently displace the binding of both 3 nM EGF-AF488 ( $pIC_{50} = 8.63 \pm 0.05$ ,  $n=5$ ; **Figure 4.4A**) and 3 nM EGF-AF647 ( $pIC_{50} = 8.61 \pm 0.15$ ,  $n=5$ ; **Figure 4.4B**). However, there was no significant effect of Q86c on the binding of EGF-AF488 (**Figure 4.4A**) or EGF-AF647 (**Figure 4.4B**). Consistent with previous data (**Figure 4.3**), increasing concentrations of unlabelled EGF was able to displace both EGF-AF488 (**Figure 4.4A**) or EGF-AF647 (**Figure 4.4B**)

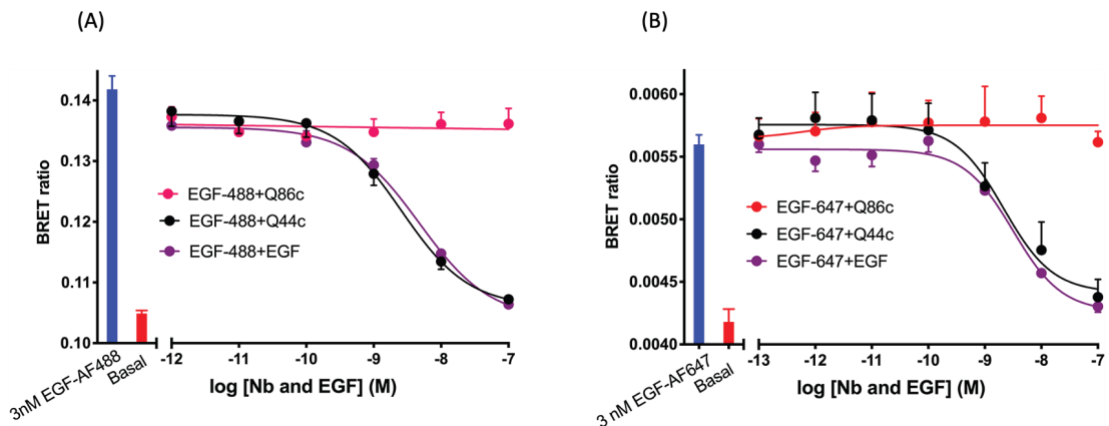


**Figure 4.4 Displacement of fluorescently labelled EGF by unlabelled EGFR nanobodies.** (A) EGF-AF488 (3 nM) or (B) EGF-AF647 (3 nM) displacement by unlabelled-EGFR nanobodies Q44c, Q86c or unlabelled EGF. NanoBRET experiments were performed using HEK293 cells stably expressing full-length N-terminal NLuc\_EGFR. Fluorescently labelled EGF and competing unlabelled ligands were added simultaneously and incubated for 30 minutes at 37°C. Experiments were performed in HBSS containing 0.2% BSA. The NLuc substrate furimazine (1/400 final dilution) was added, and plates were incubated for 5 minutes. Then, luminescence and fluorescence emissions were measured using a BMG Pherastar FS. Blue bars represent BRET ratios obtained for total EGF-AF488 or EGF-AF647 binding in the absence of competing ligands, whereas red bars represent those measured for HBSS/0.2% BSA buffer alone (basal). Data are combined mean  $\pm$  SEM from five independent experiments, where each experiment was performed in triplicate.

Next, saturation binding experiments were used to test the binding ability of fluorescently labelled Q44c-HL488 (HiLyte Fluor488; HL488) and Q86c-HL488 (HiLyte Fluor488; HL488) to NLuc\_EGFR in live HEK293 cells or purified membranes from stably transfected NLuc\_EGFR HEK293 cells. Both labelled nanobodies were successfully able to bind to NLuc\_EGFR. The ligand binding analysis showed that there was both a saturable component of specific binding and a linear component of non-specific binding and revealed  $K_d$  values of  $14.94 \pm 1.04$  nM ( $n=5$ ) and  $3.21 \pm 1.10$  nM ( $n=5$ ) for Q44c-HL488 and Q86c-HL 488 respectively (**Figure 4.5A and B**) for whole cells experiments. For purified membrane experiments, the  $K_d$  values obtained for Q44c-HL488 and Q86c-HL488 from this analysis were  $10 \pm 2$  nM and  $4.54 \pm 0.9$  (**Figure 4.6A and B**). The specific binding of Q44c-HL488 was inhibited by EGF (100 nM) (**Figure 4.5A**). In contrast, the specific binding of Q86c-HL488 was significantly increased ( $437.6 \pm 57.3$  %,  $n=5$ ) in the  $B_{MAX}$

value ( $p < 0.005$ ; paired t-test) by EGF stimulation compared to no EGF stimulation (**Figure 4.5B**). In addition, the  $K_d$  value of Q86c-HL488 obtained in the presence of 100 nM EGF was slightly decreased ( $1.18 \pm 0.28$  nM,  $n=5$ ) in whole HEK293 cells (**Figure 4.5B**) and ( $3.73 \pm 0.8$  nM,  $n=5$ ) in purified membranes (**Figure 4.6B**).

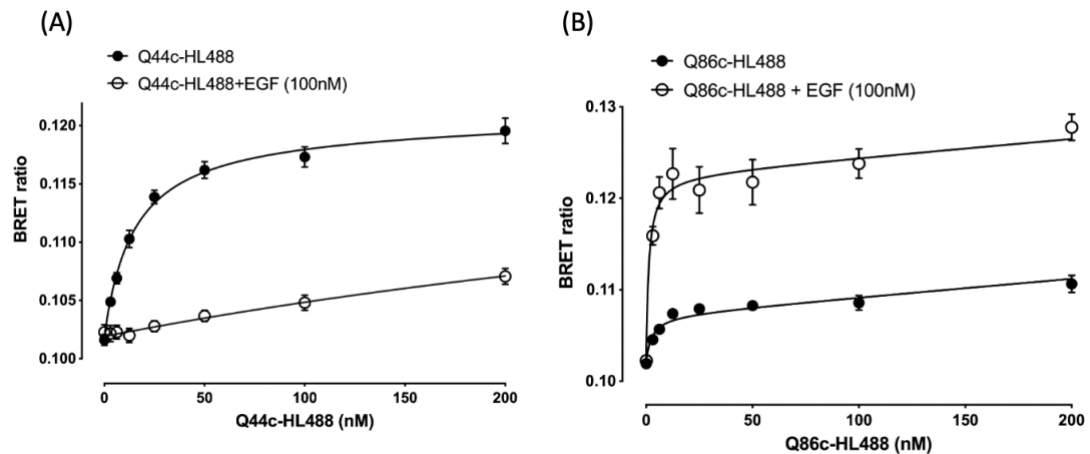


**Figure 4.5 Saturation binding of HiLyte™ 488 fluorescently labelled EGFR nanobodies performed in live cells.** Saturation binding of (A) Q44c-HL488 or (B) Q86c-HL488 in live HEK293 cells stably expressing NLuc EGFR in the absence (closed circles) or presence (open circles) of 100 nM EGF. Nanobodies and EGF were added simultaneously and incubated for 30 minutes at 37°C. NanoBRET experiments were performed in HBSS containing 0.2 % BSA. The NLuc substrate furimazine (1/400 final dilution) was added, and plates were incubated for 5 minutes. Then, luminescence and fluorescence emissions were measured using a BMG Pherastar FS. Data are combined mean  $\pm$  SEM from five independent experiments, where each experiment was performed in triplicate.

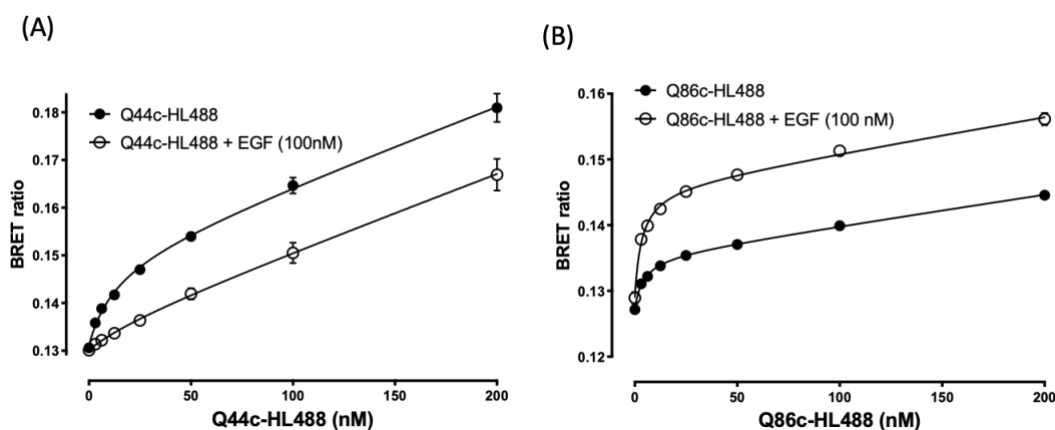


**Figure 4.6 Saturation binding of HiLyte™ 488 fluorescently labelled EGFR nanobodies performed on purified cell membranes prepared from HEK293 cells.** Saturation binding of (A) Q44c-HL488 or (B) Q86c-HL488 in membranes purified from HEK293 cells stably expressing NLuc EGFR in the absence (closed circles) or presence (open circles) of 100 nM EGF. Nanobodies and EGF were added simultaneously and incubated for 30 minutes at 37°C. NanoBRET experiments were performed in HBSS containing 0.2 % BSA. The NLuc substrate furimazine (1/400 final dilution) was added, and plates were incubated for 5 minutes. Then, luminescence and fluorescence emissions were measured using a BMG Pherastar FS. Data are combined mean  $\pm$  SEM from five independent experiments, where each experiment was performed in triplicate.

Next, the ability of EGFR ligands to displace fluorescently labelled nanobodies was studied. A very similar rank order of potency was obtained with unlabelled EGFR ligands (**Figure 4.7**) for their inhibition of Q44c-HL488 (**Figure 4.7A** and **Table 4.1**). Surprisingly an enhancement of the specific binding of Q86c-HL488 to NLuc\_EGFR (**Figure 4.7B** and **Table 4.1**) in presence of all EGFR ligands was observed. The rank order of potencies was comparable to that obtained from inhibition of the binding of 3 nM EGF-AF488 and EGF-AF647 (**Table 4.1**). However, the actual  $EC_{50}$  and  $IC_{50}$  values for modulating the binding of both Q44c-HL488 and Q86c-HL488 were generally at lower concentrations than the  $pK_i$  value calculated from displacement of EGF-AF488 and EGF-AF647 binding (**Table 4.1**). This was most marked for TGF- $\alpha$  (when using EGF-AF488 as a probe) and suggests that the  $EC_{50}$  and  $IC_{50}$  values also relate to agonist efficacy and the consequences of suggested conformational changes that occur with receptor activation

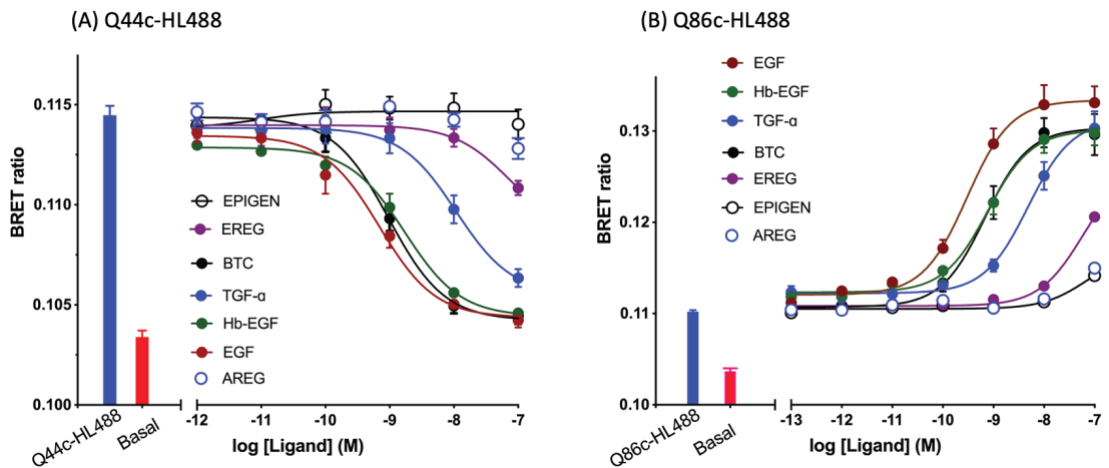


**Figure 4.7 Effect of EGFR ligands on the binding of fluorescently labelled EGFR nanobodies.** Effect of EGFR ligands on the binding of fluorescent (A) Q44c-HL488 (14.6 nM) or (B) Q86c-HL488 (12.5 nM) to full-length N-terminal NLuc\_EGFR stably expressed in HEK293 cells. Cells were treated with either nanobody and EGFR ligands simultaneously and incubated for 30 minutes at 37°C. Experiments were performed in HBSS containing 0.2 % BSA. The NLuc substrate furimazine (1/400 final dilution) was added, and plates were incubated for 5 minutes then, luminescence and fluorescence emissions were measured using a BMG Pherastar FS. Blue bars represent BRET ratios obtained for total Q44c-HL488 or Q86c-HL488 in the absence of competing ligand, whereas red bars represent those measured for HBSS/0.2% BSA buffer alone (basal). Data are combined mean  $\pm$  SEM from five independent experiments, where each experiment was performed in triplicate.

**Table 4.1** pIC<sub>50</sub> and pEC<sub>50</sub> values for the effect of EGFR ligands on the binding of 14.6 nM Q44c-HL488, 12.5 nM Q86c-HL488, 3 nM EGF-AF488 and 3 nM EGF-AF647 to full-length N-terminal NLuc\_EGFR in living HEK293 cells. The number of experiments is shown in parenthesis.

<b>EGFR Ligand</b>	<b>Q44c-HL488 (pIC<sub>50</sub>)</b>	<b>Q86c-HL488 (pEC<sub>50</sub>)</b>	<b>EGF-AF488 (pKi)</b>	<b>EGF-AF647 (pKi)</b>
<b>EGF</b>	9.23 ± 0.11 (n=5)	9.52 ± 0.06 (n=5)	8.86 ± 0.07 (n=5)	9.05 ± 0.21 (n=5)
<b>Hb-EGF</b>	8.80 ± 0.13 (n=5)	9.20 ± 0.17 (n=5)	8.43 ± 0.08 (n=5)	8.87 ± 0.16 (n=5)
<b>TGF-α</b>	7.96 ± 0.19 (n=5)	8.32 ± 0.09 (n=5)	6.83 ± 0.05 (n=5)	-
<b>BTC</b>	9.02 ± 0.14 (n=5)	9.17 ± 0.09 (n=5)	8.45 ± 0.05 (n=5)	8.51 ± 0.06 (n=5)

Moreover, NanoBRET kinetics assays were performed to observe the binding dynamics of the fluorescently labelled nanobodies in time course manner in real time to help us to understand the timing of the nanobody binding at EGFR. Hence, the kinetics NanoBRET experiments showed that fluorescently labelled EGFR nanobodies Q44c-HL488 (**Figure 4.8A**) or Q86c-HL488 (**Figure 4.8B**) were able to bind NLuc\_EGFR in 7 different concentrations. BRET ratios were read for 100 minutes. (Here, timepoints -10 to 0 represents the BRET reads before the labelled nanobodies added in wells. At timepoint 0, fluorescently labelled nanobodies were added.) Higher concentrations of labelled nanobodies showed faster and more potent binding profiles. Both labelled nanobodies established fast peaks, less than 5 minutes from the start point of either nanobody being added to the plate. This was followed by a decline in BRET ratios for both fluorescently labelled nanobodies, which was more pronounced for Q86c-HL488 (**Figure 4.8B**). This may suggest a time-dependent

change in receptor conformation induced by Q86c-488 that leads to a decrease in energy transfer or that this nanobody may be inducing EGFR internalisation.

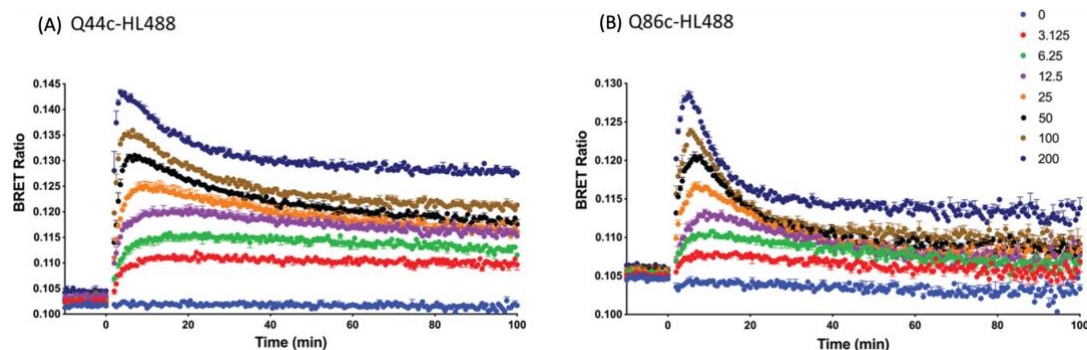


**Figure 4.8 Kinetics of fluorescently labelled EGFR nanobodies by NanoBRET.** Kinetic NanoBRET experiments showing the binding of different concentrations of fluorescent (A) Q44c-HL488 or (B) Q86c-HL488 to full-length N-terminal NLuc\_EGFR expressed in living cells. The concentrations of Q44c-HL488 and Q86c-HL488 are given in nM. HEK293 cells stably expressing NLuc\_EGFR were treated with furimazine (1/400 final dilution), and luminescence and fluorescence values were read for 15 minutes (every 60 sec) at 37°C using a BMG Pherastar FS. Experiments were performed in HBSS containing 0.2 % BSA. Following this period, cells were treated with various concentrations of either fluorescent nanobody, and the luminescence and fluorescence emissions were simultaneously recorded for a further 100 min at 37°C. Data are mean  $\pm$  SEM from triplicate determinations in a single experiment. This single experiment is representative of five independent experiments performed.

Furthermore, various concentrations of unlabelled EGF were added 30 min after the initial addition of Q44c-HL488 (**Figure 4.9A**), or Q86c-HL488 (**Figure 4.9B**). These data showed a decrease in BRET ratios for Q44c-HL488 following the addition of unlabelled EGF. Conversely, an increase in BRET was observed for Q86c-HL488 following EGF addition. These changes in BRET were EGF concentration dependent as higher concentrations of EGF had a more prominent effect on the BRET measured between the NLuc EGFR and either labelled nanobody. This effect of EGF on the increase on Q44c-HL488 binding and decrease on Q86c-HL488 binding was comparable in kinetics experiments as well.

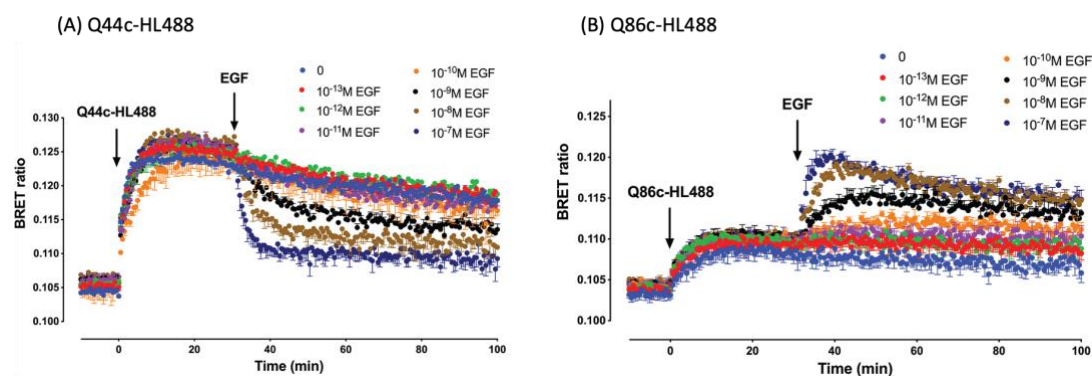


**Figure 4.9 Kinetics of EGF-induced changes in the NanoBRET signal of fluorescently labelled EGFR nanobodies in live HEK293 cells.** BRET signal obtained with fluorescent (A) Q44c-HL488 or (B) Q86c-HL488 binding to NLuc\_EGFR. HEK293 cells stably expressing N-terminal NLuc\_EGFR were treated with furimazine (1/400 final dilution), and luminescence and fluorescence values were read for 15 minutes (every 60 sec) at 37°C using a BMG Pherastar FS. Following this period, cells were treated with 25 nM of either respective fluorescent nanobody and luminescence and fluorescence emissions were simultaneously recorded for a further 30 min at 37°C. After 30 minutes, various concentrations of EGF were added to the wells, and measurements continued for an additional 30 minutes at 37°C. Data are mean  $\pm$  SEM from triplicate determinations in a single experiment. This single experiment is representative of five independent experiments performed.

Similar kinetic experiments were performed on purified cell membranes prepared from HEK293 cells stably expressing NLuc EGFR and showed comparable results to those obtained in whole cell assays. The purified cell membranes were used to eliminate the internalisation of the receptors. Q44c-HL488 (**Figure 4.10A**) binding was decreased following the addition of unlabelled EGF at the 30 min timepoint. Conversely, Q86c-HL488 (**Figure 4.10B**) binding was increased after the addition of 100 nM unlabelled EGF. The higher concentrations of Q44c-HL488 and Q86c-HL488 exhibited larger changes in relative BRET ratios after EGF addition at minute 30. Like whole cell experiments, the BRET signal fell slowly during kinetics measurements.

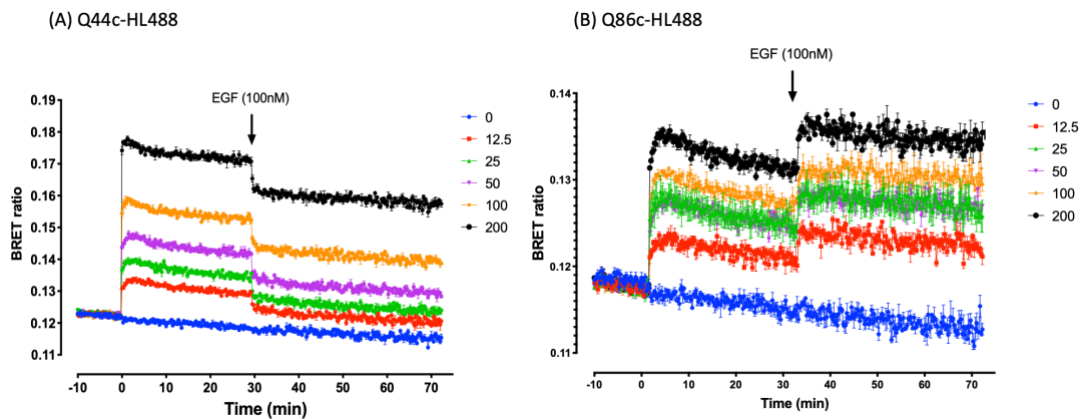


**Figure 4.10** Kinetics of EGF-induced changes in the NanoBRET signal of fluorescently labelled EGFR nanobodies on purified HEK293 cell membranes. BRET signal of association and dissociation phase curves of the binding of increasing concentrations of (A) Q44c-HL488 and (B) Q86c-HL488 (0–200 nM) added at time zero to HEK293T membranes overexpressing NLuc\_EGFR. Purified membranes were treated with furimazine (1/400 final dilution), and luminescence and fluorescence values were read for 15 minutes (every 60 seconds) at 37°C using a BMG Pherastar FS. At 30 min, 100 nM EGF was added, and the dissociation or association phase followed. Data are mean  $\pm$  SEM from triplicate determinations in a single experiment. This single experiment is representative of five independent experiments performed.

Even though Q44 and Q86 nanobodies bind to different sites on EGFR, the conformational change on EGFR due to ligand binding could influence the other ligands' binding at the receptor. To demonstrate potential binding interactions between Q44 and Q86, we performed competition binding experiments with fluorescently labelled Q44c-HL488 and Q86c-HL488 and unlabelled Q44c, Q86c and EGF. While Q44c has no effect on the binding of Q86c-HL488 to NLuc\_EGFR, Q86c competed with it. Similar to previous results, EGF enhanced Q86c-HL488 binding in both whole HEK293 cells stably expressing NLuc\_EGFR (**Figure 4.11B**) or purified membranes prepared from the same cells (**Figure 4.11D**). Q44c-HL488 binding was inhibited by unlabelled Q44c and EGF in both whole cells and purified membranes (**Figure 4.11 A and B**). In contrast, Q86c significantly ( $p < 0.05$ ; One-way ANOVA) increased Q44c-HL488 binding to NLuc\_EGFR in whole cells (**Figure 4.11A**), reminiscent of the effect of the low-affinity EGF ligands on the binding of Q86c-HL488 (**Figure 4.3B**).

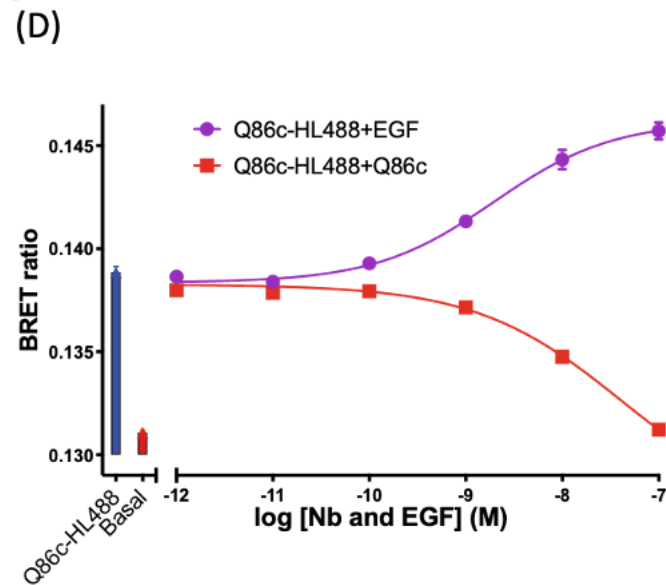
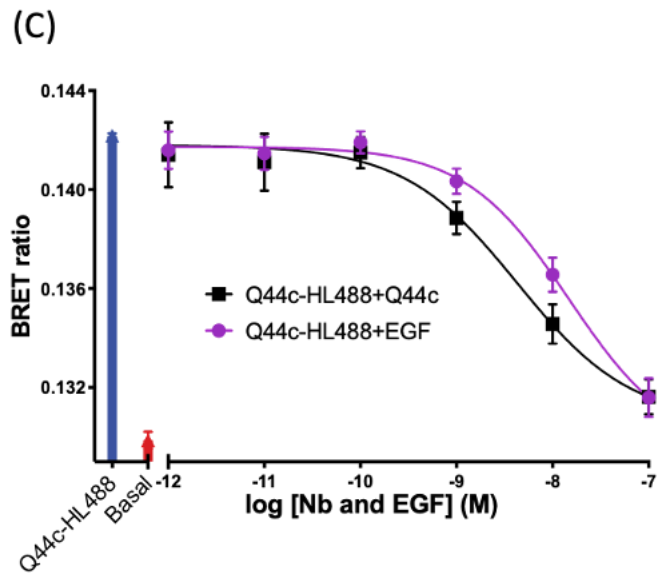
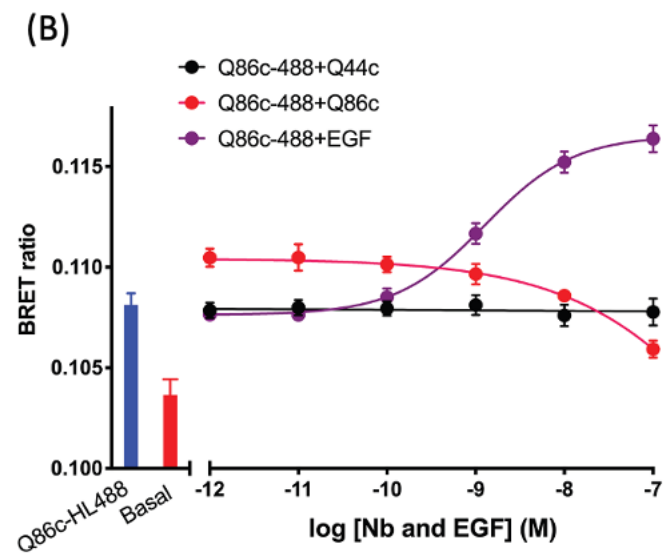
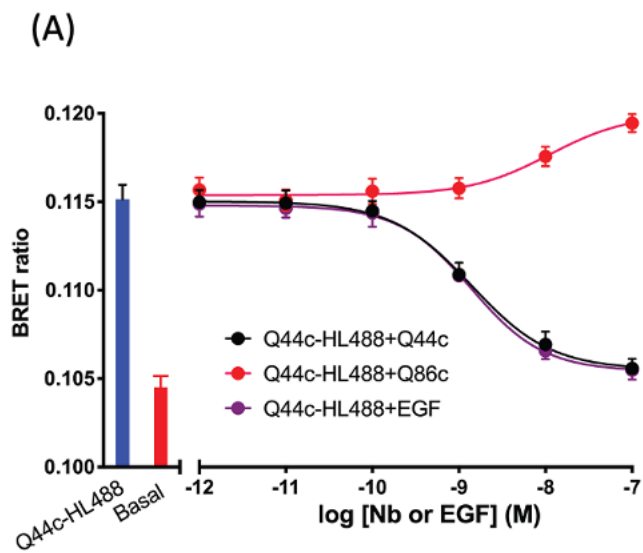


**Figure 4.11 The effect of unlabelled EGFR nanobodies and EGF on fluorescently labelled EGFR nanobodies.** The impact of Q44c, Q86c and EGF in live HEK293 cells stably expressing NLuc\_EGFR on the binding of fluorescent (A) Q44c-HL488 (14.6 nM) and (B) Q86c-HL488 (12.5 nM) and on purified cell membranes from HEK293 cells stably expressing NLuc\_EGFR (C) Q44c-HL488 (14.6 nM) and (D) Q86c-HL488 (12.5 nM). Cells/purified membranes were treated with either nanobody or EGF simultaneously and incubated for 30 minutes at 37°C. The NLuc substrate furimazine (1/400 final dilution) was added, and plates were incubated for 5 minutes then, luminescence and fluorescence emissions were measured using a BMG Pherastar FS. Experiments were performed in HBSS containing 0.2 % BSA. Data are combined mean  $\pm$  SEM from five independent experiments, where each experiment was performed in triplicate.

### 4.2.3 Internalisation of EGFR by EGF nanobody binding

The reason for the decreasing trend in kinetics nanobody binding experiments (**Figure 4.8**) during time might be an indicator of the internalisation of the EGFR. To evaluate the internalisation of HiBiT\_EGFR via EGFR nanobodies Q44c and Q86c, and EGF, we performed a HiBiT internalisation assay by transiently transfecting HEK293 cells with HiBiT\_EGFR (Soave, Goulding, et al., 2020). The experimental setup of NanoBiT internalisation experiments was explained in detail in **Figure 2.7**. The luminescence signal is produced by LgBiT complementation. The internalisation of the HiBiT labelled receptor decreases the luminescence signal since LgBiT is not membrane permeable. The remaining luminescence signal is likely coming from the HiBiT tagged EGFR remaining on the cell surface. It is well known that EGF binding leads to EGFR internalisation (Henriksen et al., 2013; Tanaka et al., 2018); therefore, EGF was used as a positive control at 4 different time points (5,30, 60 and 120 minutes) for EGF and nanobody stimulation (Hofman et al., 2010b). EGF stimulation resulted in a significant decrease in cell surface HiBiT\_EGFR levels. However, incubation with either Q44c or Q86c nanobodies did not result in a significant decrease in luminescence at any time point of EGF stimulation indicative of no significant internalisation of EGFR at any time points (**Figure 4.12**). (Data produced by Laura E. Kilpatrick)

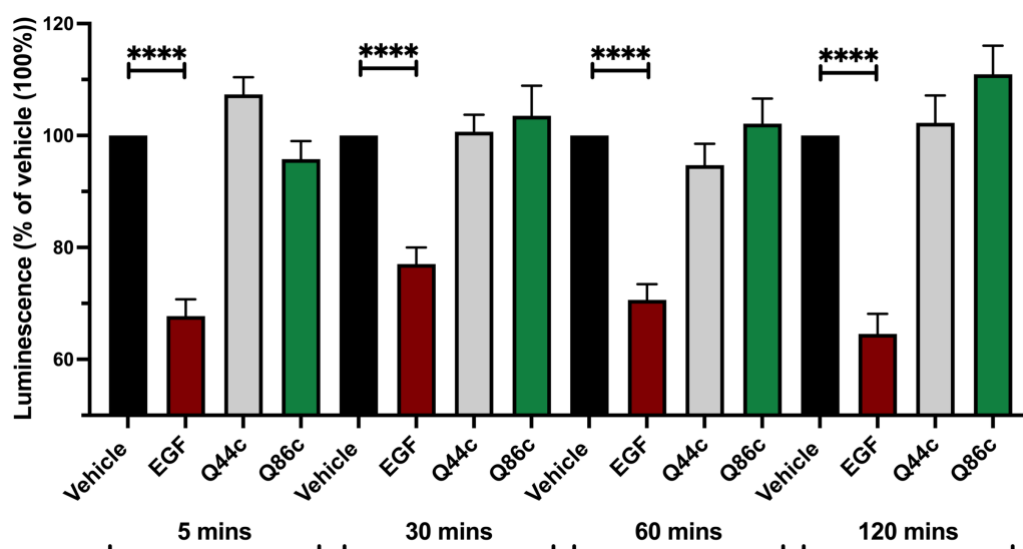


**Figure 4.12 Effect of unlabelled EGFR nanobodies and EGF on EGFR internalisation.**

The effect of Q44c, Q86c and EGF on HiBiT\_EGFR internalisation measured using NanoBiT. HEK293 cells transiently expressing HiBiT\_EGFR cDNA, were treated with EGF (100 nM), Q44c (100 nM) or Q86c (100 nM) in HBSS/0.02% BSA for 5, 30, 60 or 120 minutes at 37°C. Purified LgBiT (10 nM) and furimazine (1/400 dilution) were then added, and cells were incubated for a further 20 minutes at 37°C to allow NanoBiT re-complementation (leading to the formation of full-length nanoluciferase) and furimazine oxidation to occur. Luminescence emissions were then measured using a BMG Pherastar FS. Data are mean  $\pm$  SEM from quadruplicate observations in a single experiment pooled from 5 (120 minutes incubation) and 7 (5, 30, 60 minutes incubations) independent experiments. Data were normalised to vehicle controls (100%), and statistical significance determined using a one-way ANOVA (\*\*\*\* =  $P < 0.0001$ ).

### 4.3 Discussion

In this chapter, I used fluorescently labelled EGFR nanobodies and NanoBRET to study the binding modes of these nanobodies and ligands of EGFR. I have also examined the conformational alterations of EGFR driven by different endogenous ligands and these EGFR targeting nanobodies. One of the nanobodies, Q44c, has been shown previously to compete with EGF via binding to an epitope close to the EGF-binding site on domain III (Low-Nam et al., 2011; Schmitz et al., 2013b).

To investigate this, we have used N-terminal nanoluciferase-tagged EGFR (NLuc\_EGFR) in living cells and membrane preparations extracted from NLuc\_EGFR expressing cells along with fluorescently labelled EGFR ligands and two fluorescently labelled nanobodies termed Q44c-HL488 and Q86c-HL488. Q44c-HL488 showed high affinity binding to ligand-free EGFR in both living cells and purified membrane preparations with similar affinity values. Q44c-HL488 could be inhibited by 100 nM of EGF, however there was still a residual non-specific binding. The non-specific binding was higher in membrane preparations as expected likely because the fluorescent nanobodies has access to non-specific binding sites on the inside of the membrane leaflet in membrane preparations. Consistent with this, EGFR-AF488 and EGF-AF647 were displaced by 100 nM of Q44c in living cells. Additionally, a similar Q44c-HL488 displacement pattern by the high affinity (TGF $\alpha$ , BTC, HB-EGF) and low affinity (epiregulin, epigen and amphiregulin) EGFR ligands was observed in EGF-AF488 and EGF-AF647 displacement. Since high-affinity ligands potently prevent the binding of Q44c-HL488 (TGF- $\alpha$  shows slightly weaker potency), low-affinity ligands showed almost no inhibition except epiregulin which induced a small but significant displacement of Q44c-HL488 at 100 nM.

Nevertheless, Q44c-HL488 binding was inhibited by unlabelled Q44c in both living cells and membranes. Interestingly, incubation with unlabelled Q86c increased the binding of Q44c-HL488 to NLuc\_EGFR in living cells. This might suggest that this could be due to a conformational change of EGFR that is favourable for Q44c binding at its epitope on EGFR. Although Q86c does not change the binding affinity of EGFR, this is consistent with the previous studies showing that Q44c and EGF have a similar but not identical binding epitope/site on the EGFR domain III (Schmitz et al., 2013). This could be due to EGFR dimerization and that will be investigated in chapter 5.

In previous studies, Q86 (termed EgB4) has been shown not compete EGF binding to EGFR (Hofman et al., 2008)(Low-Nam et al., 2011). I observed similar results, whereby, fluorescent Q86c-HL488 could not be displaced by EGF. Conversely, the binding of Q86c-HL488 was increased (by 438%) in both whole cells and purified membrane preparations in the presence of EGF (**Figure 4.5** and **Figure 4.6**). This enhancement of Q86c-HL488 binding to EGF-bound EGFR was also observed for other EGFR ligands, with the high-affinity ligands (Hb-EGF, BTC and TGF- $\alpha$ ) being the most potent and low-affinity ligands epiregulin showing a modest enhancement in BRET ratios. Both epigen and amphiregulin produced very weak but observable increases in BRET ratios between NLuc EGFR and Q86c-HL488 at the highest ligand concentration used (100 nM). This might be due to conformational changes of EGFR by agonist binding that lead to exposure of the dimerisation interface in domain II promoting receptor homodimerisation (Bessman et al., 2014; Burgess et al., 2003; Dawson et al., 2005; Defize et al., 1989; Freed, 2017; Macdonald-Obermann & Pike, 2009). This is in keeping with the recent receptor X-ray crystal structures of Q86 (EgB4) alone and bound to the full extracellular EGFR-EGF complex in its extended active conformation (Zeronian et al., 2022). Consistent with this, Q86c did not compete with either EGF-AF488 or EGF-AF647 for binding to the EGFR, indicating that Q86c's epitope is not the same as the site of EGF binding. The other possible reason for the increase in BRET ratios observed with Q86c-HL488 with EGF stimulation, might be the orientation of the donor and acceptor moieties. This conformational change of EGFR might influence both the relative orientation and proximity of the donor and acceptor elements (Lay et al., 2022; Schihada et al., 2018). This change on the orientation and proximity of NLuc and fluorescent nanobody leads to increase energy transfer from the NLuc to fluorescent label of the nanobody resulting an increase on BRET signal. It can also be explained by the asymmetrical dimerisation of EGFR, which is created by low-affinity ligands and leads to different conformational changes in monomers (Freed, 2017). Moreover, this EGFR dimerisation might lead to an increased BRET signal between Q86c-HL488 and the N-terminal nanoluciferase on the opposing dimer monomer. Meaning that BRET signal cannot be assumed to be 1:1 (donor: acceptor) interaction particularly for a receptor that is known to dimerise. There is possibility for the fluorescent ligand to

interact with both monomers forming dimers which can cause an increase on BRET signal. That is also why we investigate the dimer formation on chapter 5.

To assess the time course of binding of Q44c-HL488 or Q86c-HL488 to NLuc EGFR we performed NanoBRET kinetic experiments. They showed a fast pronounced peak in the BRET ratio for both nanobodies, followed by a decline to a lower plateau (**Figure 4.8**). This decline could suggest that it might be caused by a conformational change of the receptor induced by the nanobodies. Alternatively, either nanobody may be inducing the internalisation of the EGFR after binding. Internalisation of the NLuc tagged receptors have the potential to decrease the BRET signal since internalised receptors can't transfer energy to the extracellularly localised ligands. That was shown previously with a parallel decline on VEGF binding on VEGFR2 in kinetics experiments and internalisation of VEGFR2 (Kilpatrick et al., 2017). The nanobody internalisation experiments indicated that none of the nanobodies led to EGFR internalisation in living cells. Additionally, the same decline in the BRET signal pattern detected in kinetic experiments using purified membranes expressing NLuc\_EGFR suggest that this drop might suggest that this could be due to possible conformational changes of the receptor induced by either nanobody that move the NLuc donor and acceptor further apart rather than internalisation.

Besides, EGF stimulation (30 minutes after the labelled nanobodies addition) marked that Q44c-HL488 was inhibited and Q86c-HL488 enhanced by EGF as expected. These results were comparable in profile to that observed with binding of Q44c-HL488 or Q86c-HL488, showing a similar fall to a lower plateau after an initial rapid peak in BRET. These data could also be explained by conformational change, internalisation of the receptor or the decay of the luminescence signal due to furimazine. The decay of the signal from the nanoluciferase due to furimazine can be seen in conditions with no labelled nanobodies or EGF stimulation. To eliminate this effect, long-lasting and more stable nanoluciferase substrates like endurazine (Ogrodzinski et al., 2023) might be used in future experiments. If it is conformational changes causing the decrease on BRET signal, it might be due to negative cooperativity, meaning that the binding of a ligand to one monomer of a dimer reduces the affinity of the other monomer for the same or different ligand (Ferguson et al., 2020; Freed, 2017; Macdonald-Obermann & Pike, 2009). This phenomenon may be reflected in our study as nanobody or EGF binding on one of the EGFR monomers

---

changes the conformation of the other monomer, reducing its ligand binding capacity and leading to a decrease in the BRET signal (asymmetrical dimers). Previous work has shown ligand-independent dimerisation of EGFR via their intracellular juxtamembrane domains (Macdonald-Obermann et al., 2012; Nevoltris et al., 2015; Yu et al., 2002). We have also shown ligand-independent dimerisation of NLuc\_EGFR-Halotag\_EGFR with BRET homodimerisation experiments in HEK293 cells (chapter 5). Negative cooperativity across the juxtamembrane dimer interface of ligand-independent dimers of EGFRs could also explain the complex kinetic profiles of the binding of Q44c-HL488 and Q86c-HL488 in the absence of EGF.

#### 4.4 Conclusion

- NanoBRET and NanoBiT technologies were used to detect the direct binding of fluorescently labelled EGFR nanobodies Q44c-HL488 and Q86c-HL488. Both nanobody was shown to bind to two different sites of the full-length EGFR receptor when expressed in whole cells or membrane preparations.
- Q44c is an EGF competitive nanobody suggesting overlap between its epitope and the EGF binding site found on domains I and III of the EGFR in a similar manner to 7D12 (Schmitz et al., 2013).
- Q86c does not compete with EGF; instead, the presence of EGF enhances Q86c binding to the EGFR (**Figure 4.13**).
- These data suggest that the binding of EGF and other EGFR ligands might cause a conformational change, leading to an enhanced binding of Q86c to the EGFR. Q86c can therefore be suggested to act as a conformational sensor for EGF ligand induced activation.

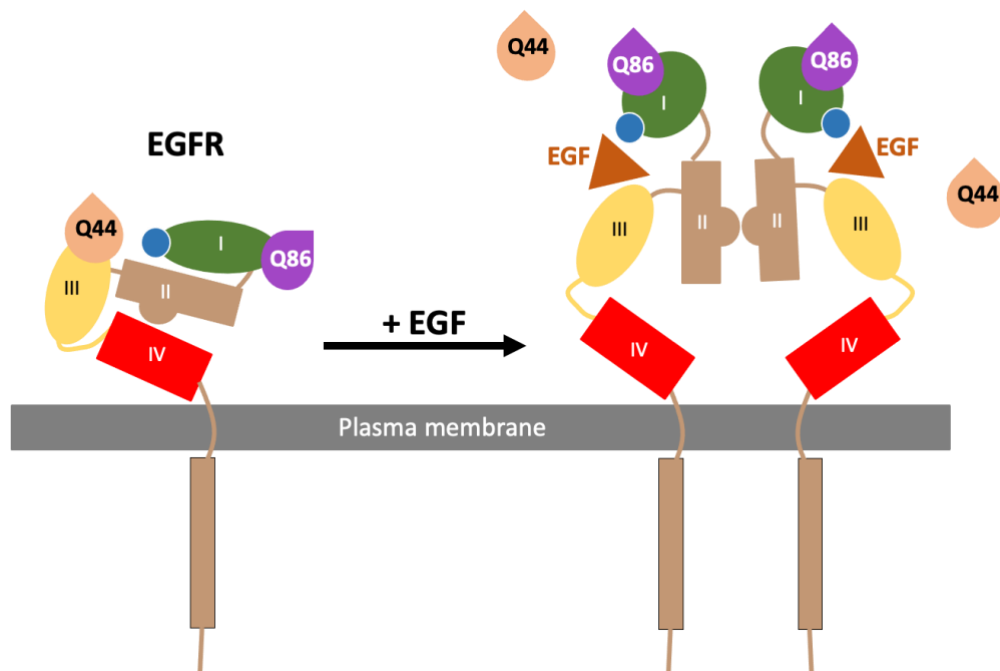


**Figure 4.13 Schematic of possible conformational change of EGFR and Q44, Q86 binding.** Q86 nanobody binds more to EGF bound conformation of EGFR. Nevertheless, Q44 nanobody competes with endogenous ligands of EGFR.

**Chapter 5: Determination  
of CXCR4/EGFR  
Homodimerisation and  
Heterodimerisation using  
NanoBRET**

## 5.1 Introduction

The crystal structures produced by Wu et al. (B. Wu et al., 2010a), suggest a symmetric dimer architecture for CXCR4 (**Figure 1.8**). There have been many studies demonstrating oligomerisation of CXCR4 using various techniques. Ligand independent homodimerisation of CXCR4 was demonstrated by co-immunoprecipitation (Babcock et al., 2003). BRET studies showed the dimerisation of CXCR4 with different expression levels (Armando et al., 2014; Percherancier et al., 2005). Single molecule imaging study suggested that CXCR4 is mostly monomeric at low expression state and oligomeric at high expression levels (Lao et al., 2017). Additionally, CXCR4 dimer formation has been shown with proximity based biotinylation (Steel et al., 2014), SPIDA (Işbilir et al., 2020; Ward et al., 2021), crystallization (B. Wu et al., 2010b) and cryo-EM (Saotome et al., 2024).

The epidermal growth factor receptor (EGFR) is a crucial receptor for targeted therapies in several cancers, such as lung and brain cancers (Jorissen et al. 2003). A crystal structure of EGFR indicated EGF docking occurs at the extracellular domains of EGFR within domains I–III, which adopt a C shape conformation; thus, EGF binding leads to a conformational change (Ogiso et al., 2002b). EGF binding between domain I and III breaks the tethered formation of domains II and IV leading to an extended formation of domain II. Extended domain II plays role as a dimerisation arm between two EGFR monomers' extracellular regions (Bessman, Bagchi, et al., 2014a). The ligand binding causes dimerisation of two monomers or alteration of pre-existing dimers. This dimerisation followed by proximity autophosphorylation starts a signal transduction cascade leading to activation of other downstream proteins creating cellular responses such as proliferation, survival and migration (Burgess, 2008a) (Ray et al., 2018). X-ray crystallography using purified extracellular domains of EGFR demonstrated the ligand-induced dimerisation of EGFR (Burgess, 2008b; Burgess et al., 2003). Although ligand binding has been shown to induce EGFR homodimerisation, pre-formed dimers have also been observed without ligand binding (Mudumbi et al., 2023). (Purba et al., 2022). (Tao & Maruyama, 2008).

There have been several studies showing the signalling cross-talk between CXCR4 and EGFR (Y. Cheng et al., 2020; M. Neves et al., 2020, 2022). Co-expression of CXCR4 and EGFR is associated with poor prognosis, aggressive phenotype, shorter

---

overall survival and disease-free survival rates in breast cancer (Cabioglu et al., 2007; Li et al., 2017) (Li et al., 2017) pancreatic ductal adenocarcinoma (H. Wu et al., 2015) and non-small cell lung carcinoma (Zobair et al., 2013) patients. Interestingly, transactivation of CXCR4 downstream mediators Gi protein activation by EGF and EGFR have been shown (M. Neves et al., 2020; Roy et al., 2024). Although there have been several studies focusing on CXCR4/EGFR expression profiles and their cross-talk in various cancer types, no study has elucidated specific heterodimerisation of CXCR4 and EGFR. In this chapter, we aim to investigate CXCR4/EGFR homodimerisation using bioluminescence resonance energy transfer approaches to monitor close proximity between the two different receptors expressed in living cells. Since these studies showed the significance of CXCR4 and EGFR, this complex can signal differently than its subcomponents. Hence EGFR/CXCR4 complex can be a target for novel cancer therapy. Therefore, this chapter aims to determine the homodimerisation and heterodimerisation dynamics of CXCR4/EGFR complex formation. The chapter has the following objectives:

- To elucidate the dynamics of CXCR4/EGFR homo and heterodimerisation.
- To gain insight into the effect of the binding of CXCR4 and EGFR receptor specific ligands and nanobodies on CXCR4/EGFR complexes.
- To detect the CXCR4/EGFR heterodimerisation at endogenous expression levels via BRET and proximity ligation assay (PLA).

To achieve the objectives for this chapter, NanoBRET technology was used (see section [2.13](#)). NanoBRET dimerisation assay was performed to determine homodimerisation and heterodimerisation of CXCR4/EGFR complexes. For this, HEK293T cells were transiently transfected with NLuc tagged receptors (donor) and fluorescently labelled SNAPTag/HaloTag receptors (acceptor). In this chapter, four different configurations were used. These configurations were: (A) NLuc\_CXCR4/SNAP\_CXCR4 for CXCR4 homodimerisation, (B) NLuc\_EGFR/Halo\_EGFR for EGFR homodimerisation, (C) NLuc\_CXCR4/Halo\_EGFR and (D) NLuc\_EGFR/SNAP\_CXCR4 for CXCR4/EGFR heterodimerisation. BRET ratios were calculated by dividing fluorescence emissions by luminescence emissions. Increase in BRET ratios were indicative of a close proximity/dimerisation of the two receptors. PLA experiments were performed as mentioned at section [2.23](#).

---

## 5.2 Results

### 5.2.1 Formation of CXCR4 and EGFR homodimers and heterodimers

Initially to test CXCR4 homodimerisation, we performed a NanoBRET assay using NLuc-tagged CXCR4 (NLuc\_CXCR4) and N-terminal SNAP tagged CXCR4 (SNAP\_CXCR4) (**Figure 5.1A**). A constant amount of NLuc\_CXCR4 cDNA (20 ng/well) and increasing concentrations of SNAP\_CXCR4 cDNA were transiently transfected into HEK293T cells. These experiments showed a saturable increase in BRET ratios indicating a specific NLuc\_CXCR4/SNAP\_CXCR4 homodimerisation (**Figure 5.1B**). The fluorescence intensity of SNAP\_CXCR4 was measured prior to the addition of the NLuc substrate furimazine. These measurements were performed to determine the transfection efficiency of SNAP\_CXCR4 between experiments. Additionally SNAP fluorescence increased linearly in parallel to increasing concentrations of SNAP\_CXCR4 cDNA added as expected. (**Figure 5.1C**).

EGFR homodimerisation was detected using the same NanoBRET system using NLuc-tagged EGFR (NLuc\_EGFR) and Halotag-labelled EGFR (Halo\_EGFR) constructs (**Figure 5.2A**). Similar to CXCR4 homodimerisation, HEK293T cells were transiently transfected with a constant amount of NLuc\_EGFR (20 ng cDNA/well) and increasing concentrations of Halo\_EGFR cDNA. Increasing concentrations of Halo\_EGFR showed a saturable BRET signal between NLuc\_EGFR/Halo\_EGFR indicative of homodimerisation (**Figure 5.2B**). A linear increase in fluorescence intensity with increasing amounts of Halo\_EGFR cDNA transfection was obtained confirming the transfection efficiency (**Figure 5.2C**).

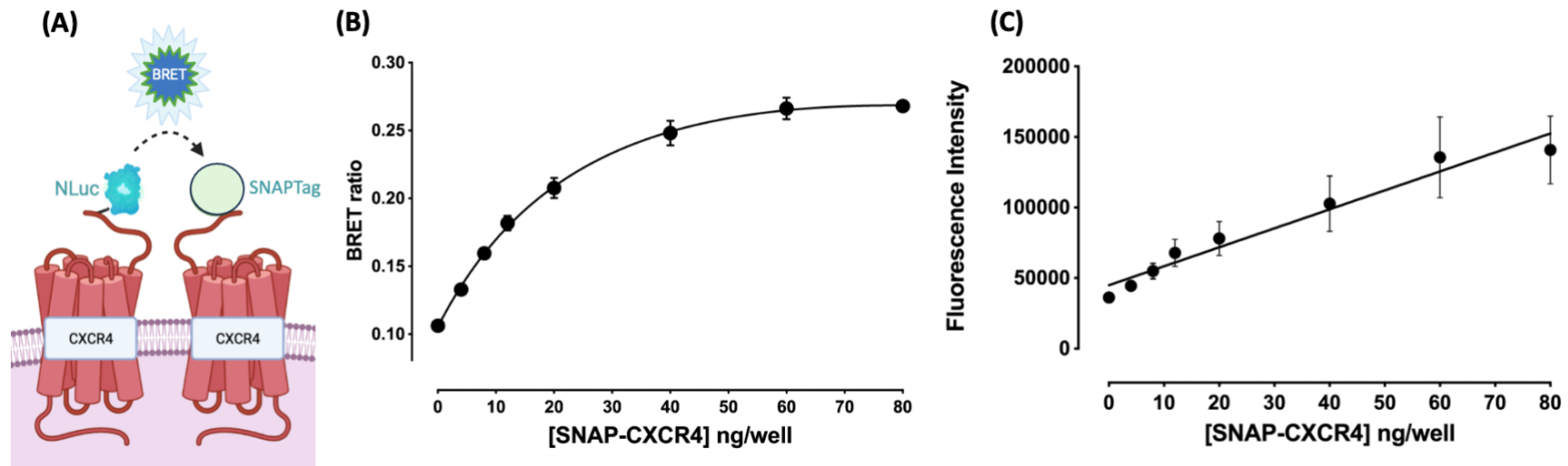


**Figure 5.1 Using NanoBRET to characterise CXCR4 homodimerisation.** BRET experiments to determine the homodimerisation of CXCR4. HEK293 cells were transiently transfected with a fixed concentration of donor NLuc\_CXCR4 cDNA (20 ng/well) and increasing concentrations of acceptor SNAP\_CXCR4 cDNA (0-80 ng/well). (A) Schematic of BRET configuration for the study of NLuc\_CXCR4/SNAP\_CXCR4 homodimers. (B) BRET ratio of SNAP\_CXCR4/NLuc\_CXCR4. (C) Fluorescence intensity measurements of increasing concentrations of transfected SNAP\_CXCR4 cDNA. SNAPTag AlexaFluor® 488 labelling was performed at 0.2  $\mu$ M concentration and incubated for 30 minutes at 37°C in DMEM. NanoBRET experiments were performed in HBSS containing 0.2 % BSA. Fluorescence emissions were measured before NLuc substrate furimazine incubation. Furimazine (1/400 final dilution) was added, and plates were incubated for 5 minutes then luminescence and fluorescence emissions were measured using a BMG Pherastar. Data are combined mean  $\pm$  SEM from 5 independent experiments, where each experiment was performed in 7 replicates.

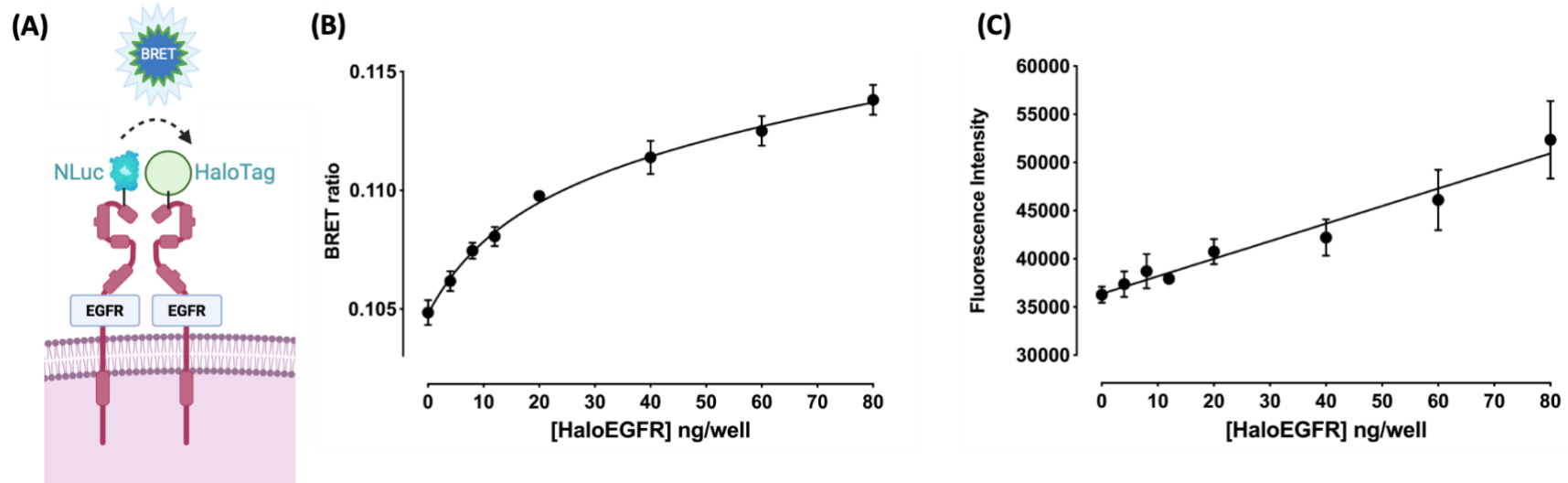


**Figure 5.2 Using NanoBRET to characterise EGFR homodimers.** BRET experiments to determine the homodimerisation of EGFR. HEK293 cells were transiently transfected with a fixed concentration of donor NLuc\_EGFR cDNA (20 ng/well) and increasing concentrations of acceptor Halo\_EGFR cDNA (0-80 ng/well). (A) Schematic of BRET configuration for the study of NLuc\_EGFR/Halo\_EGFR homodimers. (B) BRET ratio of Halo\_EGFR/NLuc\_EGFR. (C) Fluorescence intensity measurements of increasing concentrations of transfected Halo\_EGF cDNA. HaloTag AlexaFluor® 488 labelling was performed at 0.2  $\mu$ M concentration and incubated for 30 minutes at 37°C in DMEM. NanoBRET experiments were performed in HBSS containing 0.2 % BSA. Fluorescence emissions were measured before NLuc substrate furimazine incubation. Furimazine (1/400 final dilution) was added, and plates were incubated for 5 minutes then luminescence and fluorescence emissions were measured using a BMG Pherastar. Data are combined mean  $\pm$  SEM from 8 independent experiments for BRET ratio and 4 independent experiments for fluorescence intensity, where each experiment was performed in 6 replicates.

Furthermore, to detect whether CXCR4 and EGFR could form heterodimers we used a similar NanoBRET setup as used to study CXCR4 and EGFR homodimers, however this time using two different configurations of EGFR and CXCR4 vectors to confirm heterodimer formation was not dependent on NanoLuciferase or SNAPTag/HaloTag configurations. The first configuration used to detect EGFR/CXCR4 protein-protein interaction was (i) NLuc\_CXCR4/Halo\_EGFR and the second configuration was (ii) NLuc\_EGFR/SNAP\_CXCR4 (**Figure 5.3A** and **Figure 5.4A**). Both configurations gave saturable CXCR4/EGFR heterodimerisation (**Figure 5.3B** and **Figure 5.4B**). At NLuc\_EGFR/SNAP\_CXCR4 configuration a small decrease in BRET ratios were observable at 60 and 80 ng of SNAP\_CXCR4 cDNA concentration most likely due to the transfection and expression efficiency of the vector at higher concentrations. The transfection efficiencies of SNAP\_CXCR4 and Halo\_EGFR vectors was shown with the linear fluorescence increases of SNAPTag AlexaFluor® 488 and HaloTag AlexaFluor® 488 labelled receptors' fluorescence intensities respectively (**Figure 5.3C** and **Figure 5.4C**). 20 ng/well of donor and acceptor cDNA (1:1 ratio) was decided to use as optimal concentrations for CXCR4/EGFR homodimers and heterodimer configurations. 20 ng/well (1:1 ratio of both cDNAs) had a good level of transfection efficiency and optimal receptor expression level. Overly elevated amount of receptor density on the membrane due to highly overexpressed receptors might lead to non-physiological membrane dynamics conditions meaning non-specific/forced receptor dimerisation.

To observe the transfection efficiency and confirm proper membrane localisation of the SNAP\_CXCR4 receptor we used a fluorescence microscopy method (**Figure 5.5**). For this, a IX Micro widefield plate reader was used to image those HEK293T cells transiently transfected with increasing amounts of SNAP\_CXCR4 cDNA and a constant amount of NLuc\_EGFR (20 ng) in 96-well plates. SNAP\_CXCR4 receptor was labelled with SNAPTag AlexaFluor® 488, cells were then fixed using 3% PFA/PBS and H33342 used to stain the cell nuclei. Imaging showed the adequate expression levels of the SNAP\_CXCR4 with co-transfection of NLuc\_EGFR. The receptor transfected cell numbers and the fluorescence intensity were enhanced with the increased concentration of the SNAP\_CXCR4 cDNA introduced. Over-expressed SNAP\_CXCR4 receptors were localised on the cell membrane as expected (**Figure 5.5**).

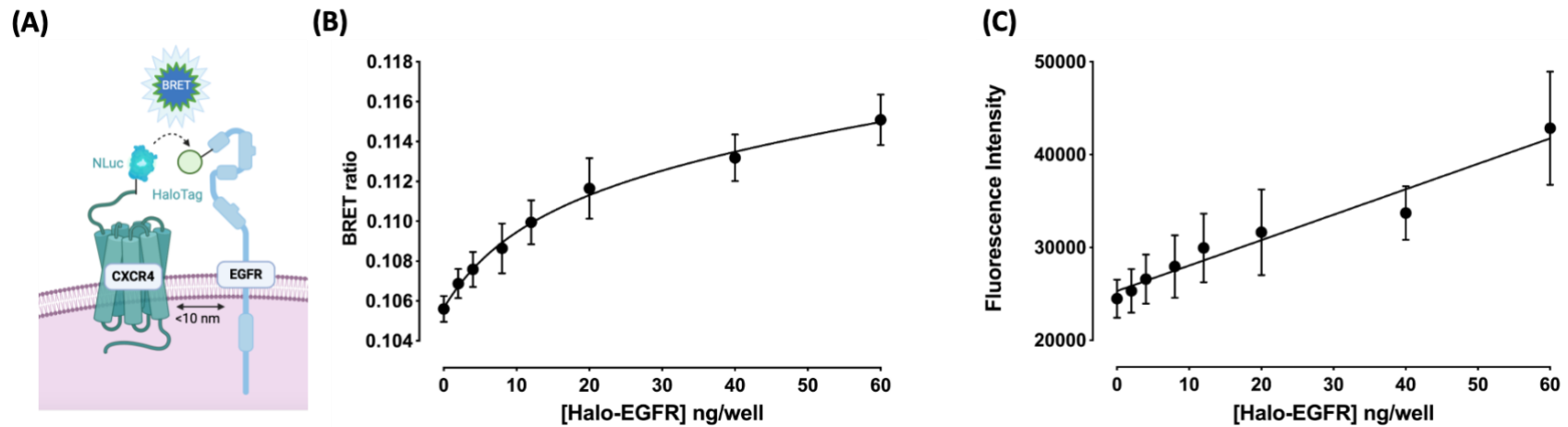


**Figure 5.3 Using NanoBRET to characterise CXCR4-EGFR heterodimers.** BRET experiments determined heterodimerisation of CXCR4 and the EGFR. HEK293 cells were transiently transfected with a fixed concentration of donor NLuc\_CXCR4 cDNA (20 ng/well) and increasing concentrations of acceptor Halo\_EGFR cDNA (0-60 ng/well). (A) Schematic of BRET configuration for the study of NLuc\_CXCR4/Halo\_EGFR heterodimers. (B) BRET ratio of Halo\_EGFR/NLuc\_CXCR4. (C) Fluorescence intensity measurements of increasing concentrations of transfected Halo\_EGFR. HaloTag AlexaFluor® 488 labelling was performed at 0.2  $\mu$ M concentration and incubated for 30 minutes at 37°C in DMEM. NanoBRET experiments were performed in HBSS containing 0.2 % BSA. Fluorescence emissions were measured before the NLuc substrate furimazine incubation. Furimazine (1/400 final dilution) was added, and plates were incubated for 5 minutes then luminescence and fluorescence emissions were measured using a BMG Pherastar. Data are combined mean  $\pm$  SEM from 5 independent experiments where each experiment was performed in 6 replicates.

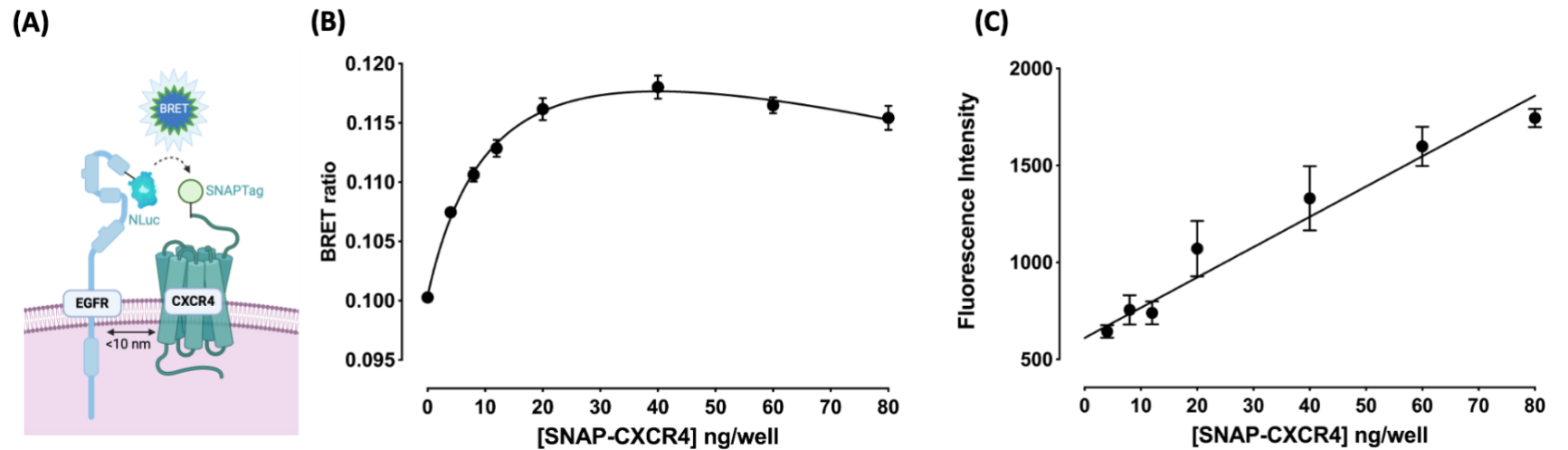


**Figure 5.4 Using NanoBRET to characterise CXCR4-EGFR heterodimers.** BRET experiments determined heterodimerisation of CXCR4 and EGFR. HEK293 cells were transiently transfected with a fixed concentration of donor NLuc\_EGFR cDNA (20 ng/well) and increasing concentrations of acceptor SNAP\_CXCR4 cDNA (0-80 ng/well). (A) Schematic of BRET configuration for the study of NLuc\_EGFR/SNAP\_CXCR4 heterodimers. (B) BRET ratio of SNAP\_CXCR4/NLuc\_EGFR. (C) Fluorescence intensity of increasing concentrations of transfected SNAP\_CXCR4. SNAPTag AlexaFluor® 488 labelling was performed at 0.2  $\mu\text{M}$  concentration and incubated for 30 minutes at 37°C in DMEM. NanoBRET experiments were performed in HBSS containing 0.2 % BSA. Fluorescence emissions were measured before the NLuc substrate furimazine incubation. Furimazine (1/400 final dilution) was added, and plates incubated for 5 minutes then luminescence and fluorescence emissions were measured using a BMG Pherastar. Data are combined mean  $\pm$  SEM from 5 independent experiments where each experiment was performed in 6 replicates for BRET ratio and 4 independent experiments for fluorescence intensity, where each experiment was performed in 5 replicates.

SNAP\_CXCR4  
DNA (ng)

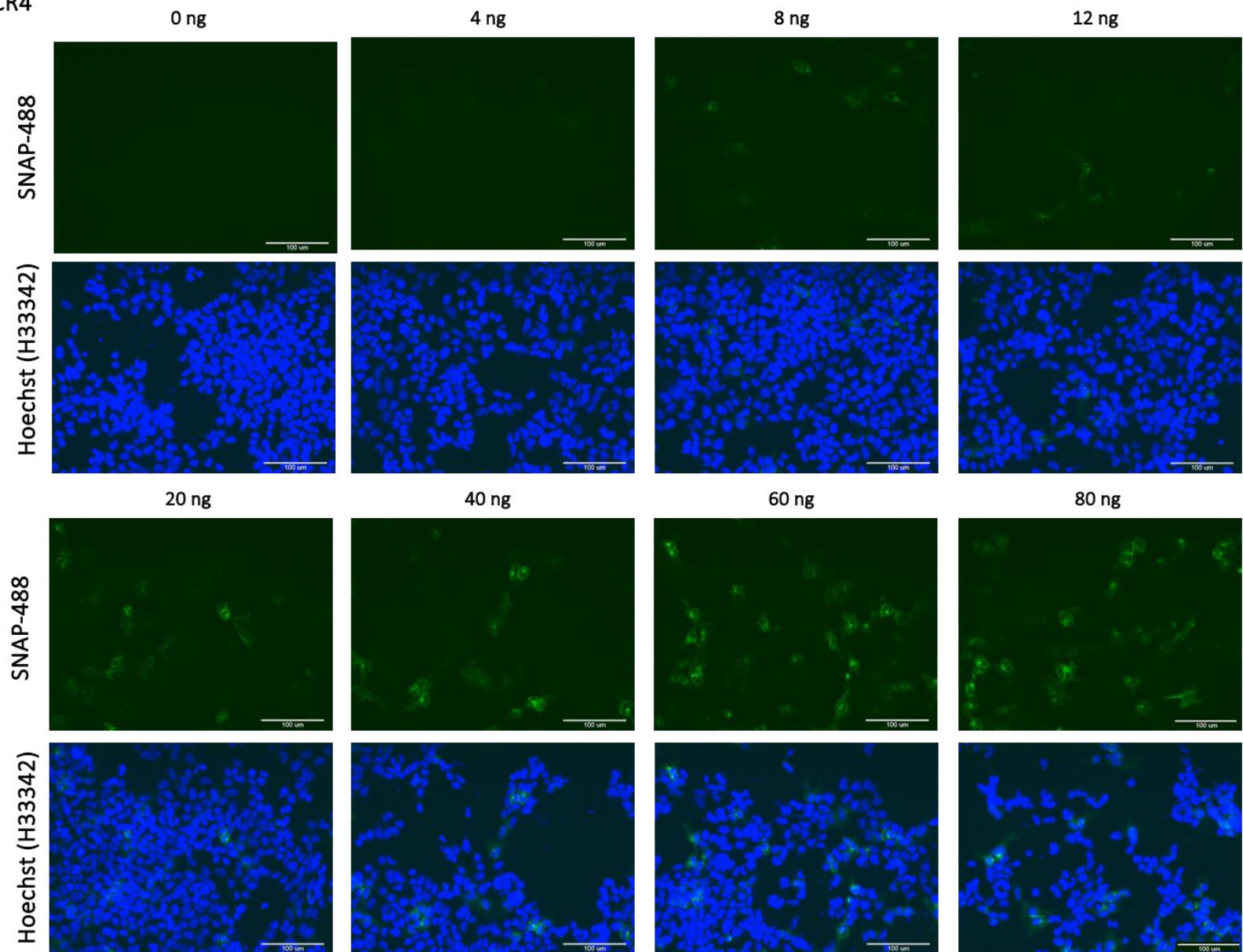


**Figure 5.5 NLuc\_EGFR and SNAP\_CXCR4 co-transfection efficiency via SNAP\_CXCR4 imaging.** HEK293T cells were seeded in 96-well plates and 24 hours later they were transiently co-transfected with 20 ng of NLuc\_EGFR cDNA and increasing concentrations (0-80 ng) of SNAP\_CXCR4 cDNA. Following 16 hours, cells were labelled with SNAPTag AlexaFluor® 488 at 0.2  $\mu$ M concentration and incubated for 30 minutes at 37°C in DMEM. Cells were fixed (3% PFA/PBS), nuclei were stained (2 mg/ml H33342) and cells were imaged using a IX Micro widefield plate reader (20X objective) with a FITC filter and a DAPI filter imaging nuclei. Images are representative from 2 independent experiments.

### 5.2.2 Impact of the serum starvation on EGFR/CXCR4 heterodimerisation

When preparing previous BRET experiments, cells were not serum starved before the BRET assay. However, it is known that fetal calf serum (FCS) contains several growth factors that bind to growth factor receptors. Next, to determine the effect of endogenous ligands and growth factors in fetal calf serum (FCS) in DMEM we performed NanoBRET experiments were performed with and without FCS conditions. For this, the NLuc\_EGFR/SNAP\_CXCR4 BRET configuration was used (**Figure 5.6A**). A constant amount of NLuc\_EGFR and SNAP\_CXCR4 cDNA (20 ng each) were transiently transfected into HEK293T cells. 16 hours later, cells were serum starved (0 % FCS) for an hour. SNAP\_CXCR4 was labelled with SNAPTag AlexaFluor® 488 in DMEM containing 0 % FCS and then cells were treated with EGF (100 ng) for 30 minutes. There was no significant difference between starvation (0 % FCS) and 10 % FCS containing media conditions in respect to NLuc\_EGFR/SNAP\_CXCR4 heterodimerisation without EGF treatment (**Figure 5.6B**). Interestingly, EGF treatment decreased the CXCR4/EGFR heterodimer formation in a concentration dependent manner (**Figure 5.6B**). However, consistent with the no EGF treatment conditions, there was no difference between 1 hour FCS starvation and no starvation conditions when exogenous EGF is added (**Figure 5.6B**). The obtained  $\log IC_{50}$  calculations from the inhibition curve of the NLuc\_EGFR/SNAP\_CXCR4 BRET heterodimerisation were similar to each other for 0% FCS starvation ( $\log IC_{50} = -9.50 \pm 0.11$ , n=5) and 10% FCS containing DMEM conditions ( $\log IC_{50} = -9.27 \pm 0.06$ , n=5) (**Figure 5.6B**).

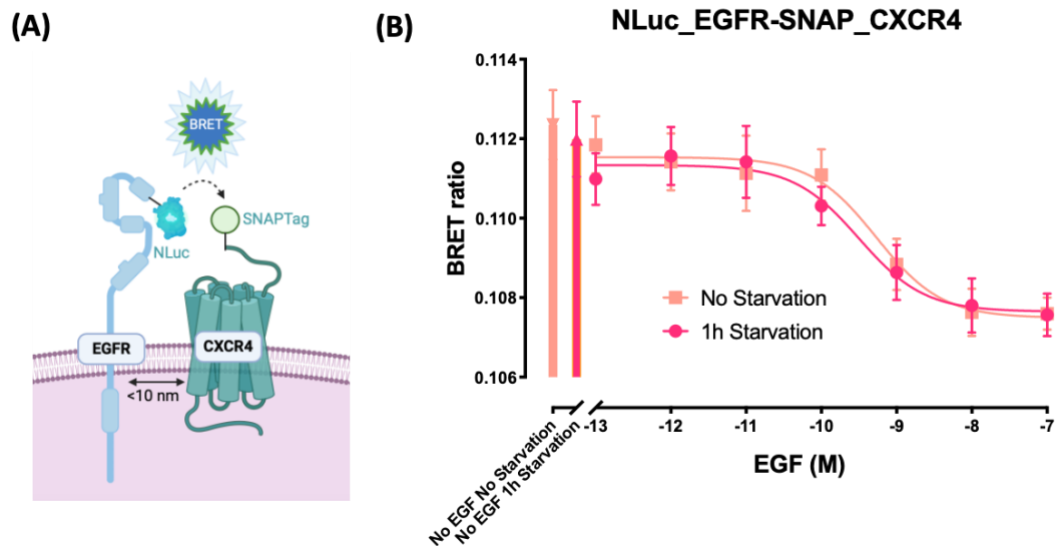


**Figure 5.6 The effect of serum starvation on EGFR/CXCR4 dimerisation.** (A) Schematic of BRET configuration for the study of NLuc\_EGFR/SNAP\_CXCR4 heterodimers. (B) Raw BRET ratio curve of NLuc\_EGFR/SNAP\_CXCR4 formation after 1 hour of 0 % FCS starvation and treatment with EGF. HEK293 cells were transiently transfected with a fixed concentration of donor NLuc\_EGFR cDNA (20 ng/well) and acceptor SNAP\_CXCR4 cDNA (20 ng/well) and 16 hours later cells were starved for 1 hour with 0% FCS DMEM. After starvation, SNAPTag AlexaFluor® 488 labelling was performed at 0.2  $\mu$ M concentration and incubated for 30 minutes at 37°C in 0 % FCS DMEM. Cells were then incubated for 30 minutes with increasing concentrations of EGF in HBSS/0.2 % BSA for 30 minutes. NanoBRET experiments were performed in HBSS containing 0.2 % BSA. Fluorescence emissions were measured before NLuc substrate furimazine incubation. Furimazine (1/400 final dilution) was added, and plates incubated for 5 minutes then luminescence and fluorescence emissions were measured using a BMG Pherastar. Data are means  $\pm$  SEM from five separate experiments, each performed with 6 replicates.

Although NanoBRET experiments between the pairings of NLuc\_EGFR with SNAP\_CXCR4 or NLuc\_CXCR4 with Halo\_EGFR showed saturable BRET indicative of an interaction, to eliminate the question of bystander (random interaction between the donor and acceptor at BRET) effects, NanoBRET experiments were repeated using receptors where there is no existing evidence of an interaction with EGFR. The adenosine receptor subtypes A1 or A3 were chosen for EGFR interaction experiments. To distinguish the receptor specificity on heterodimerisation, we performed NLuc\_EGFR/Adenosine 1 and Adenosine 3 heterodimerisation

NanoBRET experiments transiently transfection HEK293T cells with a constant amount of NLuc\_EGFR and increasing concentrations of SNAP\_A1, SNAP\_A3 or SNAP\_CXCR4 cDNA. In contrast to BRET ratios observed using the SNAP\_CXCR4 receptor as an acceptor, SNAP\_A1 and SNAP\_A3 receptors did not show increased BRET with NLuc\_EGFR (**Figure 5.7**) indicative of no dimerisation between NLuc\_EGFR and SNAP\_A1 or SNAP\_A3 receptors. This suggests that NLuc\_EGFR/CXCR4 heterodimerisation NanoBRET experiments show high specificity and even at high amount of cDNA transfection, the non-specific heterodimer formation is at a minor level.

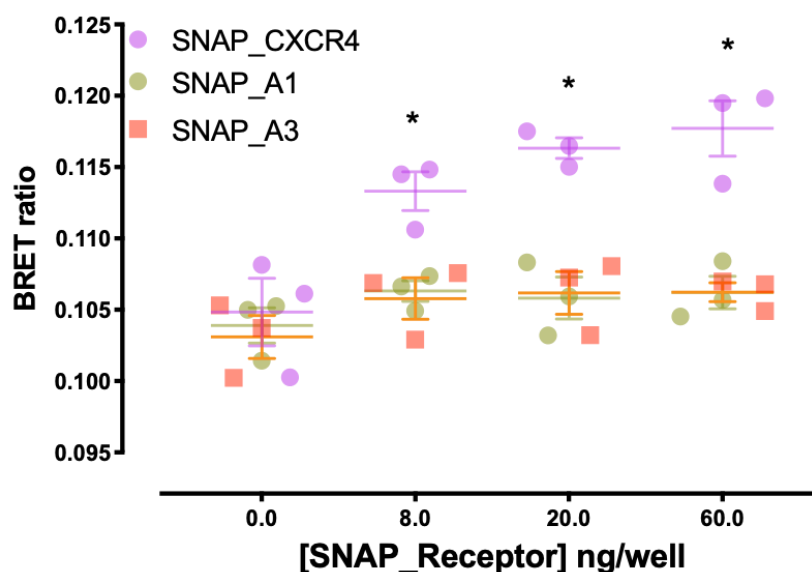


**Figure 5.7 EGFR/Adenosine 1 and EGFR/Adenosine 3 receptors dimerisation as negative control for EGFR/CXCR dimerisation.** BRET experiments to detect possible heterodimerisation of EGFR and Adenosine receptor 1 and 3 subtypes. HEK293 cells were transiently transfected with a fixed concentration of donor NLuc\_EGFR cDNA (20 ng/well) and increasing concentrations of acceptor SNAP\_A1, SNAP\_A3 or SNAP\_CXCR4 cDNA (0, 8, 20 and 60 ng/well). BRET ratios for SNAP\_A1 (green circles), A3 (orange squares) or CXCR4/NLuc\_EGFR (lilac circles) are shown. SNAPTag AlexaFluor® 488 labelling was performed at 0.2  $\mu$ M concentration and incubated for 30 minutes at 37°C in DMEM. NanoBRET experiments were performed in HBSS containing 0.2 % BSA. Furimazine (1/400 final dilution) was then added, and plates incubated for 5 minutes then luminescence and fluorescence emissions were measured using a BMG Pherastar. Data are combined mean  $\pm$  SEM from 3 independent experiments where each experiment was performed in 4 replicates. \*  $P < 0.05$  (with respect to vehicle control; one-way ANOVA with Holm-Sidak multiple comparison test).

### 5.2.3 Impact of ligand and nanobody binding on CXCR4/EGFR heterodimers.

After the determination of specific heterodimerisation of CXCR4/EGFR with no ligand or nanobody present, we aimed to understand the effect of specific ligands and nanobodies of CXCR4 and EGFR. The binding properties of several ligands and nanobodies were demonstrated in chapter 3 and chapter 4 previously. Binding properties of fluorescently labelled CXCR4 and ACKR3 ligands determined using NanoBRET . The specific binding of unlabelled CXCR4 nanobodies VUN415c, VUN400c and VUN401 has previously been showed in competition with the CXCR4 fluorescent agonist CXCL12-AlexaFluor647 (CXCL12-AF647) in HEK293T cells stably expressing (**Figure 5.8A**) or with CRISPR-Cas9-edited (Clustered regularly interspaced short palindromic repeats) (**Figure 5.8B**) NLuc\_CXCR4. All three nanobodies were able to fully compete with CXCL12-AF647 and their affinities were comparable in both NLuc\_CXCR4 over-expressed and CRISPR/Cas9-edited HEK293 NLuc\_CXCR4 cells (**Figure 5.8**). This is consistent with previous data from (Van Hout et al., 2018).

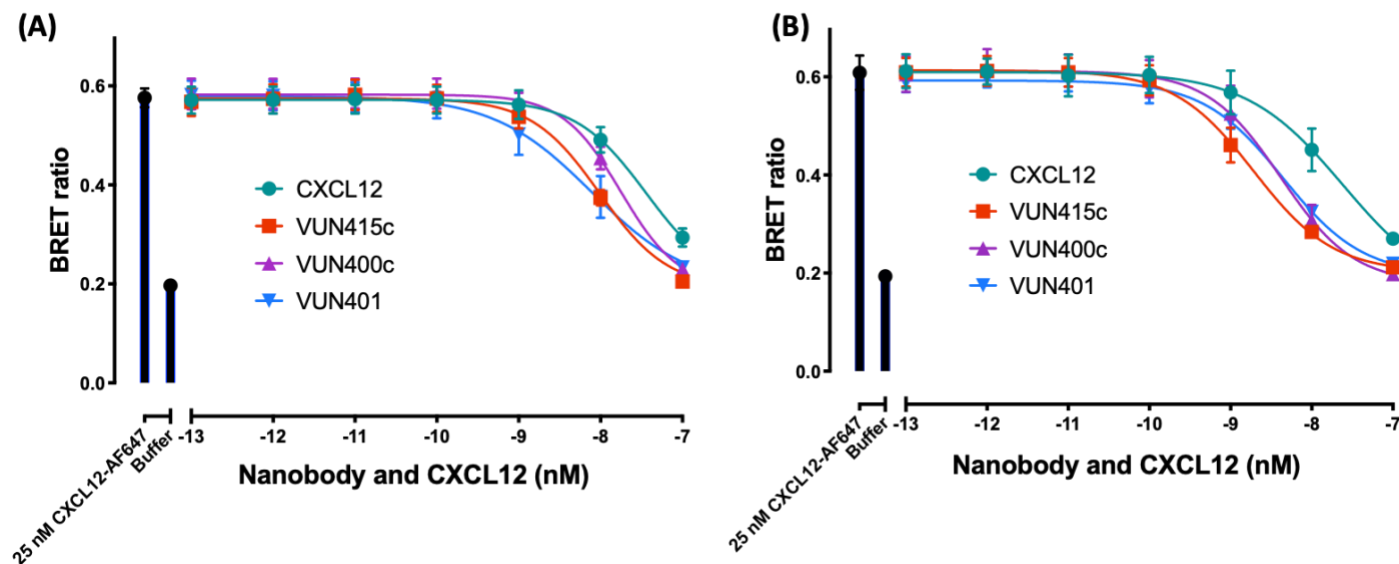


**Figure 5.8 Competition binding of CXCL12-AF647 by CXCL12 or CXCR4 targeting nanobodies.** Inhibition of the binding of CXCL12-AF647 at NLuc\_CXCR4. Binding of 25 nM CXCL12-AF647 at (A) HEK293T cells stably expressing NLuc\_CXCR4 or (B) CRISPR/Cas9-edited HEK293T cells endogenously expressing CXCR4 tagged with NLuc (NLuc\_CXCR4). Cells were incubated with CXCL12-AF647 (25 nM) in the absence or presence of increasing concentrations of unlabelled CXCL12, VUN415c, VUN400c, VUN401 for 1 hour at 37°C. Furimazine was added to each well as 1/400 final dilution and plates were equilibrated for 5 min at room temperature before simultaneous filtered light emissions were detected using a PHERASstar FS plate reader using 460 nm and >610 nm filters. BRET ratios were calculated by dividing the 610 nm emission (acceptor) by the 460 nm emission (donor). Data are means  $\pm$  SEM from (A) five separate or (B) four separate experiments, each performed with triplicate determinations. Total binding of 25nM CXCL12-AF647 alone and basal (obtained in the absence of fluorescent ligand) were also determined for each experiment.

The calculated LogIC<sub>50</sub> values for HEK293T cells overexpressing NLuc\_CXCR4 were  $-7.54 \pm 0.14$  for CXCL12,  $-7.90 \pm 0.15$  for VUN415c,  $-7.43 \pm 0.24$  VUN400c and  $-7.87 \pm 0.09$  for VUN401. The calculated LogIC<sub>50</sub> values for CRISPR/Cas9-edited NLuc\_CXCR4 cells were  $-7.65 \pm 0.15$  for CXCL12,  $-8.73 \pm 0.10$  for VUN415c,  $-8.44 \pm 0.14$  for VUN400c and  $-8.34 \pm 0.02$  for VUN401 (**Table 5.1**). The affinities of all three CXCR4 nanobodies, VUN415 ( $p=0.0032$ ), VUN400c ( $p=0.0120$ ) and VUN401 ( $p=0.0024$ ) were significantly higher at HEK293T cells overexpressing NLuc\_CXCR4 than CRISPR/Cas9-edited NLuc\_CXCR4 (unpaired t test was performed to calculate p values).

**Table 5.1 Concentration-response parameters for nanobody inhibition of NanoBRET binding of 25 nM CXCL12-AF647 to NLuc\_CXCR4.** N denotes the number of individual experiments performed for each ligand.

<b>Ligand</b>	<b>Over-expressed NLuc_CXCR4 HEK293T cells</b>		<b>P value</b>	<b>CRISPR-Cas9 NLuc_CXCR4 HEK293T cells</b>	
	<b>Log IC<sub>50</sub></b>	<b>n</b>		<b>Log IC<sub>50</sub></b>	<b>n</b>
<b>CXCL12</b>	$-7.54 \pm 0.14$	5	-	$-7.65 \pm 0.15$	4
<b>VUN415c</b>	$-7.90 \pm 0.15$	5	0.0032	$-8.73 \pm 0.10$	4
<b>VUN400c</b>	$-7.43 \pm 0.24$	5	0.0120	$-8.44 \pm 0.14$	4
<b>VUN401</b>	$-7.87 \pm 0.09$	5	0.0024	$-8.34 \pm 0.02$	4

#### 5.2.4 The effect of ligand binding on CXCR4/EGFR homodimers/heterodimers

After the initial experiments that confirmed that CXCR4 and EGFR can form homodimer and heterodimer complexes with no necessary ligand binding (**Figure 5.1**, **Figure 5.2**, **Figure 5.3**, **Figure 5.4**), we then moved to investigate the effects of ligand and nanobody binding on CXCR4/EGFR complexes. First, the effect of CXCR4 ligands and nanobodies on CXCR4 homodimerisation was determined using NLuc\_CXCR4/SNAP\_CXCR4 configuration. For this, 20 ng/well of donor and acceptor cDNA (1:1 ratio) was chosen from the saturation transfection experiments (**Figure 5.1**, **Figure 5.2**, **Figure 5.3**, **Figure 5.4**) since these were the optimal concentrations for CXCR4/EGFR homodimers and heterodimer configurations. As mentioned above 20 ng/well (1:1 ratio of both cDNAs) had an excellent level of transfection efficiency and optimal receptor expression level since the overly elevated amount of receptor density on the membrane due to highly overexpressed receptors might lead to non-physiological membrane dynamics conditions meaning non-specific/forced receptor dimerisation.

Firstly, a constant concentration of cDNA (20ng/well) encoding NLuc\_CXCR4 and SNAP\_CXCR4 was transiently transfected into HEK293T cells to confirm that the formation of CXCR4 homodimers was modulated by CXCR4-selective ligands and nanobodies (**Figure 5.9A**). As expected, the agonist CXCL12 (0.1 $\mu$ M) caused a significant increase in the dimerisation of CXCR4, whereas EGF (0.1 $\mu$ M) did not (**Figure 5.9B**). While the CXCR4 antagonists IT1t (10  $\mu$ M) and AMD070 (10  $\mu$ M) have an inhibiting effect on CXCR4 homodimerisation, AMD3100 (10  $\mu$ M) had no monomerization effect. The CXCR4 targeting nanobody VUN401 induced a significant monomerization of CXCR4 oligomers. In contrast, VUN400c caused a small but significant increase in BRET ratio whereas another nanobody with a C-terminal cysteine VUN415c had no effect on CXCR4 homodimerisation. This is in keeping with a previously shown monomerization effect of IT1t while AMD3100 demonstrated no decline when measured using the SPIDA technique (Işbilir et al., 2020; Ward et al., 2021). Inhibition of CXCR4 homodimerisation by VUN401 was compatible with previous results as well (Işbilir et al., 2020). Combination of CXCL12 and EGF (both 0.1 $\mu$ M) treatment showed a similar effect as CXCL12 only on CXCR4 homodimerisation. As expected, the EGFR targeting ligands EGF (0.1 $\mu$ M) and the receptor tyrosine kinase erlotinib (10  $\mu$ M), in addition to the EGFR targeting

nanobodies Q44c (0.1 $\mu$ M) and Q86c (0.1 $\mu$ M) had no significant effect on CXCR4 oligomerisation (**Figure 5.9B**).

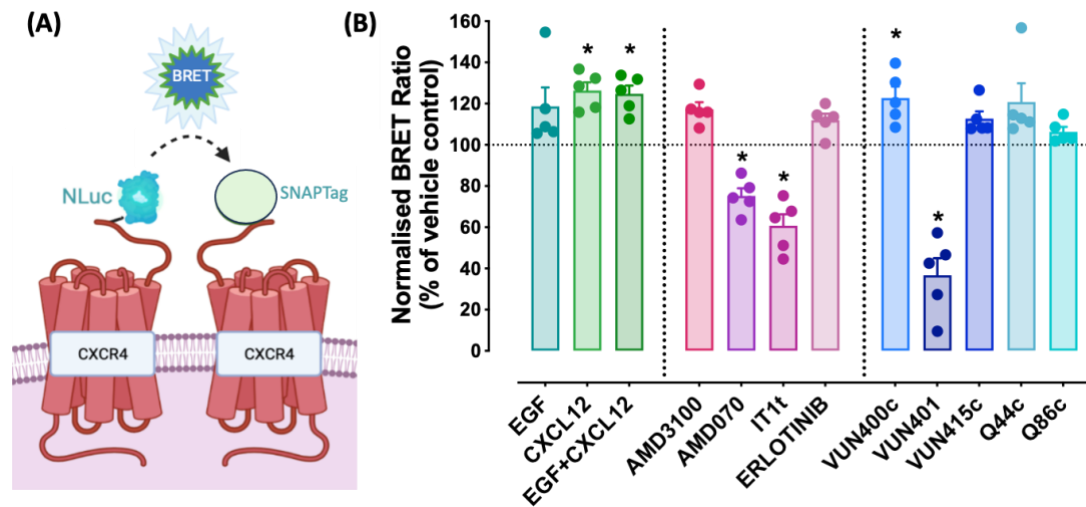


**Figure 5.9 NanoBRET experiments to investigate the effect of ligands and nanobodies on CXCR4 homodimer formation.** HEK293 cells were transiently transfected with a fixed concentration of donor NLuc\_CXCR4 cDNA (20 ng/well) and acceptor SNAP\_CXCR4 cDNA (20 ng/well). (A) Schematic of BRET configuration for the study of NLuc\_CXCR4/SNAP\_CXCR4 homodimers. (B) Normalised BRET ratio (% vehicle control) of NLuc\_CXCR4/SNAP\_CXCR4 formation. SNAPTag AlexaFluor® 488 labelling was performed at 0.2  $\mu$ M concentration and incubated for 30 minutes at 37°C in DMEM. Cells were then incubated for 30 minutes with EGF (0.1 $\mu$ M), CXCL12 (0.1 $\mu$ M), EGF+CXCL12 (both 0.1 $\mu$ M), AMD3100 (10  $\mu$ M), AMD070 (10  $\mu$ M), IT1t (10  $\mu$ M), erlotinib (10  $\mu$ M), VUN400c (0.1 $\mu$ M), VUN401 (0.1 $\mu$ M), VUN415c (0.1 $\mu$ M), Q44c (0.1 $\mu$ M) or Q86c (0.1 $\mu$ M). NanoBRET experiments were performed in HBSS containing 0.2 % BSA. Fluorescence emissions were measured before NLuc substrate furimazine incubation. Furimazine (1/400 final dilution) was added, and plates incubated for 5 minutes then luminescence and fluorescence emissions were measured using a BMG Pherastar FS. Data are normalized against no SNAPTag labelled condition (luciferase subtracted) and against vehicle control (only HBSS incubation). Data are means  $\pm$  SEM from five separate experiments, each performed with 6 replicates. \*  $P < 0.05$  (with respect to vehicle control; one-way ANOVA with Holm-Sidak multiple comparison test).  $P = 0.02$  (AMD070),  $p < 0.0001$  (IT1t),  $p = 0.03$  (VUN400c),  $p < 0.0001$  (VUN401),  $p = 0.01$  (CXCL12),  $p = 0.02$  (EGF+CXCL12). The dotted line at 100% presents the normalisation against vehicle (BRET signal from CXCR4/CXCR4 dimer with no ligand treatment).

Additionally, the effect of ligands and nanobodies on EGFR homodimers was determined via the same NanoBRET system. A constant amount of donor NLuc\_EGFR and acceptor Halo\_EGFR cDNA (20 ng/well each) was used to transfect HEK293T cells (**Figure 5.10A**). EGFR endogenous ligands EGF, TGF- $\alpha$  and Hb-EGF (0.1 $\mu$ M each) increased the EGFR homodimer formation as expected from previous studies (Freed, 2017b; Haubrich et al., 2024; Hofman et al., 2010b; Kovacs et al., 2015b) (**Figure 5.10B**). As previously demonstrated using FRET (Haubrich et al., 2024), erlotinib (erlotidine) (10  $\mu$ M) increased the EGFR homodimer formation. One of the EGFR targeting nanobodies Q44c which mainly binds at domain III of the EGFR ECD and competes with EGF (Binding properties of fluorescently labelled CXCR4 and ACKR3 ligands determined using NanoBRET)(Comez et al., 2022; Schmitz et al., 2013b), increased the homodimerisation between EGFR whereas another EGFR targeting nanobody which mainly binds at domain I and is non-competitive with EGF, Q86c, had a marginal decreasing effect on EGFR BRET homodimers. Expectedly, CXCR4 ligands CXCL12, AMD3100, AMD070, IT1t and nanobodies VUN400c, VUN401 and VUN415c did not have any significant effect on EGFR homodimerisation (**Figure 5.10B**).

Finally, to observe the impact of CXCR4 and EGFR ligands and nanobodies on CXCR4/EGFR heterodimers, a NLuc\_EGFR/SNAP\_CXCR4 configuration was used (**Figure 5.11A**). For BRET experiments, HEK293T cells were transfected with a constant amount of NLuc\_EGFR and SNAP\_CXCR4 cDNA (20 ng/well each) and incubated with ligands and nanobodies for 30 minutes at 37°C. EGF and CXCL12 both decreased BRET ratios obtained indicating a decline of EGFR/CXCR4 heterodimer formation (**Figure 5.11B**). None of the CXCR4 antagonists AMD3100, AMD070 and IT1t or the EGFR RTK inhibitor erlotinib showed any significant effect on EGFR/CXCR4 heterodimerisation. Interestingly, the CXCR4 nanobody VUN401 significantly increased heterodimer formation, whereas VUN400c and VUN415c significantly reduced it. In contrast to EGFR homodimerisation, there was no significant effect of the EGFR nanobody Q44c and only a slight decrease with incubation of Q86c on EGFR/CXCR4 heterodimerisation (**Figure 5.11B**).

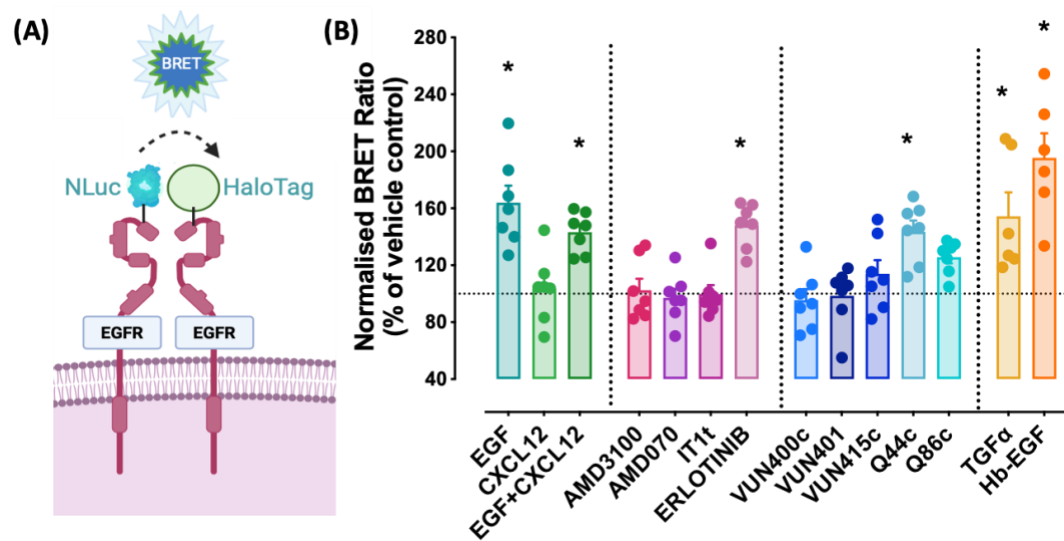


**Figure 5.10 NanoBRET experiments to investigate the effect of ligands and nanobodies on EGFR homodimer formation.** HEK293 cells were transiently transfected with a fixed concentration of donor NLuc\_EGFR cDNA (20 ng/well) and acceptor Halo\_EGFR cDNA (20 ng/well). (A) Schematic of BRET configuration for the study of NLuc\_EGFR/Halo\_EGFR homodimers. (B) Normalised BRET ratio (% vehicle control) of NLuc\_EGFR/SNAP\_EGFR formation. HaloTag AlexaFluor® 488 labelling was performed at 0.2  $\mu$ M concentration and incubated for 30 minutes at 37°C in DMEM. Cells were then incubated for 30 minutes at 37°C with EGF (0.1 $\mu$ M), CXCL12 (0.1 $\mu$ M), EGF+CXCL12 (both 0.1 $\mu$ M), AMD3100 (10  $\mu$ M), AMD070 (10  $\mu$ M), IT1t (10  $\mu$ M), erlotinib (10  $\mu$ M), VUN400c (0.1 $\mu$ M), VUN401 (0.1 $\mu$ M), VUN415c (0.1 $\mu$ M), Q44c (0.1 $\mu$ M) or Q86c (0.1 $\mu$ M), TGF- $\alpha$  (0.1 $\mu$ M) and Hb-EGF (0.1 $\mu$ M). NanoBRET experiments were performed in HBSS containing 0.2 % BSA. Fluorescence emissions were measured before NLuc substrate furimazine incubation. Furimazine (1/400 final dilution) was added, and plates incubated for 5 minutes then luminescence and fluorescence emissions were measured using a BMG Pherastar FS. Data are normalized against no HaloTag labelled condition (luciferase subtracted) and against vehicle control (only HBSS incubation). Data are means  $\pm$  SEM from six or seven separate experiments, each performed with 6 replicates. \*  $P < 0.05$  (with respect to vehicle control; one-way ANOVA with Holm-Sidak multiple comparison test).  $P < 0.0001$  (EGF),  $p = 0.0026$  (erlotinib),  $p = 0.0079$  (Q44c),  $p = 0.008$  (EGF+CXCL12),  $p < 0.0001$  (Hb-EGF),  $p = 0.0009$  (TGF- $\alpha$ ). The dotted line at 100% presents the normalisation against vehicle (BRET signal from EGFR/EGFR dimer with no ligand treatment)

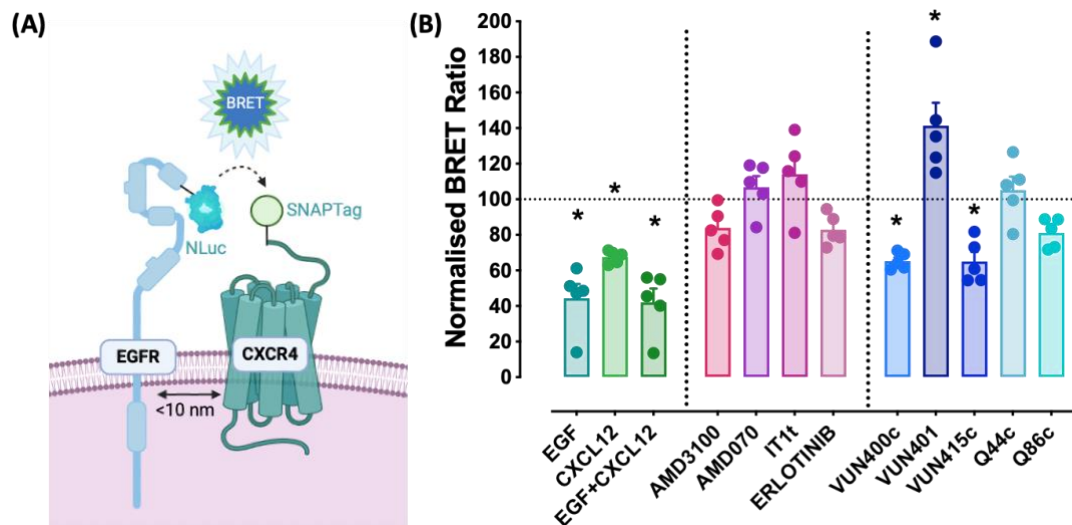


**Figure 5.11 NanoBRET experiments to investigate the effect of ligands and nanobodies on EGFR-CXCR4 heterodimer formation.** HEK293 cells were transiently transfected with a fixed concentration of donor NLuc\_EGFR cDNA (20 ng/well) and acceptor SNAP\_CXCR4 cDNA (20 ng/well). (A) Schematic of BRET configuration for the study of NLuc\_EGFR/SNAP\_CXCR4 homodimers. (B) Normalised BRET ratio (% vehicle control) of NLuc\_EGFR/SNAP\_CXCR4 formation. SNAPTag AlexaFluor® 488 labelling was performed at 0.2  $\mu$ M concentration and incubated for 30 minutes at 37°C in DMEM. Cells were then incubated for 30 minutes at 37°C with EGF (0.1 $\mu$ M), CXCL12 (0.1 $\mu$ M), EGF+CXCL12 (both 0.1 $\mu$ M), AMD3100 (10  $\mu$ M), AMD070 (10  $\mu$ M), IT1t (10  $\mu$ M), erlotinib (10  $\mu$ M), VUN400c (0.1 $\mu$ M), VUN401 (0.1 $\mu$ M), VUN415c (0.1 $\mu$ M), Q44c (0.1 $\mu$ M) or Q86c (0.1 $\mu$ M). NanoBRET experiments were performed in HBSS containing 0.2 % BSA. Fluorescence emissions were measured before the NLuc substrate furimazine incubation. Furimazine (1/400 final dilution) was added, and plates incubated for 5 minutes then luminescence and fluorescence emissions were measured using a BMG Pherastar. Data are normalized against no SNAPTag labelled condition (luciferase subtracted) and against vehicle control (only HBSS incubation). Data are means  $\pm$  SEM from five separate experiments, each performed with 6 replicates. \*  $P < 0.05$  (with respect to vehicle control; one-way ANOVA with Holm-Sidak multiple comparison test).  $P < 0.0001$  (EGF),  $p = 0.004$  (VUN400c),  $p = 0.0005$  (VUN401),  $p = 0.004$  (VUN415c),  $p = 0.0075$  (CXCL12),  $p < 0.0001$  (EGF+CXCL12). The dotted line at 100% presents the normalisation against vehicle (BRET signal from CXCR4/EGFR dimer with no ligand treatment)

We (**Figure 5.9B**) and others (Işbilir et al., 2020) have shown that the CXCR4 nanobody VUN401 can disrupt CXCR4 homodimerisation. However, in marked contrast, VUN400c caused a small but significant increase in CXCR4 dimerisation (**Figure 5.9A**) which may be due to the C-terminal cysteine present on this nanobody causing a fraction of the VUN400 nanobodies to be dimeric and subsequently leading to an increase in CXCR4 dimerisation. To investigate this possibility, this cysteine was removed from VUN400c and VUN415 nanobodies and NanoBRET experiments were performed for CXCR4 homodimers and CXCR4/EGFR heterodimers, using the same configurations as in **Figure 5.9A** for NLuc\_CXCR4/SNAP\_CXCR4 and **Figure 5.11A** for NLuc\_EGFR/SNAP\_CXCR4. In contrast with the increasing effect of VUN400c (**Figure 5.9B**), VUN400 decreased the CXCR4 homodimer formation (**Figure 5.12A**). The effect of VUN415 (**Figure 5.12A**) was the same as VUN415c (**Figure 5.9B**) which was neutral in respect to CXCR4 homodimerisation. The same NLuc\_EGFR/SNAP\_CXCR4 configuration (**Figure 5.11A**) was used to detect EGFR/CXCR4 dimerisation. Both VUN400 and VUN415 nanobodies had no significant effect on the formation of NLuc\_EGFR/SNAP\_CXCR4 heterodimers (**Figure 5.12B**) in contrast to the inhibitory effect observed with the two cysteine containing variants (**Figure 5.11B**). These data suggest that the inhibition of the formation of NLuc\_EGFR/SNAP\_CXCR4 heterodimers by VUN400c and VUN415c (**Figure 5.11B**) may be a consequence of the C-terminal cysteines causing a fraction of the VUN400c and VUN415c nanobodies to be dimeric leading to an increase in CXCR4 homodimerisation and an attenuation of EGFR/CXCR4 heterodimers. This would be in keeping with VUN401 significantly decreasing CXCR4 homodimerisation (**Figure 5.9B**) and increasing EGFR/CXCR4 heteromers (**Figure 5.11B**). In contrast to the increasing effect of Q44c on NLuc\_EGFR/Halo\_EGFR BRET homodimers (**Figure 5.10B**) and similar to the neutral effect on NLuc\_EGFR/SNAP\_CXCR4 dimers (**Figure 5.11B**), conjugation of the C-terminal cysteine on the EGFR nanobody Q44c with biotin (to remove the nanobody dimerisation effect of C-terminal cysteine) did not lead to any changes in its effect on EGFR/CXCR4 heterodimer formation (**Figure 5.12B**).

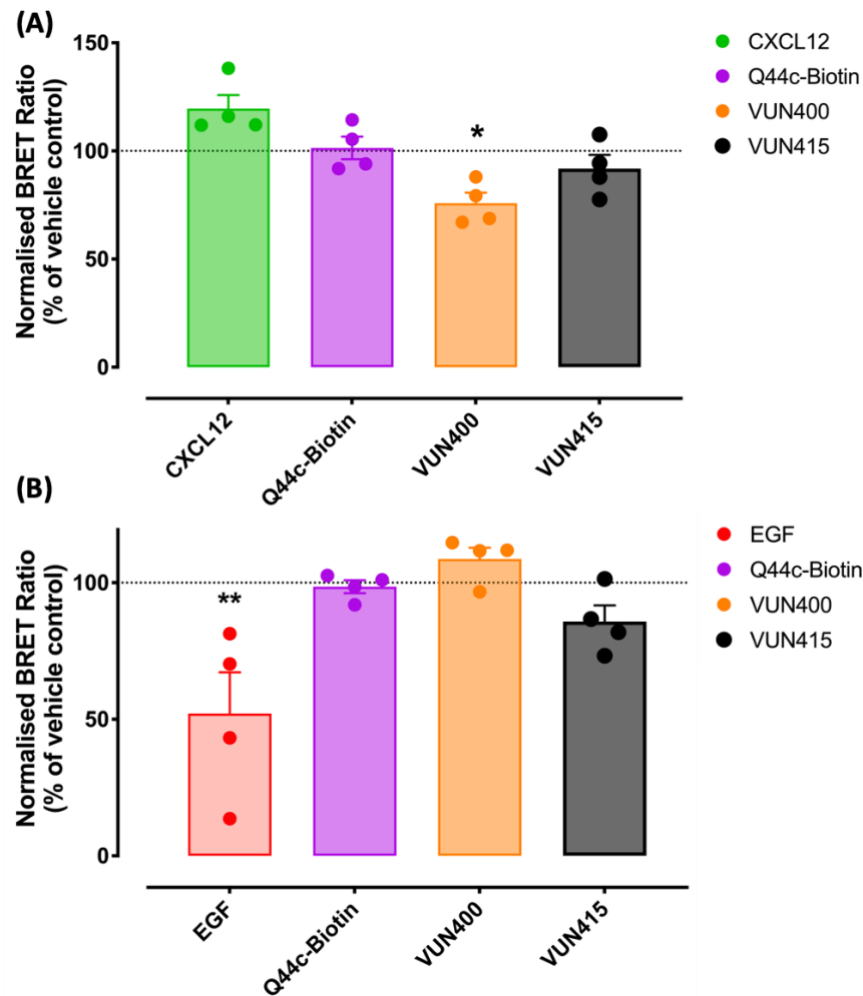


**Figure 5.12 Effect of CXCR4 nanobodies lacking C-terminal cysteines on CXCR4 homodimer and EGFR-CXCR4 heterodimer formation.** (A) Cells were transfected with a constant amount (20ng) of donor (NLuc\_CXCR4) and acceptor (SNAP\_CXCR4) cDNA. Cells were labelled with SNAP-Surface-AlexaFluor488® (0.2  $\mu$ M final concentration) for 30 min before experimentation. Cells were then incubated for 30 minutes at 37°C with CXCL12 (0.1 $\mu$ M), Q44c-Biotin (0.1 $\mu$ M), VUN400 (0.1 $\mu$ M) or VUN415 (0.1 $\mu$ M), Data are means  $\pm$  SEM from four separate experiments, each performed with 6 replicates. \*  $P < 0.05$  (with respect to vehicle control; one-way ANOVA with Holm-Sidak multiple comparison test).  $P = 0.017$  for VUN400 versus vehicle control. (B) Cells were transfected with a constant amount (20ng) of donor (NLuc\_EGFR) and acceptor (SNAP\_CXCR4). Cells were labelled with SNAP-Surface-AlexaFluor488® (0.2  $\mu$ M final concentration) for 30 min before experimentation. Cells were then incubated for 30 minutes at 37°C with EGF (0.1 $\mu$ M), Q44c-Biotin (0.1 $\mu$ M), VUN400 (0.1 $\mu$ M) or VUN415 (0.1 $\mu$ M), Data are means  $\pm$  SEM from four separate experiments, each performed with 6 replicates. \*\*  $P < 0.01$  (with respect to vehicle control; one-way ANOVA with Holm-Sidak multiple comparison test).  $P = 0.0018$  for EGF versus vehicle control.

To understand the concentration dependent effects of EGFR agonists on CXCR4/EGFR heterodimerisation, we have performed NanoBRET assays using the same NLuc\_EGFR/SNAP\_CXCR4 configuration (**Figure 5.11A**) with HEK293T cells transiently transfected with a constant concentration of NLuc\_EGFR and SNAP\_CXCR4 (20 ng/well each) cDNA. As mentioned previously (Chapter 4, **Figure 4.3**), endogenous EGFR ligands are classified according to their high and low affinity binding (Freed et al., 2017). Here, we showed that increasing concentrations of high affinity ligands EGF, TGF- $\alpha$ , Hb-EGF and BTC potently inhibited the BRET signal between NLuc\_EGFR and SNAP\_CXCR4 indicative of a decline in heterodimerisation (**Figure 5.13 A and B**). The potency of these ligands was similar to those reported previously for inhibition of EGF-binding and conformational enhancement of Q86c-HL488 binding to EGFR (Chapter 4, **Figure 4.7** and **Table 4.1**) (Comez et al., 2022). Similarly, the lower affinity EGFR ligands (Freed et al., 2017) EREG, epigen and AREG exhibited lower potency in inhibiting NLuc\_EGFR/SNAP\_CXCR4 NanoBRET signal (**Figure 5.13**) which was also similar to their conformational enhancement of Q86c-HL488 binding to EGFR (Chapter 4, **Figure 4.7** and **Table 4.1**). TGF- $\alpha$  showed the lowest potency amongst the high affinity ligands of EGFR with lower maximal level of inhibition of CXCR4/EGFR heterodimers. And epigen demonstrated lowest potency amongst the low affinity ligands with lower maximal level of inhibition of CXCR4/EGFR heterodimers (**Figure 5.13, Table 5.2**).

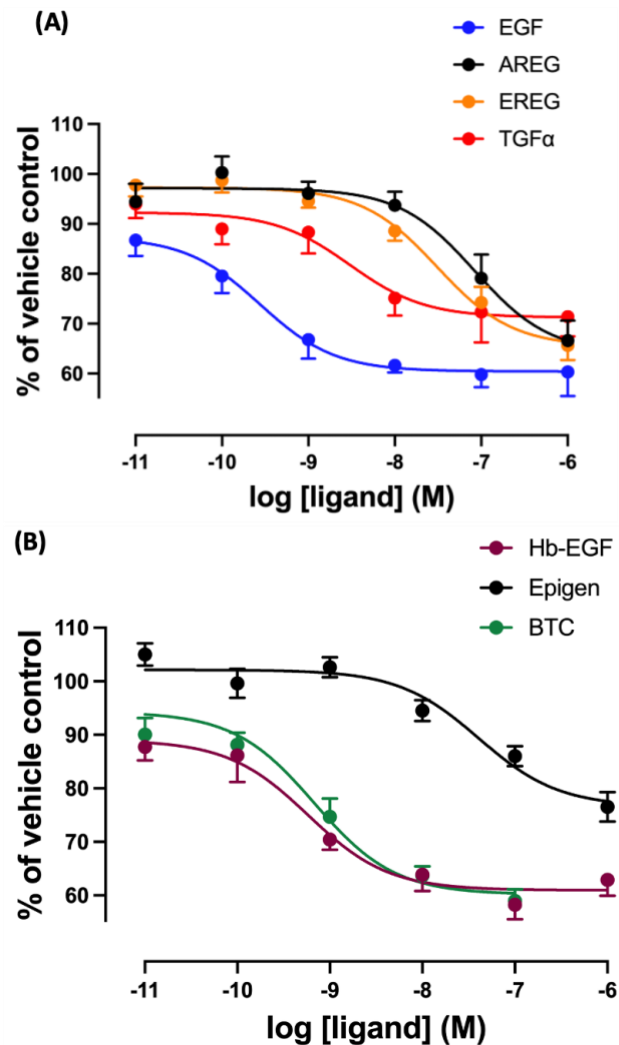


**Figure 5.13 Concentration-response curves for inhibition of EGFR-CXCR4 heterodimer formation by EGFR ligands.** HEK293 cells were transiently transfected with a fixed concentration of donor NLuc\_EGFR cDNA (20 ng/well) and acceptor SNAP\_CXCR4 cDNA (20 ng/well). (A) BRET ratio and % vehicle control by EGF, AREG, EREG and TGF- $\alpha$ . Data are means  $\pm$  SEM from 7 separate experiments, each performed with triplicates. (B) BRET ratio and % vehicle control Hb-EGF, epigen and BTC. SNAP-Surface-AlexaFluor488@ labelling was performed at 0.2  $\mu$ M concentration and incubated for 30 minutes at 37°C in DMEM. The ligands were incubated for 30 minutes at 37°C. All the ligands were used at (-6 to -11 M) concentrations except BTC (-7 to -12 M). NanoBRET experiments were performed in HBSS containing 0.2 % BSA. Furimazine (1/400 final dilution) was added, and plates incubated for 5 minutes then luminescence and fluorescence emissions were measured using a BMG Pherastar FS. Data are combined mean  $\pm$  SEM from 7 independent experiments, where each experiment was performed in triplicates. BRET ratio was calculated by dividing the fluorescence signal to the luminescence signal. BRET signal was normalized against the vehicle control (no ligand).

**Table 5.2 Concentration-response parameters for EGFR agonist-induced reduction in EGRF-CXCR4 oligomer formation in HEK293T cells.**

<b>Ligand</b>	<b>log IC<sub>50</sub></b>	<b>Max inhibition (%)</b>	<b>n</b>	<b>Log Ki (Inhibition of EGF-AF488 binding) *</b>	<b>Log EC<sub>50</sub> (enhancement of Q86c-HL488 binding) *</b>
<b>EGF</b>	-9.54 ± 0.17	38.89 ± 2.74	7	-8.86	-9.52
<b>Hb-EGF</b>	-9.08 ± 0.17	39.48 ± 1.94	7	-8.43	-9.20
<b>BTC</b>	-9.16 ± 0.25	41.27 ± 2.90	7	-8.45	-9.17
<b>TGF<math>\alpha</math></b>	-8.60 ± 0.15	21.89 ± 4.56	7	-6.83	-8.32
<b>EREG</b>	-7.61 ± 0.17	34.94 ± 3.38	7	/	/
<b>AREG</b>	-7.14 ± 0.15	39.77 ± 2.43	6	/	/
<b>Epigen</b>	-7.25 ± 0.25	26.95 ± 3.59	7	/	/

Values are mean ± S.E.M. from n separate experiments. \* Data from Chapter 4, **Table 4.1**

### 5.2.5 Detection of endogenous receptor heterodimerisation of CXCR4/EGFR

The previous BRET experiments to detect CXCR4/EGFR heterodimerisation were performed with overexpression of both CXCR and EGFR receptors in HEK293 cells (**Figure 5.3** and **Figure 5.4**). The overexpression of the donor and acceptor receptors brings up the question of bystander effect for the BRET experiments which might mean the non-specificity of the dimerisation signal due to high density of the receptor proteins on the cell membrane. To detect CXCR4/EGFR heterodimerisation in endogenously expressed cells first we have used CRISPR/Cas9 gene-edited HEK293T cells whereby NanoLuc was inserted onto the N terminus of endogenously expressed CXCR4 (clonal cell line created by (White et al., 2020a)). These cells were transiently transfected with a constant concentration of Halo\_EGFR cDNA (12 ng/well). Following 16 hours incubation, cells were labelled with HaloTag AlexaFluor® 488 for 30 minutes at 37°C. After washing steps, the fluorescence intensity of HaloTag AlexaFluor® 488 was measured using a Pherastar FS to detect the viable transfection of Halo\_EGFR. Following furimazine addition, luminescence and fluorescence emissions were measured and BRET ratios calculated. It was shown that endogenously expressed CXCR4 was able to form heterodimers with Halo\_EGFR suggesting that the overexpression of CXCR4 is not necessary for protein-protein interaction and heterodimer formation can be obtained at low expression levels of CXCR4 (**Figure 5.14**).

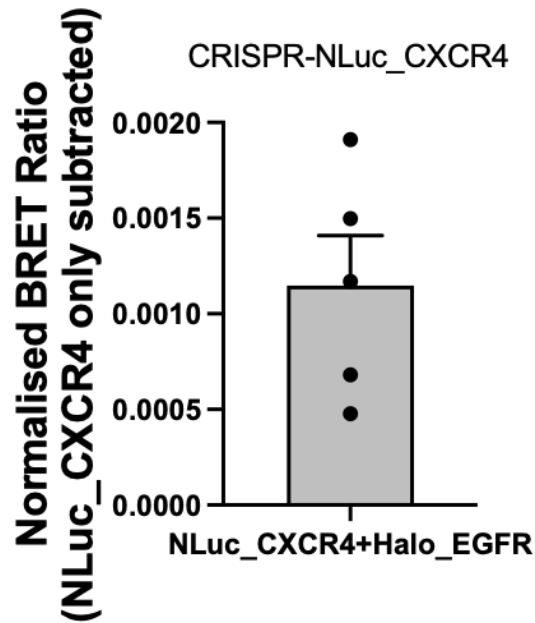


**Figure 5.14** BRET experiments performed in CRISPR/Cas9 edited HEK293T cells expressing endogenous CXCR4 tagged with NLuc and transiently transfected with Halo\_EGFR. CRISPR/Cas9 gene edited NLuc\_CXCR4 HEK293T cells were transfected with 12 ng of Halo\_EGFR. Following 16 hours incubation, HaloTag AlexaFluor® 488 labelling was performed at 0.2  $\mu$ M concentration and incubated for 30 minutes at 37°C in DMEM. NanoBRET experiments were performed in HBSS containing 0.2 % BSA. Furimazine (1/400 final dilution) was added, and plates incubated for 5 minutes then luminescence and fluorescence emissions were measured using a BMG Pherastar FS. Data are normalized against NLuc\_CXCR4 alone in the absence of Halo\_EGFR transient transfection (Only 100 ng of empty pcDNA 3.1). Data are means  $\pm$  SEM from five separate experiments, each performed with 6 replicates.

After the detection of CXCR4/EGFR heterodimerisation at HEK293 cells with endogenously expressing NLuc\_CXCR4 and transient overexpression of Halo\_EGFR (**Figure 5.14**), a new experimental system developed with both CXCR4 and EGFR receptors were expressed endogenously with no modification of NanoLuc or HaloTag. To be able to detect the receptor-receptor interactions without modification on CXCR4 and EGFR an alternative method proximity ligation assay where oligonucleotides conjugated to receptor-targeted antibodies can act as probes to target a protein complex was used. These oligonucleotides can be joined by ligation if they have been brought into close proximity by receptor oligomerisation (Soderberg et al., 2008). The

DNA ligation product formed can then act as a template for PCR amplification of a single-stranded rolling circle product that can be visualized by hybridization of a fluorescence-labelled complementary oligonucleotide detection probe (Soderberg et al., 2008). The resulting labelled rolling circle amplified DNA product can then be imaged microscopically (Raykova et al., 2016). This approach, used in conjunction with receptor-targeted nanobodies, provided an opportunity to study the formation of CXCR4/EGFR complexes in HeLa cells endogenously expressing the two receptors. Nanobodies equipped with a C-terminal cysteine were conjugated to azide-modified oligonucleotides via Dibenzocyclooctyne(DBCO)-maleimide (**Figure 5.15**). In this series of experiments, we generated VUN416-oligo1 and VUN416-oligo2 to assess CXCR4 homodimer formation. We also used Q44-oligo2 in conjunction with VUN416-oligo1 to evaluate CXCR4-EGFR heterodimers. Binding of each nanobody to endogenous CXCR4 or EGFR in CRISPR-edited HeLa cells expressing endogenous NLuc-CXCR4 was assessed using biotinylated anti-sense oligonucleotides and streptavidin-HRP (**Figure 5.15B**). The specific binding of VUN416-oligo1 ( $pK_d$   $8.7 \pm 0.3$ ,  $n=3$ ; **Figure 5.15C**) or VUN416-oligo2 to CXCR4 ( $pK_d$   $8.6 \pm 0.1$ ,  $n=3$ ; **Figure 5.15D**) and Q44-oligo2 to EGFR ( $pK_d$   $8.4 \pm 0.4$ ,  $n=3$ ; **Figure 5.15E**) in HeLa cells is shown in **Figure 5.15**. (The PLA experiments were performed by Dr Stephanie M. Anbuhl, VU University of Amsterdam).

These nanobody-oligonucleotide conjugates were then employed to detect endogenous CXCR4/CXCR4 homodimers and CXCR4/EGFR heteromers in native HeLa cells using confocal imaging (**Figure 5.16**). Use of VUN416-oligo1 and VUN416-oligo2 enabled a clear demonstration of CXCR4 homodimer formation (**Figure 5.16D**). This homodimer PLA signal was prevented by incubation of cells with unlabelled VUN416 (**Figure 5.16E**). Similarly, VUN416-oligo1 and Q44-oligo2 enabled detection of endogenous CXCR4-EGFR dimers in HeLa cells (**Figure 5.16A**). Incubation with  $1\mu\text{M}$  of un-tagged VUN416 (**Figure 5.16B**) or  $1\mu\text{M}$  Q44 (**Figure 5.16C**) completely prevented the PLA signal. (The experiments were performed by Dr Stephanie M. Anbuhl, VU University, Amsterdam).

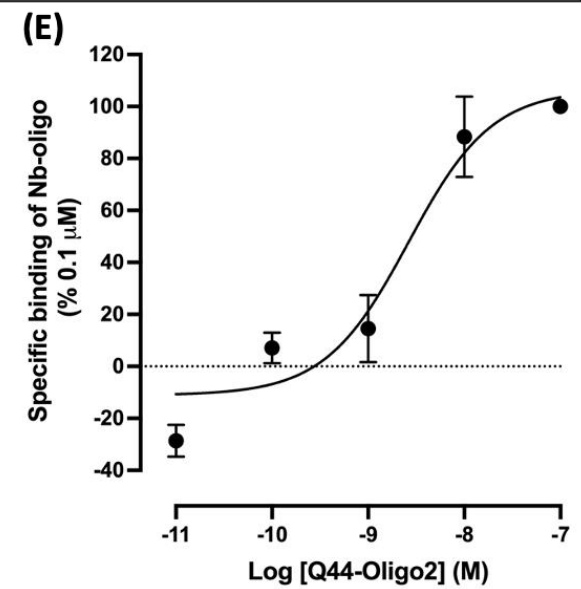
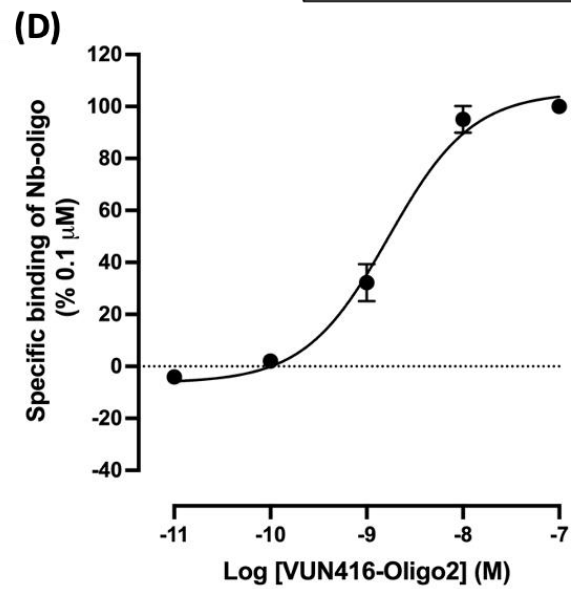
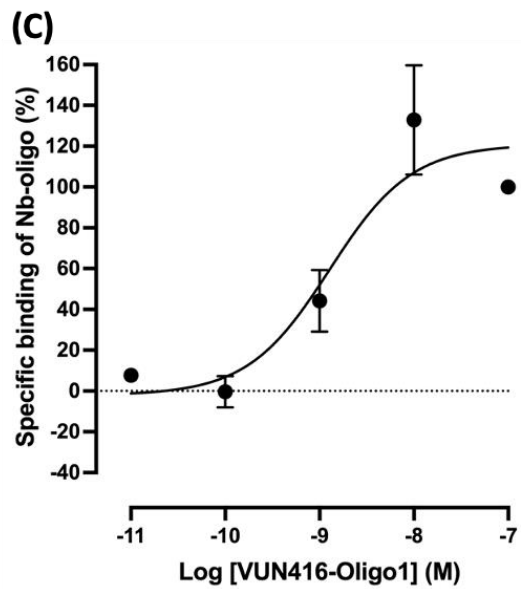
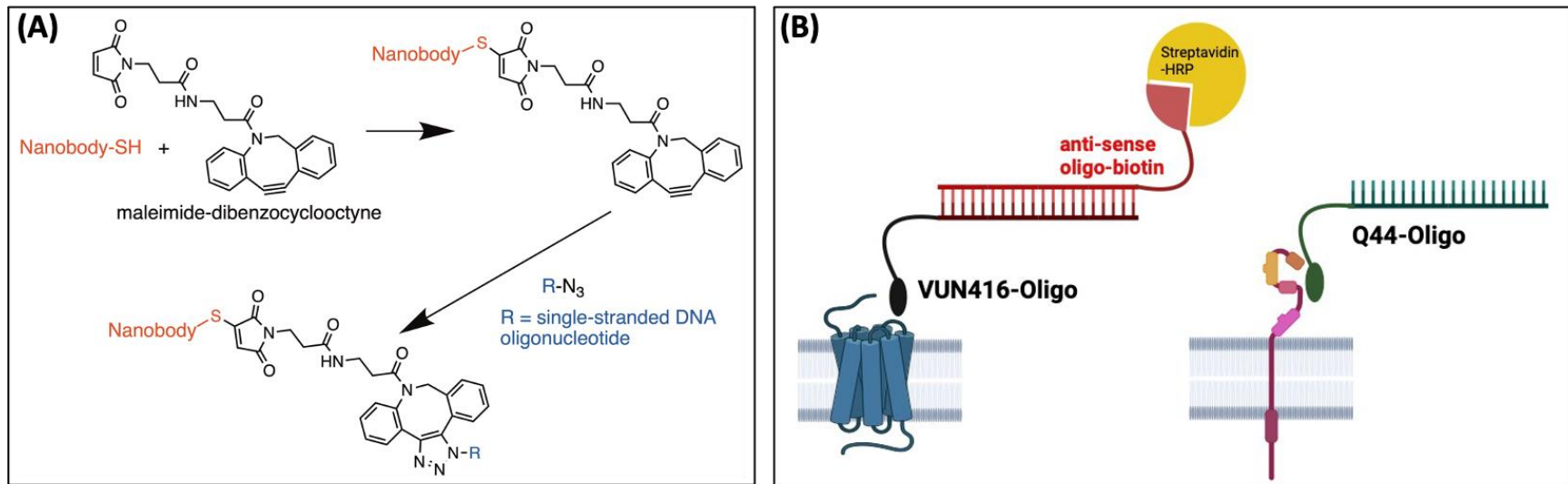


**Figure 5.15 Binding of nanobody-oligonucleotide conjugates to CRISPR-Cas9 edited HeLa cells expressing endogenous levels of NLuc\_CXCR4 and EGFR.** (A) Scheme for conjugation of C-terminally Cys-tagged nanobodies with maleimide-dibenzocyclooctyne and azide-modified oligonucleotides. (B) Illustration of the assay format to determine nanobody-oligonucleotide binding affinity. Nluc\_CXCR4 CRISPR HeLa cells containing endogenous levels of CXCR4, or EGFR were incubated with Nb-oligo. After washing, bound Nb-oligo was detected using a complementary biotinylated oligonucleotide. Bound biotin was quantified with streptavidin-HRP. (C-E) Binding of nanobody-oligo conjugates to Nluc\_CXCR4 CRISPR HeLa cells as determined by the assay illustrated in B). Non-specific binding was determined by blocking with the respective unconjugated nanobody (1  $\mu$ M). Values are means  $\pm$  SEM from three independent experiments, each performed in duplicate.



**Figure 5.16 Demonstration of CXCR4-CXCR4 and CXCR4-EGFR oligomerization in native HeLa cells using PLA.** (A-C) Detection of CXCR4/EGFR heteromers by PLA using 10nM VUN416-oligo1 and 10nM Q44-oligo2 in the absence (A) or presence of either (B) unlabeled VUN416 (1 $\mu$ M) or (C) Q44 (1 $\mu$ M). CXCR4 homodimers detected by PLA using VUN416-oligo1 (10nM) and VUN416-oligo2 (10nM) in the absence (D) or presence (E) of 1 $\mu$ M unlabeled VUN416. (F) Schematic demonstrating the working principle of PLA using single-stranded rolling circle product that can be visualized by hybridization of a fluorescence-labelled complementary oligonucleotide detection probe

### 5.2.6 Detection of CXCL12 and EGF binding at EGFR and CXCR4 respectively

The endogenous ligands of EGFR and CXCR4, EGF and CXCL12 promote EGFR and CXCR4 homodimer complexes (**Figure 5.9** and **Figure 5.10**) while both have negative regulatory impacts on CXCR4/EGFR BRET heterodimers (**Figure 5.11B**). Hence, we have decided to investigate whether CXCL12 binds to EGFR or EGF to CXCR4. For this, we have used HEK293T cells separately transiently transfected with NLuc\_EGFR (20 ng cDNA/well) or NLuc\_CXCR4 (20 ng cDNA/well) cDNA. To examine binding of CXCL12 at NLuc\_EGFR, increasing concentrations (0-200 nM) of fluorescently labelled CXCL12-AF647 was used. No BRET signal was detected between donor NLuc\_EGFR and CXCL12-AF647 indicative of CXCL12-AF647 having no affinity at EGFR (**Figure 5.17A**). The presence of unlabelled CXCL12 and EGF did not alter the affinity of CXCL12-AF647 to NLuc\_EGFR (**Figure 5.17A**). To confirm the BRET system was working correctly, 100 nM of fluorescent EGF-AF647 binding to NLuc\_EGFR and no fluorescent ligand basal condition were included (**Figure 5.17A**). The same strategy was applied for investigating EGF-AF647 binding at NLuc\_CXCR4 in transiently transfected HEK293T cells. Similar results were observed with no BRET signal between donor NLuc\_CXCR4 and acceptor EGF-AF647 meaning EGF-AF647 has no affinity for CXCR4 (**Figure 5.17B**). The presence of unlabelled EGF or CXCL12 did not change these results. The BRET signal obtained from 100 nM of CXCL12-AF647 binding at NLuc\_CXCR4 and no fluorescent ligand condition confirmed the viability of the BRET system (**Figure 5.17B**). These data are in keeping with the results from the CXCR4 and EGFR homodimerisation experiments that CXCL12 had no impact on EGFR homodimerisation and EGF had no impact on CXCR4 homodimerisation (**Figure 5.9** and **Figure 5.10**).

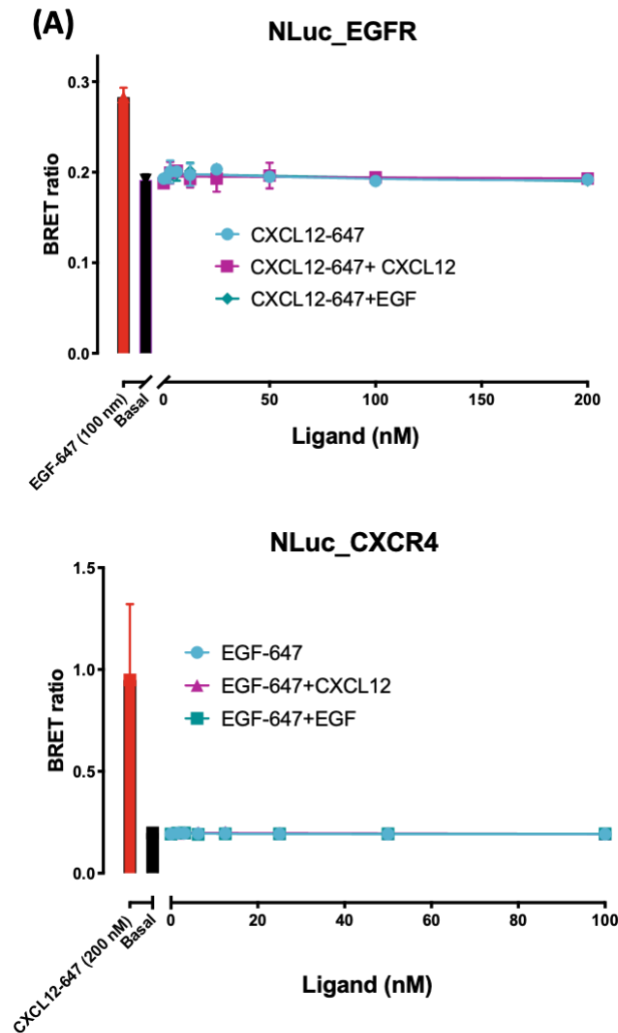


**Figure 5.17 Determination of CXCL12-AF647 binding to NLuc\_EGFR and EGF-AF647 binding to NLuc\_CXCR4.** HEK293 cells were transiently transfected with a fixed concentration of donor (A) NLuc\_EGFR or (B) NLuc\_CXCR4 cDNA (20 ng/well) and 80 ng of empty pcDNA 3.1. (A) Cells were incubated with increasing concentrations (0-200 nM) of CXCL12-AF647 in the absence or presence of 100 nM unlabelled CXCL12 or EGF for 30 minutes at 37°C. Total binding of 100 nM EGF-AF647 alone and basal (obtained in the absence of fluorescent ligand) were also determined in each experiment. (B) Cells were incubated with increasing concentrations (0-100 nM) of EGF-AF647 for 30 minutes at 37°C. Total binding of 3 nM of EGF-AF647 and 25 nM CXCL12-AF647 alone and basal (obtained in the absence of fluorescent ligand) were also determined in each experiment. Furimazine was added to each well as 1/400 final dilution and plates were equilibrated for 5 min at room temperature before sequential filtered light emissions were taken using a PHERASStar FS plate reader using 460 nm and >610 nm filters. BRET ratios were calculated by dividing the 610 nm emission (acceptor) by the 460 nm emission (donor). Data are means  $\pm$  SEM from 5 separate experiments, each performed with triplicate determinations.

Next, we performed NanoBRET experiments to answer two questions: (a) Is there any competition between CXCL12 and EGF binding at their cognate receptors? (b) Does the co-expression/dimerisation of CXCR4/EGFR have any impact on CXCL12 and EGF binding at their cognate receptors? To investigate the first question, we performed NanoBRET competition binding experiments with HEK293T cells transiently transfected (20 ng cDNA each) with (i) NLuc\_EGFR (**Figure 5.18A**) only and (ii) NLuc\_CXCR4 only (**Figure 5.18B**). The examination of the competition between EGF-AF647 (3 nM) and increasing concentrations of unlabelled CXCL12 and EGF at NLuc\_EGFR demonstrated that unlabelled EGF ( $8.9 \pm 0.1$ , n=5) fully competed with EGF-AF647 (**Figure 5.18A**). Unlabelled CXCL12 ( $8.6 \pm 0.2$ , n=5) partially displaced EGF-AF647 (**Figure 5.18A**). This might be the result of endogenous expression of EGFR or CXCR4 in HEK293T cells impacting the binding of EGF or CXCL12. Next, the competition between CXCL12-AF647 (25 nM) and increasing concentrations of unlabelled CXCL12 and EGF at NLuc\_CXCR4 only was investigated. Unlabelled CXCL12 ( $7.8 \pm 0.2$ , n=5) was able to fully displace CXCL12-AF647. EGF only had a minor reducing effect at the highest concentration (100 nM) on CXCL12-AF647 binding.

To answer the second question whether the CXCR4/EGFR co-expression/dimerisation had an impact on CXCL12 and EGF binding at the EGFR or CXCR4 we used HEK293T cells transiently transfected (20 ng cDNA each) with (iii) NLuc\_EGFR/SNAP\_CXCR4 (**Figure 5.18C**), or (iv) NLuc\_CXCR4/Halo\_EGFR (**Figure 5.18D**). No SNAPTag AlexaFluor® 488 or HaloTag AlexaFluor® 488 labelling were performed. Similar to NLuc\_EGFR only expression (**Figure 5.18A**), EGF ( $8.8 \pm 0.1$ , n=5) fully displaced and CXCL12 ( $8.6 \pm 0.8$ , n=5) partially displaced EGF-AF647 at NLuc\_EGFR/SNAP\_CXCR4 co-expression (**Figure 5.18C**). This suggested that co-expression of EGFR/CXCR4 has no significant impact on EGF binding at EGFR. In keeping with this, CXCL12 ( $7.9 \pm 0.2$ , n=5) competition with CXCL12-AF647 was not affected by CXCR4/EGFR co-expression as well (**Figure 5.18D**). Interestingly, competition of EGF with CXCL12-AF647 was slightly increased at lower concentrations of EGF (**Figure 5.18D**). This might be due to alterations of the ligand binding interface of the receptors caused by dimer formation. Additionally, the heterodimer formation between EGFR/CXCR4 might affect the CXCR4/CXCR4 homodimer interfaces leading to modification of ligand binding.

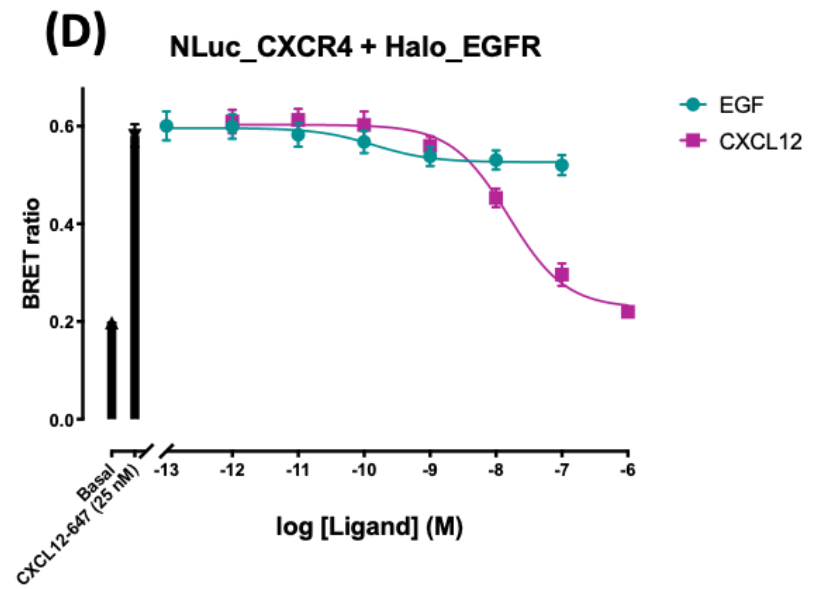
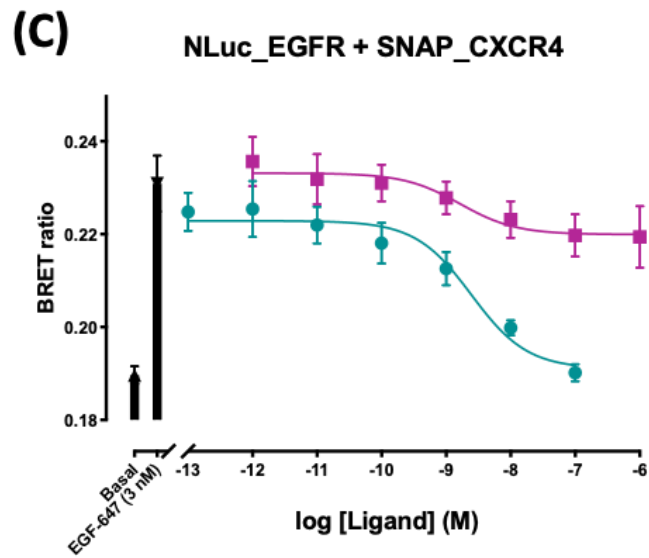
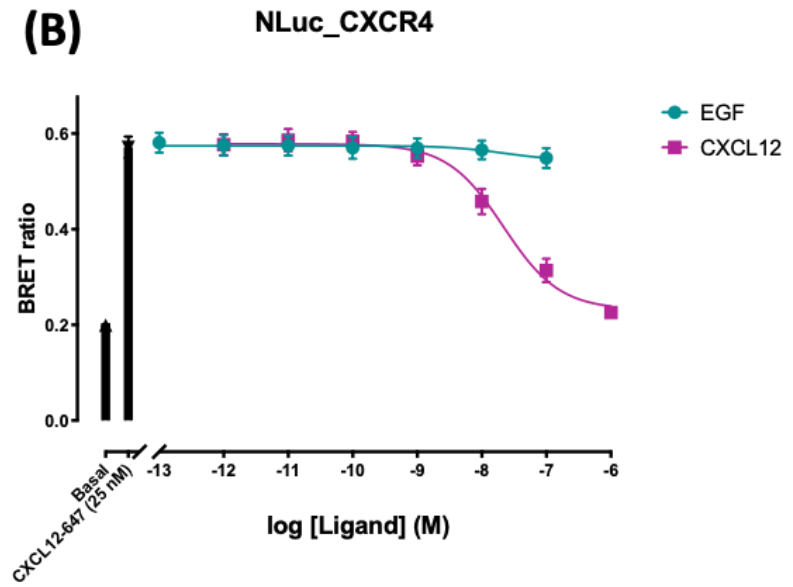
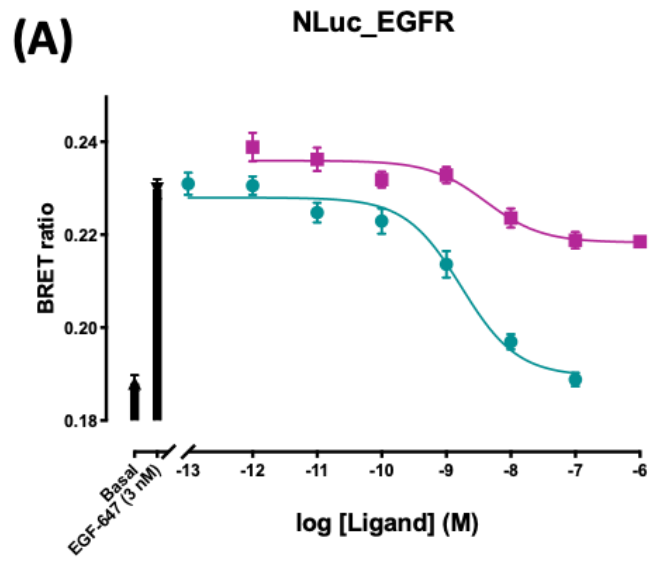


**Figure 5.18 Investigating the effect of co-expression of EGFR/CXCR4 complexes on CXCL12 and EGF binding.** HEK293 cells were transiently transfected with a fixed concentration of donor (A) NLuc\_EGFR (20 ng) or (B) NLuc\_CXCR4 cDNA (20 ng/well) and 80 ng of empty pcDNA 3.1. cDNA (C) NLuc\_EGFR and SNAP\_CXCR4 (20 ng each) and 60 ng of empty pcDNA 3.1. (D) NLuc\_CXCR4 and Halo\_EGFR (20 ng each) and 60 ng of empty pcDNA 3.1. Cells were incubated with increasing concentrations of EGF (-3 to -7 M) and CXCL12 (-12 to -6 M) with (A and C) 3 nM of EGF-AF647 and (B and D) 25 nM of CXCL12-AF647. in the absence or presence of 100 nM unlabelled CXCL12 or EGF for 30 minutes at 37°C. Total binding of 100 nM EGF-AF647 alone and basal (obtained in the absence of fluorescent ligand) were also determined in each experiment. (B) Cells were incubated with increasing concentrations (0-100 nM) of EGF-AF647 in the absence or presence of 100 nM unlabelled CXCL12 or EGF for 30 minutes at 37°C. Total binding of 200 nM CXCL12-AF647 alone and basal (obtained in the absence of fluorescent ligand) were also determined in each experiment. Furimazine was added to each well as 1/400 final dilution and plates were equilibrated for 5 min at room temperature before sequential filtered light emissions were taken using a PHERAStar FS plate reader using 460 nm and >610 nm filters. BRET ratios were calculated by dividing the 610 nm emission (acceptor) by the 460 nm emission (donor). Data are means  $\pm$  SEM from 3 separate experiments, each performed with triplicate determinations.

### 5.2.7 Investigation of conformational change of EGFR with co-expression of CXCR4

Previously, we have showed that EGFR and CXCR4 ligands significantly changed the heterodimer formation of CXCR4/EGFR (**Figure 5.11**). Yet, it is still unknown whether these ligands modify the conformation of EGFR and CXCR4 dimerisation interfaces. Ligand binding at extracellular domains of EGFR excessively reshape the conformations of those domains (Bessman, Bagchi, et al., 2014b). We have shown that Q86c-HL488 affinity was increased at the endogenous ligand bound EGFR meaning that it is recognising a specific conformation of EGFR (**Figure 4.5**). Hence, we postulated that Q86c-HL488 could be used as a conformational sensor to recognise altered conformations of EGFR (**Figure 4.13**). Co-expression and close proximity of EGFR/CXCR4 has the potential to modify EGFR conformations meaning that presence of CXCR4 may be altering the conformation of EGFR.

To investigate the conformational change of EGFR with CXCR4 co-expression we have used Q86c-HL488 as a conformational sensor. For this, HEK293T cells transiently transfected with only NLuc\_EGFR or both NLuc\_EGFR and SNAP\_CXCR4 cDNA were used. As previously shown, Q44c-HL488 nanobody competes with EGF for binding to EGFR ECM domains (**Figure 4.5**). Since, Q44 shows decreased affinity for EGF bound EGFR, it was used as a control group for these experiments. Both Q44c-HL488 and Q86c-HL488 binding to NLuc\_EGFR were not altered with SNAP\_CXCR4 co-expression (**Figure 5.19**). In keeping with previous data showing that EGF competes with Q44c-HL488 and enhances Q86c-HL488 (**Figure 4.5**), similar results were demonstrated with NLuc\_EGFR co-expressed with SNAP\_CXCR4 (**Figure 5.19**). CXCL12 has been shown as monomerizer for CXCR4/EGFR complex (**Figure 5.11**). There was no effect of CXCL12 on Q86c-HL488 binding to NLuc\_EGFR. In contrary, VUN401 has been demonstrated to increase CXCR4/EGFR heterodimer formation (**Figure 5.11**). In the presence of VUN401, there was no alteration of Q86c-HL488 binding at NLuc\_EGFR. Interestingly, erlotinib significantly increased the binding of both Q44c-HL488 and Q86c-HL488 to NLuc\_EGFR when co-expressed with SNAP\_CXCR4.

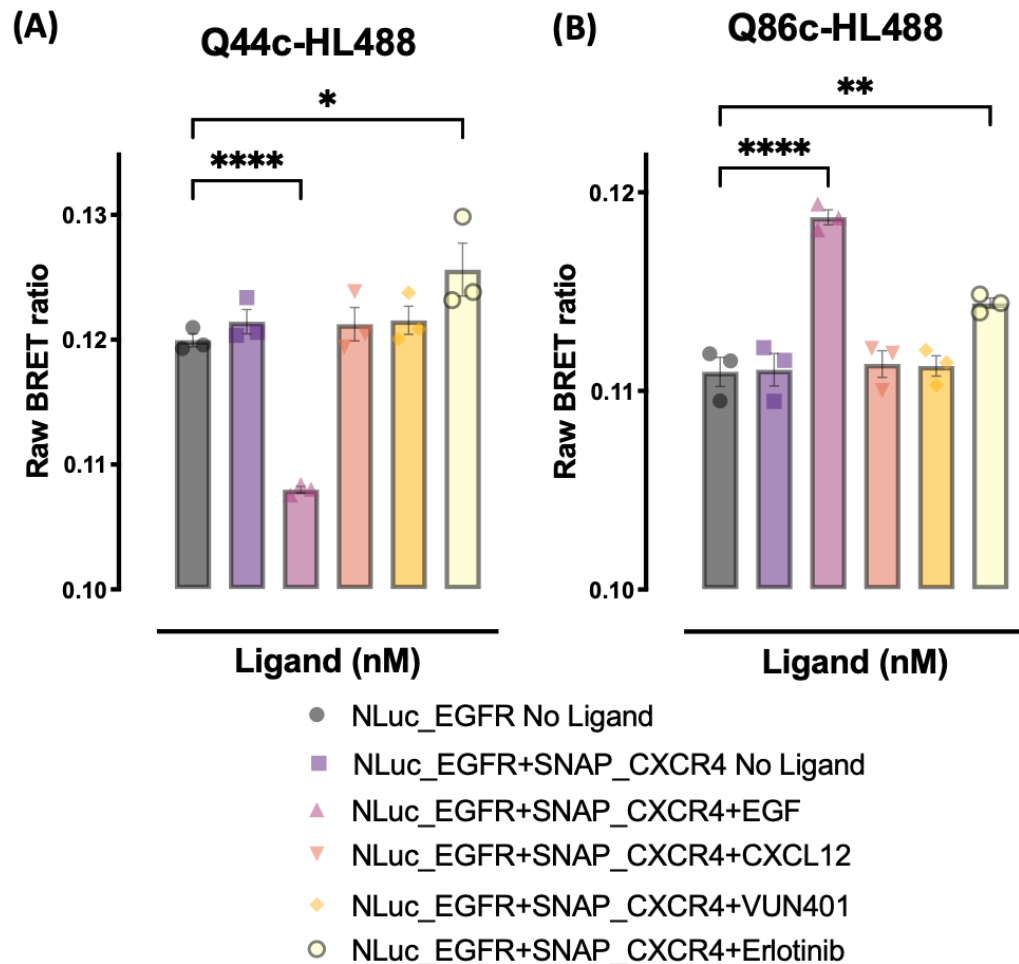


**Figure 5.19 Detection of the conformation of NLuc\_EGFR with CXCR4 co-expression via conformational sensor nanobody Q86c-HL488.** HEK293T cells were transfected with NLuc\_EGFR (20 ng cDNA) only or co-transfected with NLuc\_EGFR and SNAP\_CXCR4 (20 ng cDNA each). 30 minutes of EGF (0.1 $\mu$ M), CXCL12 (0.1 $\mu$ M), VUN401 (0.1 $\mu$ M) or erlotinib (10 $\mu$ M) incubation were performed simultaneously with (A) Q44c-HL488 (12.5 nM) and (B) Q86c-HL488 (12.5 nM) nanobodies. No SNAP labelling was performed. Furimazine was added to each well as a 1/400 final dilution and plates were equilibrated for 5 min at room temperature before simultaneous filtered light emissions were taken using a PHERASar FS plate reader. BRET ratios were calculated by dividing the 488 nm emission (acceptor-nanobodies labelled with HL488) by the 460 nm emission (donor). Data are means  $\pm$  SEM from 3 separate experiments, each performed with five replicates.

### 5.3 Summary and Discussion

In this chapter, we used a NanoBRET dimerisation system to study the complex formation of CXCR4 and EGFR receptors. The distance requirements (<10 nm) of the NanoBRET approach between the donor and acceptor receptors provided a sensitive measure of the close proximity between CXCR4 and EGFR. For the NanoBRET system we used a donor receptor which was a N-terminal nanoluciferase-tagged variant of EGFR or CXCR4 with a N-terminal fluorescently-tagged acceptor receptor which was SNAPTag or HaloTag labelled EGFR or CXCR4, all expressed in living HEK293 cells. With the same system, we examined the effects of EGFR and CXCR4 endogenous ligands, antagonists and nanobodies on CXCR4/EGFR complexes. We investigated CXCR4/EGFR complexes both in an overexpression model using NanoBRET and with endogenous expression using CRISPR-edited cells or a proximity ligation assay (PLA).

As previously shown in several studies with various techniques (Armando et al., 2014; İşbilir et al., 2020; Lao et al., 2017; Percherancier et al., 2005; Qin et al., 2015a; Saotome et al., 2024; Steel et al., 2014; Ward et al., 2021; B. Wu et al., 2010b), CXCR4 was able to form homodimers and the extent of the homodimerisation was correlated with increased amount of expressed SNAP\_CXCR4 (**Figure 5.1**). Although CXCR4 homodimerisation did not require ligand binding, the endogenous ligand of CXCR4, CXCL12 and VUN400c nanobody significantly increased the homodimerisation of CXCR4 (**Figure 5.9**). In contrast, a variant of the VUN400 nanobody without a C-terminal cysteine and the small molecular weight antagonists of CXCR4 AMD070 and IT1t showed decreasing effects on CXCR4 homodimers (**Figure 5.9** and **Figure 5.12**). This was in keeping with previous studies showing that IT1t decreased CXCR4 homodimer formation, in contrast VUN401 and AMD3100 had no significant effect on it (İşbilir et al., 2020; Ward et al., 2021). The effect of the VUN400c nanobody on increased homodimerisation of CXCR4 is possibly a secondary effect of dimerized VUN400c nanobodies caused by the cysteine-cysteine bond between two nanobodies.

As previously suggested (Mudumbi et al., 2023; Purba et al., 2022; Tao & Maruyama, 2008), EGFR formed homodimers with no requirement for ligand binding (**Figure 5.2**). Increased amounts of expressed Halo\_EGFR led to greater EGFR homodimer

---

formation (**Figure 5.2**). Additionally, the endogenous EGFR ligands EGF, TGF- $\alpha$  and Hb-EGF significantly increased the EGFR homodimer formation (**Figure 5.10**). This is in keeping with a previous study using a structural approach that showed different formations of EGFR homodimerisation induced by different endogenous ligands (Freed et al., 2017). The small molecular weight tyrosine kinase inhibitor erlotinib increased EGFR homodimer formation which was reconcilable with previous observations (Haubrich et al., 2024). While the Q44c nanobody significantly enhanced the EGFR homodimer formation, Q86c had no effect on it (**Figure 5.10**). Since Q44c binds to similar epitope as EGF (Comez et al., 2022) and competes with it, it was not unexpected that it induces an increase on EGFR homodimer formation similar to EGF. Even though, there have been several studies showing oligomeric complexes between GPCRs and RTKs (Bergelin et al., 2010; Blasco-Benito et al., 2019; Di Liberto et al., 2019c; Kilpatrick et al., 2019; Kilpatrick & Hill, 2021; Maudsley et al., 2000) and the signalling cross-talk between CXCR4 and EGFR (Y. Cheng et al., 2020; M. Neves et al., 2020, 2022) CXCR4/EGFR heterodimer complexes have not been studied yet. Similar to CXCR4 and EGFR homodimers, CXCR4/EGFR heterodimer formation did not require ligand binding (**Figure 5.3** and **Figure 5.4**). Increasing expression of Halo\_EGFR (**Figure 5.3**) and SNAP\_CXCR4 (**Figure 5.4**) lead to enhanced levels of CXCR4/EGFR heterodimer formation. Two different Nanoluciferase/fluorescent label configurations were used to detect CXCR4/EGFR heterodimer formation to eliminate the potential for false positive proximity caused by the 3D configuration of Nanoluciferase enzyme and the linkers leading to non-specific energy transfer between donor and acceptor. The few amino acid linkers provide flexibility for the luciferase and fluorescence tags that controls the positioning of the tags. Utilising two different NanoLuc/Fluorophore configurations helped to minimise a bystander effect (random interaction between the donor and acceptor leading to BRET). To investigate the potential bystander effect and demonstrate the specificity of BRET signal between pairings of CXCR4 and EGFR, NanoBRET experiments were repeated using receptors where there is no existing evidence of an interaction with EGFR. The adenosine receptor subtypes A1 or A3 were chosen for EGFR interaction experiments. In contrast to BRET ratios observed using the SNAP\_CXCR4 receptor as an acceptor, SNAP\_A1 and SNAP\_A3 receptors did not show increased BRET with NLuc\_EGFR (**Figure 5.7**) indicative of a lack of dimerisation between NLuc\_EGFR with

---

SNAP\_A1 or SNAP\_A3 receptors. This suggested that EGFR/CXCR4 heterodimerisation NanoBRET experiments are specific and demonstrated no major bystander BRET effect.

Since both configurations established a similar CXCR4/EGFR heterodimerisation trend, NLuc\_EGFR/SNAP\_CXCR4 configuration was used for subsequent ligand binding experiments. Interestingly, endogenous ligands of both the EGFR and CXCR4, EGF and CXCL12 respectively, significantly decreased CXCR4/EGFR heterodimer formation (**Figure 5.11**). This decreased effect on BRET signal was more prominent for EGF (**Figure 5.11**). While VUN401 had an increasing effect, VUN400c and VUN415c significantly decreased the EGFR/CXCR4 heterodimer formation (**Figure 5.11**). Interestingly, VUN400 and VUN415 nanobodies lacking cysteine modification did not show any impact on CXCR4/EGFR heterodimerisation (**Figure 5.12**). As mentioned previously (Chapter 4, **Figure 4.3**), endogenous EGFR ligands are classified according to their high and low affinity binding (Freed et al., 2017, Comez et al 2022). Various concentrations of endogenous EGFR ligands decreased CXCR4/EGFR BRET heterodimerisation at high concentrations (**Figure 5.13**). Even though all the EGFR ligands potently inhibited CXCR4/EGFR heterodimerisation, the rank potency of these ligands was similar to those reported previously for inhibition of EGF-binding and conformational enhancement of Q86c-HL488 binding to EGFR (Chapter 4, **Figure 4.7** and **Table 4.1**) (Comez et al., 2022). Similarly, the lower affinity EGFR ligands (Freed et al., 2017) EREG (epiregulin), epigen and AREG (amphiregulin) exhibited lower potency in inhibiting the NLuc\_EGFR/SNAP\_CXCR4 NanoBRET signal (**Figure 5.13**) which was also similar to the conformational enhancement of Q86c-HL488 binding to EGFR observed by these ligands (Chapter 4, **Figure 4.7** and **Table 4.1**).

One explanation for the the inhibiton/enhancement effect of ligands and nanobodies on CXCR4/EGFR heterodimerisation could be an enhanced homodimerisation of CXCR4 or/and EGFR which might decrease the CXCR4/EGFR heterodimerisation. EGF, TGF- $\alpha$  and Hb-EGF increasing the EGFR homodimerisation of EGFR simultaneously inhibiting the CXCR4/EGFR heterodimerisation could be the effect of homodimer formation evading the heterodimerisation. A similar effect can be seen whereby increasing CXCR4 homodimerisation induced by VUN400c and CXCL12, may consequently be inhibiting CXCR4/EGFR heteromer formation. Supporting this,

VUN401 was able to decrease CXCR4 BRET homodimerisation but led induced an enhancement in CXCR4/EGFR formation. In contrast, the small molecular weight CXCR4 antagonists (IT1t and AMD070) that inhibited CXCR4 homodimers did not significantly change CXCR4/EGFR heterodimer formation. In addition, Q44c and erlotinib which enhanced EGFR homodimer formation had no effect on CXCR4/EGFR heterodimers. Furthermore, VUN415c which had no impact on CXCR4 homodimers, decreased CXCR4/EGFR heterodimerisation. Consequently, the postulation of homodimer formation of CXCR4 or EGFR which may decrease the CXCR4/EGFR needs further research.

Fetal calf serum (FCS) contains several growth factors that bind to growth factor receptors which might have an impact on receptor oligomerization. To determine the effect of endogenous ligands and growth factors in fetal calf serum (FCS) in DMEM, NanoBRET experiments were performed with (10 % FCS) and without (0 % FCS) FCS conditions. No significant difference was detected between FCS starvation (0 % FCS) and 10 % FCS containing media conditions in respect to NLuc\_EGFR/SNAP\_CXCR4 heterodimerisation.

CXCR4 and EGFR heterodimerisation was demonstrated when overexpressing both receptors in a recombinant cell line (HEK293 cells). This raises the question of whether heterodimerisation is caused by the high density of the receptors on the cell membrane leading to more receptors being in close proximity due to overexpression of CXCR4 and EGFR rather than a ‘true’ interaction. To investigate this, CRISPR/Cas9-gene edited HEK293 cells and HeLa cells were used to detect CXCR4/EGFR heterodimers at endogenous expression levels of either one or both receptors.

Firstly, potential differences between CXCR4 targeting nanobodies binding to NLuc\_CXCR4 when overexpressed or endogenously expressed in HEK293 cells was investigated. CRISPR/Cas9 edited NLuc\_CXCR4 was used for endogenous expression of CXCR4(White et al., 2020b) . All three CXCR4 nanobodies VUN415, VUN400c and VUN401 (Van Hout et al., 2018) showed significantly higher affinities to CRISPR/Cas9-edited NLuc\_CXCR4 then overexpressed NLuc CXCR4 whereas there was no significant difference for CXCL12 binding (**Figure 5.8, Table 5.1**). An increased BRET signal was observed between CRISPR/Cas9-edited NLuc\_CXCR4

and overexpressed Halo\_EGFR in HEK293 cells indicating heterodimer formation between endogenous CXCR4 and overexpressed EGFR (**Figure 5.14**). In addition, proximity ligation assays (PLA) were able to show CXCR4/EGFR heterodimerisation (**Figure 5.16**) and CXCR4 homodimerisation (**Figure 5.16**) in native HeLa cells endogenously expressing both CXCR4 and EGFR. The successful specific binding of the nanobodies conjugated with circular oligomers and streptavidin-HRP used for PLA was also demonstrated in CRISPR/Cas9-edited NLuc\_CXCR4 HeLa cells (**Figure 5.15**).

The endogenous ligands of EGFR and CXCR4, EGF and CXCL12, promoted EGFR and CXCR4 homodimer complexes (**Figure 5.9** and **Figure 5.10**). In contrast both had negative regulatory effects on CXCR4/EGFR heterodimers (**Figure 5.11**). Hence, we decided to investigate whether CXCL12 could bind to EGFR or EGF to CXCR4. As expected, CXCL12-AF647 showed no binding affinity to NLuc\_EGFR (**Figure 5.17**). Similarly, EGF-AF647 had no affinity for NLuc\_CXCR4 (**Figure 5.17**). Two questions arose from this observation: (a) Is there competition between CXCL12 and EGF binding at their cognate receptors? (b) Does the co-expression/dimerisation of CXCR4/EGFR have any impact on CXCL12 and EGF binding at their cognate receptors? Interestingly, EGF-AF647 binding was potently and partially inhibited by EGF and CXCL12 respectively in both NLuc\_EGFR only and NLuc\_EGFR/SNAP\_CXCR4 co-expressed cells (**Figure 5.18**). CXCL12-AF647 binding was potently inhibited in both NLuc\_CXCR only and NLuc\_CXCR4/Halo\_EGFR co-expressed cells (**Figure 5.18**). However, EGF showed only partial displacement of CXCL12-AF647 binding at NLuc\_CXCR4 when co-expressed with Halo\_EGFR (**Figure 5.18D**). Hence, there was no significant difference between single expression and co-expression of CXCR4 and EGFR on inhibitory effects of CXCL12 and EGF. Interestingly, CXCL12 was more potent at displacing the binding of EGF-AF647 (**Figure 5.18A**) than it was displacing the binding of CXCL12-AF647 (**Figure 5.18B**). Since CXCL12-AF647 showed no affinity to EGFR or EGF-AF647 to CXCR4, it is curious that CXCL12 seemingly competes with EGF-AF647. The endogenous expression of CXCR4 (Busillo et al., 2010b) in cells with NLuc\_EGFR might explain these observations. Endogenous CXCR4 might tend to form homodimers since assumably homodimerisation would be the prior preference for the receptors. In NLuc\_EGFR overexpressing HEK293 cells

with endogenous expression of CXCR4, much less heterodimer formation could be seen because of more CXCR4 homodimer formation due to limited CXCR4 expression. However, overexpression of both receptors might lead to more heterodimerisation formation due to a higher density of receptors on the cell membrane. Future experiments are needed to explain this phenomenon with HEK293 cells lacking CXCR4 (CRISPR/Cas9 knock-out) to eliminate CXCR4 expression level difference. This would help understanding of homodimer/heterodimer formation dynamics alteration due to receptor density on the membrane.

Finally, the role of the extracellular domains of EGFR on homodimerisation has previously been shown (Bessman, Bagchi, et al., 2014b; Freed et al., 2017; Kovacs et al., 2015b; Mudumbi et al., 2023; Ogiso et al., 2002a). Yet, the heterodimerisation interface for EGFR/GPCR is still unknown. In our data, CXCR4/EGFR dimerisation was not affected by the conformational sensor nanobody Q86c-HL488 binding to the EGFR (**Figure 5.19**). This might demonstrate that there is a specific EGFR conformational change in presence of CXCR4, and this specific conformation would not be recognized by Q86c-HL488. Another explanation might be that the EGFR extracellular domains might play a minor role in CXCR4/EGFR heterodimerisation meaning that the dimerisation could be led by the other domains such as transmembrane, intracellular or juxtamembrane domains. A recent study showed that, similar to EGF, erlotinib has an increasing effect on EGFR homodimerisation (Haubrich et al., 2024). EGFR homodimerisation might influence the enhancement of both Q44c-HL488 and Q86c-HL488 binding on NLuc\_EGFR (**Figure 5.19**).

#### **5.4 Conclusion**

- CXCR and EGFR can form homodimers.
- CXCR4 and EGFR homodimer formations can be altered by their endogenous ligands, antagonists and nanobodies that specifically target them (
- **Table 5.3**).
- CXCR4/EGFR heterodimer formation is not restricted to cells that overexpress the receptors concerned. The PLA technique showed that endogenously expressed CXCR4/EGFR can form heterodimers in HeLa cells.

- CXCL12 has no direct binding affinity for EGFR and EGF has no direct binding affinity on CXCR4. However, they can have inhibitory effects on ligand binding as a consequence of heteromerisation.

**Table 5.3 The effect of CXCR4 and EGFR ligands and nanobodies on CXCR4/EGFR complexes** (next page). (↑ = increase, ↓ = decrease, - = no effect, / = not tested.)

	<b>CXCR4 Homodimer</b>	<b>EGFR Homodimer</b>	<b>CXCR4-EGFR Heterodimer</b>
EGF	-	↑	↓
TGF- $\alpha$	/	↑	↓
Hb-EGF	/	↑	↓
AREG	/	-	↓
EREG	/	-	↓
Epigen	/	-	↓
BTC	/	-	↓
CXCL12	↑	-	↓
EGF+CXCL12	↑	↑	↓
AMD3100	-	-	-
AMD070	↓	-	-
IT1t	↓	-	-
Erlotinib	-	↑	-
VUN400c	↑	-	↓
VUN400	↓	/	-
VUN401	↓	-	↑
VUN415c	-	-	↓
VUN415	-	/	-
Q44c	-	↑	-

---

Q44-Biotin	-	/	-
Q86c	-	-	-

---

# **Chapter 6: General Discussion and Conclusions**

## 6.1 General Discussion

CXCR4 and EGFR are key regulator receptors for cancer progression (Shi et al., 2020; Sigismund et al., 2018; Ziełńska & Katanaev, 2020b). While signalling mechanisms of both receptors are well defined the heterodimerisation of them has not studied. Considering the relevance of both receptors in drug discovery, in this project we aimed to understand the pharmacology of CXCR4/EGFR heterodimerisation. A proximity based NanoBRET assay was used to monitor the dynamics of nanoluciferase and fluorescent protein (SNAPTag and HaloTag) labelled CXCR4/EGFR complexes. As a result, we gained novel understanding of CXCR4/EGFR heterodimerisation and the effect of ligands and nanobodies on this receptor complex.

Chapter 3 characterised the binding properties of labelled and unlabelled novel compounds for CXCR4 and ACKR3 at nanoluciferase tagged full-length CXCR4 (Dekkers et al., 2023) and ACKR3 (Dekkers et al., 2024). NanoBRET was used to monitor their ligand binding to CXCR4 or ACKR3 at 37°C when expressed in living HEK293T cells.

Chapter 4 investigated the binding properties of all known endogenous EGFR ligands and nanobodies (Q44 and Q86) at stably transfected N-terminal tagged NLuc\_EGFR expressed in HEK293 cells (Comez et al., 2022; van den Bor et al., 2023). Additionally, the binding interactions between EGFR nanobodies Q44 and Q86 and ligands was studied. While Q44 has been shown to compete with EGF, Q86 binding at EGFR was enhanced in the presence of EGF. Q86 was characterised as a conformational sensor since its affinity for EGFR was increased with EGF binding. NanoBRET was used to monitor their real-time ligand binding kinetics at 37°C in living HEK293T cells. Internalisation of EGFR was studied using a HiBiT internalisation assay and no effect of both Q44 and Q86 was detected on EGFR internalisation.

Chapter 5 elucidated the dynamics of CXCR4/EGFR homodimer and heterodimer complexes using N-terminal tagged nanoluciferase and HaloTag/SNAPTag receptor (EGFR and CXCR4) configurations transiently overexpressed in HEK293 cells. Additionally, CXCR4/EGFR complexes at endogenous expression levels were detected by proximity ligation assay using circular oligomer conjugated nanobodies in HeLa cells. The effect of CXCR4 and EGFR

receptor specific ligands and nanobodies on CXCR4/EGFR complexes was monitored. These ligands and nanobodies were validated in chapter 3 and chapter 4.

*What is the pharmacology fluorescent novel compounds for CXCR4 and ACKR3?*

The generation of novel compounds for CXCR4 and ACKR3 is crucial for inflammation and cancer research. Various studies have designed, synthesized and tested the pharmacological properties of such compounds targeting either CXCR4 or ACKR3 (Bayrak et al., 2022b; Dekkers et al., 2023; Lin et al., 2020; Mishra et al., 2016; Thoma et al., 2008; Zarca et al., 2024). Yet more compounds with fluorescent labels could be used as a tool for CXCR4 and ACKR3 research. Having selective fluorescent tools allow us to work on the pharmacology of these receptors like binding affinities of non-fluorescent compounds and internalisation of the receptors. In our study we described the pharmacological evaluation of recently developed and synthesised fluorescent CXCR4 probes based on IT1t (Thoma et al., 2008) and AMD070 (Mosi et al., 2012) as well as non-fluorescent and fluorescent ACKR3 probes based on VUF11207 (Wijtmans et al., 2012) (Chapter 3). Novel BODIPY 630/650-X fluorophore conjugated CXCR4 antagonists 10 (IT1t based), and 24 (AMD070 based) maintained their affinity toward the CXCR4 receptor even after conjugation to a fluorophore which increased their size (Chapter 3). Previous results investigated the pharmacology of these compounds in purified membranes prepared from NLuc\_CXCR4 expressing HEK293 cells (Dekkers et al., 2023). Both CXCR4 compounds showed higher affinity to the purified membranes than whole HEK293 cells. In contrast to our results, AMD3100 could not fully compete with compound 10 in purified membranes (Dekkers et al., 2023), while we have shown that both AMD3100 and IT1t completely displaced compound 10 (Dekkers et al., 2023). It could be argued that the membrane properties and features might change the competitive properties of AMD3100, which might lead to a non-competitive interaction resembling allosterism because in membrane preparations the compounds would be able to bind more non-specific sites of the receptors. Fluorescent conjugates of VUF11207 (Wijtmans et al., 2012) labelled with BODIPY FL-X with linkers of three different lengths also successfully bound to the ACKR3 receptor in live cells.

*What is the pharmacology of EGFR targeting nanobodies?*

There are several heavy-chain antibodies targeting EGFR (Roovers et al., 2007) purposing to monitor EGFR oligomerisation (Hofman et al., 2010a), tumour imaging (Piramoon et al., 2017), tumour growth inhibitor (Roovers et al., 2007) and determination of conformational status (Nevoltris et al., 2015a) (Sharifi et al., 2021). Chapter 4 investigated the pharmacology of two different fluorescent label conjugated EGFR nanobodies using NanoBRET with NLuc\_EGFR in HEK293 cells. One of the nanobodies is Q86c-HL488 EgB4 (Zanetti-Domingues et al., 2018) derivative. The second nanobody Q44c-HL488 binds to EGF-binding site on domain III (Low-Nam et al., 2011; Schmitz et al., 2013b). of ECD of EGFR as a similar manner to previously studied 7D12 nanobody in (Schmitz et al., 2013b). In keeping with the previous studies Q44c-HL488 competes with the EGF at EGF binding site of EGFR (**Figure 4.5** and **Figure 4.7**). Consistent with the information that Q44c nanobody binds to similar site as EGFR ligands, Q44c-HL488 displacement rank by the high affinity (TGF $\alpha$ , BTC, HB-EGF) and low affinity (epiregulin, epigen and amphiregulin) ligands was comparable to displacement of labelled EGF on EGFR. Q86 (termed EgB4) has been shown not compete EGF binding to EGFR (Hofman et al., 2008)(Low-Nam et al., 2011). In keeping with that we showed that fluorescent Q86c-HL488 could not be displaced by EGF, oppositely the binding of Q86c-HL488 was increased in the presence of EGF (**Figure 4.5**). A rank of enhancement with all EGFR ligands was in reverse to Q44 displacement. These data suggest that the binding of EGF and other EGFR ligands might cause a conformational change, leading to an enhanced binding of Q86c to the EGFR. Q86c can therefore be considered to act as a conformational sensor for EGF ligand induced activation. This conformational change of EGFR might influence both the relative orientation and proximity of the donor and acceptor elements (Lay et al., 2022; Schihada et al., 2018). This change on the orientation and proximity of NLuc and fluorescent nanobody leads to increase energy transfer from the NLuc to fluorescent label of the nanobody resulting an increase on BRET signal. This might be due to conformational changes of EGFR by agonist binding that lead to exposure of the dimerisation interface in domain II promoting receptor homodimerisation (Bessman et al., 2014; Burgess et al., 2003; Dawson et al., 2005; Defize et al., 1989; Freed, 2017; Macdonald-Obermann & Pike, 2009).

*Do CXCR4 and EGFR form heterodimers?*

Several studies have demonstrated the signalling cross-talk between CXCR4 and EGFR (Chapter 5, Introduction) (Y. Cheng et al., 2020; M. Neves et al., 2020, 2022). Studies described in Chapter 5 investigated CXCR4/EGFR heterodimer formation using two different configurations of the NanoBRET assay (Chapter 5, **Error! Reference source not found.**) where both receptors are overexpressed. In addition, CXCR4/EGFR heterodimerisation was monitored in endogenous expression systems such as CRISPR-edited HEK293 cells and wild-type HeLa cells using proximity ligation assays. Demonstration of CXCR4/EGFR dimers with two different techniques at both overexpressed and endogenous receptor expression levels provided more insight of the pharmacology of this complex.

- With the same system, we examined the effects of EGFR and CXCR4 endogenous ligands, antagonists and nanobodies on CXCR4/EGFR complexes. All endogenous ligands of CXCR4 and EGFR decreased the BRET signal between CXCR4/EGFR complexes (Chapter 5, **Figure 5.11**,

**Table 5.3**). Additionally, the decreasing effect of EGFR ligands on CXCR4/EGFR dimers was concentration dependent. Only a CXCR4 targeting nanobody VUN401 increased EGFR/CXCR4 complex formation.

Studies have shown that transactivation of CXCR4 downstream mediators, such as G $\alpha$ i activation, can occur following stimulation of by EGF and EGFR in HEK293 and HeLa cells (M. Neves et al., 2020; Roy et al., 2024). Therefore, it is important to understand whether EGFR ligand binds on CXCR4. In our BRET ligand binding studies (Chapter 5) we have observed no EGF binding at CXCR4 and similarly no CXCL12 binding at EGFR. Therefore, CXCL12 partially displaced EGF binding at EGFR. There was a While this thesis focussed on CXCR4 and EGFR, receptor complexes could include more than two partners. For example,  $\alpha$ V $\beta$ 3 integrin can interact with both VEGFR2 (Soldi et al., 1999) and NRP1 (Robinson et al., 2009). There are specific evidences that CXCR4 and EGFR can form complexes with ACKR3 (Décaillot et al., 2011; Salazar et al., 2014b). A higher order complex including ACKR3 could modulate the pharmacology of EGFR and CXCR4.

## 6.2 Future directions

This project showed a close proximity of two membrane receptors, a GPCR (CXCR4) and a RTK (EGFR) both in overexpression and endogenous expression systems in two different cell lines with two different techniques. These cell lines are human embryonic kidney cells (HEK293T) which express a relatively low levels of endogenous EGFR expression and HeLa cells, a cervical cancer model with high CXCR4 and EGFR expression levels. Nevertheless, further studies are required to investigate the CXCR4/EGFR complex in different cell types with distinct receptor expression levels. CRISPR knock-in and knock-out approaches for both CXCR4 and EGFR could be utilized for further experiments. The nanoBRET experiments described in this thesis, were performed with N-terminal tagged receptors and membrane impermeable fluorescence labelling of Halo or SnapTagged receptors. Therefore, it gives us information about the receptors located on the cell surface. More BRET experiments with receptors tagged with a C-terminal nanoluciferase or fluorescent tags could assist us to obtain more understanding whether the dimer formation include the intracellular domains of the receptors. Accordingly, investigating the localisation of CXCR4 and or EGFR would expand our understanding of the receptor pharmacology of CXCR4/EGFR complexes. Internalisation of the CXCR4 and EGFR due to CXCL12 and EGF respectively has been reported previously (Z. J. Cheng et al., 2000b; Henriksen et al., 2013; Tanaka et al., 2018). Further investigation is required to understand the internalisation of CXCR4/EGFR complexes with or without ligand stimulation. Understanding whether dimerised CXCR4 and EGFR receptors internalise together could be vital to expand the knowledge on these receptors. Single molecule imaging with fluorescent labels can be utilized to monitor receptor trafficking or NanoBIT based HiBiT internalisation assay could be used to quantify the receptor internalisation.

To monitor for how long CXCR4/EGFR stably form dimers and the speed with which ligand stimulation could break the dimer formation could be studied with NanoBRET kinetics assay. The downstream signalling of both CXCR4 and EGFR is quite complex. Both receptors orchestrate various cellular behaviours such cell proliferation, migration and cancer progression. Therefore, the intracellular signalling

---

of both receptors after they dimerise could help to enlighten the cancer development process. Investigation of downstream signalling proteins such as  $G_i$ , GRKs and  $\beta$ -arrestin coupling to CXCR4 and GRB2 and SOS coupling to EGFR and further downstream signalling cascade proteins for both receptors like Erk, PI3K, Akt would be essential to understand the intracellular dynamics of their signalling. Regarding this, cellular behaviours like proliferation, migration, extravasation which are controlled by these intracellular signalling pathways could be a key part to understanding the response of a cell to CXCR4/EGFR dimerisation. Post-translational modifications of GPCRs and RTKs play a significant role in their receptor pharmacology. For example, phosphorylation and glycosylation profiles of both receptors and their effect on the CXCR4/EGFR complex could be another aspect for studying CXCR4/EGFR receptor biology. Regarding the indication that ACKR3 can form dimers with EGFR and CXCR4 (Décaillot et al., 2011; Salazar et al., 2014b), nanoBRET, PLA or co-immunoprecipitation studies could help us to understand whether ACKR3 also plays a part in CXCR4/EGFR complexes.

Receptor tyrosine kinase inhibitors (RTKIs) and antibodies targeting EGFR have been a significant field for cancer research (Guardiola et al., 2019b; X. Liu et al., 2017). Understanding the receptor pharmacology and the drug resistance mechanisms of EGFR is essential for further development of better inhibitors. Hence, understanding the effect of these RTKIs and antibodies on CXCR4/EGFR complexes might be useful to overcome drug resistance. More nanoBRET experiments could be done with various inhibitors and antibodies on CXCR4/EGFR dimers.

The future research for CXCR4/EGFR complex could benefit from computational modelling to distinguish the dimerisation interface and understanding which regions of the receptors play important parts in the dimer formation. Elucidating the specific residues from the dimer interface could help us to understand the pharmacology of the receptor complex. Following that, interpretation of computational research would be possible with mutagenesis studies. It would be essential to demonstrate the effect of single amino acids and their role in the dimer formation.

# Chapter 7: Appendix

## 7.1 Amino acid sequences of the receptors

The amino acid sequences of receptors used in this thesis, their N terminal tags and linkers translated from whole plasmid or/and Sanger sequencing results. The sequences are colour-coded, as demonstrated below.

### 7.1.1 NLuc\_CXCR4 (rat 5-HT3a Signal peptide)

Signalling sequences, NLuc/SNAPTag/ HaloTag/ HiBiT, linker, receptor of interest.

MRLCIPQVLLALFSMLTGPGEGRKLLVFTLEDFVGDWRQTAGYNLDQVLE  
 QGGVSSLFQNLGVSVTPIQRIVLSGENGLKIDIHVIIPYEGLSGDQMGQIEKIF  
 KVVYPVDDHHFKVILHYGTLVIDGVTPNMIDYFGRPYEGIAVFDGKKITVTG  
 TLWNGNKIIDERLINPDGSLFRVTINGVTGWRLCERILAGSLEGISYITSDNY  
 TEEMGSGDYDSMKEPCFREANANFNKIFLPTIYSIIFLTGIVGNGLVILVMGY  
 QKKLRSMTDKYRLHLSVADLLFVITLPFWAVDAVANWYFGNFLCKAVHVI  
 YTVNLYSSVLILAFISLDRYLAIVHATNSQRPRKLLAEKVVYVGVWIPALLT  
 IPDFIFANVSEADDRYICDRFYPNDLWVVVFQFQHIMVGLILPGIVILSCYCIII  
 SKLSHSHKGHQKRKALKTTVILILAFFACWLPYYIGISIDSFILLEIIKQGCEFEN  
 TVHKWISITEALAFFHCCLNPILYAFLGAKFKTSAQHALTSVSRGSSLKILSK  
 GKRGGHSSVSTESSESSSFHSS

### 7.1.2 NLuc\_EGFR (IL6 signal peptide)

Signalling sequences, NLuc/SNAPTag/ HaloTag/ HiBiT, linker, receptor of interest.

MNSFSTSAFGPVAFSLGLLLVLPAAFPAPVFTLEDFVGDWRQTAGYNLDQV  
 LEQGGVSSLFQNLGVSVTPIQRIVLSGENGLKIDIHVIIPYEGLSGDQMGQIEK  
 IFKVVPVDDHHFKVILHYGTLVIDGVTPNMIDYFGRPYEGIAVFDGKKITVT  
 GTLWNGNKIIDERLINPDGSLFRVTINGVTGWRLCERILAGSSGAIALEEKK  
 VCQGTSNKLTQLGTFEDHFSLQRMFNCEVVLGNLEITYVQRNYDLSFLK  
 TIQEVAGYVLIALNTVERIPLNLIQIRGNMYIYENSYALAVLSNYDANKTGL  
 KELPMRNLQEILHGAVRFSNNPALCNVESIQWRDIVSSDFLSNMSMDFQNH  
 L GSCQKCDPSPNGSCWGAGEENCQKLTKIICAQQCSGRCRGKSPSDCCHNQ  
 CAAGCTGPRES DCLVCRKFRDEATCKDTCPLMLYNPTTYQMDVNPEGKYS  
 FGATCVKKCPRNYVVTDHGSCVRACGADSYEMEEDGVRKCKKCEGPCRK  
 VCNGIGIGEFKDSLSINATNIKHFKNCTSIGDLHILPVAFRGDSFTHTPPLDPQ  
 ELDILKTVKEITGFLLIQAWPENRTDLHAFENLEIIRGRTKQHGQFSLAVVSL  
 NITSLGLRSLKEISDGDVIISGNKNLCYANTINWKKLFGTSGQKTKIISNRGEN  
 SCKATGQVCHALCSPEGCWGPEPKDCVSCRNVSRGRECVDKCNLLEGEPRE  
 FVENSECIQCHPECLPQAMNITCTGRGPDNCIQCAHYIDGPHCVKTCPAGVM  
 GENNTLVWKYADAGHVCHLCHPNCTYGCTGPGLEGCPNGPKIPSIATGMV  
 GALLLLLVALGIGLFMRRRHIVRKRTLRRLLQERELVEPLTPSGEAPNQAL  
 LRILKETEFKKIKVLGSGAFGTVYKGLWIPEGEKVKIPVAIKELREATSPKAN  
 KEILDEAYVMASVDNPHVCRLLGICLTSTVQLITQLMPFGCLLDYVREHKDN  
 IGSQYLLNWCVQIAKGMNYLED RRLVHRDLAARNVLV KTPQHVKITDFGL  
 AKLLGAEKEYHAEGGKVPKWMALLESILHRIYTHQSDVWSYGVTWELM  
 TFGSKPYDGIPASEISSILEKGERLPQPPICIDVYIMIMVKCWMIDADSRPKFR  
 ELIIEFSKMARDPQRYLVIQGDERMHLPSPTDSNFYRALMDEEDMDDVVDA  
 DEYLIPQQGFFSSPSTSRTPLLSSLSATSNNSTVACIDRNGLQSCPIKEDSFLQR  
 YSSDPTGALTEDSIDD TFLPVPEYINQSVPKRPAGSVQNPVYHNQPLNPAPSR  
 DPHYQDPHSTAVGNPEYLNTVQPTCVNSTFDSPAHWAAQKGS HQISLDNPDY  
 QQDFFPKEAKPNGIFKGSTAENA EYLRVAPQSSEFIGA

### 7.1.3 Halo\_EGFR (EGFR native signal peptide)

Signalling sequences, NLuc/SNAPTag/ HaloTag/ HiBiT, linker, receptor of interest.

MRPSGTAGAALLALLAALCPASRAGSEIGTGFPFDPHYVEVLGERMHYVDV  
 GPRDGTVPVFLHGNPTSSYVWRNIIPHVAPTHRCIAPDLIGMGKSDKPDLYF  
 FDDHVRFMDAFIEALGLEEVVLVIHDWGSALGFHWAKRNPERSVKGIAMFEF  
 IRPIPTWDEWPEFARETFQAFRTTDVGRKLIIDQNVFIEGTLPMGVVVRPLTEV  
 EMDHYREPFLNPVDREPLWRFPNELPIAGEPANIVALVEEYMDWLHQSPVP  
 KLLFWGTPGVLIPPAEAARLAKSLPNCKAVDIGPGLNLLQEDNPDLIGSEIAR  
 WLSTLEISGGSSGGGGSSGGSSGAIA  
 LEEKKVCQGTSNKLTQLGTFEDHFLSLQRMFNCEVVLGNLEITYVQRNYD  
 LSFLKTIQEVAGYVLIALNTVERIPLNLIQIRGNMYEYNSYALAVLSNYDAN  
 KTGLKELPMRNLQEILHGAVRFSNNPALCNVESIQWRDIVSSDFLSNMSMDF  
 QNHLGSCQKCDPSCPNGSCWGAGEENCQKLTKIICAQQCSGRRCRGKSPSDC  
 CHNQCAAGCTGPRESCLVCRKFRDEATCKDTCPLMLYNPTTYQMDVNP  
 EGKYSFGATCVKKCPRNYVVTDHGSCVRACGADSYEMEEDGVRKCKKCE  
 GPCRKVCNGIGIGEFKDSLSINATNIKHFKNCTSSISGDLHILPVAFRGDSFTHT  
 PPLDPQELDILKTVKEITGFLLIQAWPENRTDLHAFENLEIIRGRTKQHGQFSL  
 AVVSLNITSLGLRSLKEISDGDVIISGNKNLCYANTINWKKLFGTSGQKTKIIS  
 NRGENSCKATGQVCHALCSPEGCWGPEPKDCVSCRNVSRGRECVDKCNLL  
 EGEPREFVENSECIQCHPECLPQAMNITCTGRGPDNCIQCAHYIDGPHCVKTC  
 PAGVMGENNTLVWKYADAGHVCHLCHPNCTYGCTGPGLEGCPNTPKIPSI  
 ATGMVGALLLLLVALGIGLFRRRHIVRKRTLRLRLQERELVEPLTPSGEA  
 PNQALLRILKETEFKKIKVLGSGAFGTVYKGLWIPEGEKVKIPVAIKELREAT  
 SPKANKEILDEAYVMASVDNPHVCRLLGICLTSTVQLITQLMPFGCLLDYVR  
 EHKDNIGSQYLLNWCVQIAKGMNYLEDRLVHRDLAARNVLVKTTPQHVKI  
 TDFGLAKLLGAEKEYHAEGGKVPKWMALLESILHRIYTHQSDVWSYGVTV  
 WELMTFGSKPYDGIPASEISSILEKGERLPQPPICTIDVYIMVVKCWMIDADS  
 RPKFRELIIEFSKMARDPQRYLVIQGDERMHLPSPTDSNFYRALMDEEDMDD  
 VVDADEYLIPQQGFFSSPSTSRTPLLSSLSATSNNSTVACIDRNLQSCPIKED  
 SFLQRYSSDPTGALTEDSIDDTFPLVPEYINQSVPKRPAGSVQNPVYHNQPLN  
 PAPSRRPHYQDPHSTAVGNPEYLNTVQPTCVNSTFDSPAHWAAQKGS HQISL  
 DNPDYQQDFFPKEAKPNGIFKGSTAENAEYLRVAPQSSEFIGA

#### 7.1.4 SNAP\_CXCR4 (rat 5-HT<sub>3a</sub> signal peptide)

Signalling sequences, NLuc/SNAPTag/ HaloTag/ HiBiT, linker, receptor of interest.

MRLCIPQVLLALFLSMLTGPGEGRKLTLDKDCMKRTTLDSPGKLELSGC  
EQGLHEIKLLGKGTSAADAVEVPAPAAVLGGPEPLMQATAWLNAYFHQPE  
AIEFPVPALHHPVFQQESFTRQVLWKLKVVKFGEVISYQQLAALAGNPAA  
TAAVKTALSGNPVILIPCHRVSSTSGAVGGYEGGLAVKEWLLAHEGHRG  
KPGLGSLGISIYTSNYTEEMGSGDYDSMKEPCFREANANFNKIFLPTIYSIIF  
LTGIVGNGLVILVMGYQKKLRSMTDKYRLHLSVADLLFVITLFWAVDAVA  
NWFYFGNFLCKAVHVIYTVNLYSSVLILAFISLDRYLAIVHATNSQRPRKLLA  
EKVVYVGVWIPALLLTIPDFIFANVSEADRYICDRFYPNDLWVVVFQFQHI  
MVGLILPGIVILSCYCIISKLSHSGKHQKRKALKTTVILILAFFACWLPYYIGIS  
IDSFILLEIKQGCEFENTVHKWISITEALAFFHCCLNPILYAFLGAKFKTSAQH  
ALTSVSRGSSLKILSKGKRGGHSSVSTESSESSSFHSS

### 7.1.5 HiBiT\_EGFR (IL6 signal peptide)

Signalling sequences, NLuc/SNAPTag/ HaloTag/ HiBiT, linker, receptor of interest.

MNSFSTSAFGPVAFSLGLLLVLPAAFPAPVSGWRLFKKISGSSGGSSGAIALE  
 EKKVCQGTSNKLTQLGTFEDHFLSLQRMFNNCEVV LGNLEITYVQRNYDLS  
 FLKTIQEVAGYVLIALNTVERIPLNQLIIRGNMYYENSYALAVLSNYDANK  
 TGLKELPMRNLQEILHGAVRFSNNPALCNVESIQWRDIVSSDFLSNMSMDFQ  
 NHLGSCQKCDPSPNGSCWGAGEENCQKLTKIICAQQCSGRCRGKSPSDCC  
 HNQCAAGCTGPRES DCLVCRKFRDEATCKDTCPLMLYNPTTYQMDVNPE  
 GKYSFGATCVKK CPRNYVVTDHGSCVRACGADSYEMEEDGVRKCKKCEGP  
 CRKVCNGIGIGEFKDSLSINATNIKHFKNCTSISGDLHILPVAFRGDSFTHTPPL  
 DPQELDILKTVKEITGFLLIQAWPENRTDLHAFENLEIIRGRTKQHGQFSLAV  
 VSLNITSLGLRSLKEISDGDVIISGNKNLCYANTINWKKLFGTSGQKTKIISNR  
 GENSKATGQVCHALCSPEGCWGPEPKDCVSCRNVSRGRECVDKCNLLEG  
 EPREFVENSECIQCHPECLPQAMNITCTGRGPDNCIQCAHYIDGPHCVKTCPA  
 GVMGENNTLVWKYADAGHVCHLCHPNCTYGCTGPGLEGCP TNGPKIPSIAT  
 GMVGALLLLL VVALGIGLFMRRRHIVRKRTL RLLQERELVEPLTPSGEAPN  
 QALLRILKETEFKKIKVLGSGAFGTVYKGLWIPEGEKVKIPVAIKELREATSP  
 KANKEILDEAYVMASVDNPHVCRLLGICLTSTVQLITQLMPFGCLLDYVREH  
 KDNIGSQYLLNWCVQIAKGMNYLED RRLVHRDLAARNVLVKTPQHVKITD  
 FGLAKLLGAEKEYHAEGGKVPKWMALESILHRIYTHQSDVWSYGVTWV  
 ELMTFGSKPYDGIPASEISSILEKGERLPQPPICTIDVYMIMVKCWMIDADSRP  
 KFRELIIIEFSKMARDPQRYLVIQGDERMHLPSPTDSNFYRALMDEEDMDDV  
 VDADEYLIPQQGFFSSPSTSRTPLLSSLSATSNNSTVACIDRNLQSCPIKEDSF  
 LQRYSSDPTGALTEDSIDD TFLPVPEYINQSVPKRPAGSVQNPVYHNQPLNPA  
 PSRDPHYQDPHSTAVGNPEYLNTVQPTCVNSTFDSPAHWAKGSHQISLDN  
 PDYQQDFFPKAKPNGIFKGSTAENAEYLRVAPQSSEFIGAV

---

**7.1.6 Sequencing primers for EGFR**

Sequencing Primer 1	CGCAGTTGGGCACTTTTGAAG	21-mer
Sequencing Primer 2	AATCCCAAGGACCACCTCAC	21-mer
Sequencing Primer 3	AGTGTCCCCGTAATTATGTGG	21-mer
Sequencing Primer 4	CACTTCTTACACTTGCGGACG	21-mer
Sequencing Primer 5	ACCTGTGCCATCCAAACTGCA	21-mer
Sequencing Primer 6	ATCTTAGGCCCATTCGTTGGA	21-mer
Sequencing Primer 7	CGTGAGTTGATCATCGAATTCTCC	24-mer
Sequencing Primer 8	AAGTTGGAGTCTGTAGGACTTGG	23-mer
Sequencing Primer 9	TTACACCGACTAGCCAGGAAG	22-mer
Sequencing Primer 10	TTCTTGCTGGATGCGTTTCTG	21-mer
Sequencing Primer 11	TGTGTGTGCCCTGTAACCTGA	21-mer
Sequencing Primer 12	GACTGAACATAACTGTAGGCTGA	23-mer
Sequencing Primer 13	GTTCAATTCATCCTCACCAGCAG	23-mer
Sequencing Primer 14	GCTCACTCACAAAGGAGGGAAG	22-mer

---

T7P Sequencing Primer	TAATACGACTCACTATAGGG	20-mer
T7T Sequencing Primer	TATGCTAGTTATTGCTCAGCGG	22-mer

**Table 7.1 Solvents and excitation/emission of ligands, compounds and nanobodies used.**

Ligand/Compound/Nanobody	Solvent	Excitation/ Emission
EGF	PBS	-
Hb-EGF	H <sub>2</sub> O with 0.1% BSA	-
TGF-alpha	H <sub>2</sub> O with 0.1% BSA	-
BTC	H <sub>2</sub> O with 0.1% BSA	-
Amphiregulin (AREG)	PBS	-
Epiregulin (EREG)	H <sub>2</sub> O with 0.1% BSA	-
Epigen	H <sub>2</sub> O with 0.1% BSA	-
CXCL12 (SDF-1alpha)	H <sub>2</sub> O	-
AMD3100	H <sub>2</sub> O	-
AMD070	H <sub>2</sub> O	-
IT1t	H <sub>2</sub> O	-
EGF-AF488	H <sub>2</sub> O	490/525 nm
EGF-AF647	H <sub>2</sub> O	650/671 nm
CXCL12-AF647	H <sub>2</sub> O	650/671 nm

---

Compound 10	DMSO	625/642 nm
Compound 24	DMSO	625/642 nm
18a-BODIPY FL-X	DMSO	504/510 nm
18b-BODIPY FL-X	DMSO	504/510 nm
18c-BODIPY FL-X	DMSO	504/510 nm
VUF11207	DMSO	-
4 (VUF11072)	DMSO	-
9 (VUF11074)	DMSO	-
19 (VUF11403)	DMSO	-
20 (VUF16545)	DMSO	-
Q44c	PBS	-
Q86c	PBS	-
Q44c-HL488	PBS	497/526 nm
Q86c-HL488	PBS	497/526 nm
VUN400	PBS	-
VUN401c (Q84c)	PBS	-
VUN415c	PBS	-

---

# Chapter 8: References

- Adlere, I., Caspar, B., Arimont, M., Dekkers, S., Visser, K., Stuijt, J., de Graaf, C., Stocks, M., Kellam, B., Briddon, S., Wijtmans, M., de Esch, I., Hill, S., & Leurs, R. (2019). Modulators of CXCR4 and CXCR7/AckR3 function. *Molecular Pharmacology*, *96*(6), 737–752. <https://doi.org/10.1124/mol.119.117663>
- Alan V. Smrcka, I. F. (2019a). G protein  $\beta\gamma$  subunits as multi-functional scaffolds and transducers in G-protein coupled receptor signaling. *Cell Mol Life Sci.*, *176*(3), 139–148. <https://doi.org/10.1007/s00018-019-03275-2>
- Armando, S., Quoyer, J., Lukashova, V., Maiga, A., Percherancier, Y., Heveker, N., Pin, J. P., Prézeau, L., & Bouvier, M. (2014). The chemokine CXCR4 and CC2 receptors form homo- and heterooligomers that can engage their signaling G-protein effectors and  $\beta$ arrestin. *FASEB Journal*, *28*(10), 4509–4523. <https://doi.org/10.1096/fj.13-242446>
- Attwood, T. K., & Findlay, J. B. C. (1994). Fingerprinting g-protein-coupled receptors. *Protein Engineering, Design and Selection*, *7*(2), 195–203. <https://doi.org/10.1093/protein/7.2.195>
- Babcock, G. J., Farzan, M., & Sodroski, J. (2003). Ligand-independent dimerisation of CXCR4, a principal HIV-1 coreceptor. *Journal of Biological Chemistry*, *278*(5), 3378–3385. <https://doi.org/10.1074/jbc.M210140200>
- Bachelierie, F., Ben-Baruch, A., Burkhardt, A. M., Combadiere, C., Farber, J. M., Graham, G. J., Horuk, R., Sparre-Ulrich, A. H., Locati, M., Luster, A. D., Mantovani, A., Matsushima, K., Murphy, P. M., Nibbs, R., Nomiyama, H., Power, C. A., Proudfoot, A. E. I., Rosenkilde, M. M., Rot, A., ... Zlotnik, A. (2014). International union of pharmacology. LXXXIX. Update on the extended family of chemokine receptors and introducing a new nomenclature for atypical chemokine receptors. *Pharmacological Reviews*, *66*(1), 1–79. <https://doi.org/10.1124/pr.113.007724>
- Bachelierie, F., Graham, G. J., Locati, M., Mantovani, A., Murphy, P. M., Nibbs, R., Rot, A., Sozzani, S., & Thelen, M. (2015). An atypical addition to the chemokine receptor nomenclature: IUPHAR Review 15. *British Journal of Pharmacology*, *172*(16), 3945–3949. <https://doi.org/10.1111/bph.13182>

- Baker, J. G., Middleton, R., Adams, L., May, L. T., Briddon, S. J., Kellam, B., & Hill, S. J. (2010a). Influence of fluorophore and linker composition on the pharmacology of fluorescent adenosine A 1 receptor ligands: Themed section: Imaging in pharmacology research paper. *British Journal of Pharmacology*, *159*(4), 772–786. <https://doi.org/10.1111/j.1476-5381.2009.00488.x>
- Balabanian, K., Lagane, B., Infantino, S., Chow, K. Y. C., Harriague, J., Moepps, B., Arenzana-Seisdedos, F., Thelen, M., & Bachelier, F. (2005). The chemokine SDF-1/CXCL12 binds to and signals through the orphan receptor RDC1 in T lymphocytes. *Journal of Biological Chemistry*, *280*(42), 35760–35766. <https://doi.org/10.1074/jbc.M508234200>
- Bannas, P., Hambach, J., & Koch-Nolte, F. (2017a). Nanobodies and nanobody-based human heavy chain antibodies as antitumor therapeutics. *Frontiers in Immunology*, *8*(NOV), 1–13. <https://doi.org/10.3389/fimmu.2017.01603>
- Basith, S., Cui, M., Macalino, S. J. Y., Park, J., Clavio, N. A. B., Kang, S., & Choi, S. (2018a). Exploring G protein-coupled receptors (GPCRs) ligand space via cheminformatics approaches: Impact on rational drug design. *Frontiers in Pharmacology*, *9*(MAR), 1–26. <https://doi.org/10.3389/fphar.2018.00128>
- Basith, S., Cui, M., Macalino, S. J. Y., Park, J., Clavio, N. A. B., Kang, S., & Choi, S. (2018b). Exploring G protein-coupled receptors (GPCRs) ligand space via cheminformatics approaches: Impact on rational drug design. *Frontiers in Pharmacology*, *9*(MAR), 1–26. <https://doi.org/10.3389/fphar.2018.00128>
- Bayrak, A., Mohr, F., Kolb, K., Szpakowska, M., Shevchenko, E., Dicenta, V., Rohlfing, A.-K., Kudolo, M., Pantsar, T., Günther, M., Kaczor, A. A., Poso, A., Chevigné, A., Pillaiyar, T., Gawaz, M., & Laufer, S. A. (2022b). Discovery and Development of First-in-Class ACKR3/CXCR7 Superagonists for Platelet Degranulation Modulation. *Journal of Medicinal Chemistry*, *65*(19), 13365–13384. <https://doi.org/10.1021/acs.jmedchem.2c01198>
- Benovic, K. E. K. and J. L. (2018b). G protein-coupled receptor kinases: Past, present and future. *Cell Signal.*, *41*(3), 17–24. <https://doi.org/10.1016/j.cellsig.2017.07.004>

- Bergelin, N., Löf, C., Balthasar, S., Kalhori, V., & Törnquist, K. (2010). S1P1 and VEGFR-2 Form a Signaling Complex with Extracellularly Regulated Kinase 1/2 and Protein Kinase C- $\alpha$  Regulating ML-1 Thyroid Carcinoma Cell Migration. *Endocrinology*, *151*(7), 2994–3005. <https://doi.org/10.1210/en.2009-1387>
- Bessman, N. J., Bagchi, A., Ferguson, K. M., & Lemmon, M. A. (2014a). Complex Relationship between Ligand Binding and Dimerisation in the Epidermal Growth Factor Receptor. *Cell Reports*, *9*(4), 1306–1317. <https://doi.org/10.1016/j.celrep.2014.10.010>
- Bessman, N. J., Freed, D. M., & Lemmon, M. A. (2014). Putting together structures of epidermal growth factor receptors. *Current Opinion in Structural Biology*, *29*, 95–101. <https://doi.org/10.1016/j.sbi.2014.10.002>
- Blasco-Benito, S., Moreno, E., Seijo-Vila, M., Tundidor, I., Andradas, C., Caffarel, M. M., Caro-Villalobos, M., Urigüen, L., Diez-Alarcia, R., Moreno-Bueno, G., Hernández, L., Manso, L., Homar-Ruano, P., McCormick, P. J., Bibic, L., Bernadó-Morales, C., Arribas, J., Canals, M., Casadó, V., ... Sánchez, C. (2019). Therapeutic targeting of HER2–CB2R heteromers in HER2-positive breast cancer. *Proceedings of the National Academy of Sciences of the United States of America*, *116*(9), 3863–3872. <https://doi.org/10.1073/pnas.1815034116>
- Bridger, G. J., Skerlj, R. T., Hernandez-Abad, P. E., Bogucki, D. E., Wang, Z., Zhou, Y., Nan, S., Boehringer, E. M., Wilson, T., Crawford, J., Metz, M., Hatse, S., Princen, K., De Clercq, E., & Schols, D. (2010). AMD3100/CXCR4 INHIBITOR. *Journal of Medicinal Chemistry*, *53*(3), 1250–1260. <https://doi.org/10.1021/jm901530b>
- Burgess, A. W. (2008a). EGFR family: Structure physiology signalling and therapeutic target. *Growth Factors*, *26*(5), 263–274. <https://doi.org/10.1080/08977190802312844>
- Burgess, A. W., Cho, H. S., Eigenbrot, C., Ferguson, K. M., Garrett, T. P. J., Leahy, D. J., Lemmon, M. A., Sliwkowski, M. X., Ward, C. W., & Yokoyama, S. (2003). An open-and-shut case? Recent insights into the activation of EGF/ErbB receptors. *Molecular Cell*, *12*(3), 541–552. [https://doi.org/10.1016/S1097-2765\(03\)00350-2](https://doi.org/10.1016/S1097-2765(03)00350-2)

- 
- Busillo, J. M., Armando, S., Sengupta, R., Meucci, O., Bouvier, M., & Benovic, J. L. (2010a). Site-specific phosphorylation of CXCR4 is dynamically regulated by multiple kinases and results in differential modulation of CXCR4 signaling. *Journal of Biological Chemistry*, 285(10), 7805–7817. <https://doi.org/10.1074/jbc.M109.091173>
- Busillo, J. M., & Benovic, J. L. (2007). Regulation of CXCR4 signaling. *Biochimica et Biophysica Acta - Biomembranes*, 1768(4), 952–963. <https://doi.org/10.1016/j.bbamem.2006.11.002>
- Cabioglu, N., Gong, Y., Islam, R., Broglio, K. R., Sneige, N., Sahin, A., Gonzalez-Angulo, A. M., Morandi, P., Bucana, C., Hortobagyi, G. N., & Cristofanilli, M. (2007). Expression of growth factor and chemokine receptors: New insights in the biology of inflammatory breast cancer. *Annals of Oncology*, 18(6), 1021–1029. <https://doi.org/10.1093/annonc/mdm060>
- Cadena, D. L., & Gill, G. N. (1992). Receptor tyrosine kinases. *The FASEB Journal*, 6(6), 2332–2337. <https://doi.org/10.1096/fasebj.6.6.1312047>
- Cattaneo, F., Guerra, G., Parisi, M., De Marinis, M., Tafuri, D., Cinelli, M., & Ammendola, R. (2014). Cell-surface receptors transactivation mediated by G protein-coupled receptors. *International Journal of Molecular Sciences*, 15(11), 19700–19728. <https://doi.org/10.3390/ijms151119700>
- Cavallaro, S. (2013). CXCR4/CXCL12 in non-small-cell lung cancer metastasis to the brain. *International Journal of Molecular Sciences*, 14(1), 1713–1727. <https://doi.org/10.3390/ijms14011713>
- Che, T., English, J., Krumm, B. E., Kim, K., Pardon, E., Olsen, R. H. J., Wang, S., Zhang, S., Diberto, J. F., Sciaky, N., Carroll, F. I., Steyaert, J., Wacker, D., & Roth, B. L. (2020). Nanobody-enabled monitoring of kappa opioid receptor states. *Nature Communications*, 11(1). <https://doi.org/10.1038/s41467-020-14889-7>
- Cheloha, R. W., Harmand, T. J., Wijne, C., Schwartz, T. U., & Ploegh, H. L. (2020). Exploring cellular biochemistry with nanobodies. *Journal of Biological Chemistry*, 295(45), 15307–15327. <https://doi.org/10.1074/jbc.REV120.012960>
-

- 
- Chen, H. Y., Brady, D. C., & Villanueva, J. (2016). Double trouble: Kinase domain duplication as a new path to drug resistance. *Pigment Cell and Melanoma Research*, 29(5), 493–495. <https://doi.org/10.1111/pcmr.12508>
- Cheng, Y., Che, X., Zhang, S., Guo, T., He, X., Liu, Y., & Qu, X. (2020). Positive cross-talk between CXC chemokine receptor 4 (CXCR4) and epidermal growth factor receptor (EGFR) promotes gastric cancer metastasis via the nuclear factor kappa B (NF- $\kappa$ B)-dependent pathway. *Medical Science Monitor*, 26. <https://doi.org/10.12659/MSM.925019>
- Cheng, Y., Qu, J., Che, X., Xu, L., Song, N., Ma, Y., Gong, J., Qu, X., & Liu, Y. (2017a). CXCL12/SDF-1 $\alpha$  induces migration via SRC-mediated CXCR4-EGFR cross-talk in gastric cancer cells. *Oncology Letters*, 14(2), 2103–2110. <https://doi.org/10.3892/ol.2017.6389>
- Cheng, Z. J., Zhao, J., Sun, Y., Hu, W., Wu, Y. L., Cen, B., Wu, G. X., & Pei, G. (2000a).  $\beta$ -Arrestin differentially regulates the chemokine receptor CXCR4-mediated signaling and receptor internalisation, and this implicates multiple interaction sites between  $\beta$ -arrestin and CXCR4. *Journal of Biological Chemistry*, 275(4), 2479–2485. <https://doi.org/10.1074/jbc.275.4.2479>
- Comez, D., Glenn, J., Anbuhl, S. M., Heukers, R., Martine, J., Hill, S. J., Kilpatrick, L. E., & Midlands, T. (2022). *Fluorescently tagged nanobodies and NanoBRET to study ligand- binding and agonist-induced conformational changes of full-length EGFR expressed in living cells.*
- Conrath, K. E., Wernery, U., Muyldermans, S., & Nguyen, V. K. (2003). Emergence and evolution of functional heavy-chain antibodies in Camelidae. *Developmental and Comparative Immunology*, 27(2), 87–103. [https://doi.org/10.1016/S0145-305X\(02\)00071-X](https://doi.org/10.1016/S0145-305X(02)00071-X)
- Da Cunha Santos, G., Shepherd, F. A., & Tsao, M. S. (2011a). EGFR mutations and lung cancer. *Annual Review of Pathology: Mechanisms of Disease*, 6, 49–69. <https://doi.org/10.1146/annurev-pathol-011110-130206>
- Daub, H., Weiss, F. U., Wallasch, C., & Ullrich, A. (1996). *G-protein-coupled receptors Blot Ab : I- Blot Ab : 379*(February), 557–560.
-

- Dawson, J. P., Berger, M. B., Lin, C.-C., & Schlessinger, J. (2005a). *Epidermal Growth Factor Receptor Dimerisation and Activation Require Ligand-Induced Conformational Changes in the Dimer Interface*. *105*(1), 238–240. <https://doi.org/10.1128/MCB.25.17.7734>
- De Clercq, E. (2019). Mozobil® (Plerixafor, AMD3100), 10 years after its approval by the US Food and Drug Administration. *Antiviral Chemistry and Chemotherapy*, *27*. <https://doi.org/10.1177/2040206619829382>
- Debnath, B., Xu, S., Grande, F., Garofalo, A., & Neamati, N. (2013). Small molecule inhibitors of CXCR4. *Theranostics*, *3*(1), 47–75. <https://doi.org/10.7150/thno.5376>
- Décaillot, F. M., Kazmi, M. A., Lin, Y., Ray-Saha, S., Sakmar, T. P., & Sachdev, P. (2011). CXCR7/CXCR4 heterodimer constitutively recruits  $\beta$ -arrestin to enhance cell migration. *Journal of Biological Chemistry*, *286*(37), 32188–32197. <https://doi.org/10.1074/jbc.M111.277038>
- Defize, L. H. K., Boonstra, J., Meisenhelder, J., Kruijer, W., Tertoolen, L. G. J., Tilly, B. C., Hunter, T., Van Bergen en Henegouwen, P. M. P., Moolenaar, W. H., & De Laat, S. W. (1989). Signal transduction by epidermal growth factor occurs through the subclass of high affinity receptors. *Journal of Cell Biology*, *109*(5), 2495–2507. <https://doi.org/10.1083/jcb.109.5.2495>
- Dekkers, S., Caspar, B., Goulding, J., Kindon, N. D., Kilpatrick, L. E., Stoddart, L. A., Briddon, S. J., Kellam, B., Hill, S. J., & Stocks, M. J. (2023). Small-Molecule Fluorescent Ligands for the CXCR4 Chemokine Receptor. *Journal of Medicinal Chemistry*, *66*(7), 5208–5222. <https://doi.org/10.1021/acs.jmedchem.3c00151>
- Dekkers, S., Comez, D., Karsai, N., Arimont-Segura, M., Canals, M., Caspar, B., de Graaf, C., Kilpatrick, L. E., Leurs, R., Kellam, B., Hill, S. J., Briddon, S. J., & Stocks, M. J. (2024). Small Molecule Fluorescent Ligands for the Atypical Chemokine Receptor 3 (ACKR3). *ACS Medicinal Chemistry Letters*, *15*(1), 143–148. <https://doi.org/10.1021/acsmchemlett.3c00469>
- Devree, B. T., Mahoney, J. P., Vélez-Ruiz, G. A., Rasmussen, S. G. F., Kuszak, A. J., Edwald, E., Fung, J. J., Manglik, A., Masureel, M., Du, Y., Matt, R. A., Pardon, E., Steyaert, J., Kobilka, B. K., & Sunahara, R. K. (2016). Allosteric coupling

- from G protein to the agonist-binding pocket in GPCRs. *Nature*, 535(7610), 182–186. <https://doi.org/10.1038/nature18324>
- Di Liberto, V., Mudò, G., & Belluardo, N. (2019a). Crosstalk between receptor tyrosine kinases (RTKs) and G protein-coupled receptors (GPCR) in the brain: Focus on heteroreceptor complexes and related functional neurotrophic effects. *Neuropharmacology*, 152(November 2018), 67–77. <https://doi.org/10.1016/j.neuropharm.2018.11.018>
- Dixon, A. S., Schwinn, M. K., Hall, M. P., Zimmerman, K., Otto, P., Lubben, T. H., Butler, B. L., Binkowski, B. F., MacHleidt, T., Kirkland, T. A., Wood, M. G., Eggers, C. T., Encell, L. P., & Wood, K. V. (2016). NanoLuc Complementation Reporter Optimized for Accurate Measurement of Protein Interactions in Cells. *ACS Chemical Biology*, 11(2), 400–408. <https://doi.org/10.1021/acscchembio.5b00753>
- Dmitriev, O. Y., Lutsenko, S., & Muyldermans, S. (2016). Nanobodies as probes for protein dynamics in vitro and in cells. *Journal of Biological Chemistry*, 291(8), 3767–3775. <https://doi.org/10.1074/jbc.R115.679811>
- Dorsam, R. T., & Gutkind, J. S. (2007a). G-protein-coupled receptors and cancer. *Nature Reviews Cancer*, 7(2), 79–94. <https://doi.org/10.1038/nrc2069>
- Downward, J., Yarden, Y., Meyes, E., Ullrich, A., Schlessingert, J., & Waterfield, M. D. (1984). Close similarity of epidermal growth factor receptor and v-erb-B oncogene protein sequences. *Nature*.
- Du, Z., & Lovly, C. M. (2018a). Mechanisms of receptor tyrosine kinase activation in cancer. *Molecular Cancer*, 17(1), 1–13. <https://doi.org/10.1186/s12943-018-0782-4>
- Elemam, N. M., Khalil, B. A., & Maghazachi, A. A. (2021a). Chemokines and Chemokine Receptors. In *Reference Module in Biomedical Sciences* (Vol. 21). Elsevier Inc. <https://doi.org/10.1016/b978-0-12-818731-9.00061-6>
- Erlanson, S. C., McMahon, C., & Kruse, A. C. (2018). Structural Basis for G Protein Coupled Receptor Signaling. *Annual Review of Biophysics*, 47, 1–18. <https://doi.org/10.1146/annurev-biophys>

- 
- Ferguson, K. M. (2008). Structure-based view of epidermal growth factor receptor regulation. *Annual Review of Biophysics*, *37*, 353–373. <https://doi.org/10.1146/annurev.biophys.37.032807.125829>
- Ferguson, K. M., Hu, C., & Lemmon, M. A. (2020). Insulin and epidermal growth factor receptor family members share parallel activation mechanisms. *Protein Science*, *29*(6), 1331–1344. <https://doi.org/10.1002/pro.3871>
- Fredriksson, R., Lagerström, M. C., Lundin, L. G., & Schiöth, H. B. (2003). The G-protein-coupled receptors in the human genome form five main families. Phylogenetic analysis, paralogon groups, and fingerprints. *Molecular Pharmacology*, *63*(6), 1256–1272. <https://doi.org/10.1124/mol.63.6.1256>
- Freed, D. M. (2017a). EGFR ligands differentially stabilize receptor dimers to specify signaling kinetics. *Cell*, *176*(1), 139–148. <https://doi.org/10.1016/j.physbeh.2017.03.040>
- Freed, D. M., Bessman, N. J., Kiyatkin, A., Salazar-Cavazos, E., Byrne, P. O., Moore, J. O., Valley, C. C., Ferguson, K. M., Leahy, D. J., Lidke, D. S., & Lemmon, M. A. (2017). EGFR Ligands Differentially Stabilize Receptor Dimers to Specify Signaling Kinetics. *Cell*, *171*(3), 683–695.e18. <https://doi.org/10.1016/j.cell.2017.09.017>
- Fumagalli, A., Zarca, A., Neves, M., Caspar, B., Hill, S. J., Mayor, F., Smit, M. J., & Marin, P. (2019). CXCR4/AckR3 phosphorylation and recruitment of interacting proteins: Key mechanisms regulating their functional status. *Molecular Pharmacology*, *96*(6), 794–808. <https://doi.org/10.1124/mol.118.115360>
- Galazzo, L., Meier, G., Hadi Timachi, M., Hutter, C. A. J., Seeger, M. A., & Bordignon, E. (2020). Spin-labeled nanobodies as protein conformational reporters for electron paramagnetic resonance in cellular membranes. *Proceedings of the National Academy of Sciences of the United States of America*, *117*(5), 2441–2448. <https://doi.org/10.1073/pnas.1913737117>
- Gekle, M., Eckenstaler, R., Braun, H., Olgac, A., Robaa, D., Mildenerger, S., Dubourg, V., Schreier, B., Sippl, W., & Benndorf, R. (2024). Direct GPCR-EGFR interaction enables synergistic membrane-to-nucleus information transfer.
-

- 
- Cellular and Molecular Life Sciences*, 81(1). <https://doi.org/10.1007/s00018-024-05281-5>
- Ghanem, I., Riveiro, M. E., Paradis, V., Faivre, S., Vázquez de Parga, P. M., & Raymond, E. (2014). Insights on the CXCL12-CXCR4 axis in hepatocellular carcinoma carcinogenesis. *American Journal of Translational Research*, 6(4), 340–352.
- Gilman, A. G. (1987a). *G PROTEINS: TRANSDUCERS OF RECEPTOR-GENERATED SIGNALS*.
- Graham, G. J., Locati, M., Mantovani, A., Rot, A., & Thelen, M. (2012). The biochemistry and biology of the atypical chemokine receptors. *Immunology Letters*, 145(1–2), 30–38. <https://doi.org/10.1016/j.imlet.2012.04.004>
- Grande, F., Giancotti, G., Ioele, G., Occhiuzzi, M. A., & Garofalo, A. (2017). An update on small molecules targeting CXCR4 as starting points for the development of anti-cancer therapeutics. *European Journal of Medicinal Chemistry*, 139, 519–530. <https://doi.org/10.1016/j.ejmech.2017.08.027>
- Gschwind, A., Fischer, O. M., & Ullrich, A. (2004). *F O C U S O N TARGETED THERAPIES kinases : targets for cancer therapy*. 4(May), 1–10.
- Guardiola, S., Varese, M., Sánchez-Navarro, M., & Giralt, E. (2019a). A Third Shot at EGFR: New Opportunities in Cancer Therapy. *Trends in Pharmacological Sciences*, 40(12), 941–955. <https://doi.org/10.1016/j.tips.2019.10.004>
- Guo, G., Gong, K., Wohlfeld, B., Hatanpaa, K. J., Zhao, D., & Habib, A. A. (2015). Ligand-independent EGFR signaling. *Cancer Research*, 75(17), 3436–3441. <https://doi.org/10.1158/0008-5472.CAN-15-0989>
- Guo, Z., Cai, S., Fang, R., Chen, H., Du, J., Tan, Y., Ma, W., Hu, H., Cai, S., & Liu, Y. (2007a). The synergistic effects of CXCR4 and EGFR on promoting EGF-mediated metastasis in ovarian cancer cells. *Colloids and Surfaces B: Biointerfaces*, 60(1), 1–6. <https://doi.org/10.1016/j.colsurfb.2007.05.013>
- Gurevich, V. V., & Gurevich, E. V. (2019a). GPCR signaling regulation: The role of GRKs and arrestins. *Frontiers in Pharmacology*, 10(FEB), 1–11. <https://doi.org/10.3389/fphar.2019.00125>
-

- Gustavsson, M., Dyer, D. P., Zhao, C., & Handel, T. M. (2019). Kinetics of CXCL12 binding to atypical chemokine receptor 3 reveal a role for the receptor N terminus in chemokine binding. *Science Signaling*, *12*(598). <https://doi.org/10.1126/scisignal.aaw3657>
- Hall, M. P., Unch, J., Binkowski, B. F., Valley, M. P., Butler, B. L., Wood, M. G., Otto, P., Zimmerman, K., Vidugiris, G., MacHleidt, T., Robers, M. B., Benink, H. A., Eggers, C. T., Slater, M. R., Meisenheimer, P. L., Klaubert, D. H., Fan, F., Encell, L. P., & Wood, K. V. (2012). Engineered luciferase reporter from a deep sea shrimp utilizing a novel imidazopyrazinone substrate. *ACS Chemical Biology*, *7*(11), 1848–1857. <https://doi.org/10.1021/cb3002478>
- Harikumar, K. G., Hosohata, K., Pinon, D. I., & Miller, L. J. (2006). Use of probes with fluorescence indicator distributed throughout the pharmacophore to examine the peptide agonist-binding environment of the Family B G protein-coupled secretin receptor. *Journal of Biological Chemistry*, *281*(5), 2543–2550. <https://doi.org/10.1074/jbc.M509197200>
- Hattermann, K., & Mentlein, R. (2013). An Infernal Trio: The chemokine CXCL12 and its receptors CXCR4 and CXCR7 in tumor biology. *Annals of Anatomy - Anatomischer Anzeiger*, *195*(2), 103–110. <https://doi.org/https://doi.org/10.1016/j.aanat.2012.10.013>
- Haubrich, J., Zwier, J. M., Charrier-Savournin, F., Prézeau, L., & Pin, J. P. (2024). Different EGF-induced receptor dimer conformations for signaling and internalisation. *FASEB Journal*, *38*(1). <https://doi.org/10.1096/fj.202301209R>
- Hauser, A. S., Attwood, M. M., Rask-andersen, M., & Schiöth, H. B. (2019). Trends in GPCR drug discovery: new agents, targets and indications Alexander. *Nature Reviews Drug Discovery*, *16*(12), 829–842. <https://doi.org/10.1038/nrd.2017.178>. Trends
- Henriksen, L., Grandal, M. V., Knudsen, S. L. J., van Deurs, B., & Grøvdal, L. M. (2013). Internalisation Mechanisms of the Epidermal Growth Factor Receptor after Activation with Different Ligands. *PLoS ONE*, *8*(3). <https://doi.org/10.1371/journal.pone.0058148>

- 
- Heuninck, J., Viciano, C. P., İşbilir, A., Caspar, B., Capoferri, D., Briddon, S. J., Durroux, T., Hill, S. J., Lohse, M. J., Milligan, G., Pin, J. P., & Hoffmann, C. (2019). Context-dependent signaling of CXCR4 chemokine receptor 4 and atypical chemokine receptor 3. *Molecular Pharmacology*, 96(6), 778–793. <https://doi.org/10.1124/mol.118.115477>
- Hofman, E. G., Bader, A. N., Voortman, J., Van Den Heuvel, D. J., Sigismund, S., Verkleij, A. J., Gerritsen, H. C., & Van Bergen en Henegouwen, P. M. P. (2010a). Ligand-induced EGF receptor oligomerization is kinase-dependent and enhances internalisation. *Journal of Biological Chemistry*, 285(50), 39481–39489. <https://doi.org/10.1074/jbc.M110.164731>
- Hofman, E. G., Ruonala, M. O., Bader, A. N., van den Heuvel, D., Voortman, J., Roovers, R. C., Verkleij, A. J., Gerritsen, H. C., & van Bergen en Henegouwen, P. M. P. (2008a). EGF induces coalescence of different lipid rafts. *Journal of Cell Science*, 121(15), 2519–2528. <https://doi.org/10.1242/jcs.028753>
- Hsu, W. H., Yang, J. C. H., Mok, T. S., & Loong, H. H. (2018). Overview of current systemic management of EGFR-mutant NSCLC. *Annals of Oncology*, 29(Supplement 1), i3–i9. <https://doi.org/10.1093/annonc/mdx702>
- Hubbard, S. R. (1999). Structural analysis of receptor tyrosine kinases. *Progress in Biophysics and Molecular Biology*, 71(3–4), 343–358. [https://doi.org/10.1016/S0079-6107\(98\)00047-9](https://doi.org/10.1016/S0079-6107(98)00047-9)
- İşbilir, A., Möller, J., Arimont, M., Bobkov, V., Perpiñá-Viciano, C., Hoffmann, C., Inoue, A., Heukers, R., de Graaf, C., Smit, M. J., Annibale, P., & Lohse, M. J. (2020). Advanced fluorescence microscopy reveals disruption of dynamic CXCR4 dimerisation by subpocket-specific inverse agonists. *Proceedings of the National Academy of Sciences of the United States of America*, 117(46), 29144–29154. <https://doi.org/10.1073/pnas.2013319117>
- Ito, S., Sato, T., & Maeta, T. (2021). Role and therapeutic targeting of sdf-1 $\alpha$ /cxcr4 axis in multiple myeloma. *Cancers*, 13(8). <https://doi.org/10.3390/cancers13081793>
- Iwakiri, S., Mino, N., Takahashi, T., Sonobe, M., Nagai, S., Okubo, K., Wada, H., Date, H., & Miyahara, R. (2009). Higher expression of chemokine receptor
-

- CXCR7 is linked to early and metastatic recurrence in pathological stage I nonsmall cell lung cancer. *Cancer*, *115*(11), 2580–2593. <https://doi.org/10.1002/cncr.24281>
- Janssens, R., Struyf, S., & Proost, P. (2018). The unique structural and functional features of CXCL12. *Cellular and Molecular Immunology*, *15*(4), 299–311. <https://doi.org/10.1038/cmi.2017.107>
- Johnstone, E. K. M., Abhayawardana, R. S., See, H. B., Seeber, R. M., O'Brien, S. L., Thomas, W. G., & Pflieger, K. D. G. (2021). Complex interactions between the angiotensin II type 1 receptor, the epidermal growth factor receptor and TRIO-dependent signaling partners. *Biochemical Pharmacology*, *188*. <https://doi.org/10.1016/j.bcp.2021.114521>
- Jones, J. T., Akita, R. W., & Sliwkowski, M. X. (1999). Binding specificities and affinities of egf domains for ErbB receptors. *FEBS Letters*, *447*(2–3), 227–231. [https://doi.org/10.1016/S0014-5793\(99\)00283-5](https://doi.org/10.1016/S0014-5793(99)00283-5)
- Jørgensen, A. S., Daugvilaite, V., De Filippo, K., Berg, C., Mavri, M., Benned-Jensen, T., Juzenaite, G., Hjortø, G., Rankin, S., Våbenø, J., & Rosenkilde, M. M. (2021). Biased action of the CXCR4-targeting drug plerixafor is essential for its superior hematopoietic stem cell mobilization. *Communications Biology*, *4*(1). <https://doi.org/10.1038/s42003-021-02070-9>
- Jorissen, R. N., Walker, F., Pouliot, N., Garrett, T. P. J., Ward, C. W., & Burgess, A. W. (2003a). Epidermal growth factor receptor: Mechanisms of activation and signalling. *Experimental Cell Research*, *284*(1), 31–53. [https://doi.org/10.1016/S0014-4827\(02\)00098-8](https://doi.org/10.1016/S0014-4827(02)00098-8)
- Jovčevska, I., & Muyldermans, S. (2020). The Therapeutic Potential of Nanobodies. *BioDrugs*, *34*(1), 11–26. <https://doi.org/10.1007/s40259-019-00392-z>
- Kalatskaya, I., Berchiche, Y. A., Gravel, S., Limberg, B. J., Rosenbaum, J. S., & Heveker, N. (2009). AMD3100 Is a CXCR7 Ligand with Allosteric Agonist Properties. *Molecular Pharmacology*, *75*(5), 1240. <https://doi.org/10.1124/mol.108.053389>
- Kilpatrick, L. E., Alcobia, D. C., White, C. W., Peach, C. J., Glenn, J. R., Zimmerman, K., Kondrashov, A., Pflieger, K. D. G., Ohana, R. F., Robers, M. B., Wood, K.

- V., Sloan, E. K., Woolard, J., & Hill, S. J. (2019). Complex Formation between VEGFR2 and the  $\beta$ 2-Adrenoceptor. *Cell Chemical Biology*, 26(6), 830-841.e9. <https://doi.org/10.1016/j.chembiol.2019.02.014>
- Kilpatrick, L. E., Friedman-Ohana, R., Alcobia, D. C., Riching, K., Peach, C. J., Wheal, A. J., Briddon, S. J., Robers, M. B., Zimmerman, K., Machleidt, T., Wood, K. V., Woolard, J., & Hill, S. J. (2017). Real-time analysis of the binding of fluorescent VEGF165a to VEGFR2 in living cells: Effect of receptor tyrosine kinase inhibitors and fate of internalized agonist-receptor complexes. *Biochemical Pharmacology*, 136, 62–75. <https://doi.org/10.1016/j.bcp.2017.04.006>
- Kilpatrick, L. E., & Hill, S. J. (2021). Transactivation of G protein-coupled receptors (GPCRs) and receptor tyrosine kinases (RTKs): Recent insights using luminescence and fluorescence technologies. *Current Opinion in Endocrine and Metabolic Research*, 16, 102–112. <https://doi.org/10.1016/j.coemr.2020.10.003>
- Knudsen, S. L. J., Wai Mac, A. S., Henriksen, L., Van Deurs, B., & Grøvdal, L. M. (2014). EGFR signaling patterns are regulated by its different ligands. *Growth Factors*, 32(5), 155–163. <https://doi.org/10.3109/08977194.2014.952410>
- Kobilka, B. K. (2007a). G Protein Coupled Receptor Structure and Activation. *Biochim Biophys Acta.*, 1768(4), 794–807. <https://www.ncbi.nlm.nih.gov/pmc/articles/PMC3624763/pdf/nihms412728.pdf>
- Koenen, J., Bachelerie, F., Balabanian, K., Schlecht-Louf, G., & Gallego, C. (2019). Atypical chemokine receptor 3 (ACKR3): A comprehensive overview of its expression and potential roles in the immune system. *Molecular Pharmacology*, 96(6), 809–818. <https://doi.org/10.1124/mol.118.115329>
- Kogut-Günthel, M. M., Zara, Z., Nicoli, A., Steuer, A., Lopez-Balastegui, M., Selent, J., Karanth, S., Koehler, M., Ciancetta, A., Abiko, L. A., Hagn, F., & Di Pizio, A. (2024). The path to the G protein-coupled receptor structural landscape: Major milestones and future directions. In *British Journal of Pharmacology*. John Wiley and Sons Inc. <https://doi.org/10.1111/bph.17314>
- Kovacs, E., Zorn, J. A., Huang, Y., Barros, T., & Kuriyan, J. (2015a). A structural perspective on the regulation of the epidermal growth factor receptor. *Annual*

- 
- Review of Biochemistry*, 84, 739–764. <https://doi.org/10.1146/annurev-biochem-060614-034402>
- Kumar, A., Petri, E. T., Halmos, B., & Boggon, T. J. (2008a). The Structure and Clinical Relevance of the EGF Receptor in Human Cancer. *J Clin Oncol.*, 26(20), 1742–1751. <https://doi.org/10.1200/JCO.2007.12.1178>.The
- Lahiry, P., Torkamani, A., Schork, N. J., & Hegele, R. A. (2010). Kinase mutations in human disease: Interpreting genotype-phenotype relationships. *Nature Reviews Genetics*, 11(1), 60–74. <https://doi.org/10.1038/nrg2707>
- Lao, J., He, H., Wang, X., Wang, Z., Song, Y., Yang, B., Ullahkhan, N., Ge, B., & Huang, F. (2017). Single-Molecule Imaging Demonstrates Ligand Regulation of the Oligomeric Status of CXCR4 in Living Cells. *Journal of Physical Chemistry B*, 121(7), 1466–1474. <https://doi.org/10.1021/acs.jpcc.6b10969>
- Lay, C. S., Bridges, A., Goulding, J., Briddon, S. J., Soloviev, Z., Craggs, P. D., & Hill, S. J. (2022). Probing the binding of interleukin-23 to individual receptor components and the IL-23 heteromeric receptor complex in living cells using NanoBRET. *Cell Chemical Biology*, 29(1), 19-29.e6. <https://doi.org/10.1016/j.chembiol.2021.05.002>
- Leemans, M., Galicia, C., Deyaert, E., Daems, E., Krause, L., Paesmans, J., Pardon, E., Steyaert, J., Kortholt, A., Sobott, F., Klostermeier, D., & Versées, W. (2020). Allosteric modulation of the GTPase activity of a bacterial LRRK2 homolog by conformation-specific Nanobodies. *Biochemical Journal*, 477(7), 1203–1218. <https://doi.org/10.1042/BCJ20190843>
- Lemmon, M. A., & Schlessinger, J. (2010a). *Cell signaling by receptor-tyrosine kinases*. 141(7), 1117–1134. <https://doi.org/10.1016/j.cell.2010.06.011>.Cell
- Levoye, A., Balabanian, K., Baleux, F., Bachelier, F., & Lagane, B. (2009a). CXCR7 heterodimerizes with CXCR4 and regulates CXCL12-mediated G protein signaling. *Blood*, 113(24), 6085–6093. <https://doi.org/10.1182/blood-2008-12-196618>
- Li, R. H., Huang, W. H., Wu, J. D., Du, C. W., & Zhang, G. J. (2017). EGFR expression is associated with cytoplasmic staining of CXCR4 and predicts poor
-

- prognosis in triple-negative breast carcinomas. *Oncology Letters*, *13*(2), 695–703. <https://doi.org/10.3892/ol.2016.5489>
- Lin, Y., Li, Z., Ma, H., Wang, Y., Wang, X., Song, S., Zhao, L., Wu, S., Tian, S., Fu, C., Luo, L., Zhu, F., He, S., Zheng, J., & Zhang, X. (2020). Design, Synthesis, and Characterization of Novel CXCR4 Antagonists Featuring Cyclic Amines. *ChemMedChem*, *15*(13), 1150–1162. <https://doi.org/https://doi.org/10.1002/cmdc.202000268>
- Liu, X., Wang, P., Zhang, C., & Ma, Z. (2017). Epidermal growth factor receptor (EGFR): A rising star in the era of precision medicine of lung cancer. *Oncotarget*, *8*(30), 50209–50220. <https://doi.org/10.18632/oncotarget.16854>
- Liu, Y., Ji, R., Li, J., Gu, Q., Zhao, X., Sun, T., Wang, J., Li, J., Du, Q., & Sun, B. (2010). Correlation effect of EGFR and CXCR4 and CCR7 chemokine receptors in predicting breast cancer metastasis and prognosis. *Journal of Experimental and Clinical Cancer Research*, *29*(1), 1–9. <https://doi.org/10.1186/1756-9966-29-16>
- Liu, Y., Liu, A., Li, X., Liao, Q., Zhang, W., Zhu, L., & Ye, R. D. (2024). Cryo-EM structure of monomeric CXCL12-bound CXCR4 in the active state. *Cell Reports*, *43*(8), 114578. <https://doi.org/10.1016/j.celrep.2024.114578>
- Lodowski, D. T., & Palczewski, K. (2009). Chemokine receptors and other GPCRs. *Current Opinion in HIV and AIDS*, *4*(2), 88–95. <https://doi.org/10.1097/COH.0b013e3283223d8d>. Chemokine
- Lounsbury, N. (2020). Advances in CXCR7 modulators. *Pharmaceuticals*, *13*(2), 1–15. <https://doi.org/10.3390/ph13020033>
- Low-Nam, S. T., Lidke, K. A., Cutler, P. J., Roovers, R. C., Van Bergen En Henegouwen, P. M. P., Wilson, B. S., & Lidke, D. S. (2011a). ErbB1 dimerisation is promoted by domain co-confinement and stabilized by ligand binding. *Nature Structural and Molecular Biology*, *18*(11), 1244–1249. <https://doi.org/10.1038/nsmb.2135>
- Luker, K. E., Steele, J. M., Mihalko, L. A., Ray, P., & Luker, G. D. (2010). Constitutive and chemokine-dependent internalisation and recycling of CXCR7

- in breast cancer cells to degrade chemokine ligands. *Oncogene*, 29(32), 4599–4610. <https://doi.org/10.1038/onc.2010.212>
- Macdonald-Obermann, J. L., & Pike, L. J. (2009). The intracellular juxtamembrane domain of the epidermal growth factor (EGF) receptor is responsible for the allosteric regulation of EGF binding. *Journal of Biological Chemistry*, 284(20), 13570–13576. <https://doi.org/10.1074/jbc.M109.001487>
- Macdonald-Obermann, J. L., Piwnica-Worms, D., & Pike, L. J. (2012). Mechanics of EGF receptor/ErbB2 kinase activation revealed by luciferase fragment complementation imaging. *Proceedings of the National Academy of Sciences of the United States of America*, 109(1), 137–142. <https://doi.org/10.1073/pnas.1111316109>
- Machleidt, T., Woodrooffe, C. C., Schwinn, M. K., Méndez, J., Robers, M. B., Zimmerman, K., Otto, P., Daniels, D. L., Kirkland, T. A., & Wood, K. V. (2015). NanoBRET-A Novel BRET Platform for the Analysis of Protein-Protein Interactions. *ACS Chemical Biology*, 10(8), 1797–1804. <https://doi.org/10.1021/acscchembio.5b00143>
- Manglik, A., Kobilka, B. K., & Steyaert, J. (2017). Nanobodies to Study G Protein-Coupled Receptor Structure and Function. *Annual Review of Pharmacology and Toxicology*, 57(August), 19–37. <https://doi.org/10.1146/annurev-pharmtox-010716-104710>
- Martin-Fernandez, M. L., Clarke, D. T., Roberts, S. K., Zanetti-Domingues, L. C., & Gervasio, F. L. (2019). Structure and Dynamics of the EGF Receptor as Revealed by Experiments and Simulations and Its Relevance to Non-Small Cell Lung Cancer. *Cells*, 8(4), 316. <https://doi.org/10.3390/cells8040316>
- Masuda, H., Zhang, D., & Bartholomeusz, C. (2012). *Role of Epidermal Growth Factor Receptor in Breast Cancer*. 136(2), 29–31. <https://doi.org/10.1007/s10549-012-2289-9>.Role
- Maudsley, S., Pierce, K. L., Zamah, A. M., Miller, W. E., Ahn, S., Daaka, Y., Lefkowitz, R. J., & Luttrell, L. M. (2000). The  $\beta$ 2-adrenergic receptor mediates extracellular signal-regulated kinase activation via assembly of a multi-receptor

- complex with the epidermal growth factor receptor. *Journal of Biological Chemistry*, 275(13), 9572–9580. <https://doi.org/10.1074/jbc.275.13.9572>
- Maussang, D., Mujić-Delić, A., Descamps, F. J., Stortelers, C., Vanlandschoot, P., Stigter-Van Walsum, M., Vischer, H. F., Van Roy, M., Vosjan, M., Gonzalez-Pajuelo, M., Van Dongen, G. A. M. S., Merchiers, P., Van Rompaey, P., & Smit, M. J. (2013). Llama-derived single variable domains (nanobodies) directed against chemokine receptor CXCR7 reduce head and neck cancer cell growth in vivo. *Journal of Biological Chemistry*, 288(41), 29562–29572. <https://doi.org/10.1074/jbc.M113.498436>
- Meng, Q., Zhu, R., Mao, Y., Zhu, S., Wu, Y., Huang, L. S. M., Ciechanover, A., An, J., Xu, Y., & Huang, Z. (2023). Biological and mutational analyses of CXCR4-antagonist interactions and design of new antagonistic analogs. *Bioscience Reports*, 43(12). <https://doi.org/10.1042/BSR20230981>
- Meyrath, M., Szpakowska, M., Zeiner, J., Massotte, L., Merz, M. P., Benkel, T., Simon, K., Ohnmacht, J., Turner, J. D., Krüger, R., Seutin, V., Ollert, M., Kostenis, E., & Chevigné, A. (2020). The atypical chemokine receptor ACKR3/CXCR7 is a broad-spectrum scavenger for opioid peptides. *Nature Communications*, 11(1). <https://doi.org/10.1038/s41467-020-16664-0>
- Mezzapelle, R., Leo, M., Caprioglio, F., Colley, L. S., Lamarca, A., Sabatino, L., Colantuoni, V., Crippa, M. P., & Bianchi, M. E. (2022). CXCR4/CXCL12 Activities in the Tumor Microenvironment and Implications for Tumor Immunotherapy. In *Cancers* (Vol. 14, Issue 9). MDPI. <https://doi.org/10.3390/cancers14092314>
- Miao, Z., Luker, K. E., Summers, B. C., Berahovich, R., Bhojani, M. S., Rehemtulla, A., Kleer, C. G., Essner, J. J., Nasevicius, A., Luker, G. D., Howard, M. C., & Schall, T. J. (2007). CXCR7 (RDC1) promotes breast and lung tumor growth in vivo and is expressed on tumor-associated vasculature. *Proceedings of the National Academy of Sciences of the United States of America*, 104(40), 15735–15740. <https://doi.org/10.1073/pnas.0610444104>
- Milligan, G., & Kostenis, E. (2006a). Heterotrimeric G-proteins: A short history. *British Journal of Pharmacology*, 147(SUPPL. 1). <https://doi.org/10.1038/sj.bjp.0706405>

- 
- Mishra, R. K., Shum, A. K., Plataniias, L. C., Miller, R. J., & Schiltz, G. E. (2016). Discovery and characterization of novel small-molecule CXCR4 receptor agonists and antagonists. *Scientific Reports*, 6. <https://doi.org/10.1038/srep30155>
- Mosi, R. M., Anastassova, V., Cox, J., Darkes, M. C., Idzan, S. R., Labrecque, J., Lau, G., Nelson, K. L., Patel, K., Santucci, Z., Wong, R. S. Y., Skerlj, R. T., Bridger, G. J., Huskens, D., Schols, D., & Fricker, S. P. (2012). The molecular pharmacology of AMD11070: An orally bioavailable CXCR4 HIV entry inhibitor. *Biochemical Pharmacology*, 83(4), 472–479. <https://doi.org/10.1016/j.bcp.2011.11.020>
- Mudumbi, K. C., Burns, E. A., Schodt, D. J., & Petrova, Z. O. (2023). *Distinct interactions stabilize EGFR dimers and higher-order oligomers in cell membranes.*
- Mueller, W., Schütz, D., Nagel, F., Schulz, S., & Stumm, R. (2013). Hierarchical Organization of Multi-Site Phosphorylation at the CXCR4 C Terminus. *PLoS ONE*, 8(5). <https://doi.org/10.1371/journal.pone.0064975>
- Murphy, P. M., Baggiolini, M., Charo, I. F., Hebert, C. A., Horuk, R., Matsushima, K., Miller, L. H., Oppenheim, J. J., & Power, C. A. (2000). International union of pharmacology. XXII. Nomenclature for chemokine receptors. *Pharmacological Reviews*, 52(1), 145–176.
- Muyldermans, S. (2021). Applications of Nanobodies. *Annual Review of Animal Biosciences*, 9, 401–421. <https://doi.org/10.1146/annurev-animal-021419-083831>
- Nagasawa, T., Hirota, S., Tachibana, K., Takakura, N., Nishikawa, S., Kitamura, Y., Yoshida, N., Kikutani, H., & Kishimoto, T. (1996). Defects of B-cell lymphopoiesis and bone-marrow myelopoiesis in mice lacking the CXC chemokine PBSF/SDF-1. *Nature*, 382(6592), 635–638. <https://doi.org/10.1038/382635a0>
- Nathan J. Pavlos, P. A. F. (2017a). GPCR Signaling and Trafficking: The Long and Short of It. *Trends Endocrinol Metab*, 28(3), 213–226. <https://doi.org/10.1016/j.tem.2016.10.007>
-

- 
- Naumann, U., Cameroni, E., Pruenster, M., Mahabaleshwar, H., Raz, E., Zerwes, H. G., Rot, A., & Thelen, M. (2010). CXCR7 functions as a scavenger for CXCL12 and CXCL11. *PLoS ONE*, *5*(2). <https://doi.org/10.1371/journal.pone.0009175>
- Neves, M., Fumagalli, A., van den Bor, J., Marin, P., Smit, M. J., & Mayor, F. (2019a). The role of ACKR3 in breast, lung, and brain cancer. *Molecular Pharmacology*, *96*(6), 819–825. <https://doi.org/10.1124/mol.118.115279>
- Neves, M., Marolda, V., Mayor, F., & Penela, P. (2022). Crosstalk between CXCR4/ACKR3 and EGFR Signaling in Breast Cancer Cells. *International Journal of Molecular Sciences*, *23*(19). <https://doi.org/10.3390/ijms231911887>
- Neves, M., Perpiñá-Viciano, C., Penela, P., Hoffmann, C., & Mayor, F. (2020). Modulation of CXCR4-Mediated Gi1 Activation by EGF Receptor and GRK2. *ACS Pharmacology and Translational Science*, *3*(4), 627–634. <https://doi.org/10.1021/acsptsci.0c00021>
- Neves, S. R., Ram, P. T., & Iyengar, R. (2002). G protein pathways. *Science*, *296*(5573), 1636–1639. <https://doi.org/10.1126/science.1071550>
- Nevoltris, D., & Chames, P. (2015). Tethered Epidermal Growth Factor Receptor Involved in EGFR / ErbB2. *ACS Nano*, *xxx*(x), xx.
- Nevoltris, D., Lombard, B., Dupuis, E., Mathis, G., Chames, P., & Baty, D. (2015a). Conformational nanobodies reveal tethered epidermal growth factor receptor involved in EGFR/ErbB2 predimers. *ACS Nano*, *9*(2), 1388–1399. <https://doi.org/10.1021/nn505752u>
- Nickoloff-Bybel, E. A., Festa, L., Meucci, O., & Gaskill, P. J. (2021). Co-receptor signaling in the pathogenesis of neuroHIV. In *Retrovirology* (Vol. 18, Issue 1). BioMed Central Ltd. <https://doi.org/10.1186/s12977-021-00569-x>
- O'Brien, S. L., Johnstone, E. K. M., Devost, D., Conroy, J., Reichelt, M. E., Purdue, B. W., Ayoub, M. A., Kawai, T., Inoue, A., Eguchi, S., Hébert, T. E., Pflieger, K. D. G., & Thomas, W. G. (2018). BRET-based assay to monitor EGFR transactivation by the AT1R reveals Gq/11 protein-independent activation and AT1R-EGFR complexes. *Biochemical Pharmacology*, *158*, 232–242. <https://doi.org/10.1016/j.bcp.2018.10.017>
-

- Ogiso, H., Ishitani, R., Nureki, O., Fukai, S., Yamanaka, M., Kim, J. H., Saito, K., Sakamoto, A., Inoue, M., Shirouzu, M., & Yokoyama, S. (2002a). Crystal structure of the complex of human epidermal growth factor and receptor extracellular domains. *Cell*, *110*(6), 775–787. [https://doi.org/10.1016/S0092-8674\(02\)00963-7](https://doi.org/10.1016/S0092-8674(02)00963-7)
- Ogrodzinski, L., Platt, S., Goulding, J., Alexander, C., Farr, T. D., Woolard, J., Hill, S. J., & Kilpatrick, L. E. (2023). Probing expression of E-selectin using CRISPR-Cas9-mediated tagging with HiBiT in human endothelial cells. *IScience*, *26*(7). <https://doi.org/10.1016/j.isci.2023.107232>
- Ohtsu, H., Dempsey, P. J., & Eguchi, S. (2006). ADAMs as mediators of EGF receptor transactivation by G protein-coupled receptors. *American Journal of Physiology - Cell Physiology*, *291*(1). <https://doi.org/10.1152/ajpcell.00620.2005>
- Oikawa, Y., Morita, K. I., Kayamori, K., Tanimoto, K., Sakamoto, K., Katoh, H., Ishikawa, S., Inazawa, J., & Harada, H. (2017). Receptor tyrosine kinase amplification is predictive of distant metastasis in patients with oral squamous cell carcinoma. *Cancer Science*, *108*(2), 256–266. <https://doi.org/10.1111/cas.13126>
- Pabla, B., Bissonnette, M., & Konda, V. J. (2015). Colon cancer and the epidermal growth factor receptor: Current treatment paradigms, the importance of diet, and the role of chemoprevention. *World Journal of Clinical Oncology*, *6*(5), 133–141. <https://doi.org/10.5306/wjco.v6.i5.133>
- Palczewski, K., Kumasaka, T., Hori, T., Behnke, C. A., Motoshima, H., Fox, B. A., Trong, I., Teller, D. C., Okada, T., Stenkamp, E., Yamamoto, M., Miyano, M., Palczewski, K., Kumasaka, T., Hori, T., Behnke, C. A., Motoshima, H., Fox, B. A., Trong, I. Le, ... Miyano, M. (2000). *Crystal Structure of Rhodopsin: A G Protein-Coupled Receptor Published*. *289*(5480), 739–745.
- Percherancier, Y., Berchiche, Y. A., Slight, I., Volkmer-Engert, R., Tamamura, H., Fujii, N., Bouvier, M., & Heveker, N. (2005). Bioluminescence resonance energy transfer reveals ligand-induced conformational changes in CXCR4 homo- and heterodimers. *Journal of Biological Chemistry*, *280*(11), 9895–9903. <https://doi.org/10.1074/jbc.M411151200>

- 
- Pérez-Gómez, E., Andradás, C., Blasco-Benito, S., Caffarel, M. M., García-Taboada, E., Villa-Morales, M., Moreno, E., Hamann, S., Martín-Villar, E., Flores, J. M., Weners, A., Alkatout, I., Klapper, W., Röcken, C., Bronsert, P., Stickeler, E., Staebler, A., Bauer, M., Arnold, N., ... Sánchez, C. (2015). Role of cannabinoid receptor CB2 in HER2 pro-oncogenic signaling in breast cancer. *Journal of the National Cancer Institute*, *107*(6). <https://doi.org/10.1093/jnci/djv077>
- Peterson, Y. K., & Luttrell, L. M. (2017). The diverse roles of arrestin scaffolds in G protein-coupled receptor signaling. *Pharmacological Reviews*, *69*(3), 256–297. <https://doi.org/10.1124/pr.116.013367>
- Phillips, R. J., Mestas, J., Gharaee-Kermani, M., Burdick, M. D., Sica, A., Belperio, J. A., Keane, M. P., & Strieter, R. M. (2005). Epidermal growth factor and hypoxia-induced expression of CXCR4 chemokine receptor 4 on non-small cell lung cancer cells is regulated by the phosphatidylinositol 3-kinase/PTEN/AKT/mammalian target of rapamycin signaling pathway and activation of hypoxia-inducible factor-1. *Journal of Biological Chemistry*, *280*(23), 22473–22481. <https://doi.org/10.1074/jbc.M500963200>
- Piramoon, M., Hosseinimehr, S. J., Omidfar, K., Noaparast, Z., & Abedi, S. M. (2017). <sup>99m</sup>Tc-anti-epidermal growth factor receptor nanobody for tumor imaging. *Chemical Biology and Drug Design*, *89*(4), 498–504. <https://doi.org/10.1111/cbdd.12871>
- Poeta, V. M., Massara, M., Capucetti, A., & Bonocchi, R. (2019). Chemokines and chemokine receptors: New targets for cancer immunotherapy. *Frontiers in Immunology*, *10*(MAR), 1–10. <https://doi.org/10.3389/fimmu.2019.00379>
- Porcile, C., Bajetto, A., Barbero, S., Pirani, P., & Schettini, G. (2004). CXCR4 activation induces epidermal growth factor receptor transactivation in an ovarian cancer cell line. *Annals of the New York Academy of Sciences*, *1030*, 162–169. <https://doi.org/10.1196/annals.1329.021>
- Pottier, C., Fresnais, M., Gilon, M., Jérusalem, G., Longuespée, R., & Sounni, N. E. (2020). Tyrosine kinase inhibitors in cancer: Breakthrough and challenges of targeted therapy. *Cancers*, *12*(3). <https://doi.org/10.3390/cancers12030731>
-

- Pozzobon, T., Goldoni, G., Viola, A., & Molon, B. (2016a). CXCR4 signaling in health and disease. *Immunology Letters*, *177*, 6–15. <https://doi.org/10.1016/j.imlet.2016.06.006>
- Prenzel, N., Zwick, E., Daub, H., Leserer, M., Abraham, R., Wallasch, C., & Ullrich, A. (1999). EGF receptor transactivation by G-protein-coupled receptors requires metalloproteinase cleavage of proHB-EGF. *Nature*, *402*(6764), 884–888. <https://doi.org/10.1038/47260>
- Purba, E. R., Saita, E. I., Akhouri, R. R., Öfverstedt, L. G., Wilken, G., Skoglund, U., & Maruyama, I. N. (2022). Allosteric activation of preformed EGF receptor dimers by a single ligand binding event. *Frontiers in Endocrinology*, *13*(November), 1–17. <https://doi.org/10.3389/fendo.2022.1042787>
- Qin, L., Kufareva, I., Holden, L. G., Wang, C., Zheng, Y., Zhao, C., Fenalti, G., Wu, H., Han, G. W., Cherezov, V., Abagyan, R., Stevens, R. C., & Handel, T. M. (2015a). Crystal structure of the chemokine receptor CXCR4 in complex with a viral chemokine. *Science*, *347*(6226), 1117–1122. <https://doi.org/10.1126/science.1261064>
- Quinn, K. E., Mackie, D. I., & Caron, K. M. (2018a). Emerging roles of atypical chemokine receptor 3 (ACKR3) in normal development and physiology. *Cytokine*, *109*(February), 17–23. <https://doi.org/10.1016/j.cyto.2018.02.024>
- Raphael Trenker, N. J. (2020a). Receptor Tyrosine Kinase activation: from the ligand perspective. *Curr Opin Cell Biol.*, *63*, 174–185. <https://doi.org/10.1016/j.ceb.2020.01.016.Receptor>
- Ray, K., Ujvari, B., Ramana, V., & Donald, J. (2018). Cross-talk between EGFR and IL-6 drives oncogenic signaling and offers therapeutic opportunities in cancer. *Cytokine and Growth Factor Reviews*, *41*(March), 18–27. <https://doi.org/10.1016/j.cytogfr.2018.04.002>
- Raykova, D., Koos, B., Asplund, A., Gelléri, M., Ivarsson, Y., Danielson, U. H., & Söderberg, O. (2016). Let there be light! In *Proteomes* (Vol. 4, Issue 4). MDPI AG. <https://doi.org/10.3390/proteomes4040036>
- Robinson, S. D., Reynolds, L. E., Kostourou, V., Reynolds, A. R., da Silva, R. G., Tavora, B., Baker, M., Marshall, J. F., & Hodivala-Dilke, K. M. (2009).  $\alpha\beta 3$

- integrin limits the contribution of neuropilin-1 to vascular endothelial growth factor-induced angiogenesis. *Journal of Biological Chemistry*, 284(49), 33966–33981. <https://doi.org/10.1074/jbc.M109.030700>
- Ronan, T., Macdonald-Obermann, J. L., Huelsmann, L., Bessman, N. J., Naegle, K. M., & Pike, L. J. (2016). Different Epidermal Growth Factor Receptor (EGFR) agonists produce unique signatures for the recruitment of downstream signaling proteins. *Journal of Biological Chemistry*, 291(11), 5528–5540. <https://doi.org/10.1074/jbc.M115.710087>
- Roovers, R. C., Laeremans, T., Huang, L., De Taeye, S., Verkleij, A. J., Revets, H., De Haard, H. J., & Van Bergen En Henegouwen, P. M. P. (2007a). Efficient inhibition of EGFR signalling and of tumour growth by antagonistic anti-EGFR Nanobodies. *Cancer Immunology, Immunotherapy*, 56(3), 303–317. <https://doi.org/10.1007/s00262-006-0180-4>
- Roovers, R. C., Laeremans, T., Huang, L., De Taeye, S., Verkleij, A. J., Revets, H., De Haard, H. J., & Van Bergen En Henegouwen, P. M. P. (2007b). Efficient inhibition of EGFR signalling and of tumour growth by antagonistic anti-EGFR Nanobodies. *Cancer Immunology, Immunotherapy*, 56(3), 303–317. <https://doi.org/10.1007/s00262-006-0180-4>
- Rosenbaum, D. M., Rasmussen, S. G. F., & Kobilka, B. K. (2009). The structure and function of G-protein-coupled receptors. *Nature*, 459(7245), 356–363. <https://doi.org/10.1038/nature08144>.The
- Rossi, D., & Zlotnik, A. (2000). THE BIOLOGY OF CHEMOKINES AND THEIR RECEPTORS. *Anni. Rev. Immunol.*, 18, 217–242.
- Roy, S., Sinha, S., Silas, A. J., Ghassemian, M., Kufareva, I., & Ghosh, P. (2024). Growth factor-dependent phosphorylation of Gai shapes canonical signaling by G protein-coupled receptors. *Science Signaling*, 17(839). <https://doi.org/10.1126/scisignal.ade8041>
- Rubin, J. B. (2009). Chemokine signaling in cancer: One hump or two? *Seminars in Cancer Biology*, 19(2), 116–122. <https://doi.org/10.1016/j.semcancer.2008.10.001>

- Salazar, N., Muñoz, D., Kallifatidis, G., Singh, R. K., Jordà, M., & Lokeshwar, B. L. (2014a). The chemokine receptor CXCR7 interacts with EGFR to promote breast cancer cell proliferation. *Molecular Cancer*, *13*(1). <https://doi.org/10.1186/1476-4598-13-198>
- Sánchez-Martín, L., Sánchez-Mateos, P., & Cabañas, C. (2013). CXCR7 impact on CXCL12 biology and disease. *Trends in Molecular Medicine*, *19*(1), 12–22. <https://doi.org/10.1016/j.molmed.2012.10.004>
- Santos, E. da S., Nogueira, K. A. B., Fernandes, L. C. C., Martins, J. R. P., Reis, A. V. F., Neto, J. de B. V., Júnior, I. J. da S., Pessoa, C., Petrilli, R., & Eloy, J. O. (2021). EGFR targeting for cancer therapy: Pharmacology and immunoconjugates with drugs and nanoparticles. *International Journal of Pharmaceutics*, *592*(July 2020). <https://doi.org/10.1016/j.ijpharm.2020.120082>
- Saotome, K., McGoldrick, L. L., Ho, J.-H., Ramlall, T. F., Shah, S., Moore, M. J., Kim, J. H., Leidich, R., Olson, W. C., & Franklin, M. C. (2024). Structural insights into CXCR4 modulation and oligomerization. *BioRxiv*, 2024.02.09.579708. <https://doi.org/10.1101/2024.02.09.579708>
- Schihada, H., Vandenabeele, S., Zabel, U., Frank, M., Lohse, M. J., & Maiellaro, I. (2018). A universal bioluminescence resonance energy transfer sensor design enables high-sensitivity screening of GPCR activation dynamics. *Communications Biology*, *1*(1), 1–8. <https://doi.org/10.1038/s42003-018-0072-0>
- Schmitz, K. R., Bagchi, A., Roovers, R. C., Henegouwen, P. M. P. van B. en, & Ferguson, K. M. (2013a). Structural evaluation of EGFR inhibition mechanisms for nanobodies/VHH domains. *Structure*, *21*(7), 1214–1224. <https://doi.org/10.1038/jid.2014.371>
- Sharifi, J., Khireghesh, M. R., Safari, F., & Akbari, B. (2021). EGFR and anti-EGFR nanobodies: review and update. *Journal of Drug Targeting*, *29*(4), 387–402. <https://doi.org/10.1080/1061186X.2020.1853756>
- Shenoy, S. K., & Lefkowitz, R. J. (2011). B-Arrestin-Mediated Receptor Trafficking and Signal Transduction. *Trends in Pharmacological Sciences*, *32*(9), 521–533. <https://doi.org/10.1016/j.tips.2011.05.002>

- Shi, Y., Riese, D. J., & Shen, J. (2020). The Role of the CXCL12/CXCR4/CXCR7 Chemokine Axis in Cancer. *Frontiers in Pharmacology*, *11*(December), 1–14. <https://doi.org/10.3389/fphar.2020.574667>
- Shigematsu, H., Lin, L., Takahashi, T., Nomura, M., Suzuki, M., Wistuba, I. I., Fong, K. M., Lee, H., Toyooka, S., Shimizu, N., Fujisawa, T., Feng, Z., Roth, J. A., Herz, J., Minna, J. D., & Gazdar, A. F. (2005). Clinical and biological features associated with epidermal growth factor receptor gene mutations in lung cancers. *Journal of the National Cancer Institute*, *97*(5), 339–346. <https://doi.org/10.1093/jnci/dji055>
- Sibilia, M., Steinbach, J. P., Stingl, L., Aguzzi, A., & Wagner, E. F. (1998). A strain-independent postnatal neurodegeneration in mice lacking the EGF receptor. *EMBO Journal*, *17*(3), 719–731. <https://doi.org/10.1093/emboj/17.3.719>
- Sierro, F., Biben, C., Martínez-Muñoz, L., Mellado, M., Ransohoff, R. M., Li, M., Woehl, B., Leung, H., Groom, J., Batten, M., Harvey, R. P., Martínez-A, C., Mackay, C. R., & Mackay, F. (2007). Disrupted cardiac development but normal hematopoiesis in mice deficient in the second CXCL12/SDF-1 receptor, CXCR7. *Proceedings of the National Academy of Sciences of the United States of America*, *104*(37), 14759–14764. <https://doi.org/10.1073/pnas.0702229104>
- Sigismund, S., Avanzato, D., & Lanzetti, L. (2018). Emerging functions of the EGFR in cancer. *Molecular Oncology*, *12*(1), 3–20. <https://doi.org/10.1002/1878-0261.12155>
- Singh, M., & Jadhav, H. R. (2018). Targeting non-small cell lung cancer with small-molecule EGFR tyrosine kinase inhibitors. *Drug Discovery Today*, *23*(3), 745–753. <https://doi.org/10.1016/j.drudis.2017.10.004>
- Soave, M., Briddon, S. J., Hill, S. J., & Stoddart, L. A. (2020a). Fluorescent ligands: Bringing light to emerging GPCR paradigms. *British Journal of Pharmacology*, *177*(5), 978–991. <https://doi.org/10.1111/bph.14953>
- Soave, M., Goulding, J., Markus, R., Hill, S. J., & Stoddart, L. A. (2020). Application of Fluorescent Purinoceptor Antagonists for Bioluminescence Resonance Energy Transfer Assays and Fluorescent Microscopy. In P. Pelegrín (Ed.), *Purinergic*

- 
- Signaling: Methods and Protocols* (pp. 163–181). Springer New York.  
[https://doi.org/10.1007/978-1-4939-9717-6\\_12](https://doi.org/10.1007/978-1-4939-9717-6_12)
- Söderberg, O., Leuchowius, K.-J., Gullberg, M., Jarvius, M., Weibrecht, I., Larsson, L.-G., & Landegren, U. (2008). Characterizing proteins and their interactions in cells and tissues using the in situ proximity ligation assay. *Methods*, *45*(3), 227–232. <https://doi.org/https://doi.org/10.1016/j.ymeth.2008.06.014>
- Soldi, R., Mitola, S., Strasly, M., Defilippi, P., Tarone, G., & Bussolino, F. (1999). Role of  $\alpha v \beta 3$  integrin in the activation of vascular endothelial growth factor receptor-2. In *The EMBO Journal* (Vol. 18, Issue 4).
- Sosa, M. S., & Lopez-Haber, C. (2010). Identification of the Rac-GEF P-REX1 As An Essential Mediator of ErbB Signaling in Breast Cancer. *Mol Cell.*, *22*(40), 877–892. <https://doi.org/10.1016/j.molcel.2010.11.029.IDENTIFICATION>
- Stamos, J., Sliwkowski, M. X., & Eigenbrot, C. (2002). Structure of the epidermal growth factor receptor kinase domain alone and in complex with a 4-anilinoquinazoline inhibitor. *Journal of Biological Chemistry*, *277*(48), 46265–46272. <https://doi.org/10.1074/jbc.M207135200>
- Steel, E., Murray, V. L., & Liu, A. P. (2014). Multiplex detection of homo- and heterodimerisation of G protein-coupled receptors by proximity biotinylation. *PLoS ONE*, *9*(4). <https://doi.org/10.1371/journal.pone.0093646>
- Stoddart, L. A., Johnstone, E. K. M., Wheal, A. J., Goulding, J., Robers, M. B., MacHleidt, T., Wood, K. V., Hill, S. J., & Pflieger, K. D. G. (2015). Application of BRET to monitor ligand binding to GPCRs. *Nature Methods*, *12*(7), 661–663. <https://doi.org/10.1038/nmeth.3398>
- Stoddart, L. A., Kilpatrick, L. E., Briddon, S. J., & Hill, S. J. (2015a). Probing the pharmacology of G protein-coupled receptors with fluorescent ligands. *Neuropharmacology*, *98*, 48–57. <https://doi.org/10.1016/j.neuropharm.2015.04.033>
- Stoddart, L. A., Kilpatrick, L. E., & Hill, S. J. (2018). NanoBRET Approaches to Study Ligand Binding to GPCRs and RTKs. *Trends in Pharmacological Sciences*, *39*(2), 136–147. <https://doi.org/10.1016/j.tips.2017.10.006>
-

- Stoddart, L. A., White, C. W., Nguyen, K., Hill, S. J., & Pflieger, K. D. G. (2016). Fluorescence- and bioluminescence-based approaches to study GPCR ligand binding. *British Journal of Pharmacology*, *173*(20), 3028–3037. <https://doi.org/10.1111/bph.13316>
- Sun, S., Ding, Z., Yang, X., Zhao, X., Zhao, M., Gao, L., Chen, Q., Xie, S., Liu, A., Yin, S., Xu, Z., & Lu, X. (2021). Nanobody: A small antibody with big implications for tumor therapeutic strategy. *International Journal of Nanomedicine*, *16*, 2337–2356. <https://doi.org/10.2147/IJN.S297631>
- Sun, X., Cheng, G., Hao, M., Zheng, J., Zhou, X., Zhang, J., Taichman, R. S., Pienta, K. J., & Wang, J. (2010). CXCL12 / CXCR4 / CXCR7 chemokine axis and cancer progression. *Cancer and Metastasis Reviews*, *29*(4), 709–722. <https://doi.org/10.1007/s10555-010-9256-x>
- Suomivuori, C.-M., Latorraca, N. R., Wingler, L. M., Eismann, S., King, M. C., Kleinhenz, A. L. W., Skiba, M. A., Staus, D. P., Kruse, A. C., Lefkowitz, R. J., & Dror, R. O. (2020). Molecular mechanism of biased signaling in a prototypical G protein-coupled receptor. *Science*, *367*(6480), 881–887. <https://doi.org/10.5281/zenodo.3629830>
- Syrovatkina, V., Alegre, K. O., Dey, R., & Huang, X. Y. (2016a). Regulation, Signaling, and Physiological Functions of G-Proteins. *Journal of Molecular Biology*, *428*(19), 3850–3868. <https://doi.org/10.1016/j.jmb.2016.08.002>
- Takeuchi, K., & Ito, F. (2011). Receptor tyrosine kinases and targeted cancer therapeutics. *Biological and Pharmaceutical Bulletin*, *34*(12), 1774–1780. <https://doi.org/10.1248/bpb.34.1774>
- Tanaka, T., Zhou, Y., Ozawa, T., Okizono, R., Banba, A., Yamamura, T., Oga, E., Muraguchi, A., & Sakurai, H. (2018). Ligand-activated epidermal growth factor receptor (EGFR) signaling governs endocytic trafficking of unliganded receptor monomers by non-canonical phosphorylation. *Journal of Biological Chemistry*, *293*(7), 2288–2301. <https://doi.org/10.1074/jbc.M117.811299>
- Tao, R. H., & Maruyama, I. N. (2008). All EGF(ErbB) receptors have preformed homo- and heterodimeric structures in living cells. *Journal of Cell Science*, *121*(19), 3207–3217. <https://doi.org/10.1242/jcs.033399>

- Thoma, G., Streiff, M. B., Kovarik, J., Glickman, F., Wagner, T., Beerli, C., & Zerwes, H.-G. (2008). Orally Bioavailable Isothioureas Block Function of the Chemokine Receptor CXCR4 In Vitro and In Vivo. *Journal of Medicinal Chemistry*, *51*(24), 7915–7920. <https://doi.org/10.1021/jm801065q>
- Tian, Z., Niu, X., & Yao, W. (2020). Receptor Tyrosine Kinases in Osteosarcoma Treatment: Which Is the Key Target? *Frontiers in Oncology*, *10*(August), 1–13. <https://doi.org/10.3389/fonc.2020.01642>
- Tripathi, A., Gaponenko, V., & Majetschak, M. (2016). Commercially available antibodies directed against  $\alpha$ -adrenergic receptor subtypes and other G protein-coupled receptors with acceptable selectivity in flow cytometry experiments. *Naunyn-Schmiedeberg's Archives of Pharmacology*, *389*(2), 243–248. <https://doi.org/10.1007/s00210-015-1196-0>
- Tsai, M. F., Chang, T. H., Wu, S. G., Yang, H. Y., Hsu, Y. C., Yang, P. C., & Shih, J. Y. (2015a). EGFR-L858R mutant enhances lung adenocarcinoma cell invasive ability and promotes malignant pleural effusion formation through activation of the CXCL12-CXCR4 pathway. *Scientific Reports*, *5*(July), 1–14. <https://doi.org/10.1038/srep13574>
- van den Bor, J., Bergkamp, N. D., Anbuhl, S. M., Dekker, F., Comez, D., Perez Almeria, C. V., Bosma, R., White, C. W., Kilpatrick, L. E., Hill, S. J., Siderius, M., Smit, M. J., & Heukers, R. (2023). NanoB2 to monitor interactions of ligands with membrane proteins by combining nanobodies and NanoBRET. *Cell Reports Methods*, *3*(3). <https://doi.org/10.1016/j.crmeth.2023.100422>
- Van Hout, A., Klarenbeek, A., Bobkov, V., Doijen, J., Arimont, M., Zhao, C., Heukers, R., Rimkunas, R., de Graaf, C., Verrips, T., van der Woning, B., de Haard, H., Rucker, J. B., Vermeire, K., Handel, T., Van Loy, T., Smit, M. J., & Schols, D. (2018). CXCR4-targeting nanobodies differentially inhibit CXCR4 function and HIV entry. *Biochemical Pharmacology*, *158*(October), 402–412. <https://doi.org/10.1016/j.bcp.2018.10.015>
- Wang, J., Tannous, B. A., Poznansky, M. C., & Chen, H. (2020). CXCR4 antagonist AMD3100 (plerixafor): From an impurity to a therapeutic agent. *Pharmacological Research*, *159*(May), 105010. <https://doi.org/10.1016/j.phrs.2020.105010>

- Ward, R. J., Padiani, J. D., Marsango, S., Jolly, R., Stoneman, M. R., Biener, G., Handel, T. M., Raicu, V., & Milligan, G. (2021). Chemokine receptor CXCR4 oligomerization is disrupted selectively by the antagonist ligand IT1t. *Journal of Biological Chemistry*, *296*, 1–13. <https://doi.org/10.1074/jbc.RA120.016612>
- Weis, W. I., & Kobilka, B. K. (2018). The Molecular Basis of G Protein–Coupled Receptor Activation. *Annual Review of Biochemistry*, *87*, 897–919. <https://doi.org/10.1146/annurev-biochem>
- White, C. W., Caspar, B., Vanyai, H. K., Pflieger, K. D. G., & Hill, S. J. (2020a). CRISPR-Mediated Protein Tagging with Nanoluciferase to Investigate Native Chemokine Receptor Function and Conformational Changes. *Cell Chemical Biology*, *27*(5), 499–510.e7. <https://doi.org/10.1016/j.chembiol.2020.01.010>
- Wijtmans, M., Maussang, D., Sirici, F., Scholten, D. J., Canals, M., Mujić-Delić, A., Chong, M., Chatalic, K. L. S., Custers, H., Janssen, E., De Graaf, C., Smit, M. J., De Esch, I. J. P., & Leurs, R. (2012). Synthesis, modeling and functional activity of substituted styrene-amides as small-molecule CXCR7 agonists. *European Journal of Medicinal Chemistry*, *51*, 184–192. <https://doi.org/10.1016/j.ejmech.2012.02.041>
- Wilson, K. J., Mill, C., Lambert, S., Buchman, J., Wilson, T. R., Hernandez-Gordillo, V., Gallo, R. M., Ades, L. M. C., Settleman, J., & Riese, D. J. (2012). EGFR ligands exhibit functional differences in models of paracrine and autocrine signaling. *Growth Factors*, *30*(2), 107–116. <https://doi.org/10.3109/08977194.2011.649918>
- Woerner, B. M., Warrington, N. M., Kung, A. L., Perry, A., & Rubin, J. B. (2005). Widespread CXCR4 activation in astrocytomas revealed by phospho-CXCR4-specific antibodies. *Cancer Research*, *65*(24), 11392–11399. <https://doi.org/10.1158/0008-5472.CAN-05-0847>
- Woodard, L. E., & Nimmagadda, S. (2011). CXCR4-based imaging agents. In *Journal of Nuclear Medicine* (Vol. 52, Issue 11, pp. 1665–1669). <https://doi.org/10.2967/jnumed.111.097733>
- Wu, B., Chien, E. Y. T., Mol, C. D., Fenalti, G., Liu, W., Abagyan, R., Brooun, A., Wells, P., Bi, F. C., Hamel, D., Kuhn, P., Handel, T. M., Cherezov, V., & Stevens,

- R. C. (2010a). Structures of the CXCR4 chemokine receptor in complex with small molecule and cyclic peptide antagonists. *Science*, *330*(6007), 1066–1071. <https://doi.org/10.1126/science.1194396.Structures>
- Wu, B., Chien, E. Y. T., Mol, C. D., Fenalti, G., Liu, W., Abagyan, R., Brooun, A., Wells, P., Bi, F. C., Hamel, D., Kuhn, P., Handel, T. M., Cherezov, V., & Stevens, R. C. (2010b). Structures of the CXCR4 chemokine receptor in complex with small molecule and cyclic peptide antagonists. *Science*, *330*(6007), 1066–1071. <https://doi.org/10.1126/science.1194396.Structures>
- Wu, H., Zhu, L., Zhang, H., Shi, X., Zhang, L., Wang, W., Xue, H., & Liang, Z. (2015). Coexpression of EGFR and CXCR4 predicts poor prognosis in resected pancreatic ductal adenocarcinoma. *PLoS ONE*, *10*(2), 1–13. <https://doi.org/10.1371/journal.pone.0116803>
- Wu, J., Liu, Y., Ma, Y., Wang, R., Ji, X., Zhang, Y., & Du, Y. (2020a). Interaction between CXCR4 and EGFR and downstream PI3K/AKT pathway in lung adenocarcinoma A549 cells and transplanted tumor in nude mice. *International Journal of Clinical and Experimental Pathology*, *13*(2), 132–141.
- Xu, L., Li, C., Hua, F., & Liu, X. (2021). The CXCL12/CXCR7 signalling axis promotes proliferation and metastasis in cervical cancer. *Medical Oncology*, *38*(5), 1–10. <https://doi.org/10.1007/s12032-021-01481-2>
- Yamada, K., Maishi, N., Akiyama, K., Towfik Alam, M., Ohga, N., Kawamoto, T., Shindoh, M., Takahashi, N., Kamiyama, T., Hida, Y., Taketomi, A., & Hida, K. (2015). CXCL12-CXCR7 axis is important for tumor endothelial cell angiogenic property. *International Journal of Cancer*, *137*(12), 2825–2836. <https://doi.org/10.1002/ijc.29655>
- Yarden, Y., & Schlessinger, J. (1987). Epidermal Growth Factor Induces Rapid, Reversible Aggregation of the Purified Epidermal Growth Factor Receptor. *Biochemistry*, *26*(5), 1443–1451. <https://doi.org/10.1021/bi00379a035>
- Yen, Y.-C., Schafer, C. T., Gustavsson, M., Eberle, S. A., Dominik, P. K., Deneka, D., Zhang, P., Schall, T. J., Kossiakoff, A. A., G Tesmer, J. J., & Handel, T. M. (2022). Structures of atypical chemokine receptor 3 reveal the basis for its promiscuity and signaling bias. In *Sci. Adv* (Vol. 8).

- Yu, X., Sharma, K. D., Takahashi, T., Iwamoto, R., & Mekada, E. (2002). Ligand-independent dimer formation of epidermal growth factor receptor (EGFR) is a step separable from ligand-induced EGFR signaling. *Molecular Biology of the Cell*, *13*(7), 2547–2557. <https://doi.org/10.1091/mbc.01-08-0411>
- Yun, C. H., Boggon, T. J., Li, Y., Woo, M. S., Greulich, H., Meyerson, M., & Eck, M. J. (2007). Structures of Lung Cancer-Derived EGFR Mutants and Inhibitor Complexes: Mechanism of Activation and Insights into Differential Inhibitor Sensitivity. *Cancer Cell*, *11*(3), 217–227. <https://doi.org/10.1016/j.ccr.2006.12.017>
- Zanetti-Domingues, L. C., Korovesis, D., Needham, S. R., Tynan, C. J., Sagawa, S., Roberts, S. K., Kuzmanic, A., Ortiz-Zapater, E., Jain, P., Roovers, R. C., Lajevardipour, A., van Bergen en Henegouwen, P. M. P., Santis, G., Clayton, A. H. A., Clarke, D. T., Gervasio, F. L., Shan, Y., Shaw, D. E., Rolfe, D. J., ... Martin-Fernandez, M. L. (2018). The architecture of EGFR's basal complexes reveals autoinhibition mechanisms in dimers and oligomers. *Nature Communications*, *9*(1). <https://doi.org/10.1038/s41467-018-06632-0>
- Zarca, A. M., Adlere, I., Viciano, C. P., Arimont-Segura, M., Meyrath, M., Simon, I. A., Bebelman, J. P., Laan, D., Custers, H. G. J., Janssen, E., Versteegh, K. L., Buzink, M. C. M. L., Nesheva, D. N., Bosma, R., de Esch, I. J. P., Vischer, H. F., Wijtmans, M., Szpakowska, M., Chevigné, A., ... Leurs, R. (2024). Pharmacological Characterization and Radiolabeling of VUF15485, a High-Affinity Small-Molecule Agonist for the Atypical Chemokine Receptor ACKR3. *Molecular Pharmacology*, *105*(4), 301. <https://doi.org/10.1124/molpharm.123.000835>
- Zeng, Z., Yan, H. hong, Zhang, X. chao, Zhong, W. zhao, He, Y. yan, Guan, J. lin, Niu, F. yu, Xie, Z., Huang, Y. sheng, Xu, C. rui, Dong, S., & Wu, Y. long. (2014). Reduced chemotherapy sensitivity in EGFR-mutant lung cancer patient with frontline EGFR tyrosine kinase inhibitor. *Lung Cancer*, *86*(2), 219–224. <https://doi.org/10.1016/j.lungcan.2014.09.008>
- Zeronian, M. R., Doukeridou, S., van Bergen en Henegouwen, P. M. P., & Janssen, B. J. C. (2022). Structural insights into the non-inhibitory mechanism of the anti-

- EGFR EgB4 nanobody. *BMC Molecular and Cell Biology*, 23(1), 1–10. <https://doi.org/10.1186/s12860-022-00412-x>
- Zhang, C., Zhu, R., Cao, Q., Yang, X., Huang, Z., & An, J. (2020). Discoveries and developments of CXCR4-targeted HIV-1 entry inhibitors. *Experimental Biology and Medicine*, 245(5), 477–485. <https://doi.org/10.1177/1535370220901498>
- Zhao, M., Jung, Y., Jiang, Z., & Svensson, K. J. (2020). Regulation of Energy Metabolism by Receptor Tyrosine Kinase Ligands. *Frontiers in Physiology*, 11(April), 1–23. <https://doi.org/10.3389/fphys.2020.00354>
- Zhao, S., Wu, B., & Stevens, R. C. (2019). Advancing Chemokine GPCR Structure Based Drug Discovery. *Structure*, 27(3), 405–408. <https://doi.org/10.1016/j.str.2019.02.004>
- Zhen, Y., Caprioli, R. M., & Staros, J. V. (2003). Characterization of glycosylation sites of the epidermal growth factor receptor. *Biochemistry*, 42(18), 5478–5492. <https://doi.org/10.1021/bi027101p>
- Zhou, Q., Yang, D., Wu, M., Guo, Y., Guo, W., Zhong, L., Cai, X., Dai, A., Jang, W., Shakhnovich, E., Liu, Z. J., Stevens, R. C., Lambert, N. A., Babu, M. M., Wang, M. W., & Zhao, S. (2019). Common activation mechanism of class a GPCRs. *ELife*, 8, 1–31. <https://doi.org/10.7554/eLife.50279>
- Zielińska, K. A., & Katanaev, V. L. (2020a). The signaling duo CXCL12 and CXCR4: Chemokine fuel for breast cancer tumorigenesis. *Cancers*, 12(10), 1–21. <https://doi.org/10.3390/cancers12103071>
- Zielińska, K. A., & Katanaev, V. L. (2020b). The signaling duo CXCL12 and CXCR4: Chemokine fuel for breast cancer tumorigenesis. *Cancers*, 12(10), 1–21. <https://doi.org/10.3390/cancers12103071>
- Zobair, A. A. A., Obeidy, B. F. A., Yang, L., Yang, C., Hui, Y., Yu, H., Zheng, F., Yang, G., Xie, C., Zhou, F., & Zhou, Y. (2013). Concomitant overexpression of EGFR and CXCR4 is associated with worse prognosis in a new molecular subtype of non-small cell lung cancer. *Oncology Reports*, 29(4), 1524–1532. <https://doi.org/10.3892/or.2013.2254>
-

- Zou, Y.-R., Kottmann, A. H., Kuroda, M., Taniuchi, I., & Littman, D. R. (1998). Function of the chemokine receptor CXCR4 in haematopoiesis and in cerebellar development. *Nature*, *393*(6685), 595–599. <https://doi.org/10.1038/31269>
- Zuo, J., Wen, M., Li, S., Lv, X., Wang, L., Ai, X., & Lei, M. (2017). Overexpression of CXCR4 promotes invasion and migration of non-small cell lung cancer via EGFR and MMP-9. *Oncology Letters*, *14*(6), 7513–7521. <https://doi.org/10.3892/ol.2017.7168>